

**Magnetostrictively Induced Mechanical Resonance  
of Electrical Steel Strips  
by  
Thant Phyu Phyu Phway**

**A thesis submitted to the Cardiff University in candidature for the degree  
of Doctor of Philosophy**

**Wolfson Centre for Magnetics  
Cardiff School of Engineering  
Cardiff University  
Wales, United Kingdom of Great Britain and Northern Ireland**

**December 2007**

UMI Number: U585084

All rights reserved

INFORMATION TO ALL USERS

The quality of this reproduction is dependent upon the quality of the copy submitted.

In the unlikely event that the author did not send a complete manuscript and there are missing pages, these will be noted. Also, if material had to be removed, a note will indicate the deletion.



UMI U585084

Published by ProQuest LLC 2013. Copyright in the Dissertation held by the Author.  
Microform Edition © ProQuest LLC.

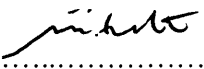
All rights reserved. This work is protected against  
unauthorized copying under Title 17, United States Code.



ProQuest LLC  
789 East Eisenhower Parkway  
P.O. Box 1346  
Ann Arbor, MI 48106-1346

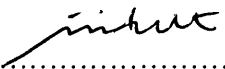
## DECLARATION

This work has not previously been accepted in substance for any degree and is not concurrently submitted in candidature for any degree.

Signed .....  ..... (candidate) Date ..... 6 JUNE 2008 .....

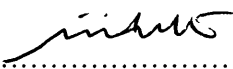
### STATEMENT 1

This thesis is being submitted in partial fulfillment of the requirements for the degree of ..... Ph.D. ..... (insert MCh, MD, MPhil, PhD etc, as appropriate)

Signed .....  ..... (candidate) Date ..... 6 JUNE 2008 .....


### STATEMENT 2

This thesis is the result of my own independent work/investigation, except where otherwise stated. Other sources are acknowledged by explicit references.

Signed .....  ..... (candidate) Date ..... 6 JUNE 2008 .....

### STATEMENT 3

I hereby give consent for my thesis, if accepted, to be available for photocopying and for inter-library loan, and for the title and summary to be made available to outside organisations.

Signed .....  ..... (candidate) Date ..... 6 JUNE 2008 .....

### STATEMENT 4 - BAR ON ACCESS APPROVED

I hereby give consent for my thesis, if accepted, to be available for photocopying and for inter-library loans after expiry of a bar on access approved by the Graduate Development Committee.

Signed .....  ..... (candidate) Date ..... 6 JUNE 2008 .....

**DECLARATION**

This work has not previously been accepted in substance for any degree and is not concurrently submitted in candidature for any degree.

Signed ..... (candidate)      Date .....

**STATEMENT 1**

This thesis is being submitted in partial fulfillment of the requirements for the degree of .....(insert MCh, MD, MPhil, PhD etc, as appropriate)

Signed ..... (candidate)      Date .....

**STATEMENT 2**

This thesis is the result of my own independent work/investigation, except where otherwise stated. Other sources are acknowledged by explicit references.

Signed ..... (candidate)      Date .....

**STATEMENT 3**

I hereby give consent for my thesis, if accepted, to be available for photocopying and for inter-library loan, and for the title and summary to be made available to outside organisations.

Signed ..... (candidate)      Date .....

**STATEMENT 4 - BAR ON ACCESS APPROVED**

I hereby give consent for my thesis, if accepted, to be available for photocopying and for inter-library loans after expiry of a bar on access approved by the Graduate Development Committee.

Signed ..... (candidate)      Date .....

*To my beloved parents U Than Tun and Daw Vidya Devi who have always  
believed in me and to my sweet sister Thaya for the laughter we share.*

## Acknowledgements



The work has been carried out at the Wolfson Centre for Magnetism, Cardiff School of Engineering, Cardiff University, to which I am grateful for providing the resources needed to complete this project.

I am grateful to my supervisors, Professor A. J. Moses for his guidance and valuable discussions, and Dr Turgut Meydan for his time and patience throughout this project. Thank you both for your continuous help and support.

I would like to express my gratitude to Professor Phil Beckley who has contributed significantly to my understanding of the subject. His enthusiasm in research has kept me motivated.

I would like to extend my heartfelt thanks to Professor David Jiles for his kind assistance during his sabbatical year in the Wolfson Centre. It was a privilege to work with him.

Finally, to several colleagues who have assisted me one way or another, especially Mr. Harshad V. Patel, Dr. Stan Zurek and Dr Paul I. Williams in challenging me with alternative views, I feel very much indebted.

## SUMMARY

Extensive research has been carried out over the years to reduce the acoustic noise resulting from vibration of electromagnetic cores mainly caused by magnetostriction. This project presents the results of a basic experimental study of magnetostriction in strips of magnetic materials commonly used in electromagnetic cores which gives an important new understanding of the phenomenon. The presence of mechanical resonance in the laminations is highlighted here for the first time.

A standard magnetising system was built and a new method of measuring magnetostriction was used. A single point laser vibrometer was used to measure magnetostrictive vibration of the samples. The magnetostriction of grain-oriented materials cut at various angles to the rolling direction, non-oriented samples with different silicon content and nickel iron strips was measured over a wide range of magnetising frequencies and at peak flux densities up to 1.0 Tesla.

Magnetostriction measurement results were used to identify magnetisation induced mechanical resonance of the samples. The magnetising frequency at resonance was derived from the relationship of velocity, frequency and wavelength of an electromagnetically excited strip. Theoretical value of the fundamental resonant frequency and its harmonics were calculated and compared with measured values. The variation of the acoustic noise in a three-phase transformer core under no-load condition with various switching frequencies and different modulation indices was measured under pulse-width modulation and sinusoidal voltage excitation. All measurements were repeated at least five times to assess experimental accuracy and uncertainties.

Results suggest that under resonance, transformer cores can produce excessive noise and potentially long term deterioration of lamination coating and possible core failure. Extrapolation of the results to larger cores infer that the phenomenon can possibly occur in cores with different length laminations leading to variability of noise output according to how close the magnetising frequency or predominant harmonics are to the resonant frequency. These findings demonstrate the importance of the interaction between basic magnetostriction and geometrical factors that are contributing towards the total noise output and care that must be taken when characterising the basic magnetostriction of samples of different sizes magnetised at different frequencies.

## LIST OF CONTENTS

CHAPTER	PAGE
DECLARATION AND STATEMENTS	ii
DEDICATION	iii
ACKNOWLEDGEMENTS	iv
SUMMARY	v
LIST OF CONTENTS	
<b>1.0 AIMS OF THE INVESTIGATION</b>	<b>1-1</b>
References	1-4
<b>2.0 MAGNETISM AND MAGNETIC MATERIALS</b>	<b>2-1</b>
2.1 Introduction	2-1
2.2 Magnetic Field, $H$	2-2
2.3 Magnetic Induction, $B$	2-3
2.4 Magnetic Materials	2-4
2.4.1 <i>Hard Magnetic Materials</i>	2-6
2.4.2 <i>Soft Magnetic Materials</i>	2-6
2.4.2.1 <i>Electrical Steels</i>	2-7
2.5 Ferromagnetism	2-11
2.6 Hysteresis in Magnetic Materials	2-13
2.7 Power Loss	2-15
References	2-16
<b>3.0 MAGNETOSTRICTION</b>	<b>3-1</b>
3.1 Introduction	3-1
3.2 Physics of Magnetostriction	3-3
3.3 Magnetostriction and Mechanical Resonance	3-6
3.3.1 <i>Theoretical Approach to Mechanical Resonance in Epstein Strips</i>	3-8
3.4 Previous Research on Magnetostriction and Resonance	3-10
3.5 Measurement of Magnetostriction	3-16
3.5.1 <i>Resistance and Semiconductor Strain Gauges</i>	3-18
3.5.2 <i>Accelerometers</i>	3-19
3.5.3 <i>Laser Interferometer Techniques</i>	3-21



3.5.3.1	<i>Laser Vibrometer</i>	3-22
3.5.4	<i>Previous Research on Measurement of Magnetostriction – Concentrating on Optical Methods</i>	3-24
3.6	Application of Magnetostriction	3-30
	References	3-33
<b>4.0</b>	<b>TRANSFORMER NOISE</b>	<b>4-1</b>
4.1	Introduction	4-1
4.2	Construction of Transformer Cores	4-3
4.3	Types of Transformers	4-4
4.4	Previous Research on Noise in Transformer Cores	4-6
	References	4-14
<b>5.0</b>	<b>EXPERIMENTAL SETUP</b>	<b>5-1</b>
5.1	Introduction	5-1
5.2	The Measurement System	5-1
5.3	Single Point Laser Displacement Vibrometer – Operating Principle	5-6
5.4	Samples	5-9
5.5	Experimental Procedure	5-9
5.6	Data Analysis using LabVIEW	5-11
5.7	Young’s Modulus Tests	5-15
5.8	3-Phase Transformer Core	5-17
5.8.1	<i>Theoretical Basis</i>	5-18
5.8.2	<i>Experimental Setup for 3-Phase Transformer Core</i>	5-19
5.9	Preliminary Tests	5-21
5.10	Measurement Repeatability	5-23
5.11	Uncertainty of Calculated Resonance Frequency $f_m$	5-25
	References	5-28
<b>6.0</b>	<b>EXPERIMENTAL RESULTS</b>	<b>6-1</b>
6.1	Introduction	6-1
6.2	Magnetisation Induced Mechanical Resonance of GO90°	6-1
6.2.1	<i>Magnetostriction against Magnetising Frequency at Various Magnetic Fields</i>	6-2

6.2.2	<i>Temperature Effects</i>	6-4
6.2.3	<i>Half Epstein Length GO90°</i>	6-6
6.2.4	<i>Stack of GO90°</i>	6-7
6.3	<b>Magnetisation Induced Mechanical Resonance of GO0°</b>	6-8
6.3.1	<i>Power Loss</i>	6-9
6.3.2	<i>3-Phase Transformer Core</i>	6-10
6.3.2.1.	<i>Displacement and acoustic noise measurements at Point 1</i>	6-10
6.3.2.2.	<i>Displacement and acoustic noise measurements at point 2</i>	6-13
6.3.2.3.	<i>Displacement measurements at point 4 (horizontal displacement)</i>	6-16
6.3.2.4.	<i>Acoustic noise measurements at point 5</i>	6-18
6.3.2.5.	<i>Resultant acoustic noise of the 3-phase core</i>	6-19
6.4	<b>Magnetisation Induced Mechanical Resonance of GO55°</b>	6-20
6.5	<b>Magnetisation Induced Mechanical Resonance of NO</b>	6-20
6.5.1	<i>3% Si NO</i>	6-21
6.5.2	<i>6.5% Si NO0°</i>	6-21
6.5.3	<i>6.5% Si NO90°</i>	6-22
6.6	<b>Magnetisation Induced Mechanical Resonance of 45% Ni-Fe</b>	6-23
	<b>References</b>	6-24
<b>7.0</b>	<b>DISCUSSION OF RESULTS</b>	<b>7-1</b>
7.1	<b>Introduction</b>	7-1
7.2	<b>Magnetisation Induced Mechanical Resonance of Grain Oriented Samples</b>	7-1
7.2.1	<i>3% Si-Fe GO90°</i>	7-1
7.2.2	<i>3% Si-Fe GO0°</i>	7-11
7.2.3	<i>3-Phase Transformer Core</i>	7-13
7.2.4	<i>3% Si-Fe GO55°</i>	7-17
7.3	<b>Magnetisation Induced Mechanical Resonance of Non Oriented Samples</b>	7-19
7.3.1	<i>3% Si NO</i>	7-19

7.3.2	6.5% Si NO	7-20
7.4	Magnetisation Induced Mechanical Resonance of Ni-Fe Sample	7-22
7.5	Damping	7-24
7.6	Summary	7-25
	References	7-27
<b>8.0</b>	<b>CONCLUSIONS AND FUTURE WORK</b>	<b>8-1</b>
8.1	Conclusions	8-1
8.2	Future Work	8-2
	<b>APPENDIX I – PUBLISHED WORK</b>	
	<b>APPENDIX II – CORRECTION TABLE</b>	

## CHAPTER 1

### AIMS OF THE INVESTIGATION

---

Magnetic materials such as grain-oriented electrical steels are widely used for the magnetic cores of transformers and motors. Extensive research has been carried out for at least two decades to reduce the transformer acoustic noise resulting from core vibration partly caused by the magnetostriction of the core material, which is the prime cause of large acoustic noise that radiates uncontrollably from the surfaces of electrical machines. Because of the interrelationship between magnetostriction and transformer noise, it is important to be able to accurately measure the properties of single laminations and to predict their effect on the noise when built into a core. This harmful effect of noise is also not well understood and is a source of energy waste as well as environmental noise concerns and not many researchers highlight the importance of mechanical resonance in the materials. The noise problem is becoming of increasing industrial importance particularly in equipment subjected to high frequency and harmonic magnetisation.

All materials or bodies possessing mass and elasticity are capable of vibration or vibration takes place in the presence of external excitation [1.1]. Thus, most engineering machines and structures experience vibration to some degree, and therefore, design of any engineering machines and structures generally requires consideration of their oscillatory behavior especially at resonant frequency.

Recently, the two most important characteristics of transformer cores, i.e. power loss and noise, have been reduced considerably with improved material and core design. However, the base value of noise that results from magnetostriction is still a major environmental noise concern of the now highly industrialised world since noise is unwanted sound, a mellow sound to some, can be completely unacceptable to others. For example, magnetostriction of 4 micro strain measured at 100 Hz on a 15 MVA transformer core limb produced a noise level of 72 dBA [1.2]. In a specification of a transformer design, the maximum allowable noise level is given to be 60 – 70 dBA [1.3]. The noise level of 60 dB is equivalent to a passenger car travelling at 60 km/h

measured at a 7 metre distance. It is clear that magnetostrictive effects partly lead to generation of acoustic noise in a transformer and the higher harmonics produced, affects the sensitivity of human ear immensely.

It has come to prominence, mainly because transformers are placed closer to the populace such as in high rise office buildings, apartments, shopping malls and in gardens. It is even more necessary to design transformer cores appropriately since resonance may cause excessive noise as well as potential effect to the efficiency of large transformer cores.

Therefore, it is important to understand the vibration modes of transformers to ensure that the next generation of transformers can be built better. This project presents investigation of magnetostriction in strips of magnetic materials commonly used in electromagnetic cores which gives an important new understanding of the phenomenon.

The main aims of the investigation can be summarised as follow:

- 1) Identify resonance modes.
- 2) Predict effects in noise and vibration output.

Methods employed to achieve the above aims are summarised as follow:

1. Selection of samples
  - a. Non oriented silicon iron strips to assess the effect of mechanical resonance on different silicon content and thickness of samples.
  - b. Grain oriented silicon iron strips to assess the effect of mechanical resonance on samples cut at different angles to rolling directions, sample length and stack of laminations.
  - c. Nickel iron to assess the effect of mechanical resonance.
2. Identify and derive resonance equation(s)
  - a. To cater for the sample sizes and shapes in (1).
  - b. Calculate resonance modes for clamped end situations.

- c. List principal resonance harmonics of all the samples.
3. Measure vibration characteristics of all the samples for;
  - a. Active (magnetised) and mechanical lengths for electrical steel in particular to gather a wide range of resonance data.
  - b. Fully assess experimental accuracy and uncertainties.
  - c. Repeat each measurement at least 5 times.
4. Full assessment of physical and magnetic characteristics of samples of different materials and shapes, etc.
  - a. Quantify and explain agreement between theory and measurement on the range of materials in 1.
5. Based on results
  - (a) Understand assembly method(s) to be able to relate test conditions and analysis of 3 and 4.
  - (b) Select suitable single phase stacked core geometry(ies) which can be magnetised in the laboratory over the expected resonance mode range.
  - (c) Assess wider implications of predictions for cores made from different materials.

**References**

- [1.1] W T Thomson, 'Theory of Vibration with Applications – Fourth Edition', Prentice Hall, 1993.
- [1.2] P Beckley, 'Electrical Steels', European Electrical Steels, Orb Works, 2000.
- [1.3] Federal Pacific, 'Online Literature – Dry Type Transformers', <http://www.federalpacific.com/>.

## CHAPTER 2

### MAGNETISM AND MAGNETIC MATERIALS

#### 2.1. Introduction

In 1820, Oersted discovered that a current carrying wire deflected a compass needle in its vicinity and then Faraday repeated and extended Oersted's experiments, discovering the Laws of Induction in 1831 [2.1]. In 1862, Maxwell created the common theoretical basis for electromagnetism with the laws which were named after him. Throughout the history of magnetism, it is evident that the availability of different types of devices operating on a magnetic basis has increased the development of special magnetic material while discovering new physical and magnetic effects.

Table 2.1. shows a number of terms and units which are commonly used in the subject of magnetism. In this thesis, magnetic terms and units will be given using the SI system.

Table 2.1  
Magnetic terms and units [2.2].

Terms		SI Units	CGS Units	Conversion
Magnetic field strength	$H$	A/m (Ampere/metre)	Oe (Oersted)	1 Oe = 79.58 A/m
Magnetisation	$M$	A/m	Oe (Oersted)	
Magnetic induction or flux density	$B$	T (Tesla)	G (Gauss)	1 G = $10^{-4}$ T
Magnetic flux	$\phi$	Wb (Weber)	Mx (Maxwell)	1 Mx = $10^{-8}$ Wb
Magnetic polarization	$J$	T	G (Gauss)	
Permeability (absolute)	$\mu$	T.m/A	G/Oe	
Permeability of vacuum (magnetic constant)	$\mu_0$	$4\pi \times 10^{-7}$ T.m/A	1	

In general, the relationship between  $B$ ,  $M$ , and  $H$  can be expressed by equation 2.1.



$$B = \mu_0(H + M) \quad (2.1)$$

Under linear conditions of a magnetic material i.e. at constant temperature and relatively low  $H$ , magnetic susceptibility  $\chi$  is constant. Therefore,

$$M = \chi \cdot H \quad (2.2)$$

Consequently, equation 2.1 can be written as:

$$B = \mu_0(1 + \chi)H \quad (2.3)$$

Magnetic susceptibility  $\chi$  is zero in vacuum and hence, in the case of free space the relationship between  $B$  and  $H$  is can be calculated as:

$$B = \mu_0 H \quad (2.4)$$

However, relative permeability  $\mu_r$  is  $\frac{\mu}{\mu_0}$  and  $\mu = \mu_0(1 + \chi)$  [2.2]. Therefore, for any other medium the correlation between  $B$  and  $H$  can be written as:

$$B = \mu H \quad (2.5)$$

## 2.2. Magnetic Field, $H$

Magnetic field,  $H$  is produced whenever there is an electrical charge in motion and the strength of  $H$  is measured in amperes per metre (A/m). Magnetic field can be produced due to an electrical current flowing in a conductor or by a permanent magnet. Magnetic field sources are essentially dipolar in nature, having a north and south magnetic pole. Direction of magnetic field is such that it circulates the conductor using the right-hand-rule. Figure 2.1 shows various sources of magnetic field including the natural magnetic field of the earth. Earth's magnetic field (and the surface magnetic field) is approximately a magnetic dipole, with one pole near the

north pole and the other near the geographic south pole. The cause of the natural earth's magnetic field is explained by dynamo theory which is described in [2.1].

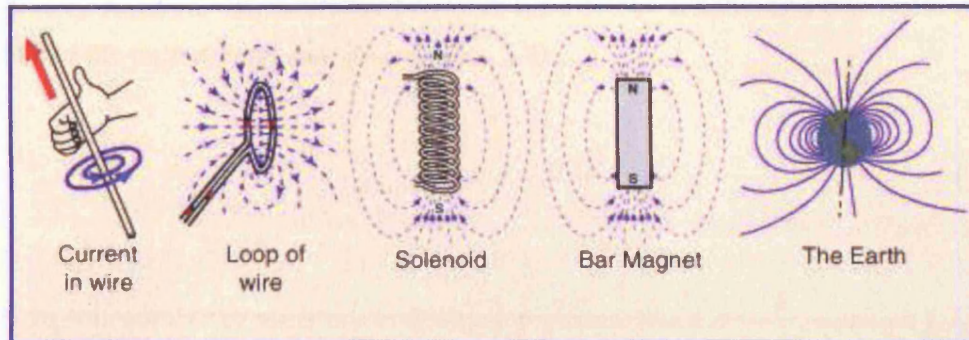


Figure 2.1. Magnetic field sources

Magnetic field,  $H$ , that is generated by an electrical current produced in a thin long solenoid can be calculated by the following equation (2.6). Note that  $H$  defined here is the magnetic field along the axis inside the coil.

$$H = \frac{Ni}{L} \text{ (A/m)} \quad (2.6)$$

where  $N$  is the number of turns on the solenoid,  $i$  is the generating current and  $L$  is the length of the solenoid. Therefore,  $H$  is determined by the size and distribution of currents producing it and is independent of the material medium.  $L$  in equation 2.1 is replaced by other parameters depending on the configuration of the solenoid or electromagnet.

### 2.3. Flux Density, $B$

Magnetic induction or flux density,  $B$  is the response to a magnetic field,  $H$  generated in a medium by a current.

Whenever there is  $H$  present in free space, there will be magnetic flux  $\phi$  (Wb) generating an electromotive force (emf) in a closed circuit of conductor through which the  $\phi$  passes. Faraday's law states that the voltage induced in an electrical

circuit is proportional to the rate of change of  $\phi$  linking the circuit. And Lenz's law states that the induced voltage is in a direction which opposes the flux change producing it. Therefore, the rate of change of flux,  $\frac{d\phi}{dt}$  linking an electric circuit is equal to the induced emf in volts (equation 2.7).

$$V_{ind} = -N \frac{d\phi}{dt} \quad (2.7)$$

where  $N$  is number of turns in a coil which  $\phi$  passes. Since  $B = \frac{\phi}{A}$ , equation 2.7, can be written as follows.

$$V_{ind} = -NA \frac{dB}{dt} \quad (2.8)$$

where voltage induced in a coil with  $N$  turns of cross sectional area  $A$ .

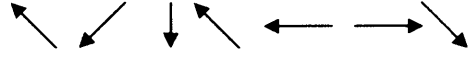

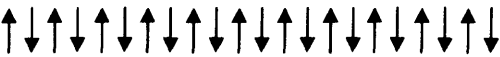

#### 2.4. Magnetic Materials

Magnetic properties of materials arise from the motion of electrons in the form of electron spin and electron orbital motion generating magnetic moment associated with the electron. Magnetic materials can be classified into three main categories; diamagnets, paramagnets and ferromagnets. Diamagnets have a net magnetic moment in the atoms however not permanent. When  $H$  is applied, orbits of electrons change and they set up orbital magnetic moment which opposes the field. Paramagnets have a net magnetic moment per atom and with external  $H$ , moments are aligned in the field direction having the magnetisation parallel to the field. Paramagnetic materials such as aluminium or platinum become magnetised in a magnetic field but when the field is removed, the net magnetic alignment is lost as the dipoles relax back to their normal random motion.

The most important and interesting magnetic materials are the ferromagnets. Ferromagnetism is explained in more details in section 2.6. Ferromagnets can retain

their magnetic properties when the magnetic field is removed. Ferromagnets have aligned magnetic moments and these become disordered when the material reaches the Curie temperature. Ferromagnets such as iron, cobalt, nickel have high relative permeability. Table 2.2 describes some of the types of magnetic materials and their arrangement of magnetic moments on neighbouring atoms.

Table 2.2  
Types of magnetic materials

<i>Types of magnetic materials</i>	<i>Arrangement of magnetic moments on neighbouring atoms</i>	
Paramagnet		
Ferromagnet		
Antiferromagnet		
Ferrimagnet		

Ferromagnetic materials can be divided into two major groups; soft magnetic materials (for Epstein strips<sup>1</sup> with coercive<sup>2</sup> field of 0 to 1 kA/m) and hard magnetic materials (for Epstein strips with coercive field of 10 kA/m and above). Soft magnetic materials are used in electromagnets and inductor cores and the primary objective of application is to generate as much magnetic induction,  $B$  as possible under action of magnetic field,  $H$ . Hard magnetic materials are used in permanent magnet applications and used to generate a magnetic induction,  $B$  without a conventional electrical power supply.

Other ferromagnetic materials include magnetic particles and magnetic thin films which are used in magnetic recording of information in the form of analogue signals or digital data. These magnetic recording materials are also known as the semi-hard magnetic materials (for Epstein strips with coercive field of 1 to 10 kA/m). Arising

<sup>1</sup> British Standards EN 60404-2:1998 states that for ac measurements of electrical steel strips by means of Epstein frame, sample sizes should be cut at width  $30 \text{ mm} \pm 0.2 \text{ mm}$  and length,  $l$  should be  $280 \text{ mm} \leq l \leq 320 \text{ mm}$ .

<sup>2</sup> See section 2.6 for definition

interest in such materials for magnetic data storage, both for long term memory such as disk drives and on-line random access memory, RAM.

#### **2.4.1. Hard Magnetic Materials**

Hard magnetic materials are also referred to as permanent magnets. The desirable properties of hard magnetic materials are high coercive field (see section 2.6) and high residual magnetisation [2.3]. The quality of permanent magnets are characterized by the so-called energy product  $(B.H)_{max}$ . It is believed that permanent magnets have been used for compasses by the Chinese since approximately 2500 B.C. In his review, Kirchmayr [2.4] said the development of permanent magnets during this century has shown a continuous increase of quality, strength and the ability to store energy.

Hard magnets were permanent magnets due to the pinning of domain walls [2.3] by dislocations and inclusions. The movement of dislocations within a material is often hindered by the same factors that affect the motion of domain walls and as a consequence these steels are mechanically very hard and are the origin of the term 'hard' magnetic.

Alnico, hard ferrites, samarium cobalt and neodymium-boron-iron (NdFeB) are among the permanent magnets widely used in various modern applications such as in the automobile industry. Other industries where permanent magnets have widespread use is telecommunications namely, loudspeakers, microphones, data processing industry making disc drives and actuators, electronic and instrumentation products such as contactless switches, sensors and many more.

#### **2.4.2. Soft Magnetic Materials**

The term 'soft' relates to the class of metals or alloys which can be easily magnetised and demagnetised as opposed to hard magnetic materials. Soft magnetic materials find extensive applications since because of their desirable properties of having high permeability, low coercivity and their ability to enhance the flux produced by an electrical current. Therefore, applications of soft magnetic materials are mostly

associated with electrical circuits in which the magnetic material is used to amplify the flux generated.

The types of applications for soft magnetic materials fall into two main categories: ac and dc. In dc applications the material is magnetised in order to perform an operation and then demagnetised at the end of the operation e.g. in the case of an electromagnet on a crane at a scrap yard which will be switched on to attract the scrap steel and then switched off to drop the steel. The main consideration for material selection for dc application is most likely to be the permeability e.g. in the case of shielding applications where flux must be channelled through the material and saturation magnetisation where the material is used to generate a magnetic field or create a force. Soft magnetic materials used for dc applications include iron and low-carbon steels, nickel-iron alloys, and cobalt-iron alloys [2.2].

In ac applications the material will be magnetised from one direction to the other in a continuous cycle, throughout the period of operation. An example of soft magnetic materials used in ac applications relate to electric circuits and primarily in transformers converting one ac voltage into another. Similarly, the most desirable property of soft magnetic material for ac application is the high permeability. Silicon-iron alloys used for transformer cores, also known as electrical steels, will be discussed further in the next section 2.4.2.1. Other soft magnetic materials used for ac applications are aluminium-iron alloys, nickel-iron alloy, amorphous ribbons and fibres and nanocrystalline materials etc.

#### ***2.4.2.1. Electrical Steels***

Electrical steels, also known as silicon steels, are soft magnetic materials normally used in lamination form to carry magnetic flux in the cores of a variety of electrical machines such as motors, generators and transformers. There are three principal types of electrical steel; grain oriented steels, non oriented fully processed steels and non oriented semi-processed steels.

In the power industry, the electrical voltage is usually low-frequency ac at 50 Hz or 60 Hz. Use of these frequencies, consequently leads to the generation of eddy currents which reduce the efficiency of transformers because some of the energy is lost through eddy current dissipation. In the 19<sup>th</sup> century, electrical machines used solid iron cores [2.6]. However the benefits of using laminations to reduce the effects of eddy currents soon become apparent. Barrett et al carried out work around 1900 into the benefits of alloying silicon with the steel [2.7]. They discovered that about 3% added silicon, reduced eddy currents and enhance the permeability of the alloy. The conductivity is also reduced and magnetostriction (explained in detail in chapter 3) is reduced when silicon is added. Silicon is also a very cheap material which makes an important consideration when so much transformer iron is needed. However, the addition of too much silicon makes the material extremely brittle and difficult to produce, giving a practical limitation of 4% to the amount of silicon that can be added [2.5]. When the silicon content exceeds 4.5% the material become quite brittle and hard to cut, making it very difficult to produce in laminations. However, in 1993 NKK Corporation managed to produce a state-of-the-art flat-rolled non oriented steel of 0.1 - 0.3 mm thickness with 6.5% silicon composition and subsequently succeeded in producing 0.05 mm thick silicon steel in 1996 [2.9]. At around 6.5% silicon the magnetic permeability of the alloy increases, iron loss decreases and magnetostriction drops to near zero. Typically most electrical steels will contain between 0.2 – 6.5% silicon with varying thickness of between 0.1 – 0.65 mm [2.8].

Grain oriented silicon iron steels are widely used as transformer core materials and such steel has superior properties in the rolling direction. The production of grain oriented steel was based on the discovery by Goss, where certain combinations of chemistry, rolling and heat treatment would give rise to material with highly directional properties [2.5]. The Goss material utilises the fact that the iron crystal has easy directions of magnetisation along its cube edges. This means that it is possible, as long as the material is magnetised along its rolling, easy, direction, to achieve high levels of magnetisation at relatively low power loss and low magnetic field intensity.

Silicon iron is made up of crystals constructed in a body-centred cubic lattice form and the easiest direction of magnetisation is along any one of the cube edge directions

which in terms of Miller indices are the  $[100]$  directions. In the finished silicon iron material, the crystals tend to be oriented with their  $[110]$  planes parallel to the surface of the sheet and their  $(001)$  directions parallel to the rolling direction [2.7] (figure 2.2a). Another grain orientation with the  $(001)$  planes parallel to the rolling direction is shown in figure 2.2b.

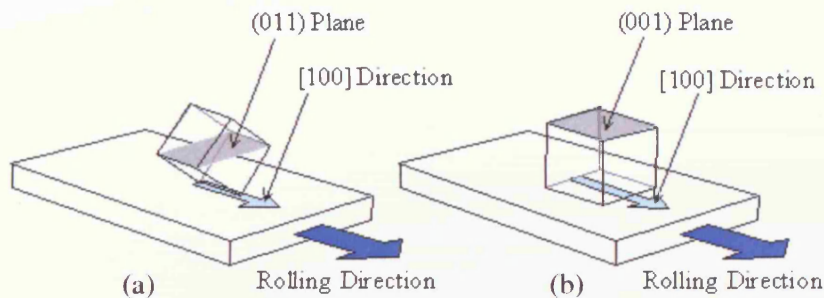


Figure 2.2. Schematic diagram of a (a) Goss-oriented grain or cube edge and (b) cube or Cubex oriented grain in a silicon iron sheet

To fabricate grain oriented electrical steel, basic steel needs to be vacuum degassed before adding carbon, silicon and manganese. The alloy is then cast into ingots which are in turn reduced to 220 mm thick slabs. These are then hot rolled (figure 2.3a), and further reduced to a thickness of 1.9 mm. As the strip cools manganese sulphide particles are formed. These particles act as a growth inhibitor for grains not of Goss texture. The next stage is to trim, descale, pickle and oil the steel ready for cold rolling (figure 2.3b) on the reversing mill. The steel is cold rolled several times and is reduced to a thickness of approximately 0.6 mm. The steel is then annealed at  $900\text{ }^{\circ}\text{C}$  to re-crystallise the material. This process is repeated and finally cold rolled twice to achieve the final thickness. By this time the grains are beginning to develop a Goss texture [2.10].

The steel is then decarburised to 0.03% carbon by annealing at  $830\text{ }^{\circ}\text{C}$  in a moist hydrogen atmosphere which prevents magnetic ageing. The strip is then cooled and covered in magnesia to prevent the steel sticking together when coiled. It is then coiled and stacked in furnaces to undergo annealing at  $1200\text{ }^{\circ}\text{C}$ , again in a hydrogen atmosphere. It is at this stage that the secondary re-crystallisation occurs. This causes the grains with Goss texture grow through the thickness of the sheet, and the magnesium sulphide stops the growth of the other grains. The magnesia which is used



to prevent the steel sticking together reacts with the steel to form a magnesium silicate layer known as 'glass film'. The strip is then washed and pickled and any excess magnesium oxide is removed. A magnesium phosphate coating is then added to the sheet and cured at 820 °C. This process is done while the sheet is under tension in order to flatten the sheet. Finally the sheet is punched and trimmed and annealed at 800 °C to relieve and residual stress [2.10].

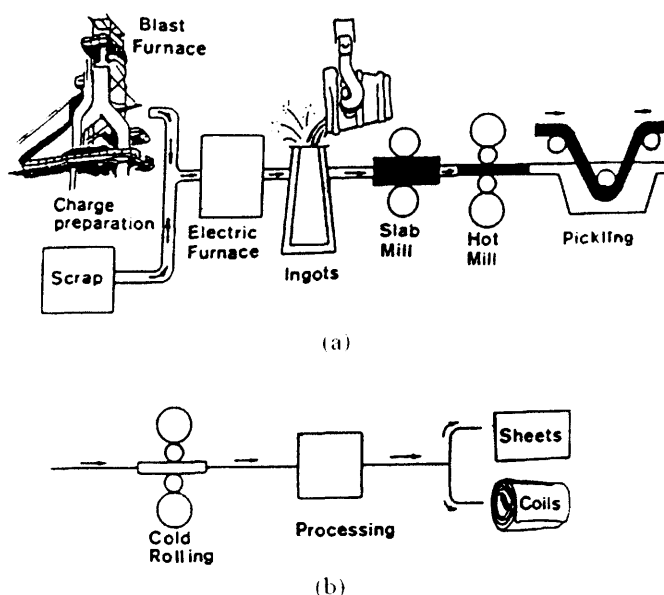


Figure 2.3. Basic operation of electrical steel production showing (a) hot rolling process (b) cold rolling process [2.10].

Grain oriented electrical steel can be further sub-categorised into conventional grain oriented (CGO) and high permeability grain oriented steels. CGO steel is processed under carefully controlled conditions to develop optimum magnetic characteristics in the rolling direction. CGO steel develops low core losses at high inductions when used as core material in designs with the flux path parallel to the rolling direction. In contrast to the conventional grain oriented process, high permeability steels are produced using a single stage rolling process. The grain size of high permeability materials is coarse in comparison to that of CGO material. The coarse grain size results in increased domain spacing with a consequential adverse effect upon eddy current losses.

Non oriented steel is very nearly isotropic (not isotropic but with small anisotropy), that is, both magnetic and mechanical properties are approximately the same in all directions in the plane of the sheet. It is thus suitable for rotating electrical machinery, but is also used for small transformers and reactors. The random grain texture is produced in the starting hot rolling stage and it is in the cold rolling process that controls the final losses and permeability.

## 2.5. Ferromagnetism

A most important and interesting magnetic state of materials are ferromagnetic. Ferromagnetic materials exhibit strong magnetic effects and ferromagnets are characterised by the fact that they can exhibit a net magnetisation without the presence of an applied magnetic field. Ferromagnetism occurs in the elements of iron, cobalt, nickel and their alloys [2.11].

Ultimately, ferromagnetism is caused by spinning electrons in the atoms of the material. Electrons produce a small magnetic field as they spin and orbit the nucleus of an atom. For many atoms, the combinations of electrons in their orbits cancel each other out. In ferromagnetic materials, however, the electron fields in the atoms do not cancel out, so they exhibit a long-range ordering phenomenon at the atomic level, which causes unpaired electron spins to line up parallel with each other in a region called a magnetic domain<sup>1</sup>. The domains are separated by domain walls, which are caused by local impurities, crystal dislocations, surface defects, etc. The domains tend to distribute themselves in order to minimise the energy so that the material does not produce any external field. In an un-magnetised material, it is expected that the magnetic moments of ferromagnetic domains are randomly aligned (figure 2.4a) so there is no overall magnetic effect. Magnetic effect starts to develop as a weak magnetic field is applied (figure 2.4b) and as the magnetic field increased, the domains align to point in the same direction (figure 2.4c), producing a strong overall magnetic effect. The presence of domains and the behaviour of domain walls when subjected to applied fields are of fundamental importance in understanding the magnetic properties of ferromagnetic materials [2.12].

---

<sup>1</sup> A magnetic domain is region in which the magnetic fields of atoms are grouped together and aligned.

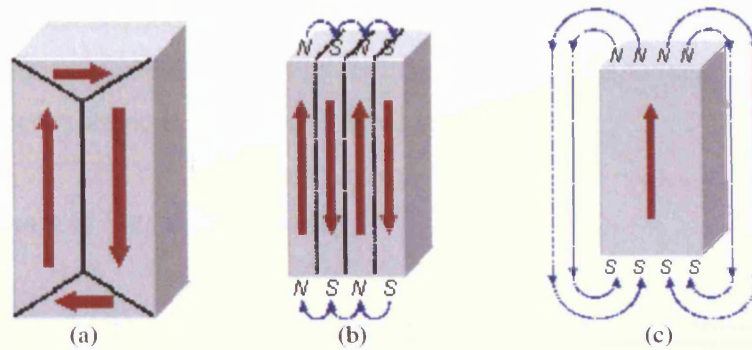


Figure 2.4 Orientation of ferromagnetic domains (a) at an un-magnetised state, (b) domains with weak magnetic field (c) aligned domain with strong magnetic field.

Ferromagnets will tend to stay magnetized to some extent after being subjected to an external magnetic field. This tendency to remember their magnetic history is called hysteresis. Hysteresis is explained later in section 2.6. However, ferromagnetic state of a material only applies below the Curie temperature. The Curie temperature marks a transition between order and disorder of the alignment of the atomic magnetic moments. All ferromagnets when heated to the Curie temperature, the material transforms to paramagnetic behaviour [2.2]. At this temperature, the permeability of the material drops suddenly and both coercivity and remanence becomes zero (see section 2.6). All ferromagnetic materials can be made paramagnetic at sufficiently high temperature. Curie temperatures of various magnetic materials are shown in table 2.3.

Table 2.3.

Curie temperatures of various materials [2.2].

<i>Material</i>	<i>Curie Temperature (°C)</i>
Iron	770
Nickel	358
Cobalt	1130
Gadolinium	20
Terfenol	380 – 430
Nd <sub>2</sub> Fe <sub>14</sub> B	312
Alnico	850
Hard ferrites	400 - 700

Another effect of ferromagnetic materials is magnetostriction. Ferromagnets will respond mechanically to an applied magnetic field by changing length slightly. This effect is called magnetostriction which is a major contributor to familiar transformer hums. Magnetostriction is explained in detail in Chapter 3.

## 2.6. Hysteresis in Magnetic Materials

Ferromagnets can retain a memory of an applied field once it is removed and this behavior is called hysteresis. A great deal of information can be learned about the magnetic properties of a material by studying its hysteresis loop. A hysteresis loop shows the relationship between the induced magnetic flux density,  $B$  and the magnetic field strength,  $H$ . Figure 2.5 shows a typical hysteresis loop of a ferromagnetic material which is often referred to as the  $B$ - $H$  loop. Initial stage of the hysteresis loop is point 1, where the ferromagnet is not magnetised having magnetic moments randomly aligned. Once magnetic field  $H$  is applied,  $B$  increases to the field direction. As  $H$  is increased to point 2, the curve flattens and  $B$  reaches saturation at which an additional increase in the  $H$  will produce very little increase in  $B$ . At this point, all magnetic moments within the material are aligned in the direction of the magnetic field. As  $H$  is reduced to zero,  $B$  does not drop to zero, but a level of residual flux density or remanence, occurs at point 3. At this point, some of the magnetic moments remain aligned but some have lost their alignment. As  $H$  is reversed, the curve moves to point 4, where the  $B$  has been reduced to zero. This point is called coercivity. The reversed  $H$  has flipped enough of the magnetic moments so that the net  $B$  within the material is zero. As  $H$  is increased further in the negative direction, material will again become magnetically saturated but in the opposite direction at point 5. Reducing the applied field  $H$  to zero again leaves a residual magnetisation with negative remanence at point 6. Increasing  $H$  back in the positive direction will return  $B$  to zero at point 7, positive coercivity. From this point,  $B$  takes a different path back to the saturation point and completes the loop.

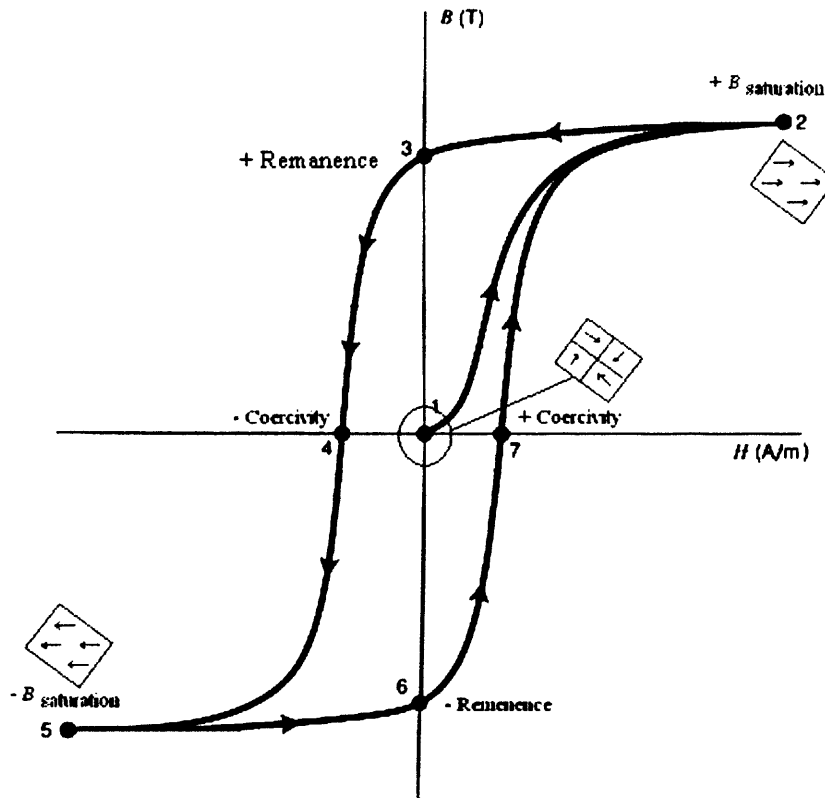


Figure 2.5 Typical hysteresis loop of a ferromagnetic material showing path 1 – 7 of  $B$  as  $H$  is varied.

The properties of a  $B$ - $H$  loop are used to characterise the ferromagnets. If the loop is narrow then such ferromagnets are called "soft magnetic materials" such as electrical steels and if the loop is wide then such ferromagnets are named as "hard magnetic materials" such as permanent magnetic as shown in figure 2.6.

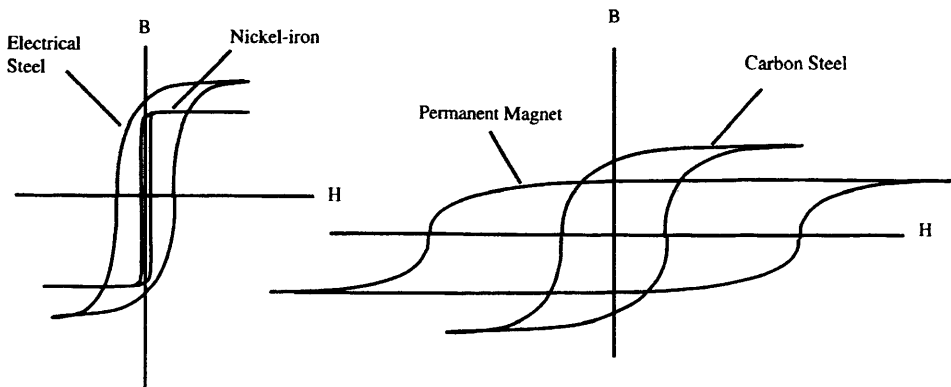


Figure 2.6 Typical hysteresis loops of range of ferromagnets [2.5].

## 2.7. Power Loss

The relationship of  $B$  and  $H$  in free space is linear and in the case of any other medium, the relationship between  $B$  and  $H$  becomes non-linear. Therefore, this non-linearity being observed in a material as a continuous series of hysteresis loops instead of having a straight line  $B$ - $H$  loops. The shapes of  $B$ - $H$  loops vary for different magnetic materials and magnetising conditions. The amount of energy lost when magnetising a magnetic material is related to the  $B$ - $H$  loop area. If the material is taken through a complete cycle the total energy,  $W$  needed is described by equation 2.9.

$$W = \int H \cdot dB \quad (2.9)$$

The unit of the power loss of a material is Watt per kilogram (W/kg) so therefore, the power loss is determined by multiplying the total energy,  $W$  by magnetising frequency  $f_{mag}$  over density  $d$ .

$$\text{Power loss} = \frac{f_{mag}}{d} \int \left( H \cdot \frac{dB}{dt} \right) dt \quad (2.10)$$

Equation 2.10 is known as the power loss for magnetic materials excited with alternating current. Other factors contributing to total power loss are eddy current losses and anomalous losses. From equation 2.10, it can be seen that power loss will increase with increasing magnetising frequencies.

**References**

- [2.1] R T Merrill, M W MscElhinny, P L MsFadden, 'The Magnetic Field of the Earth', Academic Press, 1996.
- [2.2] D Jiles, 'Introduction to Magnetism and Magnetic Materials' Chapman & Hall, 1991.
- [2.3] S Chikazumi, 'Physics of Magnetism', John Wiley & Sons, 1964.
- [2.4] H R Kirchmayr, 'Permanent Magnets and Hard Magnetic Materials', Journal of Physics D: Applied Physics, Vol 29, pages 2763 – 2778, 1996.
- [2.5] P Beckley, 'Electrical Steels', European Electrical Steels, Orb Works, 2000.
- [2.6] C G Page, 'Early Electrical Apparatus of Charles Grafton Page', American Journal of Science, Vol. XXXV, 1839.
- [2.7] W F Barrett, W Brown, R A Hadfield, 'On the Electrical Conductivity and Magnetic Permeability of Various Alloys of Iron', Science Transactions of Royal Dublin Society, page 67, 1900.
- [2.8] J Leicht, 'Magnetic Properties of Electrical Steels under Controlled Magnetisation Conditions', PhD Thesis, University of Wales, Cardiff, 2003.
- [2.9] H Haiji, K Okada, T Hiratani, M Abe, M Ninomiya, 'Magnetic Properties and Workability of 6.5% Si Steel Sheet', Journal of Magnetism and Magnetic Materials, Vol 160, pages 109 – 114, 1996.
- [2.10] K.H.J Buschow, 'Handbook of Magnetic Material, Elsevier Science B.V', pages 327-347, 1995.
- [2.11] R M Bozorth, 'Ferromagnetism', D Van Nostrand Company Inc., 1951.
- [2.12] F Brailsford, 'Physical Principles of Magnetism', D Van Nostrand Company Ltd, 1966.

## CHAPTER 3

### MAGNETOSTRICTION

---

#### 3.1. Introduction

A magnetic material is composed of domains whose magnetic moments are aligned in a random direction in a demagnetised state (see Chapter 2). When a magnetic field is applied, the magnetic moments tend to line up in the same direction as the applied field. This is accompanied by a change in dimensions of the magnetic material by few parts per million referred to as magnetostriction. In other words, a magnetostrictive material will change in dimension when it is subjected to a magnetic field. The first observation of the magnetostriction effects was in 1837 [3.1]. James Prescott Joule made the first quantitative measurements in 1842 in iron [3.2].

Magnetostriction can be divided into two types: spontaneous magnetostriction and field-induced magnetostriction [3.4]. Spontaneous magnetostriction can be described as ordering of magnetic moments into domains at the Curie temperature, whereas, field induced magnetostriction arises under applied magnetic field. Magnetostriction occurs in most ferromagnetic materials and there are various categories of magnetostrictive effects, which include Joule effect or also known as linear magnetostriction, volume magnetostriction and the  $\Delta E$  effect.

The Joule effect or linear magnetostriction involves changes in linear dimensions in the direction of the applied magnetic field and is the most commonly encountered magnetostrictive effect [3.5]. Volume magnetostriction occurs when volume of a sample changes when subjected to a magnetic field. Volume magnetostriction is sometimes referred to as the magnetovolume or Barret effect [3.6]. Typical values of volume and Joule magnetostriction in iron are 3 micro strain at 15.91 kA/m [3.2] and 0.1 micro strain at 15.91 kA/m [3.6] respectively. In this investigation only Joule magnetostriction is considered.



When a material is magnetised under applied stress, the change in length is altered from what would be expected normally simply under elastic strain because rotation of magnetic moments leads to additional strain which has the effect of altering the elastic modulus or Young's modulus. This phenomenon is referred to as the  $\Delta E$  effect because the effective Young's modulus is changed by the magnetic effects [3.7]. Young's modulus is the ratio of stress to applied strain and the  $\Delta E$  effect can be defined as  $\Delta E = (E_s - E_0)/E_0$  where  $E_0$  is Young's modulus at high field and  $E_s$  is the value of the modulus at saturation.

Magnetostriction can be either positive or negative depending on material properties and magnetization level. If a material such as grain-oriented silicon iron, has positive magnetostriction then its length in the field direction increases with increasing field strength. A material such as nickel iron is said to have negative magnetostriction since its length decreases with increasing magnetic field. However, in either case, for a positive magnetostriction material, the sample will increase in length as the flux increases to a maximum, the sample will then decrease in length as the flux returns to zero and then increase in length as the flux becomes negative and so on. It is therefore evident that the fundamental frequency of magnetostriction is twice that of the exciting waveform. Magnetostriction of a material is normally presented as the butterfly loop (figure 3.1a), which is extrapolated from a graph of magnetic flux density against magnetostriction.

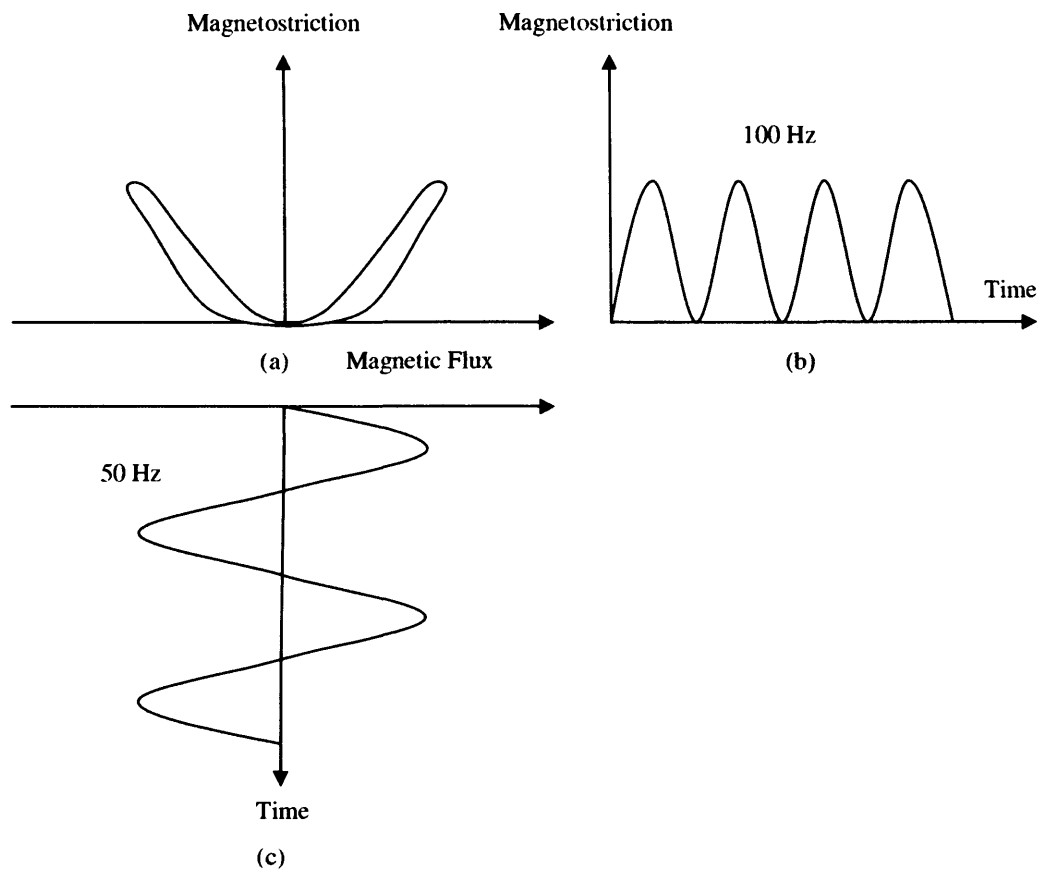


Figure 3.1. (a) Butterfly loop of a positive magnetostriction material extrapolated from the time variation of (b) magnetostriction and (c) magnetic flux density

### 3.2. Mechanism of Magnetostriction

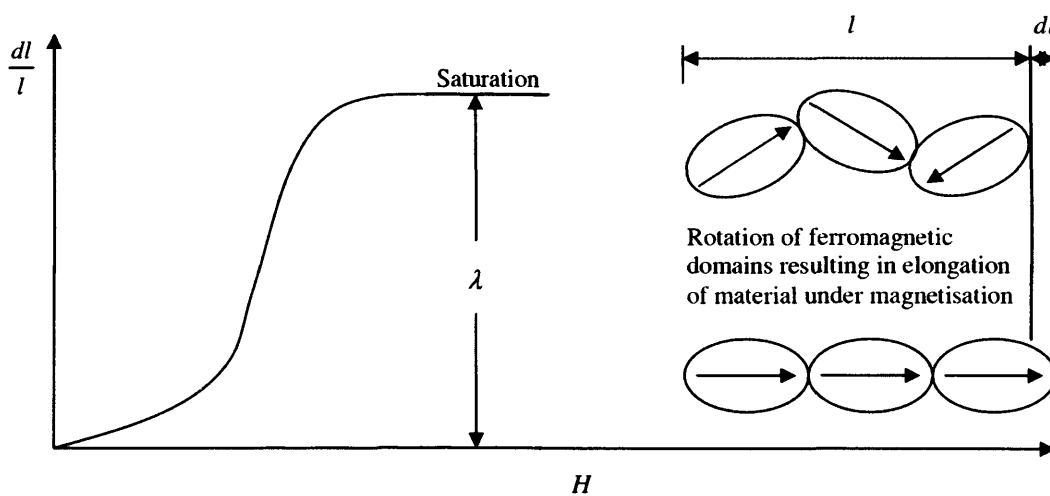


Figure 3.2. Magnetostriction change in a ferromagnetic material due to magnetisation.

The strain due to magnetostriction changes with increase of magnetic field,  $H$  (figure 3.2) and can be simply described as  $\lambda$ , the fractional change in length.

$$\lambda = \frac{dl}{l} \quad (3.1)$$

Magnetostriction originates in the interaction between the atomic magnetic moments [3.9]. This atomic moment interaction produce forces between atoms which tend to strain the lattice anisotropically.

If an isotropic sample with cubic crystals is heated to above Curie temperature and then cooled, the sample will spontaneously strain along the direction of domain magnetisation. The direction of spontaneous strain,  $e$  varies with and angle  $\theta$  from the direction of spontaneous magnetisation,  $M_s$  (Figure. 3.3).

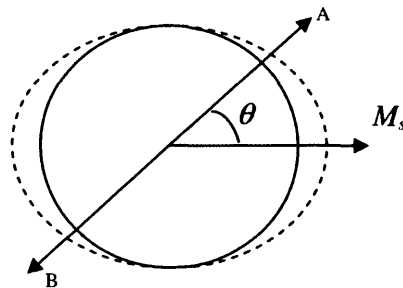


Figure 3.3. Elongation of a ferromagnetic sphere in a direction which makes an angle  $\theta$  with the axis AB of spontaneous strain,  $e$

Therefore, elongation of the diameter of the ferromagnetic sphere along  $M_s$ , is

$$\frac{dl}{l} = e \cos^2 \theta \quad (3.2)$$

However, the direction of spontaneous magnetisation varies from domain to domain throughout a ferromagnetic material having randomly oriented domains. Assuming that the spontaneous magnetostriction,  $\lambda_0$  is equal along any specific direction in the

sample, the average deformation throughout the sample can be obtained by integration.

$$\lambda_0 = \int_{-\pi/2}^{\pi/2} e \cos^2 \theta \sin \theta d\theta \quad (3.3)$$

$$= \frac{e}{3} \quad (3.4)$$

Silicon steel has a body centred cubic structure and as such a cubic anisotropy with easy axes along any of the cube edges termed [100] directions. The [110] directions are the diagonals across the cube face are harder to magnetise whilst the [111] directions are those that pass through the centre of the cube, are the hardest magnetisation direction. Consider a single Goss<sup>1</sup> oriented grain as shown in figure 3.4.  $\alpha_1$ ,  $\alpha_2$  and  $\alpha_3$  are the direction cosines of magnetisation,  $M$  and  $\beta_1$ ,  $\beta_2$  and  $\beta_3$  are the direction cosines of the strain measurement,  $R$  direction with respect to the cube edges.

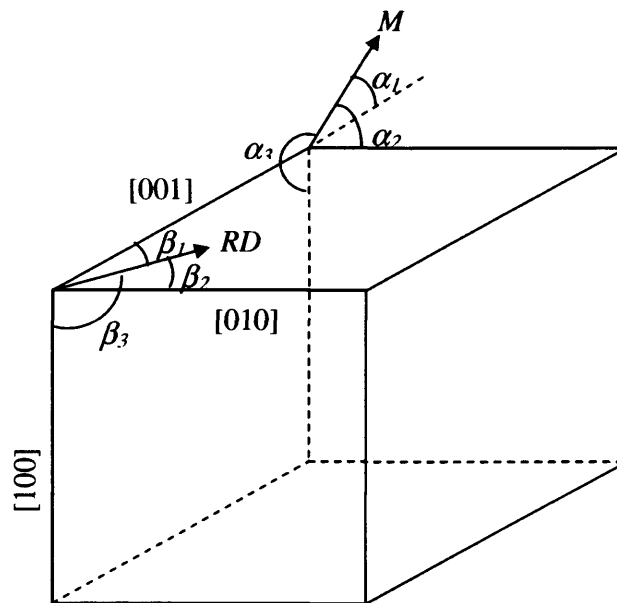


Figure 3.4. Direction cosines of a single Goss oriented grain; where  $RD$  is the rolling direction and  $M$  is direction of magnetisation

<sup>1</sup> The Goss material utilises the fact that the iron crystal has easy directions of magnetisation along its cube edges. See section 2.4.2.1.

The Becker-Doring equation [3.10] of magnetostriction for a cubic lattice structure can be written as:

$$\frac{dl}{l} = \frac{3}{2} \lambda_{100} (\alpha_1^2 \beta_1^2 + \alpha_2^2 \beta_2^2 + \alpha_3^2 \beta_3^2) + 3\lambda_{111} (\alpha_1 \alpha_2 \beta_1 \beta_2 + \alpha_2 \alpha_3 \beta_2 \beta_3 + \alpha_3 \alpha_1 \beta_3 \beta_1) \quad (3.5)$$

where  $\lambda_{100}$  and  $\lambda_{111}$  are the saturation magnetostriction constants in the [100] and [111] directions respectively.

Magnetostriction, although dimensionless, sometimes expressed in units of mm/mm. Since magnetostriction is a measure of very small strain, it is often expressed as ppm (parts per million),  $10^{-6}\epsilon$  or simply  $\mu\epsilon$ , microstrain. In this investigation, magnetostriction will be expressed in terms of  $\mu\epsilon$ .

### 3.3. Magnetostriction and Mechanical Resonance

Most machines and structures experience vibration to some degree, and resonance occurs as the tendency of a system to absorb more energy when the frequency of its oscillations matches the system's natural frequency of vibration [3.11]. Therefore, design of any engineering machines and structures generally requires consideration of their oscillatory behavior especially at resonant frequency.

In the case of this project, magnetically induced mechanical resonance in magnetic distribution or power transformer core materials are of primary interest since such transformers are a major cause of noise. Magnetostrictive vibration excites the magnetic core, and hence the winding, and the structure on which a distribution transformer is mounted. Grain-oriented steels are widely used for magnetic cores of transformers and such material produces magnetostrictive vibration under the action of a magnetic field. This magnetostrictive vibration causes acoustic noise in transformer cores, which is a known source of environmental noise. Extensive research has been carried out over many years to reduce the acoustic noise resulting from vibration of magnetic cores mainly caused by magnetostriction. However, not much research has been done to study the importance of mechanical resonance in the materials themselves.

When magnetostriction occurs due to magnetisation of a fixed end Epstein strip, a displacement is caused as a result. The displacement is the result of strain in the material itself. Hence, a displacement or vibration of a fixed end Epstein strip caused by magnetostriction, can be regarded as a forced oscillator system. Magnetostriction of the sample at any other magnetising frequency should produce similar strain whenever the sample properties are not affected by other factors such as temperature, stress etc. However, at resonant frequency of the sample, the amplitude of strain reaches a maximum. At this frequency, if damping is relatively small, or equal to zero (fig 3.5,  $\delta = 0$ ), the resonant frequency is approximately equal to natural frequency of the sample. Therefore, in the case of transformer laminations, this effect can be harmful because it produces excessive acoustic noise.

In this thesis, strain induced by magnetic field is described as magnetostriction. At the point of resonance, this strain is forced by magnetostriction to vibrate at higher amplitudes. For simplicity, all magnetostriction results presented in the thesis are labelled as 'peak-peak magnetostriction' for any magnetising frequency. However at the resonant point a rise in amplitude of magnetostriction is simply the vibration amplitude at a specific mechanical resonance frequency.

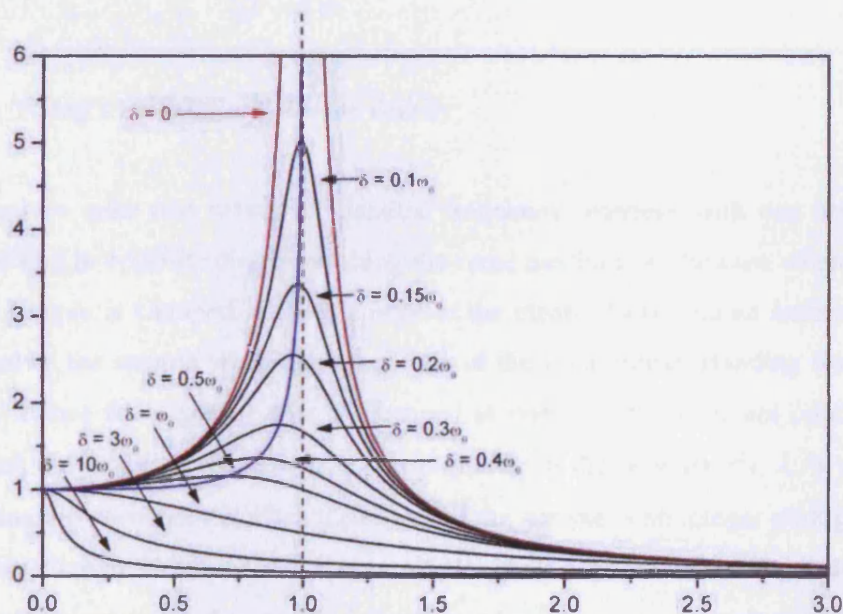


Figure 3.5 Increase of amplitude as damping,  $\delta$  decreases and frequency,  $\omega$  approaches resonance frequency,  $\omega_0$  [3.12]

### 3.3.1. Theoretical Approach to Mechanical Resonance in Epstein Strips

A wave can be described as a disturbance that travels through a medium from one particle to another creating a wave pattern. In a longitudinal wave the particle displacement is parallel to the direction of wave propagation i.e. the particles simply vibrate back and forth about their individual equilibrium positions. The frequency,  $f$  at which each individual particle vibrates is equal to the frequency at which the source vibrates. Similarly, the period of vibration is equal to the period of the source excitation. Distance of the maximum amplitude of the displacement travels is equal to one complete wavelength,  $\lambda_w$ . It is known that speed,  $v$  is equal to  $\frac{\text{distance}}{\text{time}}$  and

therefore it follows that the speed of a wave,  $v_w$  is also  $\frac{\text{wavelength}}{\text{period}}$ . As the period is the reciprocal of the frequency, and so the equation for  $v_w$  can be written as

$$v_w = \lambda_w f \quad (3.6)$$

In a longitudinal wave in a solid sample, the  $v_w$  takes the following form

$$v_w = \sqrt{\frac{E}{d}} \quad (3.7)$$

where  $E$  is Young's modulus and  $d$  is the density.

Standing waves arise two waves of identical frequency interfere with one another while travelling in opposite directions along the same medium. In the case where one end of the sample is clamped, there is a node at the clamped end and an antinode at the free end of the sample where the amplitude of the longitudinal standing wave is maximum. Hence for a sample that is clamped at one end, the resonant condition occurs when the length of the sample,  $l$  is one quarter of the wavelength,  $\lambda_w/4$  in the sample. Standing waves occur when the length of the sample is an integer multiple of a quarter wavelength. However with even multiples there is no vibration of the end, so harmonic vibrations occur for an odd integer number of quarter wavelengths  $\lambda_w/4$ . Hence combining equation 3.6 and 3.7, and expressing in terms of resonant frequency,  $f_n$  as a function of sample length,  $l$  gives

$$f_n = \frac{n}{4l} \sqrt{\frac{E}{d}} \quad (3.8)$$

where  $n$  is the  $n^{\text{th}}$  order harmonic and first harmonic resonance mode is when  $n = 1$ , third harmonic resonance mode is when  $n = 3$  etc.. As explained earlier in section 3.1, the magnetising waveform is half of the magnetostriction frequency. Therefore, the magnetising frequency at resonance,  $f_m$ , can be described as:

$$f_m = \frac{n}{8l} \sqrt{\frac{E}{d}} \quad (3.9)$$

The main objective of this research was to study magnetically induced strains and the associated vibrational modes of different electrical steel samples. These were in the form of Epstein frame strips that were magnetised at a single frequency but over a wide frequency range. The resonant frequency  $f_m$  was then obtained as the frequency at which a sharp rise in amplitude of peak-to-peak magnetically induced magnetostriction occurred, since at the point of resonance, displacement is at its maximum. The measured  $f_m$  values were then compared with the calculated values of  $f_m$  which were obtained using a simple model of the specimen which assumed uniform, homogeneous material of a given length, density and elastic modulus using (3.9).

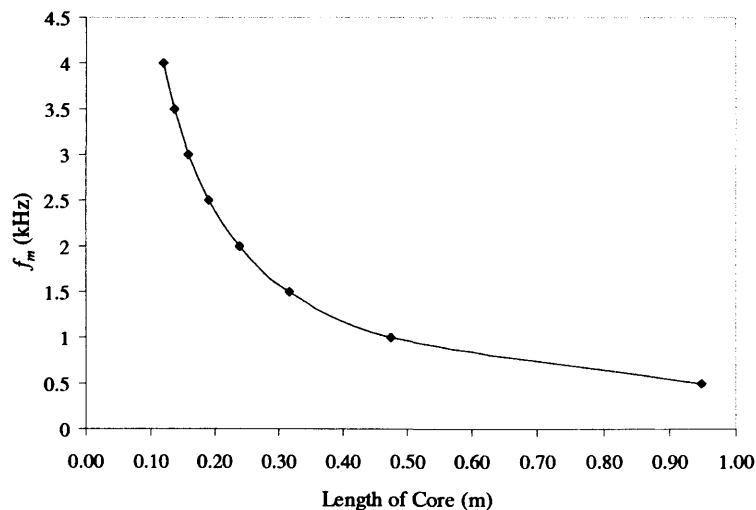


Figure 3.6.  $f_m$  as a function of core length,  $l$  for a lamination in a single-phase transformer core assembled from 3 % Si-Fe grain-oriented cut at  $0^\circ$  to its rolling direction.



Figure 3.6. shows calculated  $f_m$  in the fundamental mode of vibration with corresponding core length using (3.9) for 3 % Si-Fe grain-oriented steel cut at  $0^\circ$  to the rolling direction. This suggests that a lamination in a transformer core having length of approximately 0.3 m would resonate under 1.5 kHz magnetisation. In a transformer core of 0.3 m length that is not magnetised at 1.5 kHz, harmonics of induced flux can coincide with the resonance frequency. Such resonance may produce excessive core vibration and noise as well as possible failure in transformer cores. Hence, it is important to identify resonance and its harmonics of laminations in order to avoid this situation particularly in high frequency cores. The noise problem is becoming of increasing industrial importance particularly in equipment subjected to high frequency and harmonic magnetisation.

#### ***3.4. Previous Research on Magnetostriction and Resonance***

Magnetostriction is a known major source of acoustic noise in transformer cores. The acoustic noise becomes a major concern for transformers such as distribution transformer as they are placed closer to the populace. Although grain-oriented silicon iron is used as transformer core material because of its magnetic properties such as high permeability and low power loss, magnetostriction of the material produces noise in the core. Extensive work have been carried out over the past 50 years to reduce this unwanted noise but only a few have referred to resonance of such transformer core materials. However, mechanical resonance have been reported as ‘unusual high-frequency behaviour’ [3.13] for various magnetostrictive materials in relation to energy loss and mostly magnetomechanical coupling.

In 1973, Moses and Pegler [3.14] demonstrated the possibility of producing improved transformers by bonding stacks of silicon iron laminations together with flexible adhesive thereby reducing magnetostrictive vibrations of the laminations. They showed that the pattern of vibration of certain harmonics of the core were reduced by a factor of between five and ten, which was accompanied by a reduction in the noise output at the same frequencies. The overall reduction in total noise output was only about 3 dBA below that of a bolted core (see section 5.8.1. for A-weighted noise). It was assumed that other factors such as resonance of external parts of yoke clamps, tie rods etc were contributing to noise in transformer cores.

Thottuvelil et al investigated the behaviour of two types of amorphous metallic-alloy tape-wound magnetic cores excited under sine wave voltage conditions in the 1 kHz to 100 kHz frequency range [3.13]. Unusual behaviour of both energy loss (figure 3.7) and core characteristic loops of flux density was observed (figure 3.8). The unexpected results were due to mechanical resonances of the toroidal core structures. A model was used to calculate resonant frequencies of the cores which led to good agreement with experimental results for fundamental mode of resonance using the following equation [3.13]:

$$f = \frac{1}{2\pi r} \sqrt{\frac{E}{d}} \quad (3.10)$$

where the radius  $r$ , of the mean circumference of the ring is obtained from the mean magnetic path length  $l_m$  as  $r = l_m/2\pi$ . It is said in [3.13] that this mechanical vibration under ac excitation at twice the frequency of the exciting voltage is in contrast to the magnetostrictively induced mechanical vibrations of cores under dc biased small signal excitation.

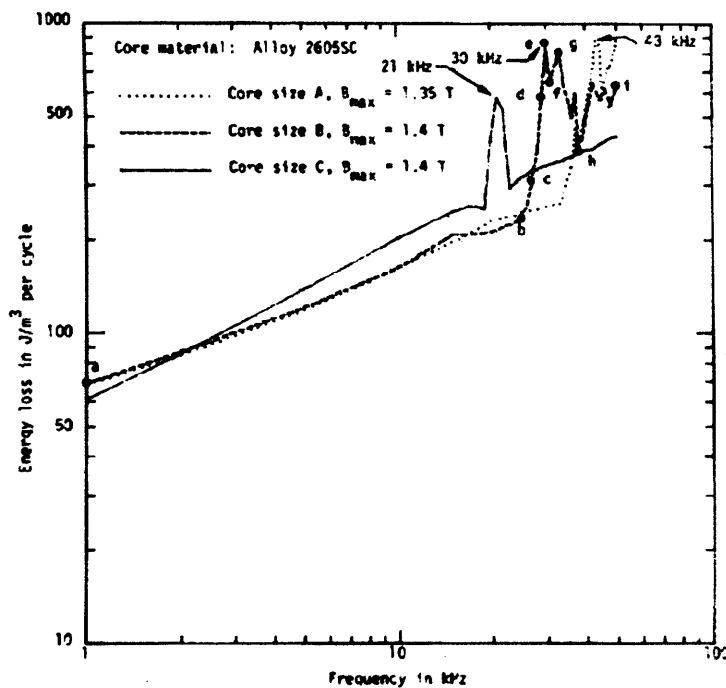


Figure 3.7. Energy loss per unit volume of Metglas<sup>1</sup> 2605SC at various frequencies under sine wave voltage excitation of  $B_{max} = 1.4$  T [3.13].

<sup>1</sup> Metglas is a producer of amorphous metal ribbons. Metglas © Inc. is a wholly-owned subsidiary of Hitachi Metals America Ltd.

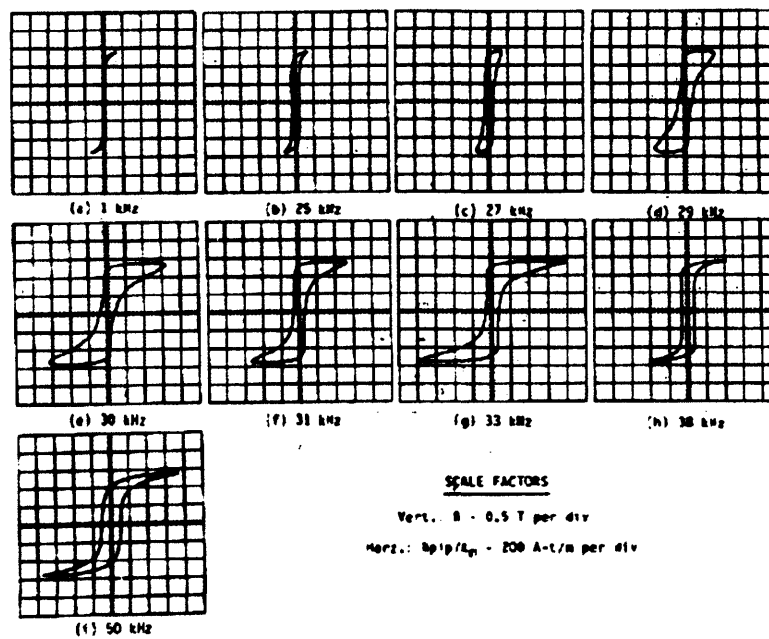


Figure 3.8. Characteristic loops of Metglas 2605SC at various frequencies under sine wave voltage excitation of  $B_{max} = 1.4$  T [3.13].

In 1989, H C Kim and C G Kim [3.15] calculated the change in elastic strain due to the nucleation and annihilation of  $180^\circ$  domain wall using magneto-elastic coupling of ferromagnetic materials, and investigated the dependence of the magneto-acoustic emission on the magnetising frequency,  $f$  and the micro tensile stress,  $\sigma$ . Measurements were performed on a (110)[001] oriented 3% silicon iron single crystal of dimensions  $29.5 \text{ mm} \times 125 \text{ mm} \times 0.8 \text{ mm}$ . the sample was clamped at both ends and magneto-acoustic emission was measured using a resonant acoustic emission transducer. The output signal of the transducer is said to be affected by the resonance mode of the plate at length  $2L$  (3.9) [3.15].

$$f_k = \frac{2.98hk^2}{\pi L^2} \sqrt{\left(\frac{E}{\rho(1-\nu^2)}\right)} \quad (3.9)$$

Where  $k$  is the order of the mode,  $h$  is the plate thickness,  $\rho$  is the material density,  $E$  is Young's modulus and  $\nu$  is the Poisson's ratio.

Kelley [3.16] stated that if a mechanical resonant frequency corresponds to a power system harmonic, the acoustic noise emission of a transformer core at that frequency

may be amplified. Transformer flux is not always sinusoidal and can contain harmonic fluxes in addition to the fundamental frequency flux. However, the effect is said to be minimised in practice. A theoretical equation to calculate the mechanical resonant frequency was not given but values of resonant frequency in the fundamental extensional mode of vibration was tabulated according to core sizes A, B, C and D (D being the largest dimension) used in the investigation (table 3.1). The resonant frequency of core size D was 24.7 kHz and is was found to be near enough to the 20 kHz excitation frequency. Thus, the core size D was found to be more efficient emitter of 20 kHz noise than any of the smaller size cores.

Table 3.1.  
Mechanical resonant frequency of the four core sizes as in [3.16]

Core sizes	Resonant frequency in the fundamental mode of vibration (kHz)
A	98.6
B	65.6
C	49.2
D	24.7

Wakiwaka et al [3.17] have measured the mechanical vibrations of samples indirectly through the determination of impedance characteristics. They have described the behaviour of an acoustic vibration element in which the measurements were made using a laser Doppler vibrometer but their analysis was based on an analogy with the vibration of a mass on a spring (figure 3.9) which is not appropriate for this situation. Analysis in terms of magnetostrictively induced sound waves, in the material is the correct procedure to use where the whole specimen is vibrating and the mass is distributed. The mechanical resonance frequency in [3.17] was expressed as:

$$f_0 = \frac{1}{2\pi} \sqrt{\frac{k}{m}} \quad (3.11)$$

Where  $k$  is the spring stiffness matrix and  $m$  is the mass.

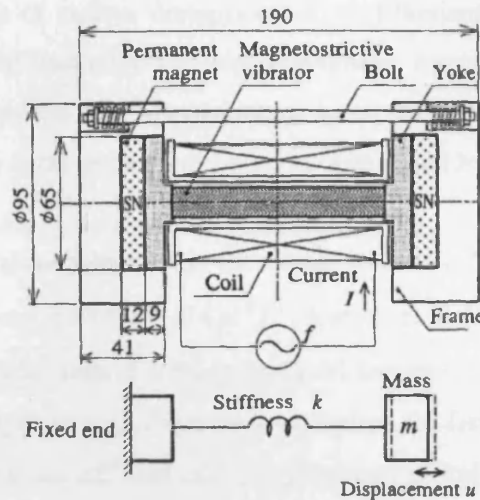


Figure 3.9. Structure and vibration system used in [3.17]

Takada [3.18] investigated mechanical resonance in both strip and toroidal non-oriented electrical iron samples using semiconductor strain gauges. Variation of magnetostriction with magnetising frequency was observed with resonance points occurring at several frequencies (Figure 3.10).

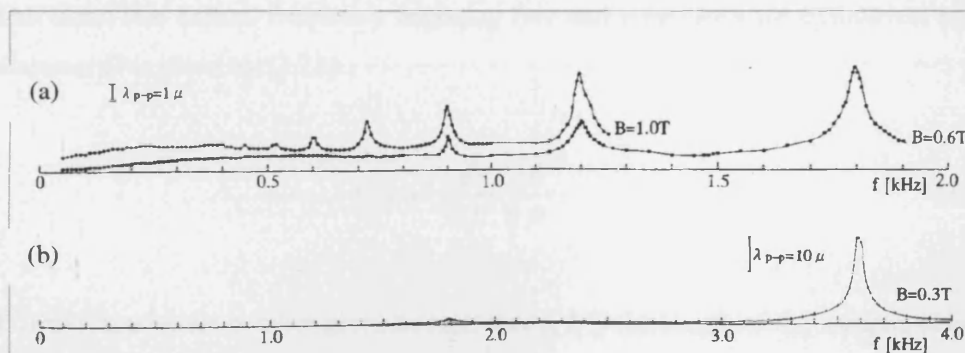


Figure 3.10. Dependence of peak to peak magnetostriction of non-oriented strip sample on magnetising frequency at (a)  $B = 1.0$  T and  $0.6$  T (b)  $B = 0.3$  T [3.18]

In 1996, Mogi et al [3.19] developed a system to measure ac magnetostriction of high permeability grain-oriented steel from 20 Hz to 100 kHz. Here, resonance frequency was detected at 5, 10 and 15 kHz. Although no comparisons with theoretical predictions were made, it was suggested that emerging new materials should avoid such resonance hence lower transformer noise. Ozturk et al [3.20] also suggested that electromagnetic forces can cause large displacements and loud noise when the forcing frequencies are equal or close to the natural frequency of the stator core laminations.

Mechanical resonance of various dimensions of steel laminations were obtained and Ozturk et al suggested that effects of electromagnetic forces on the resonance of a stator core can be avoided with improvements in electronics, changes in lamination structure and changes in the geometry of core thickness and length.

Chicharro [3.21] has demonstrated that the elastic modulus,  $E$  can be calculated from the resonance frequency,  $f$  where  $E = 4\rho l^2 f^2$ . Karimi et al [3.22] have looked at the magnetomechanical behaviour of ternary Fe-Cr-Al and Fe-CrMo alloy films between  $f = 0.2$  and 2 kHz. Bayon et al [3.23] have investigated the field dependence of elastic modulus by measuring the  $\Delta E^1$  and  $\Delta G^2$  in cylindrical nickel bars from the torsional and transverse natural frequencies. The torsional natural frequency of vibration is given as a function of shear modulus,  $G$  [3.23]:

$$f_{\tau} = \frac{n}{2L} \sqrt{\frac{G}{\rho}} \quad (3.12)$$

The transverse natural frequency imposing free end conditions for cylindrical bar of diameter  $D$  is given by [3.23]:

$$f_t = n^2 \frac{\pi D}{32L^2} \sqrt{\frac{E}{\rho}} \quad (3.13)$$

Where  $n$  is a whole number given to each mode,  $L$  is the length of the sample,  $G$  is the shear modulus,  $E$  is the Young's modulus of the sample and  $\rho$  is the density. Recently, Chicharro, Bayon and Salazar [3.24] measured damping in nickel rods and wires by using optical heterodyne interferometry as a detector of longitudinal vibration of the samples. The attenuation constant is determined by examining free vibration of the sample and damping is indirectly measured from the sharpness of its resonance curve using the following equation [3.24] for resonance frequency of damped longitudinal vibrations.

<sup>1</sup> The variation of Young's modulus  $E$  of a material

<sup>2</sup> The variation shear modulus  $G$  of a material

$$f_n = \sqrt{\frac{n^2}{4l^2} \left( \frac{E_H}{\rho} \right) - \frac{\gamma^2}{16\pi^2}} \quad (3.14)$$

where  $n$  is the number for each mode,  $E_H$  is the Young's modulus for magnetic field  $H$ ,  $l$  is the length of sample,  $\rho$  is the density and  $\gamma$  is the attenuation constant.

This section of some previous research on magnetostriction and mechanical resonance shows that not much research has been carried out on magnetisation induced mechanical resonance of grain oriented silicon iron strips for transformer core applications.

### 3.5. Measurement of Magnetostriction

A transducer is a device which transforms one type of energy into another. A specific class of transducers are devices which translate an input of mechanical energy into equivalent electrical signals for measuring and/or controlling the input phenomena. Transducers are designed to operate based on many different principles - resistive, inductive, capacitive, piezoelectric, etc. Certain forms of transducers have their own family names which usually derive from the physical phenomena they measure such as accelerometers, extensometers and vibrometers [3.25].

Displacement caused by magnetostriction can be measured using a transducer that produces a signal proportional to the displacement,  $\Delta l$  of the vibrating end of a magnetised strip, or by determining the velocity of vibration,  $v$  or acceleration,  $a$  of the strip and then performing a single or double integration on the measured signal (3.15 and 3.16).

$$v = \frac{d(\Delta l)}{dt} \quad \therefore \Delta l = \int v dt \quad (3.15)$$

$$a = \frac{dv}{dt} \quad \therefore \Delta l = \iint a dt \quad (3.16)$$

In this project, displacement due to magnetostriction is measured under ac magnetisation. Methods of measuring displacement such as resistance strain gauges, semiconductor strain gauges, accelerometers and various optical techniques discussed

in the following sections could be applied. Advantages and disadvantages of the techniques are compared.

The desired transducer should also be unaffected by a magnetic field, since the measurement ends of the sample are in close proximity to the magnetisation windings and yoke. Minimum specifications of the required displacement measuring device for this investigation are:

*1. Resolution*

Magnetostriction varies with samples composition. In this investigation it was anticipated that it might vary between 0.05  $\mu\epsilon$  and 100  $\mu\epsilon$ . Therefore, a transducer of at least 0.01  $\mu\epsilon$  resolution is desired.

*2. Frequency range*

Magnetising frequency is an important factor to consider when choosing a transducer to measure magnetostriction. The calculated 3<sup>rd</sup> harmonic of resonance frequency of an Epstein sized [3.26] grain-oriented 3% silicon iron sample cut at 0° to rolling direction is 8 kHz (4 kHz magnetising frequency). Therefore, by requiring at least 10 kHz magnetisation frequency, the desired transducer must be able to measure displacements at 20 kHz.

*3. Sample Rate*

When plotting and reading a voltage waveform, it is preferable to have as many number of data points per magnetising cycle as possible so the waveform, including harmonics can be accurately analysed. It is desired to have at least 100 points for a 20 kHz cycle. Hence, a sampling rate of 2 mega samples per second is required in a transducer to measure magnetostriction for this project.

*4. Temperature range*

Heating of a sample can be a significant factor when making measurements at high frequencies. The maximum temperature of a sample was measured to be about 70 °C at 4 kHz magnetisation. Therefore, the chosen transducer should be able to withstand temperatures up to 100 °C.



The samples to be tested will be fixed at one end and displacement at the free end will be measured. A suitable measurement system was to be chosen for this project. To comply with the minimum specifications mentioned above.

### 3.5.1. Resistance and Semiconductor Strain Gauges

Strain gauge based transducers have been an important engineering tool since shortly after the invention of the first strain gauge in late 1930s [3.25]. Resistance strain gauges are simple yet highly effective devices for converting material surface strain into a measurable electrical output. The gauges themselves are sometimes metal foil resistors fitted to an insulation backing (Figure 3.11a), which is bonded to the surface of the material under test. Resistance strain gauges have gauge factor<sup>1</sup> of 2 to 6 and they have been widely used to measure magnetostriction [3.27]. Resistance strain gauges have fatigue life cycle<sup>2</sup> (100-10<sup>6</sup> cycles of strain) and most strain gauge materials are also sensitive to temperature variations and differences in expansion coefficients between the gauge and base materials may cause dimensional changes in the gauge element. For high frequency displacement measurement using resistance strain gauges, fatigue life cycle and operating temperature could be a disadvantage.

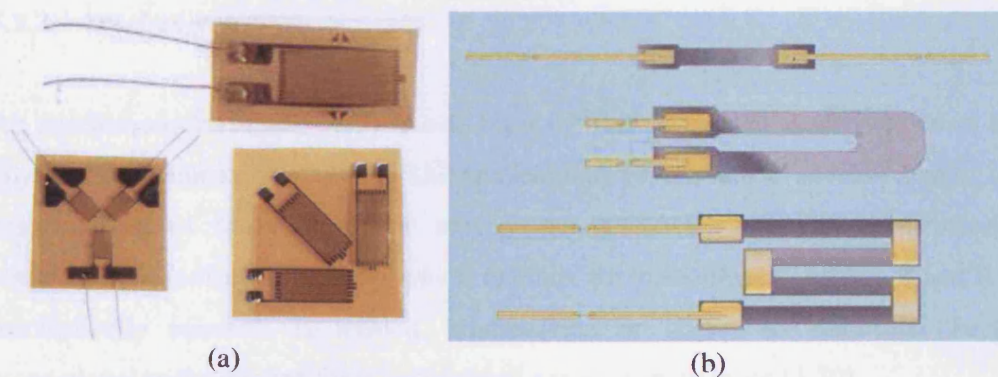


Figure 3.11. Different types of (a) resistance strain gauges [3.27] and (b) semiconductor strain gauges [3.28]

<sup>1</sup> The gauge factor is the measure of strain sensitivity or output produced by the strain sensor. Gauge factor is a dimensionless quantity and is determined through calibration of the specific gauge type and is the ratio between  $\Delta R/R_0$  and strain, where  $R_0$  is the initial resistance of the gauge.

<sup>2</sup> Number of repeated cycles that gauge can endure; when strain is repeatedly applied to the gauge, it causes increased resistance under zero strain, peeling-off of the gauge or disconnection, resulting in failure

A spin-off from semiconductor technology, semiconductor strain gauges are produced in the form of gauge patterns deposited on to suitable insulating substrates, and as small bars or ribbons of doped silicon (Figure 3.11b), equipped with fine lead wires and bonding them to the strained surface requires great care. In the case of semiconductor strain gauges, the resistivity also changes with strain, along with the physical dimensions as in resistance gauges. Although, the semiconductor materials have gauge factors more than 50 times, sensitivity more than a 100 times, and better fatigue life cycle than that of the resistance strain gauges, such gauges exhibit substantial nonlinearity and greater sensitivity to temperature change [3.27]. The gauge factor is not always constant as the strain takes place (the gauge factor may be -150 with no strain, but drop nonlinearly to -50 at 5000 mm/m) [3.29]. Once again, due to operating temperature limitation, semiconductor strain gauges have a disadvantage for high frequency displacement measurements as desired for this investigation.

Although both resistance and semiconductor gauges are relatively low in cost, small size and very low mass, for the disadvantages mentioned above, both gauges are not favourable for high frequency magnetostriction measurement related to this investigation.

### 3.5.2. Accelerometers

An accelerometer (Figure 3.12) is one form of transducer that is derived from the physical phenomena it measures i.e. acceleration. Piezoelectric accelerometers are universally used for vibration or motion measurements. Such an accelerometer contains a piezoelectric material which exhibits the piezoelectric effect. When it is mechanically stressed, in tension, compression or shear, an electrical charge, proportional to the applied force is generated across its pole faces [3.30].

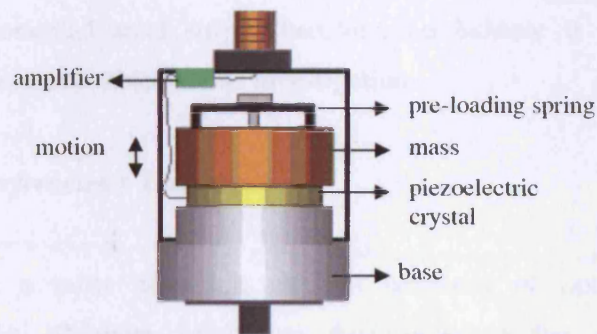


Figure 3.12. Typical piezoelectric accelerometer

When selecting an accelerometer, it is important to determine if it is designed for measuring motion or vibration. In vibration measurement, the vibratory responses of the object under test are of concern. While in the motion measurement, speed or the displacement of the test sample is of interest. When using an accelerometer to measure displacement accurately, the measured acceleration data must not contain any zero offset error. A small zero offset in the acceleration output can lead to gross displacement errors after numerical integration.

Accelerometers are self generating and require no power supply. Accelerometers can tolerate operating temperatures up to 250 °C and for temperatures up to 400 °C, accelerometers with a special piezoelectric ceramic can be used. Accelerometers also have a robust structure with no moving parts.

The resonance frequency of the accelerometer should be sufficiently high that it stays above the high frequency displacement signals of the sample itself [3.30]. Also, high resonance accelerometer designs usually are associated with very low output sensitivity which is a given constraint in any given spring-mass transducer design. The mass of the accelerometer is also an important factor to consider when measuring on light and thin grain-oriented samples. The additional mass of the accelerometer can significantly alter the vibration levels and frequencies at the measuring point.

Although accelerometers have advantages to measure displacement due to magnetostriction, there are factors to consider such as the additional mass and low output sensitivity before high frequency magnetostriction measurements can be taken

on a thin grain-oriented steel strip. Therefore, on balance it is concluded that accelerometers are not suitable for this investigation.

### 3.5.3. Laser Interferometer Techniques

Interferometry is a most important element or basis of optical measurement techniques. Albert Abraham Michelson first invented the setup for optical interferometry technique [3.31]. Interferometry is simply combining two or more waves, which are said to interfere with each other. Therefore, an interferometer works on the principle that two waves that coincide with the same phase ( $0^\circ$  phase) will amplify each other while two waves that have opposite phases ( $180^\circ$  phase) will cancel each other out.

Figure 3.13 shows the Michelson interferometer setup where there are two paths from the laser source to the detector. One reflects off the beam splitter, goes to mirror 1 and then reflects back, goes through the beam splitter, to the detector. The other first goes through the beam splitter, to mirror 2, reflects back to the beam splitter, then reflects from the beam splitter into the detector. The detector takes the difference between the two paths and interprets into measured data such as displacement.

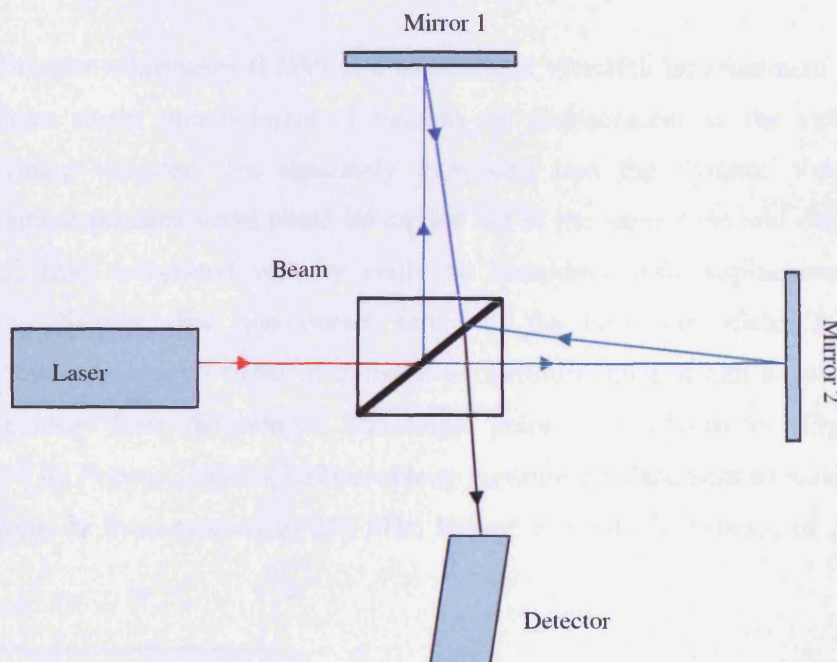


Figure 3.13. Example of a Michelson interferometer

Optical methods such as laser interferometers are non-contact vibration or displacement measurement techniques which permit measurement of hot, soft, rough, wet surfaces etc. avoiding the loading effects of contact or attached transducers. Therefore, surface texture and temperature of the measured object is not a concern. It is also an added advantage by being not susceptible to magnetic fields. Most lasers used in optical methods are eye-safe class 2 laser instruments that use a low power Helium-Neon<sup>1</sup> laser can operate over distances of hundreds of meters [3.31]. Laser methods measures displacement on the nano meter scale, which is needed in the case of materials with low magnetostriction compared to strain gauges and accelerometers that only measures displacement down to micro meter scale.

### ***3.5.3.1. Laser Vibrometer***

Laser Doppler vibrometers are industrially engineered modernised version of an interferometer (Figure 3.13). The basic principle behind the laser Doppler vibrometer is the Doppler effect. A coherent laser beam is projected on to the surface of a sample. Light scattered back from the surface is shifted in frequency by an amount proportional to the velocity of the surface, which is can be defined as the Doppler effect.

Laser Doppler vibrometry (LDV) is a non-contact vibration measurement technique that allows direct measurement of velocity or displacement as the velocity and displacement decoders are separately integrated into the system. Velocity and displacement measurements could be carried out at the same time and displacement obtained from integrated velocity could be compared with displacement that is measured directly. The non-contact nature of the laser vibrometer is also not susceptible to magnetic fields or extreme temperature since it can be placed some distance away from the sample. The single point laser vibrometer (Figure 3.14) produced by Polytec GmbH [3.32] is able to measure displacement as small as 2 nm at frequencies from near dc to 250 kHz, having a stand-off distance of  $\geq 230$  mm.

---

<sup>1</sup> Helium-Neon laser is a type of small laser with a mixture of helium and neon gasses approximately in the ratio of 5:1. The laser operation wavelength is usually 632.8 nm having optical output power ranging from 1 mW to 100 mW.

Laser beam spot diameter is 25  $\mu\text{m}$  and therefore, minimum thickness of the measured object could be as low as 25  $\mu\text{m}$ .

Other laser techniques include laser displacement meter, laser velocimeter, scanning vibrometer etc. All these laser techniques including the laser vibrometer are now commercially available as a single compact unit which requires little operator skill. The displacement and velocity measurement is fundamentally non-destructive, easily aligned and minimizes the need for time-consuming accelerometer mounting, strain gauge wiring, and signal conditioning. Whereas traditionally, all laser techniques have complex optics and requires high operating skill for time consuming process of developing the measurement setup as well as conducting the experiment itself. However, laser vibrometers are sensitive to external vibrations and can be high in cost (tens of thousands of pounds). Sensitivity to external vibrations can be resolved by having the laser head and measured sample placed on vibration isolated table or in an acoustic room. Cost of the system becomes a major disadvantage where potential cost of the system becomes even higher if the laser source has to be replaced, in which case will be followed by re-calibration of the entire laser system.



Figure 3.14. Single point laser vibrometer (Polytec GmbH) for measuring displacement caused by magnetostriction

Magnetostriction measurement method using strain gauges is used from the point of cost effectiveness while, compact laser methods open the possibility of measuring magnetostriction in instances where it is not practical to attach strain gauges or simple

because of its sensitivity, accuracy, mobility and ease of use. Although optical techniques have greater advantages compared to traditional strain gauges or accelerometers and becoming more favourable in measuring magnetostriction, one must consider the cost and specifications that will suit individual applications.

In conclusion, for the high frequency displacement measurement on the micro meter scale and funds available for this project, the single point laser vibrometer, SPLV from Polytec GmbH (Figure 3.14) appeared most favourable as a displacement measurement system for this project.

#### 3.5.4. Previous Research on Measurement of Magnetostriction – Concentrating on Optical Methods

Various techniques have been used to measure magnetostrictive displacement. Methods such as resistance strain gauges, semiconductor strain gauges, accelerometers, laser velocimeters and laser vibrometers have been used to measure

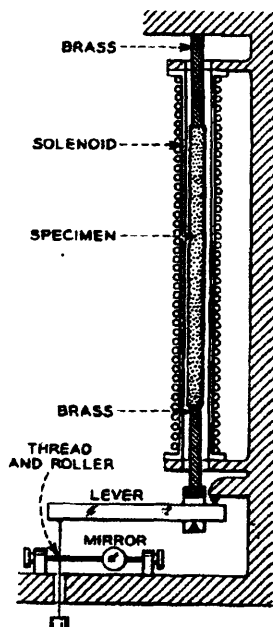


Figure 3.15. One of the older methods of magnetostriction measurement system [3.33].

displacement at specific magnetizing frequencies. Previous researchers have investigated magnetostriction at magnetizing frequencies of 0.05 kHz – 2 kHz. However at the higher magnetizing frequencies within this range, typically at 1 kHz and above, optical methods such as the laser displacement meter and the laser vibrometer have become more widely used.

One of the older methods of measuring magnetostriction was referenced by Bozorth [3.33]. Figure 3.15 shows the method of measuring magnetostriction that is dependent on the use of mechanical and optical levers. The change in length of the specimen moves the lever arm which is attached to a wire that turns a carefully constructed roller on which the mirror is mounted. This turn of the mirror is

observed with a telescope or light and expansion or contraction of the specimen can be obtained from a scale.

The strain gauge method was first introduced by Goldman in 1947 [3.34]. With this method, an experimental and theoretical study of the relationship between saturation magnetostriction and the order-disorder transformation in an iron-cobalt alloy has been carried out in 1949. Goldman et al claimed a strain sensitivity,  $\Delta l/l$  per mm equals to  $2.15 \times 10^{-8}$  can be achieved with good accuracy and reproducibility with the magnetostriction measurement system shown in figure 3.16 [3.34].

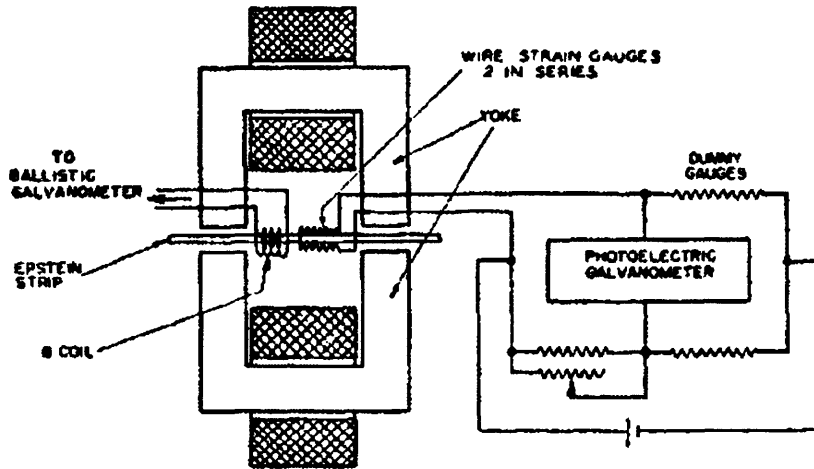


Figure 3.16. Circuit diagram of magnetostriction measurement system used in [3.33]

Since 1947, measurement of magnetostriction using strain gauges significantly improved. Greenough et al [3.35] investigated the temperature dependence of gauge factor and magnetoresistance for two types of foil strain gauges.

Little [3.36] and Alexander [3.37] used the free end surface of a standard Epstein test specimen and a fixed capacitor plate to produce a change of capacitance in the tuned circuit of an oscillator. The change of frequency with reference to a fixed frequency oscillator produced a voltage signal proportional to the change in length of the sample. An essentially similar method has been used by Whitaker in 1960 [3.38] and George et al [3.39] in 1962. In the latter experiment, the magnetising field is produced by a large coil and the current is supplied from either an accumulator or a power oscillator. Flux density along the grain-oriented silicon iron strip was not uniform due to the open path of their magnetising circuit. However, this was reported to have a negligible effect on the magnetostrictive measurements. The authors managed to achieve a sensitivity of  $\Delta l/l \cong 4 \times 10^{-6}$  for 1 cm movement on the oscillograph using this measurement system.



Other methods such as piezoelectric transducers were used to measure magnetostriction by Mapps et al [3.40] in 1982. Magnetostriction of a half Epstein sample of grain oriented silicon iron was measured by a refined ‘double transducer’ technique where two piezoelectric stereo transducers were placed on the surface of the sample (figure 3.17). Although the sensitivity of the system was not specified, it is said that the transducer output was carefully designed to detect low magnitude magnetostriction harmonics ( $\sim 1 \times 10^{-6}$  m/m).

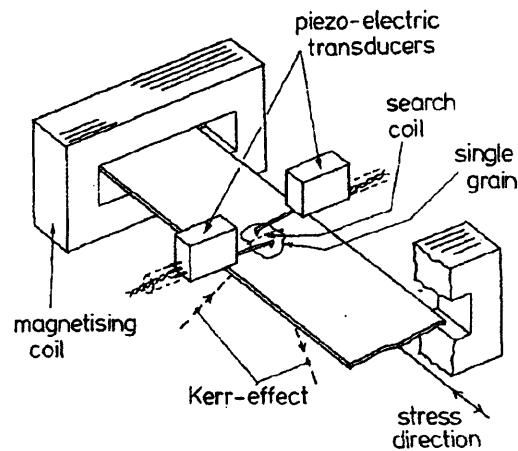


Figure 3.17. Schematic diagram of the experimental arrangements for measurement of magnetostriction harmonics [3.40]

Squire and Gibbs [3.41] described a method employing a fibre-optic dilatometer (Figure 3.18) for measuring magnetostriction in 1986. The changes in sample length vary the optical power transmitted across a narrow gap in the optical fibre. It is claimed that the method is suitable for making routine measurements on samples in the form of thin ribbons, as only minimal mechanical load is imposed on the sample and it is not necessary to attach any ancillary load components to the sample. Results (Figure 3.19) indicate sensitivity of the fibre-optic dilatometer in the order of  $10^{-7}$  for magnetostriction measurements as a function of applied field and  $10^{-8}$  for measurements of saturation magnetostriction.

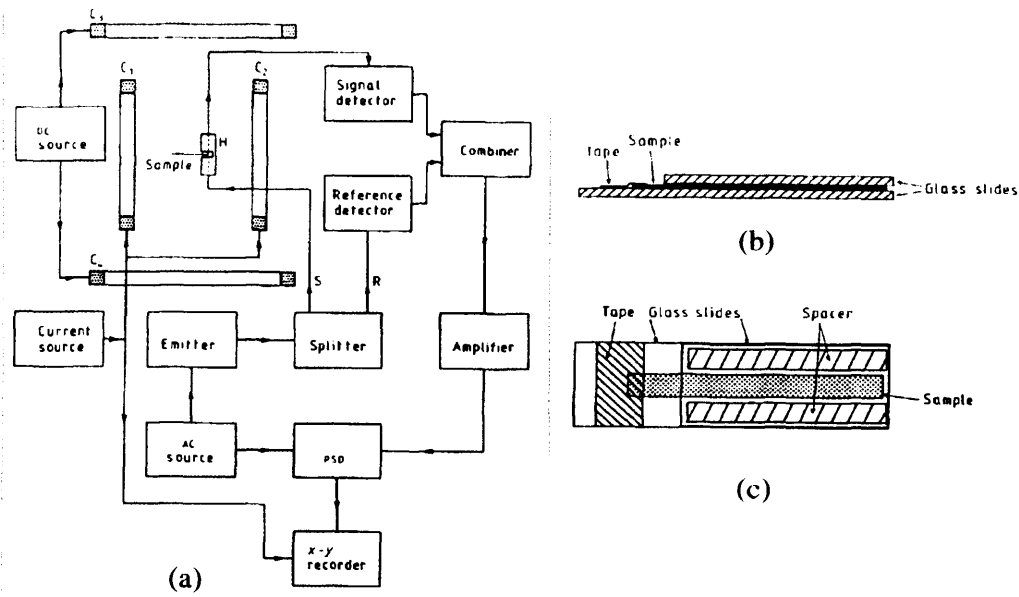


Figure 3.18. (a) Block diagram of the system used in [3.41], sample holder (b) elevation view and (c) plan view [3.41]

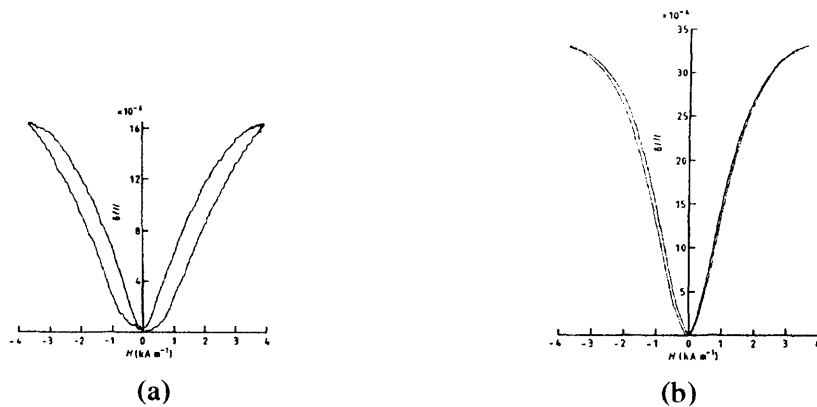


Figure 3.19. Measured magnetostriction results of (a) nickel sample, and (b) Metglas 2605SC [3.41]

Optical methods using laser as the object illumination source are relatively new for use in strain and vibration analysis. Recently, this application has yielded a notable volume of work in measuring displacement due to magnetostriction. However, most researchers used complex optical systems which require high operating skills. Andrew and Schroeder [3.42] constructed an optical setup as shown in figure 3.20 to measure the magnetostriction of a thin magnetic film deposited on a substrate. Although the system has significant advancements over traditional methods in terms of sensitivity and long term stability, further development is needed to eliminate external vibration and noise. The source of such vibration and noise are table vibrations, air turbulence,

laser pointing stability, light intensity fluctuations, amplifier noise, detector shot noise, etc which are mainly due to the complexity of the optical setup itself.

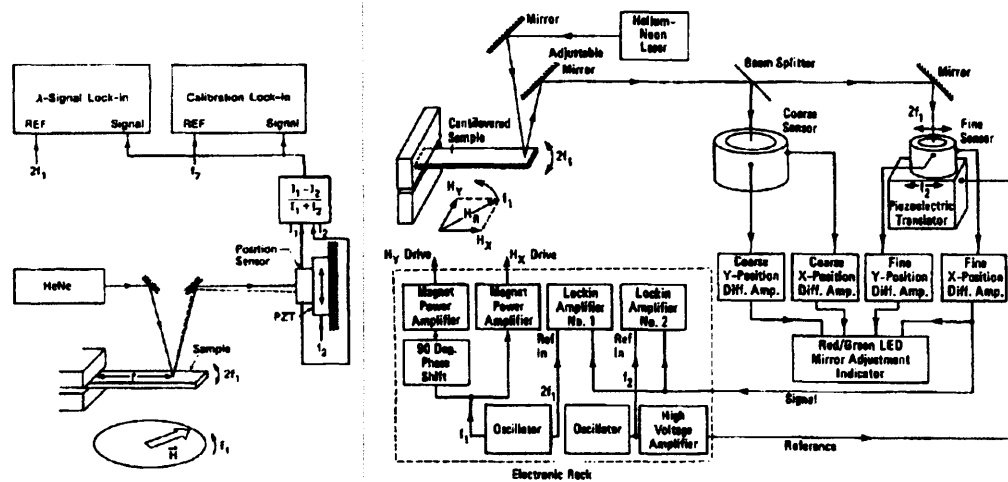


Figure 3.20. Optical setup to measure magnetostriction in thin films [3.42]

Development of laser optical methods continued with Bellesis et al [3.43] in 1993, introducing a laser Doppler interferometer to measure magnetostriction. Although this system is said to have avoided many of the lower frequency noise sources in [3.42] and measures sample deflection instead of bending angle, it is not a direct measurement of sample displacement. Magnetostriction as small as  $1 \times 10^{-9}$  could be measured on films of  $1 \mu\text{m}$  thick on  $100 \mu\text{m}$  substrates with the system used in [3.43].

In 1994, Nakata et al [3.44] introduced the method of measuring magnetostriction with a laser Doppler velocimeter. The authors expressed the advantages of using the laser Doppler velocimeter and measured magnetostriction in arbitrary directions in anisotropic material at flux density  $1.0 \text{ T}$  with  $50 \text{ Hz}$  magnetizing frequency and were able to achieve resolution of displacements of  $4 \times 10^{-8} \text{ m}$ . In 1999, Mogi et al [3.45] published a paper on ac magnetostriction hysteresis and magnetisation direction in grain-oriented silicon steel. They also used a laser Doppler velocimeter to measure ac magnetostriction of a grain-oriented silicon iron in directions deviating from the rolling direction of the sample at  $50 \text{ Hz}$ . This system then had the advantage of being used to precisely measure ac magnetostriction waveforms up to  $4 \text{ kHz}$  including harmonic components.

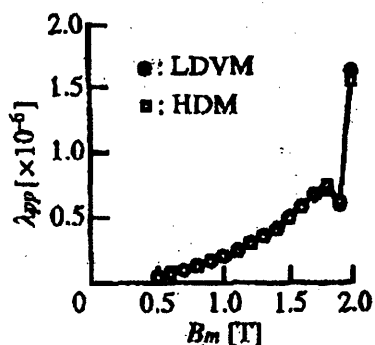


Figure 3.21. Comparison of laser Doppler vibrometer, LDVM and heterodyne displacement meter, HDM used in [3.46].

Nakase et al [3.46] developed a system for measuring magnetostriction of silicon steel in a single sheet tester using an optical method. Their aim was to establish a standard test method for IEC (International Electrotechnical Commission) and JIS (Japanese Industrial Standards). Two optical instruments, i.e. a laser Doppler vibrometer and a heterodyne displacement meter were used and the results were compared. Magnetostriction under 50 Hz ac excitation in rolling, transverse and thickness direction of a silicon steel sheet was investigated [3.46]. The results obtained from the two instruments (figure 3.21) were within  $\pm 5\%$  and an error of 1% obtained for minimum magnetostriction measured at  $4 \times 10^{-7}$ . Environmental noise problems were said to be removed considerably by implementing a vibration eliminator and by averaging the measurements.

Over the past ten years, compact laser systems have become available commercially by companies such as Polytec GmbH, Neoark Corporation, Keyence Corporation, and Ultra-Optec Inc. In 2003, Hirano et al. studied [3.47] comparison of measurement of magnetostriction silicon steel sheets using commercial compact laser displacement meter and optical methods of laser Doppler vibrometer [3.47]. The silicon steel sheet was 500 mm x 100 mm and 50 Hz magnetisation was excited  $90^\circ$  to the rolling direction of the sheet. The laser displacement meter was able to measure displacements as low as  $5 \times 10^{-8}$  meter and Hirano et al. found that characteristics of peak-peak magnetostriction measured by laser displacement meter agreed well with that of the laser vibrometer (figure 3.22).

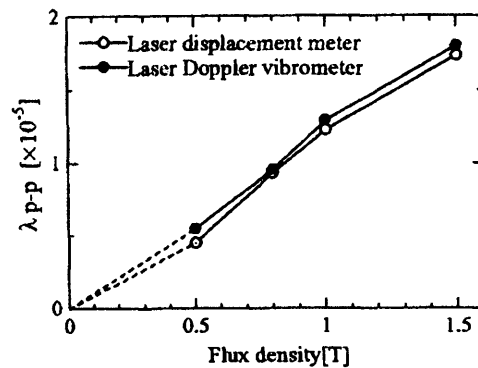


Figure 3.22. Comparison of laser displacement meter and laser Doppler vibrometer used to measure magnetostriction of silicon steel sheets magnetised at 50 Hz [3.47]

Laser techniques open the possibility of measuring magnetostriction in instances where it is not practical to attach strain gauges and allow measurement of magnetostriction in any direction of anisotropic material. Although laser techniques have advantages over the traditional methods of measuring magnetostriction, one must consider the cost and specifications that will suit individual applications.

### 3.6. Application of Magnetostriction

According to Dapino [3.5], magnetostrictive materials are a class of smart materials which can convert energy between the magnetic and elastic states. Magnetostriction is used in transducers to generate and receive sound waves i.e. ultrasonic generation and detection. Low frequency underwater communications such as echo depth recorders (Figure 3.23a) [3.48], fish finders and sonar utilize magnetostriction transducers. Magnetostrictive vibrators are also used to provide ultrasonic energy for devices such as the ultrasonic dental scaler. In such applications, variation of magnetic field is employed to produce varying strains in the magnetostrictive material to produce a mechanical output.

One advantage of magnetostrictive transducers over other types of transducers is that they can be driven with conventional low impedance amplifiers, particularly at frequencies well below resonance [3.5]. The low impedance of a magnetostrictive transducer means that driving voltages can be low. This is useful in medical applications and in general can greatly simplify amplifier design. In processes such as

ultrasonic cleaning, welding, machining and drilling, considerable energy is usually needed and magnetostriction transducers (figure 3.23b) are particularly suitable because of their robustness and power handling capabilities [3.48].

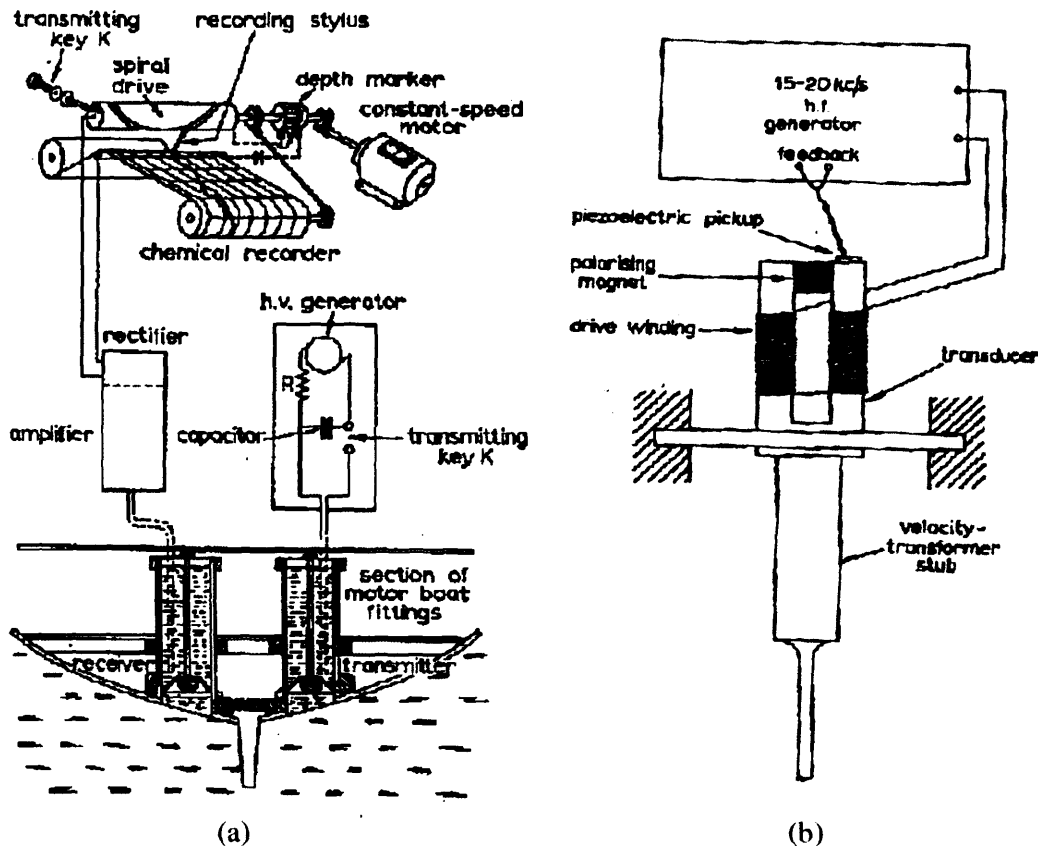


Figure 3.23 (a) A general arrangement of an echo depth recorder shown in [3.48] (b) A magnetostriction transducer as in [3.48]

Magnetostrictive materials have applications in devices such as sensors and actuators. The reversible effect of magnetostriction i.e. changes in a material's applied stress generated magnetic energy; can be used as a sensor. As for actuators, the magnitude of the strain and the available force are the most important properties. Some of the earliest uses of magnetostrictive materials during the first half of this century include telephone receivers, hydrophones, magnetostrictive oscillators, torque-meters and scanning sonars. In 1980, Terfenol-D with composition of terbium, dysprosium and iron was found to have the highest magnetostriction of all known materials of  $1600 \times$

$10^{-6}$  at room temperature [3.5]. Since then, Terfenol-D has created an increasing interest as a magnetostrictive actuator material because of its high energy density, high force and broad frequency bandwidth [3.5]. Dentsply Research and Development Corporation claimed a patent [3.49] for an ultrasonic dental scaler rod using Terfenol-D ( $\text{Tb}_{0.30}\text{Dy}_{0.70}\text{Fe}_{1.92}$ ) to maximise the performance of the device.

Other applications for magnetostrictive devices include robotics, high force linear motors, positioners for adaptive optics, active vibration or noise control systems, medical and industrial ultrasonics. In addition, magnetostrictive linear motors, reaction mass actuators, and tuned vibration absorbers have been designed, while less obvious applications include high cycle accelerated fatigue test stands, mine detection, hearing aids, razor blade sharpeners, and seismic sources.

---

**References**

- [3.1] J P Joule, 'On the Effects of Magnetism Upon the Dimensions of Iron and Steel Bars', *Philosophical Magazine*, Vol. 30, Part 3, pages 76-87, 1847.
- [3.2] W Alexander, 'Principles and Applications of Magnetostriction', *Electronics & Power*, pages 186-190, 1966.
- [3.3] Practical Physics, <http://www.practicalphysics.org>
- [3.4] D Jiles, 'Introduction to Magnetism and Magnetic Materials' Chapman & Hall, 1991.
- [3.5] M J Dapino, 'On Magnetostrictive Materials and Their Use In Smart Material Transducers', *Structural Engineering and Mechanics: An International Journal*. Submitted October 2002.
- [3.6] F Brailsford, 'Physical Principles of Magnetism', D Van Nostrand Company, 1966.
- [3.7] J B Restorff, 'Magnetostrictive Materials and Devices', *Encyclopedia of Applied Physics*, Vol. 9, 1994.
- [3.8] Federal Pacific, 'Understanding Transformer Noise',  
<http://www.federalpacific.com/university/transnoise/transnoise.html>
- [3.9] S Chikazumi, 'Physics of Magnetism', John Wiley & Sons, 1964.
- [3.10] R Becker, 'Electromagnetic Fields and Interactions', Vol. I *Electromagnetic Theory and Relativity*, Blackie: London and Glasgow, 1964.
- [3.11] W T Thomson, 'Theory of Vibration with Applications – Fourth Edition', Prentice Hall, 1993.
- [3.12] H J Pain, 'The Physics of Vibrations and Waves – Sixth Edition', John Wiley & Sons Inc, 2005.
- [3.13] A J Thottuvelil, T G Wilson and H A Owen Jr, 'Unusual High-Frequency Behaviour of Some Amorphous Metallic-Alloy Tape-Wound Magnetic Cores', *IEEE Transactions on Magnetics*, Vol. Mag-20, No. 4, pages 570-578, 1984
- [3.14] A. J. Moses and S. M. Pegler, 'The Effects of Flexible Bonding of Laminations In a Transformer Core' *Journal of Sound and Vibration*, Vol 29(1), pages 103-112, 1973.



- [3.15] H C Kim and C G Kim, 'Effect of Magnetising Frequency and Stress On Magneto-Acoustic Emission From 3% Si-Fe Crystals', *Journal of Physics D: Applied Physics* 22, pages 192-198, 1989.
- [3.16] A W Kelley, 'Measurement of Spacecraft Power Transformer Acoustic Noise', *IEEE Transactions on Magnetics*, Vol. 26, No. 1, pages 281-289, 1990.
- [3.17] H Wakiwaka, T Umezawa, K Kuwahara, H Kamata, T Yoshikawa, S Kitazawa, H Yamada, 'Measurement of Vibration Mode of An Acoustic Vibration Element Using Giant Magnetostrictive Material', *Proceedings of ISEM Conference*, 1994.
- [3.18] S Takada, 'Magnetostrictions of Electrical Iron Sheets under Controlled Magnetization', *Journal of Magnetism and Magnetic Materials* 133, pages 226-228, 1994.
- [3.19] H Mogi, M Yabumoto, M Mizokami and Y Okazaki, 'Harmonic Analysis of AC Magnetostriction Measurements Under Non-Sinusoidal Excitation', *IEEE Transactions on Magnetics*, Vol. 32, No. 5, pages 4911-4913, 1996.
- [3.20] C Ozturk and A Bahadir, 'Significance of Electromagnetic Forces on The Mechanical Resonances of Stator Laminations', *Mechanical Systems and Signal Processing*, 10 (5), pages 501-515, 1996.
- [3.21] J M Chicarro, A Bayon, F Salazar, 'Measurement of Field-Dependence Elastic Modulus and Magnetomechanical Coupling Factor by Optical Heterodyne Interferometry', *Journal of Magnetism and Magnetic Materials* 202, pages 465-472, 1999.
- [3.22] A Karimi, Ch Azcoitia, Degauque, 'Relationships Between Magnetomechanical Damping and Magnetic Properties of Fe-Cr (Al/Mo) Alloys', *Journal of Magnetism and Magnetic Materials* 215-216, pages 601-603, 2000.
- [3.23] A Bayon, Chicarro, F Salazar, 'Simultaneous Measurement of Field Dependence of Elastic Moduli by Laser Interferometry', *Journal of Magnetism and Magnetic Materials* 219, pages 229-235, 2000.
- [3.24] J M Chicarro, A Bayon and F Salazar, 'Measurement of Damping in Magnetic Materials by Optical Heterodyne Interferometry', *Journal Magnetism and Magnetic Materials* 268, pages 348-356, 2004.

- [3.25] Measurement Group Inc., 'Strain Gauge Based Transducers, Their Design and Construction'.
- [3.26] BS EN 60404-2:1998, 'Magnetic Materials – Part 2: Methods of Measurement of the Magnetic Properties of Electrical Steel Sheet and Strip by Means of An Epstein Frame'.
- [3.27] Technical Reference Series by Omega, 'Force Related Measurements', Transactions in Measurement and Control, Vol. 3, 2<sup>nd</sup> Edition, 1998.
- [3.28] Micron Instruments, [www.microninstruments.com](http://www.microninstruments.com)
- [3.29] National instruments, <http://www.ni.com/academic/>
- [3.30] 'Measuring Vibration', Brüel & Kjær, 1982.
- [3.31] M Bass, J M Enoch, E W Van Stryland, W L Wolfe, 'Handbook of Optics, Classical, Vision & X-ray Optics' Second Edition, Volume III, 2001.
- [3.32] Polytec GmbH, 'Vibrometer University', <http://www.polytec.com/>
- [3.33] R M Bozorth, 'Ferromagnetism', D Van Nostrand Company Inc., 1951.
- [3.34] J E Goldman and R Smoluchowski, 'Magnetostriction and Order-Disorder', Physical Review, Vol. 75, No. 1, pages 140-147, 1949.
- [3.35] R D Greenough and C Underhill, 'Strain Gauges for the Measurement of Magnetostriction in The Range 4K to 300K', Journal of Physics E, Scientific Instruments, Vol. 9, pages 451-454, 1976.
- [3.36] C W Little, 'Instrumentation for the Rapid Measurement of Magnetostriction', Conference on Magnetism and Magnetic Materials (proceedings), Boston, pages 236, 1956.
- [3.37] W Alexander, 'An Electronic Ultramicrometer', Electronics Engineering, 23, pages 479, 1951.
- [3.38] J D Whitaker, 'Measurement methods of electrical sheet', Electrical times, 137, pages 675, 1960.
- [3.39] W R George, C Holt and J E Thompson, 'Magnetostriction in Grain-Oriented Silicon-Iron', Proceedings IEE, Vol. 109, Part A, No 43, pages 101-108, 1962.
- [3.40] D J Mapps and C E White, 'Phase-Shifted Flux Harmonics and Magnetostriction in (110) [001] Silicon-Iron', IEEE Transactions on Magnetics, Vol. Mag-18, No.6, pages 1505-1507, 1982.
- [3.41] P T Squire and M R Gibbs, 'Fibre-Optic Dilatometer for Measuring Magnetostriction in Ribbon Samples', Journal of Physics E: Science Instrumentation 20, pages 499-502, 1986.

- [3.42] C T Andrew and H Schroeder, 'A New High-Precision Optical Technique to Measure Magnetostriction of A Thin Magnetic Film Deposited on A Substrate', IEEE Transactions on Magnetics, Vol. 25, No. 3, pages 2629-2638, 1989.
- [3.43] G H Bellesis, P S Harllee, A Renema II and D N Lambeth, 'Magnetostriction Measurement by Interferometry,' IEEE Transactions on Magnetics, Vol. 29, No. 6, pages 2989-2991, 1993.
- [3.44] T Nakata, N Takahashi, M Nakano, K Muramatsu, P Miyake, 'Magnetostriction Measurements With Laser Doppler Velocimeter', IEEE Transactions on Magnetics Vol. 30 Issue 6, pages 4563-4565, 1994.
- [3.45] H Mogi, Y Matsuo and T Kumano, 'AC Magnetostriction Hysteresis and Magnetisation Direction in Grain Oriented Silicon Steel', IEEE Transactions on Magnetics, Vol 35, No. 5, pages 3364-3366, 1999.
- [3.46] T Nakase, M Nakano, K Fujiwara and N Takahashi, 'Measuring System for Magnetostriction of Silicon Steel Sheet under AC excitation Using Optical Methods', IEEE Transactions on Magnetics, Vol. 34 No 4, pages 2072-2074, 1998.
- [3.47] M Hirano, Y Ishihara, K Harada, T Tokada, 'A Study on Measurement of Magnetostriction of Silicon Steel Sheet by Laser Displacement Meter', Journal of Magnetism and Magnetic Materials 254-255, pages 43-46, 2003.
- [3.48] M J Dapino, 'Magnetostrictive Materials: Their Use in Smart Structure Applications', Encyclopaedia of Smart Materials, pages 600-620, J. A. Harvey, Editor, John Wiley & Sons, Inc. New York, 2002.
- [3.49] Mosch et al, 'Ultrasonic scaler – United States Patent', Dentsply Research and Development Corporation, US patent no. US6,619,957 B1, September 16, 2003.

## CHAPTER 4

### TRANSFORMER NOISE

---

#### 4.1. Introduction

Noise is defined as unwanted sound. Transformer “humming” has been known to soothe a person, which makes it a sound, but generally it is thought to be a nuisance, which makes it a noise. The causes and reduction of transformer noise has been the subject of many articles even before discovering that magnetostriction was the main source of noise in transformer cores in mid 1900s [4.1]. Reduction of transformer noise has come to prominence, mainly because transformers are placed closer to the populace i.e. in high-rise office buildings, apartments, shopping malls and in their gardens. Therefore, when designing a transformer, it is necessary to consider each case on its merits and to be familiar with causes of transformer noise. Many users build special rooms to house their transformers in order to damp the noise. A high number of transformers operate below ground for the same reason.

The transformer acoustic noise resulting from core vibration is mainly caused by magnetostriction of the core material [4.2]. Other sources of noise are the periodic mechanical deformation of the transformer core and the coil windings, under the influence of fluctuating electromagnetic flux associated with these parts. Noise from the cooling fans and the pumps are negligible contributors to the far-field noise. Figure 4.1 shows a schematic diagram of the noise generation and transmission from a transformer [4.2]. In this chapter, only transformer core noise contributed by magnetostriction is discussed.

A transformer core is magnetically excited by an alternating voltageso that it becomes extended and contracted twice during a full cycle of magnetisation. Magnetostriction is not uniform and consequently, it varies all over a magnetic steel lamination (this is discussed in chapter 8 – figure 8.8). Therefore, each lamination in a stacked transformer core behaves erratically with respect to its neighbour. Although

magnetostriction cannot be seen by the naked eye, it is sufficient to cause a vibration and noise as a result.

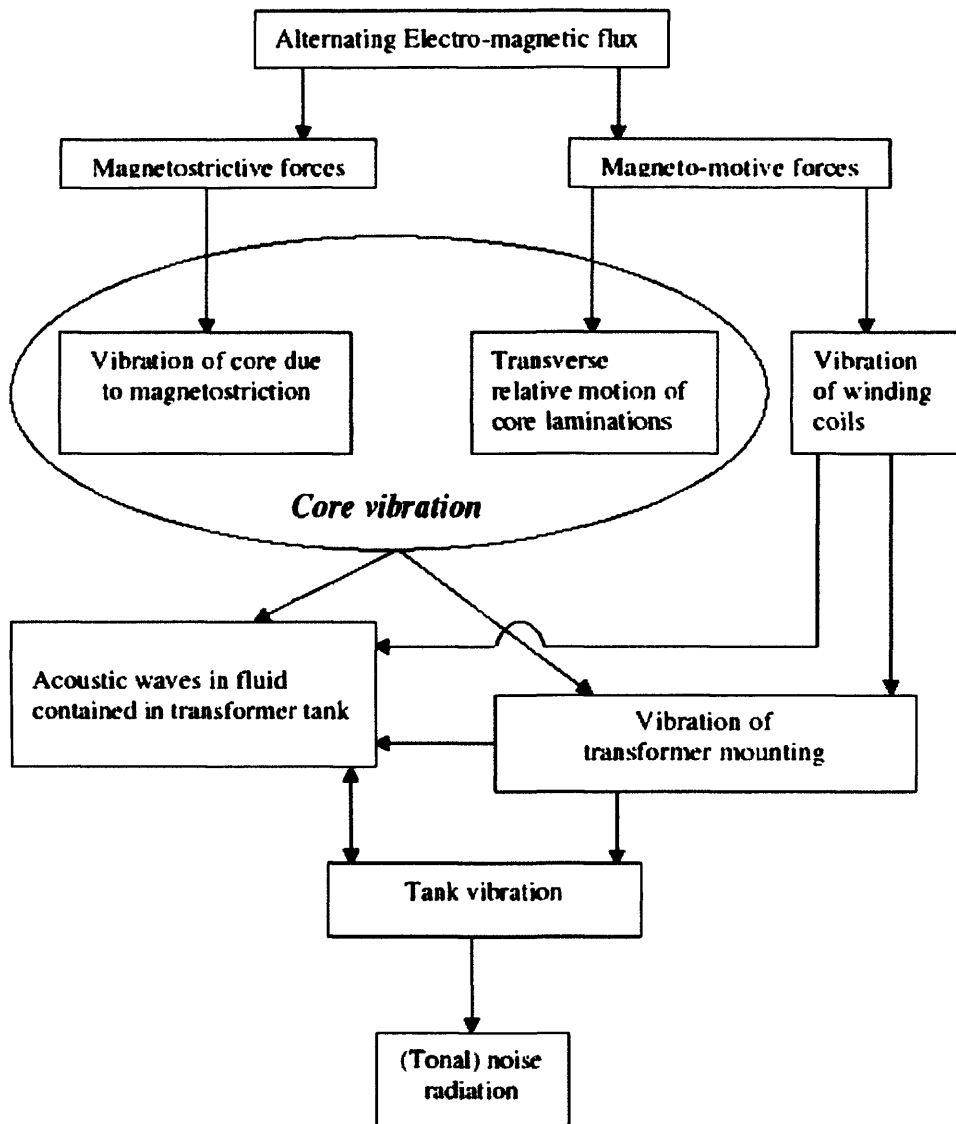


Figure 4.1. Schematic diagram of noise generation and transmission in a power transformer [4.2].

Transformer voltages are fixed by system requirements such as the ratio of the voltages to the number of turns in the winding (see section 4.2. equation 4.1) and the amount of magnetisation. The decision on what this turns ratio should be is mainly made for economic reasons. Trying to reduce noise level at the source by means of changing turns ratio or amount of magnetisation, is costly with hardly any improvement in the noise level since increasing (or decreasing) magnetisation does

not increase or decrease the magnetostriction by the same amount i.e. the relationship is not linear.

## 4.2. Construction of Transformer Cores

A transformer is an electrical device used to convert ac power at a certain voltage level to ac power at a different voltage, but at the same frequency. The development of the transformer is closely linked with the development of soft magnetic materials. In 1886, the first transformer core was constructed and until 1907, cores were assembled from non-silicon steel [4.3]. Immediately after the introduction of silicon into the iron (see section 2.4.2.1), the magnetic properties of transformer cores were found to improve and a significant reduction in magnetostriction occurred. Nowadays, the acoustic noise produced by a 15 MVA grain-oriented steel core is around 72 dBA having a  $4 \mu\epsilon$  magnetostriction measured on a core limb [4.4]. The British Standards BS EN 60551: 1993 [4.5] states that when designing a transformer, the maximum allowable acoustic noise level emitted by the transformer should be around 60 - 70 dBA, equivalent to a car travelling at 60 km/h at 7 m distance.

A transformer core is often made up of stack of electrical steel laminations. Figure 4.2a shows a single phase transformer core and figure 4.2b shows its typical schematic circuit. The basic construction of a transformer includes a ferromagnetic core with primary and secondary coils, or windings of copper or aluminium wire are wrapped around the core. The input line connects to the primary coil, while the output line connects to the secondary coil. The alternating current in the primary coil induces an alternating magnetic flux that flows around the ferromagnetic core, changing direction during each electrical cycle. The alternating flux in the core in turn induces an alternating voltage in the secondary coil. The voltage at each of the secondary coils,  $V_s$  is directly related to the primary voltage,  $V_p$  by the turns ratio,  $r$  the ratio of the number of turns in the primary coil,  $N_p$  to that in the secondary coil,  $N_s$ .

$$\frac{V_s}{V_p} = \frac{N_s}{N_p} = r \quad (4.1)$$

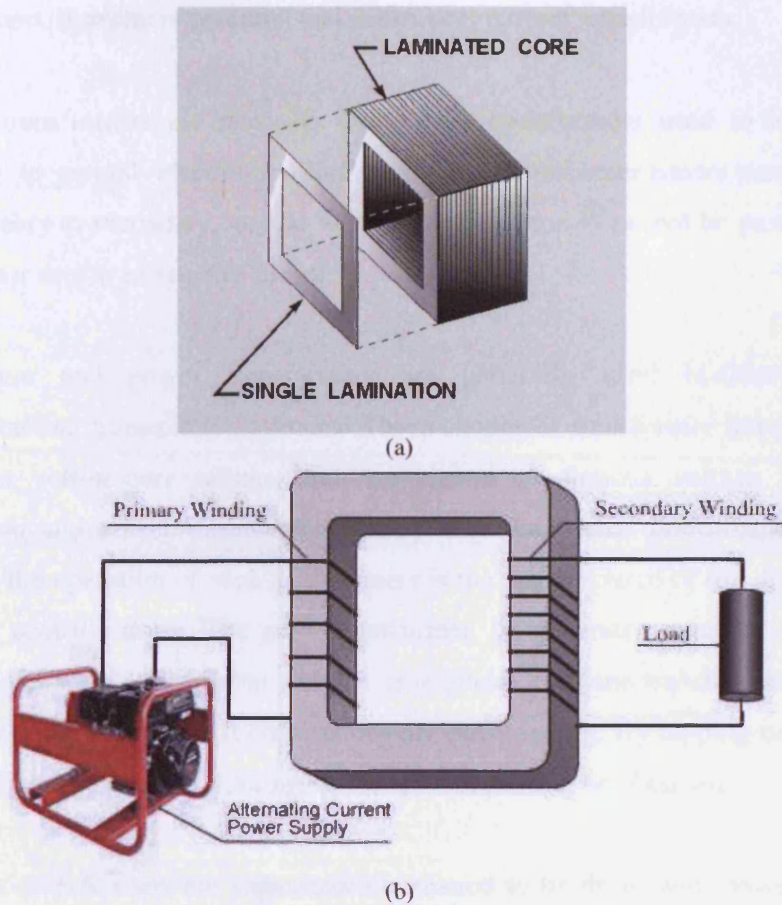


Figure 4.2. (a) Single phase transformer core made up of stack of steel laminations (b) Schematic diagram of a single phase transformer circuit.

A transformer may have multiple secondary coils to feed a number of electrical loads; however, power must be conserved, so the sum of the output power must equal the sum of the input power less the internal losses. The most efficient transformer core is one that offers the best path for the flux with the least loss.

### 4.3. Types of Transformers

Transformers are constructed so that their characteristics match the application for which they are intended. The differences in construction may involve the size of the windings or the relationship between the primary and secondary windings. Transformer types are also designated for the function the transformer serves in a

circuit, such as an isolation transformer. Other applications are distribution, power, control, auto, instrument potential and instrument current transformers.

Isolation transformers are normally low power transformers used to isolate noise from or to ground electronic circuits. Since a transformer cannot pass dc voltage from primary to secondary, any dc voltage (such as noise) cannot be passed, and the transformer acts to isolate this noise.

Distribution and power transformers are generally used in electrical power distribution and transmission systems. These classes of transformer have the highest power, or volt-ampere ratings, and the highest continuous voltage rating. Both distribution and power transformers satisfy their functional performance objective; however, the operation of such transformers is the major source of the disturbing and annoying acoustic noise. The auto transformer is generally used in low power applications where a variable voltage is required. The auto transformer is a special type of power transformer. It consists of only one winding. By tapping or connecting at certain points along the winding, different voltages can be obtained.

Electronic transformers are sometimes considered to be those with power ratings of 300 volt-amperes and below [4.4]. These transformers normally provide power to the power supply of an electronic device, such as in power amplifiers in audio receivers. Control transformers are generally used in electronic circuits that require constant voltage or current with a low power or volt-amp rating. Various filtering devices, such as capacitors, are used to minimize the variations in the output to obtain the constant voltage or current.

The instrument potential transformer steps down voltage of a circuit to a low value that can be effectively and safely used for operation of ammeters, voltmeters, watt meters, and relays used for protective purposes. The instrument current transformer steps down the current of a circuit to a lower value and is used in the same types of equipment as a potential transformer. This is done by constructing the secondary coil consisting of many turns of wire, around the primary coil, which contains only a few turns of wire.



The requirement for more electrical power associated with the growing density of population, especially in urban areas, has resulted in enhancing the supply capacity of local electrical substations by adding more transformers, or building new substations of high power ratings closer to the neighborhoods. This result in residents in the vicinity being exposed to increased, and often disturbing, noise levels. A growing awareness and concern about public health problems due to noise pollution has brought transformer substations under the concerns of strict regulations on excessive noise emission which requires the design of efficient passive/active control systems for onsite noise control measures. For this purpose, a proper understanding of the noise generation in a transformer and an accurate estimation of its radiation characteristics are necessary.

#### **4.4. Previous Research on Noise in Transformer Cores**

As opposed to the huge improvements in the magnetic materials sector, the transformer, as a magnetic circuit, has not changed much over the last century. The difference between a late 1880's transformer core and a modern one is that the later was made from thin sheets of magnetic material, whereas the former would probably be made out of solid iron. Many investigations have been carried out especially in the second half of the 20<sup>th</sup> century in order to take full advantage of grain-oriented silicon iron. Since then improvements in the magnetic properties of transformer cores have been a combination of improved design and build, the development of superior magnetic materials used for the construction of the cores as well as an improvement in the design of windings. However, even with such improvements, it is still necessary to reduce transformer acoustic noise.

In the review written by Alexander in 1966, it was established that transformer core noise was almost entirely due to magnetostriction, with a small contribution due to joint noise [4.6]. Alexander and Swaffield developed a method of measuring the magnetostrictive effect in the core of a model transformer. It was shown that a reduction of flux density from 1.3 T to 1.0 T halved the noise. Unless the transformer runs at a very low flux density, Alexander suggested that the only way to reduce the undesirable effect is to use 6% Si-Fe. However, at that time, it was not practicable to use such alloys since the brittle material was difficult to produce and cut.

Majed and Thompson said that during the construction of large power transformers, the magnetostriction of the material is increased, so that the noise output of the core is higher than that predicted from laboratory measurements [4.7]. They investigated a way of producing improved transformers by analysing the magnetostriction/stress behaviour of groups of similar samples held together by taping and bonding under tensile and compressive stresses. Stress sensitivity of magnetostriction of silicon iron in the form of individual Epstein strips was measured followed by the behaviour of groups of strips held together in various ways, such as used in a transformer core. Further experiments on the vibration pattern or modes of vibration of the 100 (figure 4.3), 200 and 300 Hz harmonics for each assembly of strips held vertically between two fixed end points in such a way as to simulate a transformer limb was also investigated and it was found that the amplitude of vibration at all frequencies of eight taped silicon iron strips, with negative, near zero and positive magnetostriction in the unstressed state, was comparatively larger than that in corresponding bonded stacks.

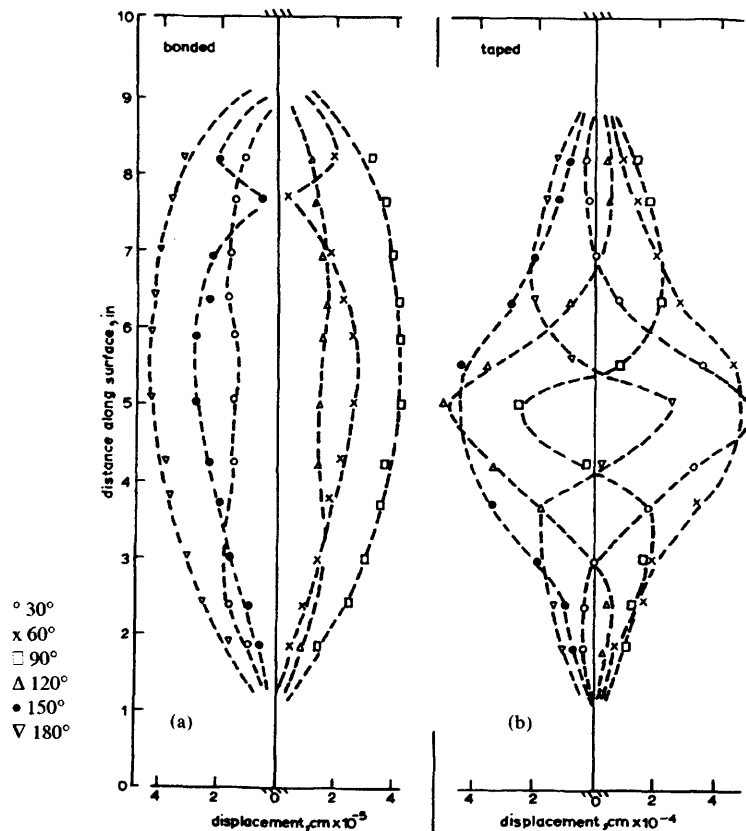


Figure 4.3. 100 Hz component of the vibration pattern of group of strips in (a) bonded and (b) taped conditions at different phase angle between flux (reference) signal and vibration signal [4.7].

Moses highlighted that the control of transformer noise is a costly problem which increases as core size become greater [4.8]. It was mentioned that the origin of noise is the core vibration brought about by the mechanical effects of the alternating flux i.e. magnetic attraction producing flapping laminations and magnetostriction causing changes in core dimensions. Although there was no mention about mechanical resonance in the core laminations, it was said that noise produced by the harmonics of magnetostriction has a much greater effect to the human ear. It is shown in this paper that the stress sensitivity of grain-oriented 3.2% silicon iron bonded laminations is far less than that of taped laminations; although the magnetostriction in the stress free state was higher. Corresponding effects were found to occur with the harmonics of magnetostriction.

Moses and Pegler [4.9] demonstrated the possibility of producing improved transformers by bonding stacks of silicon iron laminations together with flexible adhesive instead of bolted core since bonding with flexible adhesive reduced magnetostrictive vibrations of the laminations. They showed that the pattern of vibration at certain lower frequencies and the total noise output of a 100 kVA transformer core was reduced only by 3 dB (A-weighted noise) below that of a bolted core at the same magnetising frequencies. It was assumed that other factors such as resonance of yoke clamps, tie rods etc contributed to the noise although the core vibration itself fell up to tenfold.

White and McNally presented a complete design procedure for assessing and subsequently controlling the noise emitted by large power transformers and their associated equipment [4.10]. They proposed four types of enclosure for satisfying a range of noise control requirements. The proposed enclosures that suit a particular calculated relative noise level were categorised as follows:

Type A – Unroofed enclosures

- (i) 3 walls approximately 2 metres above tank with acoustic liner.
- (ii) 4 walls approximately 2 metres above tank with acoustic liner.

Type B – Roofed enclosure.

Type C - Unroofed enclosure with resonating cavity lining.

Type D – Roofed enclosure with resonating cavity lining.

For any application, one of the above enclosures can be selected to be able to achieve acceptability sound level using White and McNally's enclosure selection chart (figure 4.4). Although placing an enclosure to reduce transformer noise emission contains the noise, it does not reduce the noise from the source and it is expensive.

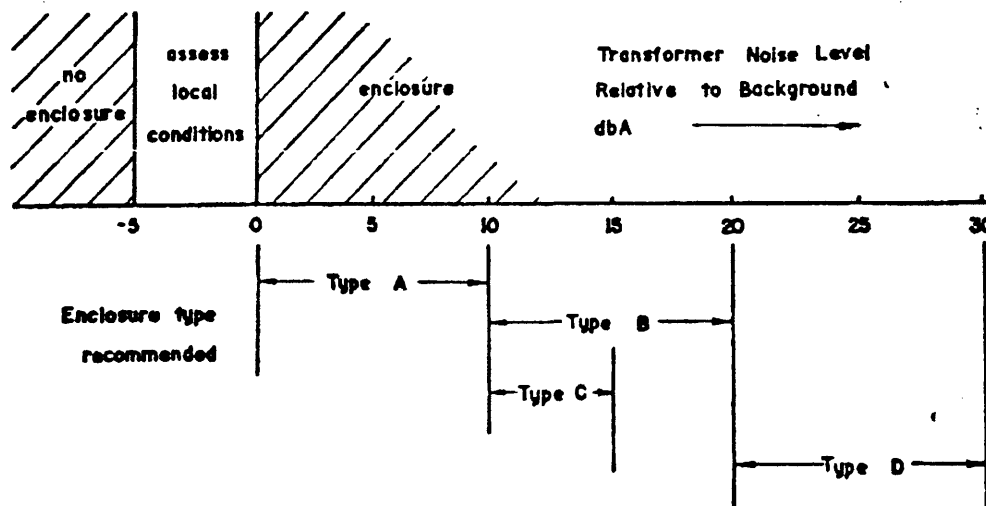


Figure 4.4. Enclosure selection chart as recommended by White and McNally [4.10].

The principle advantage of an ac power system is the use of transformers for changes in voltage [4.11]. However, power transformers normally operate at 0.4 kHz to 20 kHz and this may lead to generation of unwanted acoustic noise. In 1990s, transformer noise studies at power system frequencies other than 60 Hz were nearly rare although sources of transformer noise were found to originate from both windings and core vibration. It is said that windings vibration can be reduced during manufacture by ensuring winding integrity. In addition, Kelly suggested that magnetostrictive vibration excites the mechanical system consisting of the core, winding and the structure on which transformer is mounted. Subsequently, the resonant frequencies of the mechanical system are excited by magnetostrictive vibration of the core. If a mechanical resonant frequency corresponds to a power system harmonic, the acoustic noise emission at that frequency will be amplified.

Kelley chose three comparisons for acoustic noise considerations namely power system frequencies, magnetic materials and core types [4.11]. Power frequencies for the study were 0.4 to 20 kHz. Four types of single-phase tape wound cores of

different sizes were constructed from 3% Si-Fe and 79% Ni 17% Fe 4% Mo. Figure 4.5 shows the overall sound pressure level of the four core sizes (A = 0.6" to D = 1.2") of square shaped toroidal cores. A trend was observed where larger cores and higher excitation frequencies produce higher noise. It was also observed that cores made from Si-Fe produced higher noise than the Ni-Fe-Mo cores, the difference being more apparent for larger cores. Figure 4.6 shows the qualitative guidelines from Kelley's transformer design study when acoustic noise is considered [4.11]. It was observed that the Ni-Fe-Mo material was favoured acoustically due to low magnetostriction, tape wound toroidal cores are favoured acoustically over tape wound rectangular cores and square shaped toroidal cores are acoustically favoured over the rectangular toroidal cores.

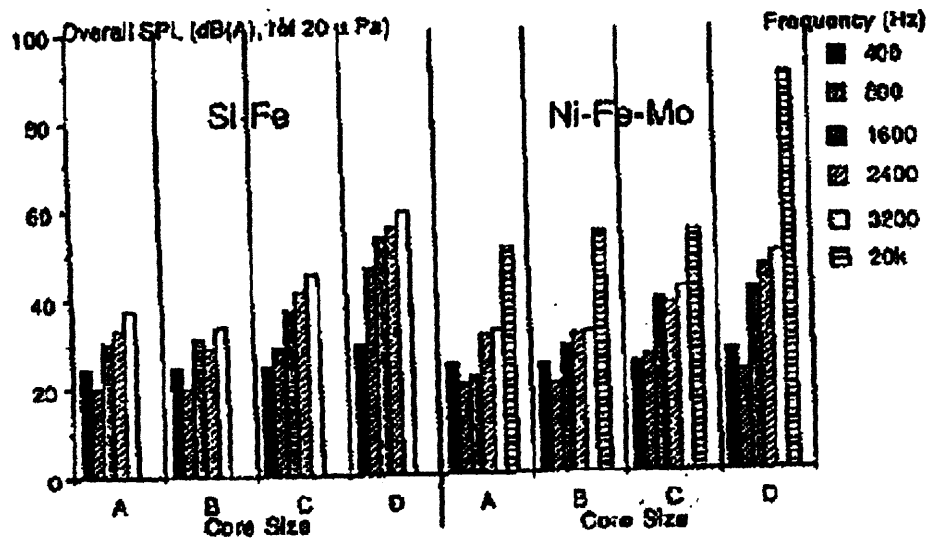


Figure 4.5. Summary of overall A-weighted sound pressure level measured for boxed tape wound toroidal cores for sizes A-D (D being the largest) for various excitation frequencies of Si-Fe and Ni-Fe-Mo [4.11]

Moses et al [4.12] reported a reduction of magnetostriction with frequency under longitudinal stress in non-oriented electrical steels (figure 4.7). It is also shown that magnetostriction was dependent on texture (figure 7.8). AC magnetostriction of single Epstein strips of non-oriented electrical steels cut parallel (RD) and perpendicular (TD) to the rolling direction was measured using surface mounted accelerometers. It was suggested that further experimental studies and more rigorous theoretical calculations were necessary to verify the size trends with frequency. The reduction in

magnetostriction at high frequency would have important applications in analysis and prediction of electrical machine noise.

Basis for Comparison	Favored Acoustically	Favored in VA Rating	Other Comparisons
Power system frequency	low frequency	high frequency	must avoid resonance of mechanical structures at excitation frequency
Magnetic material	Ni-Fe-Mo	Si-Fe below 2400 Hz, Ni-Fe-Mo above 2400 Hz	VA rating depends heavily on transformer cooling constraint
Core type: toroidal cores versus rectangular cores	toroidal cores	toroidal cores may be slightly higher	gapped rectangular cores much easier to assemble into completed transformer
Core type: bare versus boxed toroidal cores	boxed tape-wound toroids	bare tape-wound toroids	slight additional window area used by box
Core type: gapped versus ungapped rectangular cores	ungapped	no difference	gapped rectangular cores much easier to assemble into completed transformer
Core type: gap pressure for gapped rectangular cores	high pressure	no difference	maintaining consistent gap pressure may be difficult in manufacturing environment

Figure 4.6. Qualitative recommendations for transformer design when acoustic noise is a consideration [4.11]

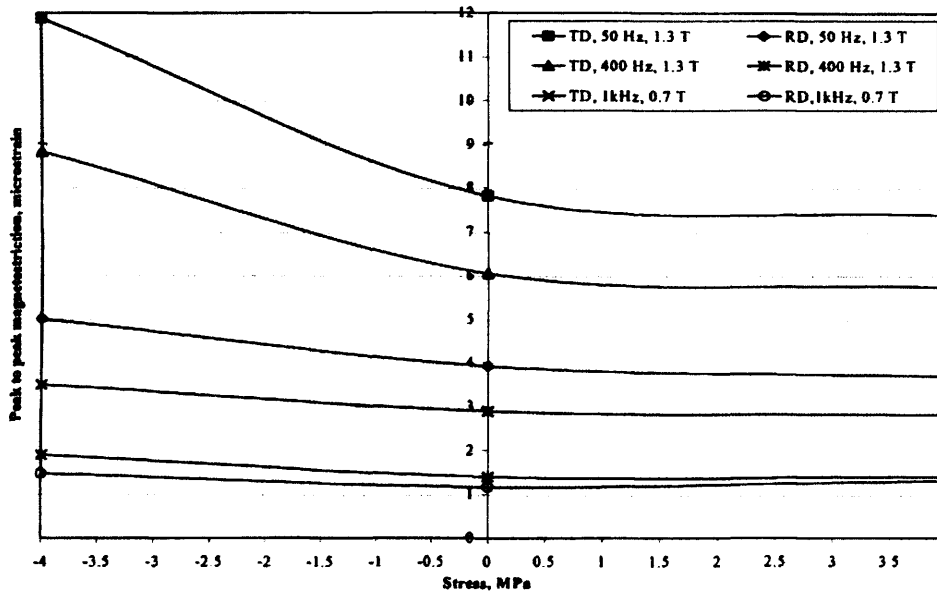


Figure 4.7. Peak-peak magnetostriction against stress applied along rolling and transverse direction of V700-50A non-oriented strips sinusoidally magnetised at various frequencies and flux densities [4.12].

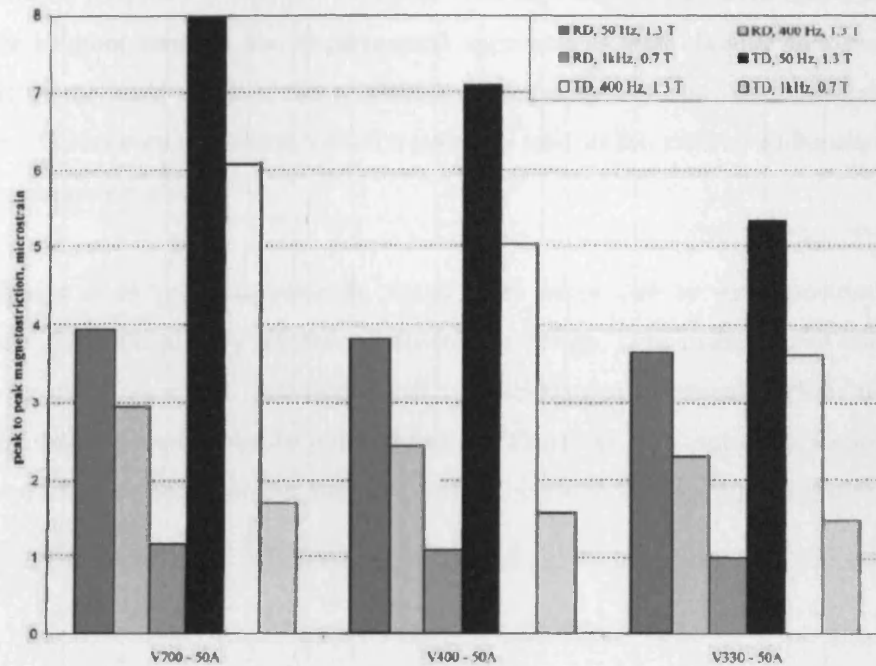


Figure 4.8. Peak-peak magnetostriction of different grades of non-oriented steel strips sinusoidally magnetised at different frequencies and flux densities [4.12]

In 2004, Masti et al [4.2] investigated the influence of core laminations on transformer core noise. They mentioned that when a core's natural frequency coincides with an excitation frequency, the core can resonate with large deformations if not properly designed. Although the core has to meet a transformer's electrical system requirements, it is important that its structure does not resonate at any of its excitation frequencies that are related to the power system frequency and its harmonics. Masti et al used a finite element model analysis to understand the dynamic of a Si-Fe laminated core structure. A rectangular core block was modeled for three degree of lamination refinements under free boundary conditions; 1) single solid block with no lamination 2) an assembly of several blocks and 3) a fully laminated core. The sizes of the modeled cores was not given, However, lamination thickness was 0.28 mm and the properties of the core material were; Young's Modulus: 210 GPa, density: 7650 kg/m<sup>3</sup> and Poisson's Ratio: 0.3. Results indicate a significant lowering of resonance frequencies of the assembly of 9 blocks and the fully laminated core compared to the single solid block. Masti et al also compared the first resonance frequencies obtained from finite element analysis to experimentally obtained results of the fully laminated core. However, a theoretical approach to obtaining the

resonance frequencies was not included. Although differences were observed in the finite element analysis and experimental approach, it was claimed that the results were of the same order of the magnitude. This study indicates that some structural borne vibrations exist which, would eventually lead to the exterior radiation of noise from the tank surface.

Although from previous research, transformer noise due to magnetostriction was reduced significantly by improved transformer design, core material and enclosures, at present, increased environmental consciousness demands that unwanted transformer acoustic noise be reduced further. Therefore, it is important to understand the transformer noise phenomena and continue research in reducing the audible noise.



---

**References**

- [4.1] P Marketos, 'Consolidated Cores', PhD Thesis, Cardiff University, 2003.
- [4.2] R S Masti, W Desmet, W Heylen, 'On the Influence of Core Laminations upon Power Transformer Noise', Proceedings of ISMA, 2004.
- [4.3] G A V. Sowter, 'Soft magnetic materials for audio transformers: History, production, and applications', Journal of Audio Engineering Society, Vol. 35, No. 10, pages 760-777, 1987.
- [4.4] P Beckley, 'Electrical Steels', European Electrical Steels, Orb Works, 2000.
- [4.5] BS EN 60551:1993, 'Determination of Transformer and Reactor Sound Levels', British Standards, 1993.
- [4.6] W Alexander, 'Principles and Applications of Magnetostriction', Electronics and Power, pages 186 – 190, 1966.
- [4.7] S A Majed and J E Thompson, 'Magnetic Properties of Grain-Oriented Silicon Iron. Part 3 – Magnetostrictive Stress Sensitivity of Simple Assemblies of Strips', Proceedings of the IEE, Vol. 117, No 1, pages 243 – 248, 1970.
- [4.8] A J Moses, 'Measurement of Magnetostriction and Vibration with Regard to Transformer Noise', IEEE Transactions on Magnetics, Vol. Mag 10, No 2, page 154 – 156, 1974.
- [4.9] A J Moses and S M Pegler, 'The Effects of Flexible Bonding of Laminations in a Transformer Core', Journal of Sound and Vibration, Vol. 29 (1), pages 103 – 112, 1973.
- [4.10] J M White and R G McNally, 'Transformer Noise Control', Electrical Engineering Transactions, The Institution of Engineers Australia, pages 32 - 37, 1973.
- [4.11] A W Kelley, 'Measurement of Spacecraft Power Transformer Acoustic Noise', IEEE Transactions of Magnetics, Vol. 26, No 1, pages 281 – 289, 1990.
- [4.12] A J Moses, A Ntatsis, T Kochmann and J Schneider, ' Magnetostriction in Non-oriented steels: General Trends', Journal of Magnetism and Magnetic Materials, Vol. 215-216, pages 669 – 672, 2000.

## CHAPTER 5

### EXPERIMENTAL SETUP

---

#### 5.1. Introduction

The purpose of the magnetostriction measurement is to identify the magnetising frequency at resonance for single strip and stack of magnetic materials used in transformer cores since magnetostriction is a contributing factor to transformer core noise. At resonance, displacement due to magnetostriction of the sample is expected to be at maximum and this will contribute towards the acoustic noise emission of transformer cores. Magnetostriction of grain-oriented 3% Si-Fe samples cut at 0°, 55°, 90° to rolling direction, non-oriented 6.5% Si-Fe samples cut at 0° and 90°, Fe based amorphous sample and Ni-Fe samples of dimensions 300 mm length x 30 mm wide were measured over a magnetising frequency,  $f_{mag}$  range of 0.5 kHz – 8 kHz at sinusoidal flux densities from 0.5 T to 1.0 T.

#### 5.2. The Measurement System

The measurement system has been assembled from instruments, which were individually calibrated, where applicable. The system comprises two parts; the SPLV (see Chapter 3) and magnetising system. The SPLV was purchased from Polytec GmbH and the magnetising system was assembled in the Wolfson Centre. All measurements took place in an acoustically insulated room to help reduce external noise. The laser head and measured object was placed in the acoustic chamber (figure 5.1) and the rest of the system was placed outside the acoustic chamber (figure 5.2) to ensure that noise and vibration from the equipments did not affect the measurement.

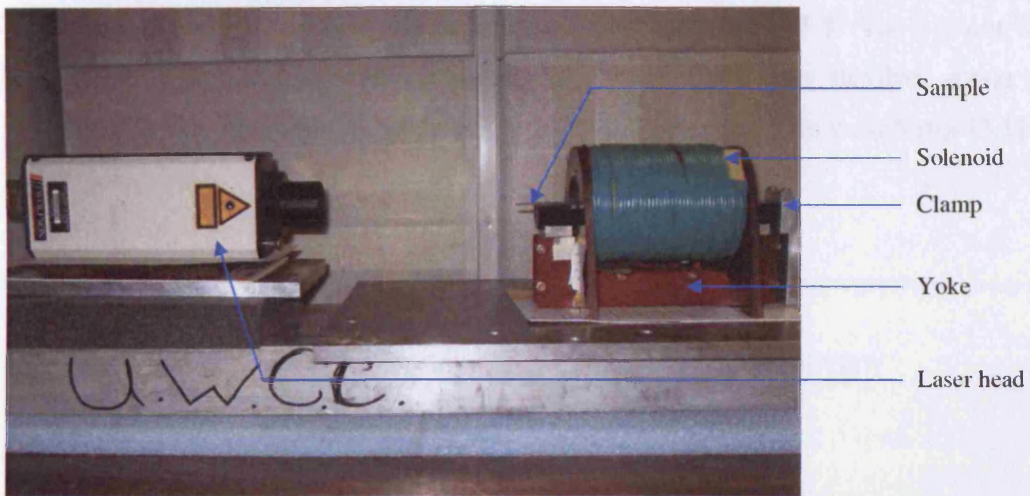


Figure 5.1. Laser head, sample and magnetising setup located in the acoustic chamber

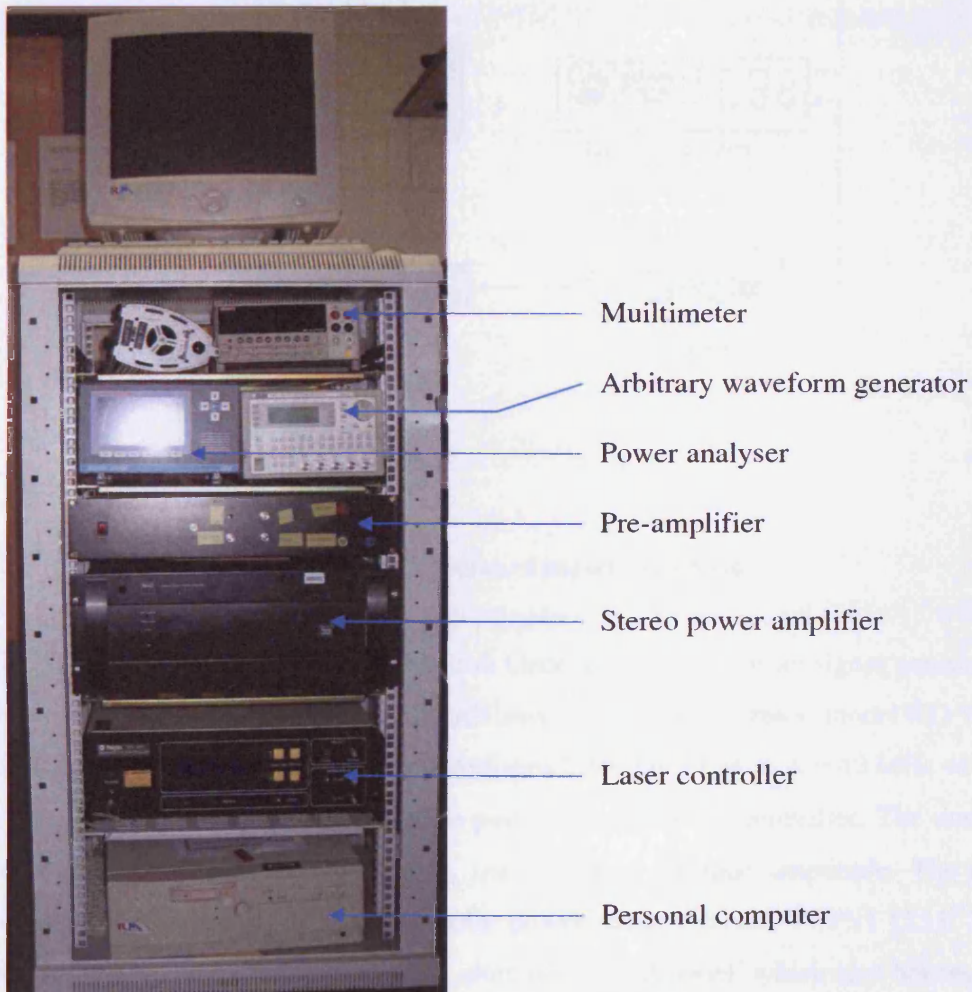


Figure 5.2. Measurement system and laser controller located outside the acoustic chamber

The magnetising system was connected as shown in figure 5.3. The system is comprised of discrete instruments, which makes the system very flexible, giving a wide magnetising frequency range and access to arbitrary excitation waveforms [5.1].

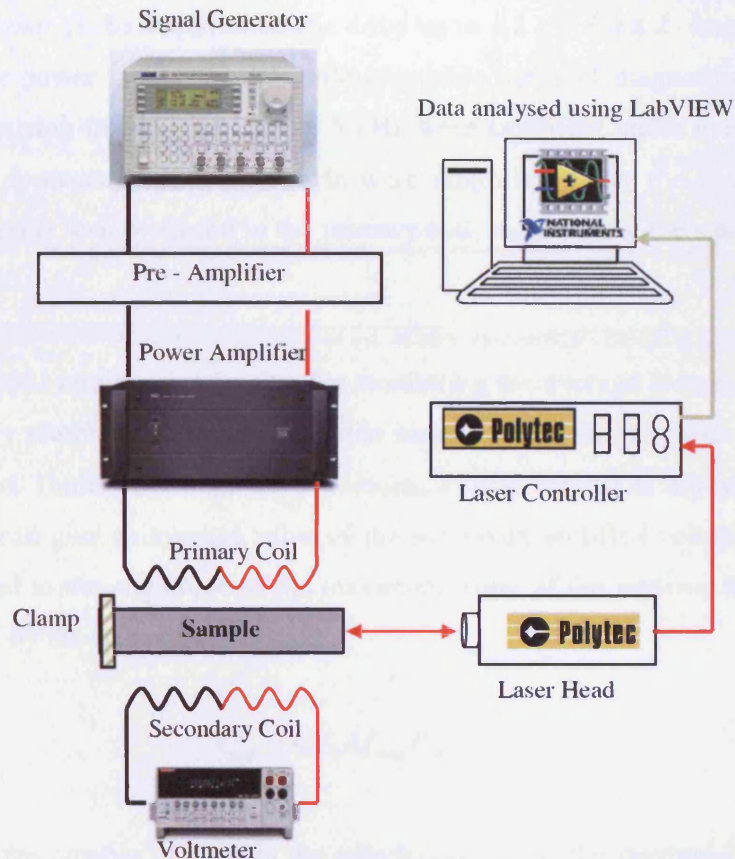


Figure 5.3 Block diagram of magnetising system

The Thurlby Thandar Arbitrary Waveform Generator is used for ac signal generation with amplitude 2 volts peak-peak. The arbitrary waveform generator, model TTi TGA 1241, can generate a wide variety of waveforms between 0.1 mHz and 40 MHz within  $\pm 1\%$  error [5.2]. The ac signal is then passed through a pre-amplifier. The custom made pre-amplifier is used to control the secondary voltage amplitude. The pre-amplifier is powered by a Farnell bipolar power supply, model TOPS1 [5.1]. This circuit is mounted on the reverse of an aluminium front panel, which also houses the potentiometers and switches. The potentiometers are used for the coarse and fine

adjustments of the power amplifier which is connected in parallel with the pre-amplifier.

The power amplifier (NAD: stereo power amplifier 218 THX) has two modes i.e. stereo and mono (bridged) mode with a voltage gain of 29 dB. In the bridged mode the output power of the amplifier can be drive up to 1.2 kW for a 2 ohms load, which is double the power in stereo mode, allowing wide range of magnetising frequency [5.3]. Magnetising frequencies up to 0.5 kHz were amplified under mono mode and magnetising frequencies above 0.5 kHz were amplified under the stereo mode. A Magnetic field is then produced in the primary coil, magnetising the sample from 0.5 kHz to 8 kHz.

A Keithley 2001 multimeter was use for monitoring the average voltage appearing at the secondary search coil wound around the sample where the magnetic flux density,  $B$  is obtained. Under sinusoidal ac conditions, source voltage is adjusted using the pre-amplifier to give an average value of the secondary rectified voltage  $V_{avg}$ , which can be related to the amplitude of the maximum value of the intrinsic magnetic flux density,  $B_{max}$  by the equation:

$$V_{avg} = 4N_2 A f_{mag} B_{max} \quad (5.1)$$

where  $N_2$  is the number of turns in the search coil,  $f_{mag}$  is the magnetising frequency and  $A$  is the cross sectional area of the test sample. Even if the ac flux density does not vary sinusoidally with time,  $B_{max}$  can be calculated from equation 5.1.

The primary core turns were varied from 39 to 1415 turns to maintain a low impedance value when the magnetising frequency was increased. Impedance,  $Z$  can be described as:

$$Z = \sqrt{R^2 + \omega^2 L^2} \quad (5.2)$$

where  $R$  is the resistance of the solenoid,  $\omega = 2\pi f_m$ ,  $f_m$  is the magnetising frequency, and  $L$  is the inductance.  $L$  is directly proportional to  $Z$  and  $L$  is a function of  $N_1^2$ . From equation 5.2, it can be seen that  $Z$  increases with increasing  $f_m$  and  $N_1$ . Therefore, the

appropriate numbers of turns,  $N_l$  were used according to the magnetising frequency,  $f_m$ . The characteristics of the solenoid are given in Table 5.1.

Table 5.1.  
Characteristics of solenoid

$N_l$	Number of turns for solenoid	1415 for magnetising frequencies 0 - 0.5 kHz 39 for magnetising frequencies 0.5 - 8 kHz	-
$l_s$	Length of solenoid	0.17	m
$l_p$	Path length	0.21	m
$d$	Diameter of Solenoid (mean diameter)	0.1	m
$R$	Resistance of Solenoid (at room temperature)	4.6 for 1415 turns 0.3 for 39 turns	$\Omega$
$A_s$	Area of solenoid	$\pi \times r^2 = 0.007853$	$m^2$
$L$	Inductance	$\frac{\mu_0 \mu_r A_s N_l^2}{l_s}$ (for $N_l = 39$ )	mH

The sample was clamped at one end and the laser beam pointed on the other end. The laser beam was focused on an adhesive reflective thin film which was attached to the sample to optimise reflection back to the laser head.

A digital oscilloscope (Yokogawa: model DL708E) was used to display and record data of displacement output from the SPLV, the voltage signal in the search coil,  $V_{ind}$  and voltage induced in the primary coil. The voltage induced in the primary coil was taken as a reference signal for triggering. Averaging of the signals was carried out using the digital oscilloscope which is accomplished by using the following equation:

$$\bar{x} = \frac{1}{n} \sum_{i=1}^n x_i \quad (5.3)$$

where  $\bar{x}$  is the average of each point of the waveform over 10 cycles,  $n$  is the number of cycles,  $x$  is the value of the measured data point and  $i$  is number of iterations.

The digital oscilloscope has plug-in high voltage isolation modules that displays and saves waveforms in 12-bit resolution with 10 MS/s. All displayed waveforms are saved on a floppy disk and data was processed using algorithms embedded in LabVIEW software.

### **5.3. Single Point Laser Doppler Vibrometer – Operating Principle**

The Polytec GmbH SPLV measures the velocity and absolute displacement of the point at the end of the sample in a completely non-contact manner. The SPLV system comprises an optical interferometric laser head OFV-303 (figure 5.1) and an electronics controller unit OFV-3001 (figure 5.2). The controller demodulates the signal from the laser head and provides an analogue voltage proportional to the velocity or displacement of the sample.

The laser head works on the principle of laser interferometry. Figure 5.4 shows the basic optical arrangement found incorporated in the laser head. The light source is a visible and safe, low power HeNe laser source which provides a linear polarized beam. The polarizing beam splitter, BS1 splits the beam into the object beam and the reference beam. The object beam that passes through the polarizing beam splitter BS2 is then focused by the lens on the object and scattered back from there. The polarizing beam splitter BS2 then functions as an optical directional coupler and deflects the object beam to the beam splitter BS3.

The light scattered from the point at the end of the sample experiences a Doppler frequency shift which is proportional to the instantaneous velocity of the sample in the direction of the laser beam. The frequency difference between the object beam and the reference beam shows up as a light intensity modulation, which is an electrical signal in the photo detector and subsequently decoded in the controller. The detector is utilized to minimise noise and drift. In order to distinguish between motion towards and away from the optical head, the Bragg cell<sup>1</sup> in the reference arm of the

---

<sup>1</sup> A Bragg cell is known to be the most reliable, stable and accurate means for frequency shifting of a laser beam.

interferometer is used to introduce a static 40 MHz frequency shift onto the reference beam.

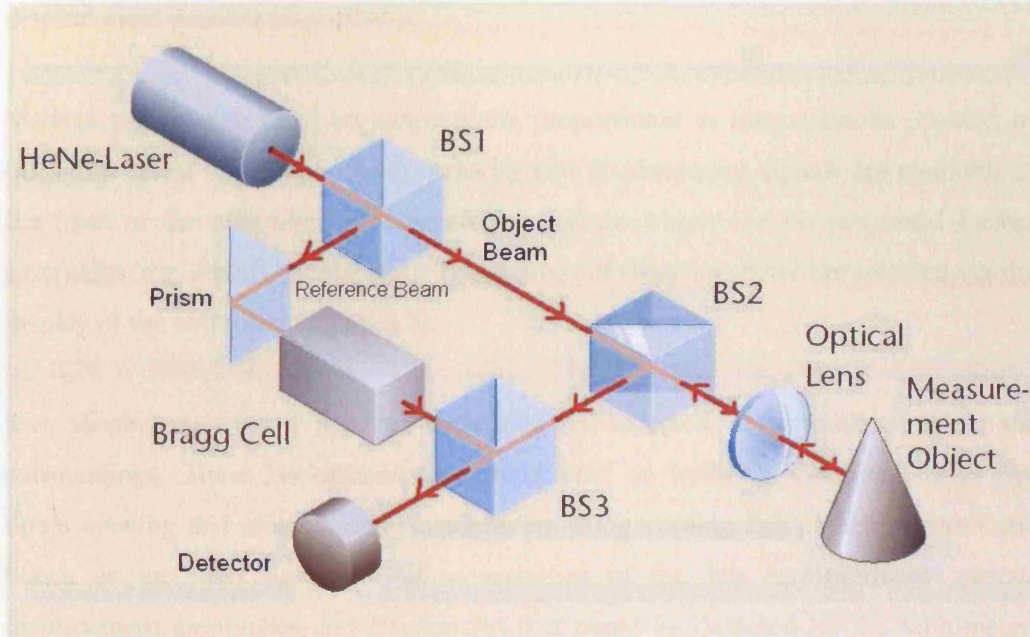


Figure 5.4 Optical configuration of the interferometer in the sensor head OFV-303

Since the optical interference results from coinciding two coherent light beams, the resulting intensity,  $I$  vary with phase difference  $\Delta\phi$  between the two beams according to the following equation:

$$I(\Delta\phi) = \frac{I_{\max}}{2} \cdot (1 + \cos(\Delta\phi)) \quad (5.4)$$

$\Delta\phi$  is a function of path length difference  $\Delta L$  between the two beams according to:

$$\Delta\phi = 2\pi \frac{\Delta L}{\lambda} \quad (5.5)$$

where  $\lambda$  is the laser wavelength. If one of the two beams is scattered back from the object beam, the path difference becomes a function of time  $\Delta L = \Delta L(t)$ . The interference fringe pattern moves on the detector and the displacement of the object can be determined by directionally counting the passing fringe pattern [5.5].



The main function of the controller is to demodulate the radio frequency signal provided by the interferometer in the laser head. The frequency of the signal is the carrier of the velocity information and the optical phase difference is the carrier of the displacement information. The resulting signal is decoded using the velocity and displacement decoder respectively.

Voltage signals generated are respectively proportional to instantaneous position or displacement of the sample. Both, velocity and displacement signals are available at the front of the controller as an analogue voltage which can be processed further externally (e.g. using oscilloscope). The settings of the vibrometer are selected via the display of the controller (figure 5.2).

The displacement or vibration measured is affected by vibration from the surroundings. These background vibrations such as building vibrations from fire doors opening and closing, other equipments using cooling fan placed on the same bench as the laser head and other activities in the lab can produce various displacement amplitudes and frequencies that could be detected by the vibrometer. Therefore, the measurements were carried out in the acoustic room so the background noise can be minimised. Also, to prevent over-ranging, the displacement measurement range was selected taking the background vibrations into consideration.

After setting a given displacement measurement range, a dc offset voltage is present at the output which depends on the distance from the measured point of the sample to the sensor head and on the thermal drift of the interferometer. This dc offset could be removed using the CLEAR input (figure 5.5) of the displacement decoder which allows synchronized resetting of the displacement decoder.



Figure 5.5. Front display panel of the laser controller

## 5.4. Samples

The main aim of the project is to identify resonance modes of materials used in transformer cores in the interest of acoustic noise and vibration produced by core laminations under magnetisation. Therefore, materials widely used as transformer core are chosen as test samples of Epstein dimensions (300 mm x 30mm). Electrical steel samples of different silicon content were cut at different angles to rolling direction. Iron based amorphous ribbon Metglas 2605SC and 48% nickel iron samples were also cut to Epstein dimensions since the measurement setup only catered for single Epstein strip. Table 5.2 shows properties of samples tested where all properties are as given by manufacturer. Other property of the samples such as the Young's modulus of the samples,  $E$  are later measured by stressing each sample and obtaining the slope of a stress-strain curve as explained later in section 5.7.

Table 5.2.

Properties of samples used in the experimental work of the project.

Sample	Cut Direction to rolling direction	Silicon Content (%)	Density, $d$ (kg/m <sup>3</sup> )	Width (mm)	Length, $l$ (mm)	Thickness (mm)
GO	0°	3.0	7650	30.0	305	0.27
GO	55°	3.0	7650	30.0	305	0.27
GO	90°	3.0	7650	30.0	305	0.27
NO	-	3.0	7850	30.0	305	0.50
NO	0°	6.5	7430	30.0	280	0.10
NO	90°	6.5	7430	30.0	280	0.10
Ni-Fe	-	45% Ni content	8071	30.0	305	0.36

Where GO is grain-oriented and NO is non-oriented silicon steel.

## 5.5. Experimental Procedure

The mass of each samples to be tested (table 5.2) were measured to calculate cross sectional area,  $A$ .  $A$  is calculated from the *mass*, *length* and *density* of the sample tested (equation 5.6).

$$A = \frac{\text{mass}}{\text{length} \times \text{density}} \quad (5.6)$$

Each sample was then wound with 10 secondary windings at the centre of the path length,  $l_p$ .  $V_{avg}$  was calculated using equation 5.1 for corresponding  $B_{max}$  at 0.5 T, 0.7 T, 0.9 T and 1.0 T. Measurements were taken only at  $B_{max}$  0.5 T to 1.0 T because no feedback control was used to obtain a sinusoidal waveform of flux density above 1.0 T. A feedback control can be used to control a waveform to maintain a sinusoidal shape within 1% error. For the current magnetising system, only analogue feedback can be used if desired since using a digital feedback will be an extra added cost as well as time consuming process for high frequency measurements. Also, analogue feedback can only be used up to  $B_{max} = 1.5$  T for high frequency measurements. Therefore, no feedback control was utilised and below  $B_{max} = 1.0$  T,  $B$  waveform is fairly sinusoidal within 1% error of the form factor,  $FF$ . Also  $B_{max}$  above 1.0 T is not possible to achieve for high magnetising frequencies since voltage amplitude is limited by the power amplifier for the solenoid configuration that is used. Therefore, only magnetostriction at  $B_{max}$  0.5 T to 1.0 T is measured so that results could be compared for all magnetising frequencies. In a practical situation, well designed transformers saturate only during abnormal operation, if at all. Hence, it is more practical to focus on flux densities below saturation so that sinusoidal flux is maintained.

A sample was placed in the solenoid and clamped as shown in figure 5.6. The reflective film was placed at the centre of the free end of the sample on which the laser spot was focused. The He-Ne laser in the sensor head required a certain period of time to reach optimum stability. Both, the SPLV and the power amplifier were switched on 20 minutes before the first measurements are made to ensure that it is in thermal equilibrium with the surroundings. The sample was then magnetised from 0.05 kHz to 0.45 kHz using  $N_l = 1415$  turns and 0.5 kHz to 8 kHz using  $N_l = 39$  turns.

$B_{max}$  from 0.5 T to 1.0 T was adjusted using potentiometers in pre-amplifier at each magnetising frequency and saved onto a floppy disk using the digital oscilloscope together with measured displacement at each  $B_{max}$ . The saved data was then processed in LabVIEW (see section 5.6).

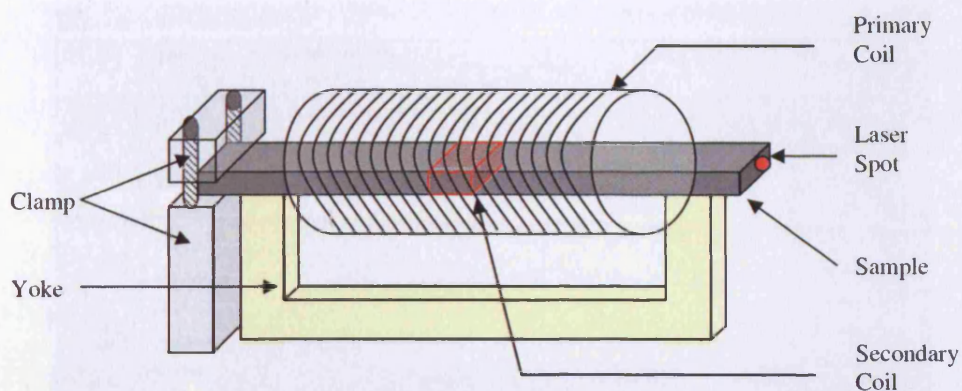


Figure 5.6. Schematic diagram of closed magnetic circuit

### 5.6. Data Analysis using LabVIEW

LabVIEW 7.0™ is a National Instruments' graphic programming language that can be installed on a personal computer (PC) with most operating systems [5.6]. The LabVIEW package is user friendly and allow creating and editing written programs easily since no compilation is required [5.6]. The graphics programming language of LabVIEW requires less programming skill from the operator and the program is easily understandable by any other user. Figure 5.7 shows an example of the LabVIEW program, known as a 'vi' (virtual instrument), used to calculate magnetostriction from displacement and display magnetostriction plot against number of points.

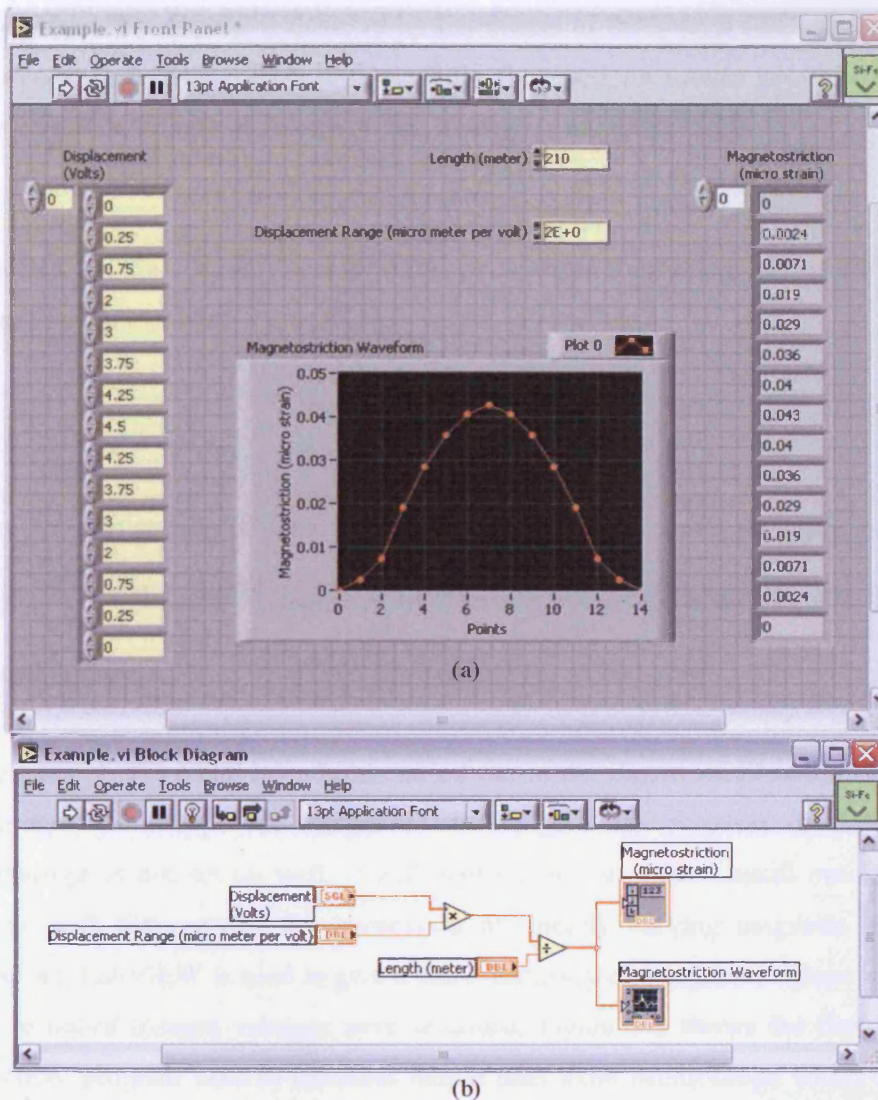


Figure 5.7. Example of LabVIEW Vi (a) front panel view corresponding from program in (b) the block diagram view where program is graphically written

LabVIEW is used to calculate data recorded from the digital oscilloscope. Files saved in Augmented Syntax Diagram (.asd) format from the digital oscilloscope are opened and columns containing displacement and  $V_{ind}$  are extracted individually. Displacement is obtained in  $\mu\text{m}$  as follow:

$$\epsilon = \frac{\Delta l}{l} = \frac{\text{displacement} \times \text{displacement.range}}{l_p} \quad (5.7)$$

where  $l_p$  is the path length presented in table 5.1 and the displacement range is the displacement range set at the laser controller for each magnetising frequency.

The average flux density is detected by the means of the search coil. The changing flux density induces a voltage in the coil ( $V_{ind}$ ) around the sample and this voltage is proportional to the rate of change of flux density as in equation 5.8

$$V_{ind} = -N \cdot A \cdot \frac{dB}{dt} \quad (5.8)$$

Therefore, the flux density waveform can be calculated by integrating the  $V_{ind}$  in the coil as in equation 5.8a:

$$B = -\frac{1}{N \cdot A} \cdot \int V_{ind} dt \quad (5.8a)$$

where  $N$  is the number of turns in the search coil,  $A$  is the cross sectional area of the sample,  $\frac{dB}{dt}$  is the rate of change of flux density with respect to time and  $V_{ind}$  is the induced voltage.

Integration of  $V_{ind}$  could have been carried out in the digital oscilloscope. However, using the oscilloscope for integration would give the problem of drift. If the oscilloscope is not set up well, it will continue to integrate a small out-of-balance voltage with time, giving the impression of linearly varying magnetic induction. Therefore, LabVIEW is used to give a better accuracy of integrated values where any drift or out-of-balance voltages were removed. Figure 5.8 shows the flow chart of LabVIEW program used to calculate output data from oscilloscope where table 5.3 shows a typical data file recorded from the oscilloscope and table 5.4 is the calculated LabVIEW data output obtained from saved spreadsheet file. Once all data have been processed in LabVIEW, results are then analysed and plotted using Microsoft Excel.

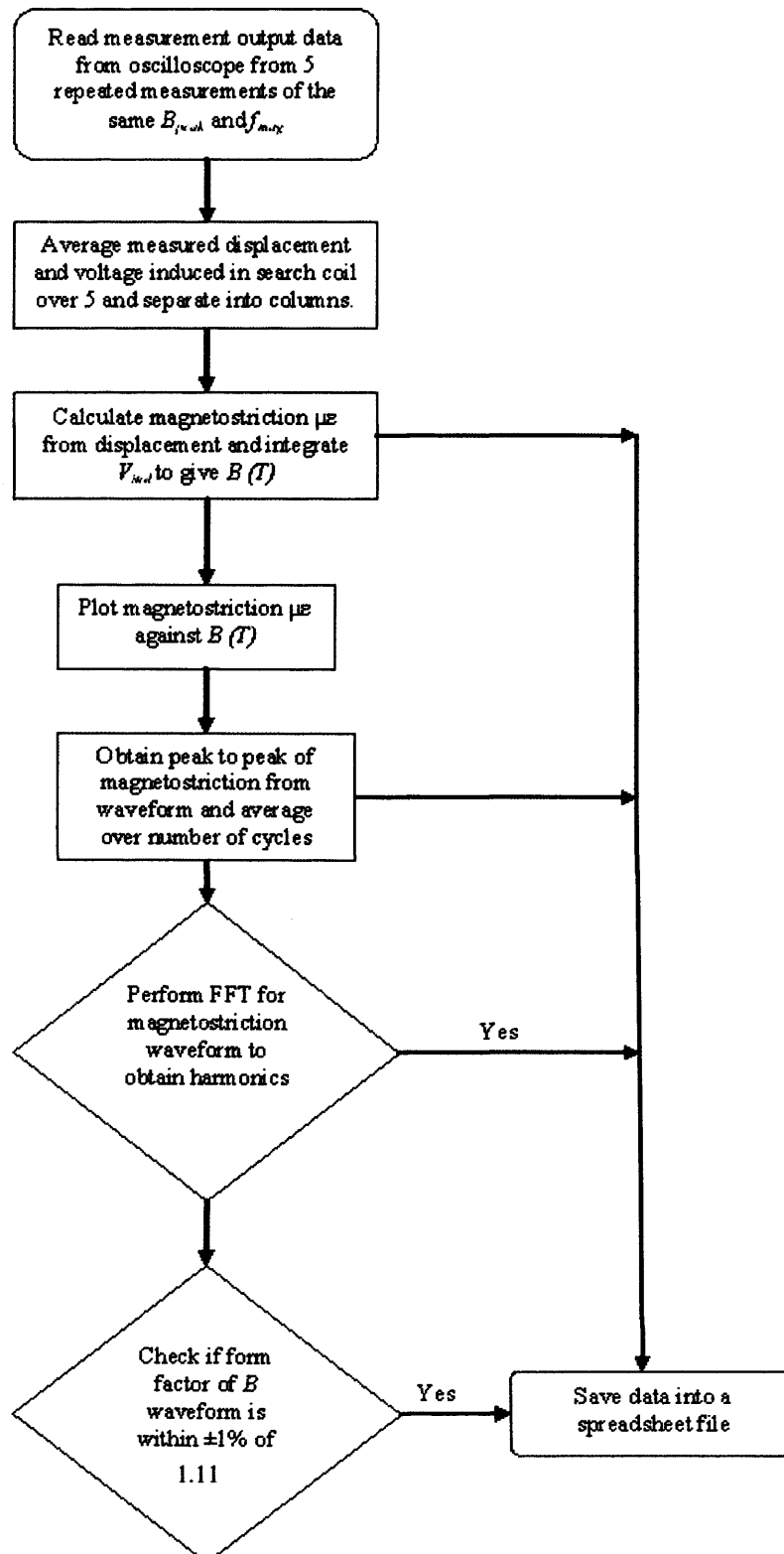


Figure 5.8 Flow chart for calculation carried out in LabVIEW

Table 5.3.

Typical data recorded from oscilloscope which is processed in LabVIEW.

Model	DL700			
BlockNumber	1			
TraceName	TRIGGER	CURRENT	DISPLACEMENT	V <sub>IND</sub>
BlockSize	1002	1002	1002	1002
Vertical Unit	Volts	Volts	Volts	Volts
SampleRate	5.00E+05	5.00E+05	5.00E+05	5.00E+05
Horizontal Unit	s	s	s	s
DisplayBlockSize	1002	1002	1002	1002
PhaseShift	0	0	0	0
Date	06/05/2005			
Time	15:54:52			
	-5.53E-01	-1.53E-02	-7.00E-04	1.83E-01
	-5.88E-01	8.00E-03	-7.55E-04	2.42E-01
	-6.21E-01	3.15E-02	-8.46E-04	3.02E-01
	.	.	.	.
	.	.	.	.
	.	.	.	.

Table 5.4.

Typical data output from LabVIEW which is saved into a spreadsheet file.

B (T)	$\lambda$ ( $\mu\epsilon$ )	Harmonics	H (A/m)	$B_{max}$ (T)	$\lambda$ ( $\mu\epsilon$ )	Form
Waveform	Waveform				Peak to peak	Factor of B (T)
For B <sub>peak</sub> = 0.5T				For all $B_{max}$ measured at each $f_{mag}$		
-0.401	0.003	0.031	-7.567	0.5	0.032	1.112
-0.395	0.003	0.001	1.448	0.7	0.079	1.101
-0.389	0.002	0	10.54	0.9	0.137	1.101
-0.381	0.001	0	19.594	1.0	0.192	1.172
-0.371	0	0	28.725	0	0	0
-0.36	0	0	37.817	0	0	0
-0.348	0.001	0	46.329	0	0	0
-0.334	0.002	0.001	55.228	0	0	0
-0.319	0.002	0.001	63.353	0	0	0
.	.	.	.	.	.	.
.	.	.	.	.	.	.
.	.	.	.	.	.	.
.	.	.	.	.	.	.

### 5.7. Young’s Modulus Tests

Young’s modulus,  $E$  of each sample in table 5.2 was measured using the experimental setup shown in figure 5.9. A Shimadzu Autograph AG-IS universal testing system (figure 5.9 b) was used to apply tensile stress on the sample. The test system is connected to the PC for controlling the amount of load applied when stressing the samples using a software called Trapezium and all measurement parameters such as



cross-sectional area of the sample and maximum limit of load to be applied was set to 1 kN.

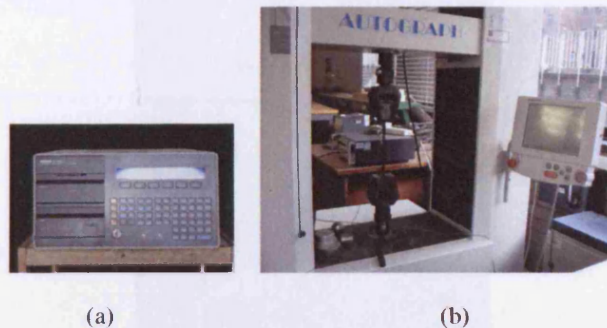


Figure 5.9 Diagram of experimental setup for Young's Modulus test (a) data acquisition system where strain gauges are connected to (b) test system where the samples were stressed.

A  $120 \Omega$  strain gauge with gauge factor 2.1 was attached at the centre of the sample (figure 5.10) and the strain gauge leads were connected to Solartron Schlumberger 3135D Data Acquisition System. The data acquisition system is also connected to the test system so that both strain and applied load values can be monitored at the same time. The data acquisition system calculates the strain values by dividing the displacement of the sample when stress is applied with the distance between the clamping jaws instead of the sample length. The distance between the clamps is about 5 mm longer than the sample length because of the rubber padding around the clamps. This error in length of the sample used when calculating strain is adds to the error between calculated resonance frequencies and measured values shown later in section 5.11.



Figure 5.10. Test sample clamped at both ends having strain gauges attached at the centre of the sample.

Each sample was clamped at both end and tensile load was applied continuously while the data acquisition system prints the load and corresponding strain values at every 2 seconds. The test system is then stopped manually before reaching the maximum limit of 1 kN. The load values were then divided by cross-sectional area of the sample to obtain stress in  $\text{N/m}^2$  and plotted against corresponding strain using Microsoft Excel. The stress-strain test was carried out 5 times for each sample and Young's Modulus of each sample was obtained from the slope of the average stress-strain curve.

### 5.8. 3-Phase Transformer Core

A 3-phase, 3-limb laminated transformer core was constructed and acoustic noise and displacement of the 3-phase transformer were analysed under pulse-width modulation, PWM and sinusoidal excitations. subjected to PWM voltage excitation are becoming more common in industrial applications and renewable energy supply systems and very limited research work has been reported on acoustic noise for transformer core under PWM voltage excitation. Also, a PWM voltage signal would contain higher harmonic components which could coincide with the resonance frequency of the core. Displacement and acoustic noise experiment on 3-phase transformer core were carried out to assess wider implications of mechanical resonance predictions for transformer cores.

The 3-phase transformer core was excited under PWM conditions with switching frequency in the range 1 kHz - 3 kHz and different modulation indices at  $f_{mag} = 0.05$  kHz to 0.1 kHz;  $B_{max}$  1.3 T - 1.5 T and the corresponding variation of displacement and acoustic noise was measured. Under sinusoidal excitation, the 3-phase transformer core was magnetised at 50 Hz;  $B_{max} = 1.3$  T and 1.5 T.

### 5.8.1. Theoretical Basis

A PWM voltage waveform was obtained by comparing a reference voltage waveform (modulating signal, usually sinusoidal) with a carrier voltage waveform (usually triangular). That is, the PWM waveform is a synthesis of a reference voltage waveform (amplitude  $A_{ref}$ , frequency  $f$ ) and carrier voltage waveform (amplitude  $A_c$ , frequency  $f_c$ ) at different frequencies. The modulation index,  $m_i$  and frequency ratio  $m_f$  are given by (5.9) and (5.10) respectively.

$$m_i = \frac{A_{ref}}{A_c} \quad (5.9)$$

$$m_f = \frac{f_c}{f} \quad (5.10)$$

The PWM output voltage waveform synthesis is illustrated in figure 5.11.

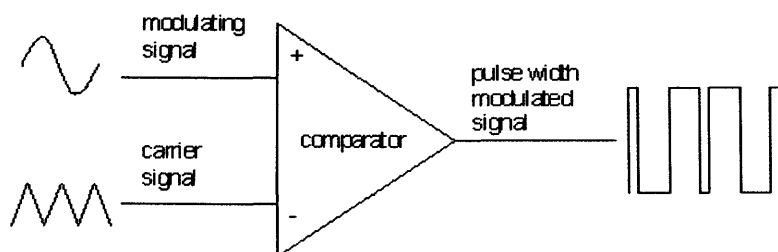


Figure 5.11. Generation of PWM voltage waveform

The three significant parameters which determine the performance of PWM inverters are modulation index  $m_i$ , carrier index (frequency ratio)  $m_f$  and the frequency of the

carrier voltage waveform or switching frequency  $f_s$ .

The acoustic Sound Pressure Level ( $SPL$ ) is given by:

$$SPL(dB) = 20 \log_{10} \frac{n_{mea}}{n_{ref}} \quad (5.11)$$

where  $n_{mea}$  is the measured pressure level,  $n_{ref}$  is the reference pressure level. The scale in equation 5.11 uses the hearing threshold of  $20 \mu\text{Pa}$  as the reference level of 0 dB.

### 5.8.2. Experimental Setup for 3-Phase Transformer Core

A 3-phase, 3-limb laminated transformer core was assembled from 200 layers of 0.27 mm thick grain-oriented 3% Si steel (UNISIL M089-27N). The density and resistivity of the core material were  $7650 \text{ kg/m}^3$  and  $46 \mu\Omega\text{cm}$  respectively. The core mass was 96.1 kg in weight. The overall dimensions as well as position of primary and secondary coil windings are shown in figure 5.12.

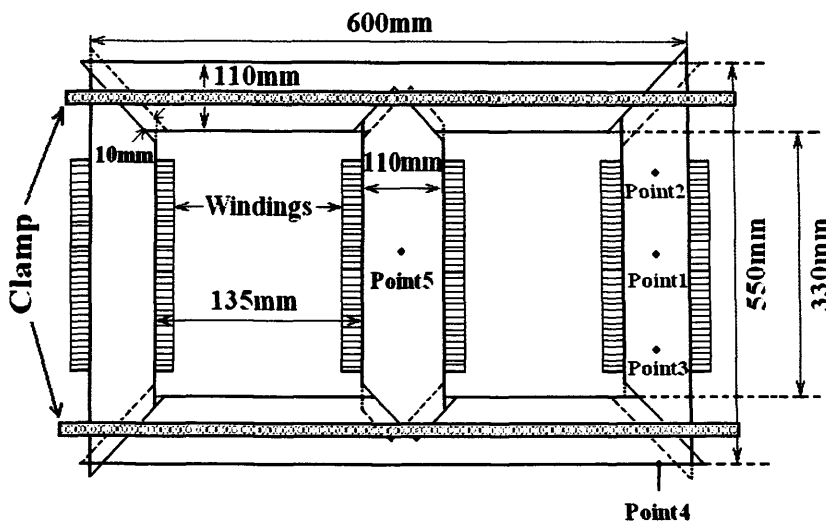


Figure 5.12. Layout of experimental 3-phase transformer core showing positions of measuring points

Figure 5.13. shows the magnetizing circuit of the core assembly for (a) PWM excitation and (b) sinusoidal excitation. A 3-phase PWM inverter (Toshiba inverter

TOSVERT VF-A3) was connected to three independent variacs, which supplied the three 50-turn primary windings of the delta-wound transformer core under no-load condition, and were used to keep the three winding voltages balanced. The voltage applied to the primary windings, the induced voltages in the 50-turn secondary windings, the sound pressure level was recorded using a microphone (Brüel & Kjaer type 4231) and vibration signal from SPLV were recorded by a digital oscilloscope (YOKOGAWA DL716 - 16CH Digital Scope). The digital oscilloscope has plug-in high voltage isolation modules, which display and save waveforms in 12-bit resolution at 10 MS/s. All displayed waveforms were saved in a floppy disk and data was analyzed using algorithms embedded in National Instrument LabVIEW software.

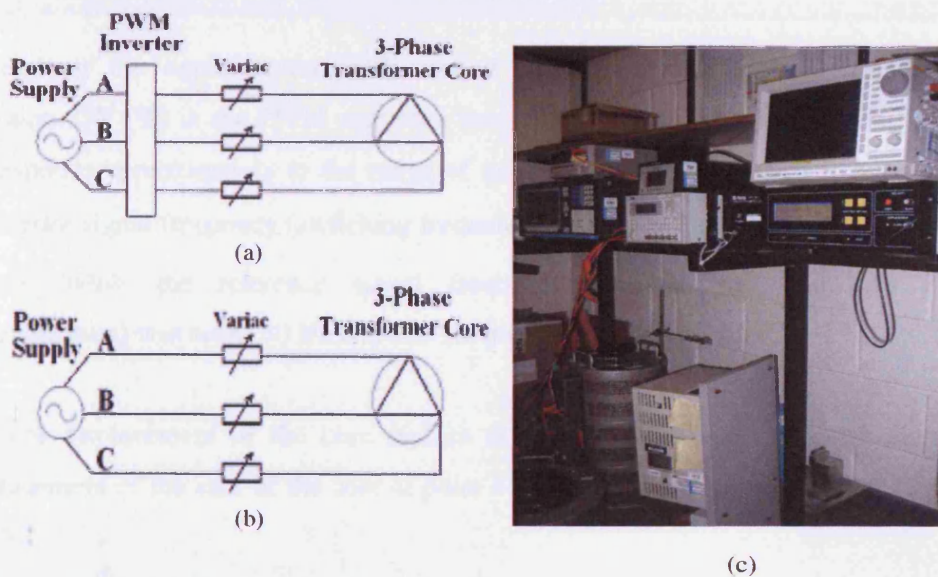


Figure 5.13. Magnetizing circuit of the 3-phase transformer core (a) under PWM excitation (b) under sinusoidal excitation (c) magnetising system

The transformer core was placed horizontally on a table in an acoustic chamber. The magnetizing system was located in a separate measurement room. Acoustic noise and vibration were measured using the setup shown in figure 5.14 where amplifier is placed in the anechoic chamber and oscilloscope placed outside the anechoic chamber. The microphone was placed 0.5 m vertically above the core and moved from points 1 to 5 in turn and moved between measurements. The vibration of the core surface at the same points were measured with the SPLV.

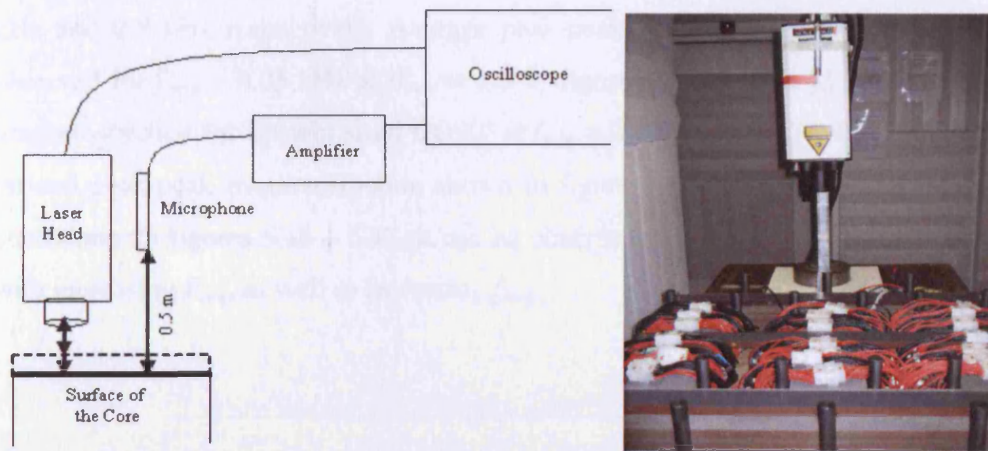


Figure 5.14. Vibration and acoustic noise measurement setup placed in an anechoic chamber

Throughout the experimental work carried out, the Output Voltage Regulation Function,  $OV$  (%) in the PWM converter was varied in the range 40% - 90%, which corresponds approximately to the range of modulation indices 0.5 – 1.2. Moreover, the carrier signal frequency (switching frequency,  $f_s$ ) was varied in the range 1 kHz - 3 kHz while the reference signal frequency (fundamental frequency  $f$  of magnetization) was set to 50 Hz and 100 Hz respectively.

Vertical displacement of the core surface at points 1, 2, 3 and 5 and horizontal displacement of the side of the core at point 4 (figure 5.12) were measured using the SPLV.

### 5.9. Preliminary Tests

Preliminary tests were carried out with the measurement system when the system was checked to be functioning correctly. These preliminary tests were also carried out to compare peak-peak magnetostriction of grain-oriented Si-Fe to those typical values suggested in [5.7 – 5.8]. Single Epstein strip of  $GO90^\circ$  was chosen for this test because magnetostriction in  $GO90^\circ$  is 10 times higher than magnetostriction in  $GO0^\circ$ . The  $GO90^\circ$  was clamped at one end and vibration of the free end was measured from  $f_{mag} = 0.05$  kHz to 0.5 kHz at  $B_{max} = 0.7$  T to 1.0 T. Figures 5.15 – 5.17 show magnetostriction against flux density of  $GO90^\circ$  sample magnetised at 0.05 kHz, 0.1

kHz and 0.5 kHz respectively. Average peak-peak magnetostriction about  $4 \mu\epsilon$  is observed for  $f_{mag} = 0.05$  kHz at  $B_{max} = 1.0$  T (figure 5.15). Moses [5.7] suggest that magnetostriction for Epstein sized GO90° at  $f_{mag} = 0.1$  kHz at  $B_{max} = 1.1$  T is about  $8 \mu\epsilon$  and peak-peak magnetostriction shown in figure 5.16 is  $8.6 \mu\epsilon$  under the same conditions. In figures 5.15 – 5.17, it can be observed that magnetostriction increases with increasing  $B_{max}$  as well as increasing  $f_{mag}$ .

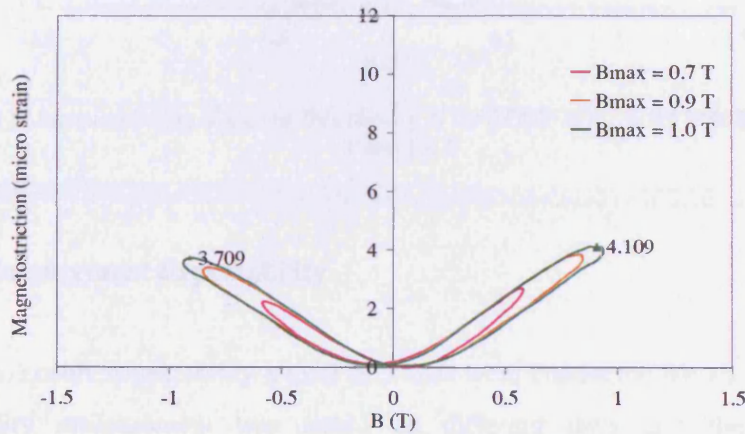


Figure 5.15 Magnetostriction,  $\lambda$  against flux density,  $B$  for GO90° at  $f_{mag} = 0.05$  kHz  $B_{max} = 0.7$  T, 0.9 T and 1.0 T

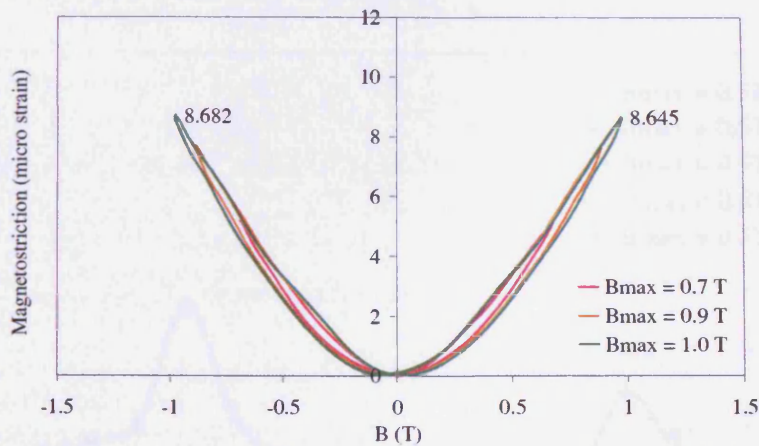


Figure 5.16 Magnetostriction,  $\lambda$  against flux density,  $B$  for GO90° at  $f_{mag} = 0.1$  kHz  $B_{max} = 0.7$  T, 0.9 T and 1.0 T

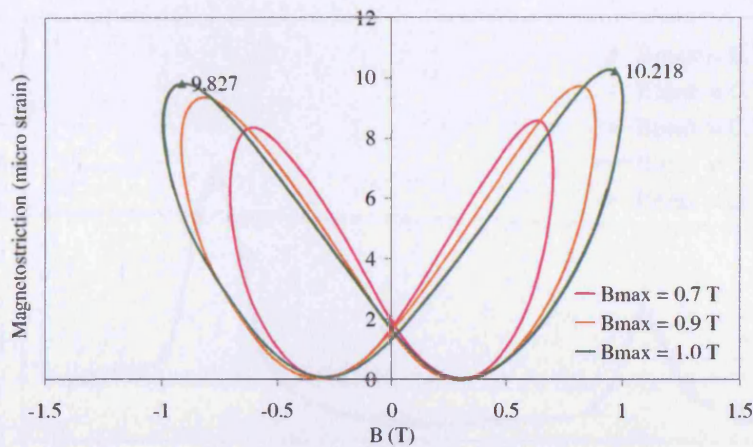


Figure 5.17 Magnetostriction,  $\lambda$  against flux density,  $B$  for  $\text{GO}90^\circ$  at  $f_{\text{mag}} = 0.5$  kHz  $B_{\text{max}} = 0.7$  T, 0.9 T and 1.0 T

### 5.10. Measurement Repeatability

In order to ensure repeatability a total of 5 tests were conducted for all samples. Each repeatability measurement was tested on different days and the sample was demagnetised after every measurement. Results presented in chapter 6 are shown as the average of 5 repeated measurements. Figures 5.18 – 5.21 show peak-peak magnetostriction of  $\text{GO}90^\circ$  against magnetising frequency,  $f_{\text{mag}}$  of 5 repeated tests at  $B_{\text{max}} = 0.5$  T, 0.7T, 0.9 T and 1.0 T respectively.

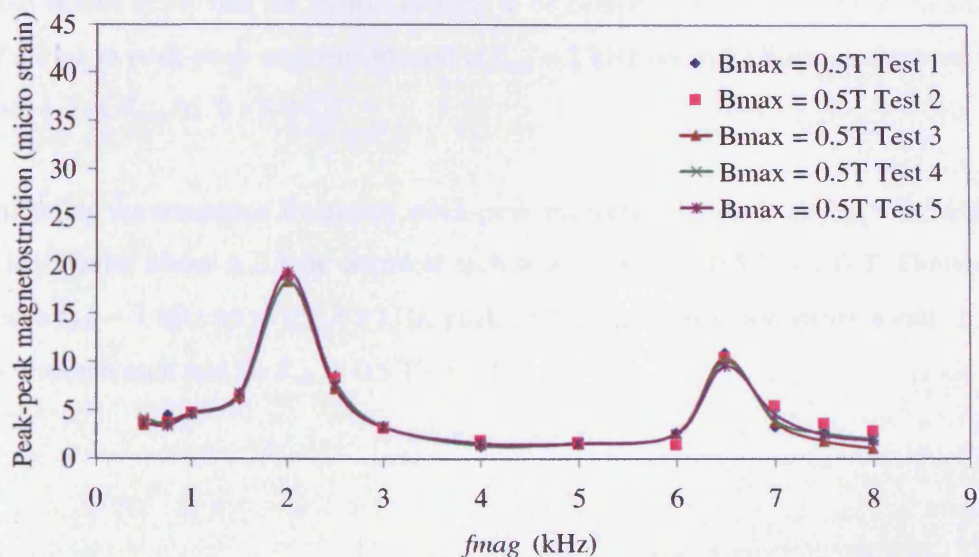


Figure 5.18 Repeatability of peak-peak magnetostriction,  $\lambda_{\text{pp}}$  against magnetising frequency,  $f_{\text{mag}}$  for  $\text{GO}90^\circ$  at  $B_{\text{max}} = 0.5$  T.



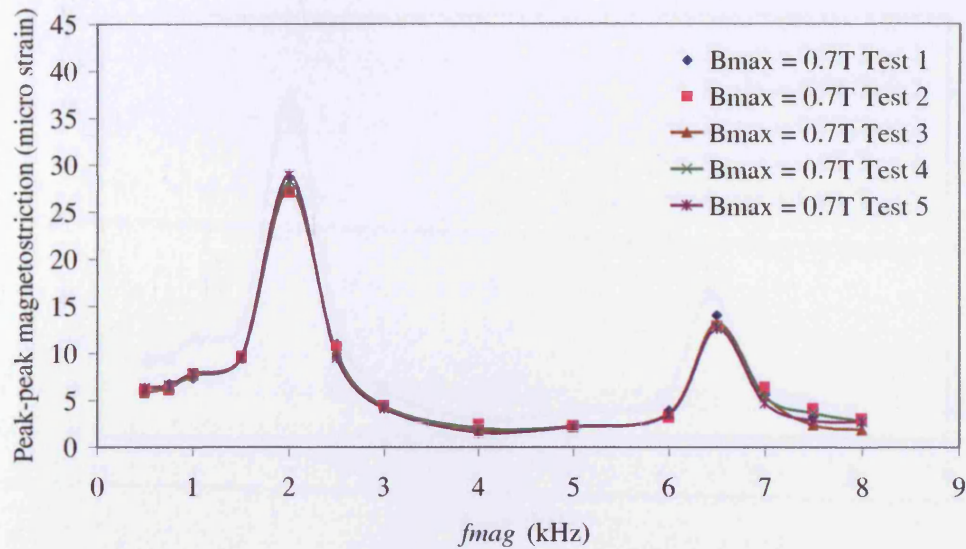


Figure 5.19 Repeatability of peak-peak magnetostriction,  $\lambda_{pp}$  against magnetising frequency,  $f_{mag}$  for GO90° at  $B_{max} = 0.7$  T.

For  $f_{mag} = 2$  kHz (figure 5.18), peak-peak magnetostriction is observed to vary from 18.8  $\mu\epsilon$  to 19.3  $\mu\epsilon$ . From equation 3.9 (Chapter 3: section 3.3.1), the sharp peak at  $f_{mag} = 2$  kHz correspond as the fundamental resonance frequency and  $f_{mag} = 6.5$  kHz as the 3<sup>rd</sup> harmonic of the resonance frequency of GO90°: which will be discussed further in chapter 6. It is known that at resonance point, an un-damped structure or a sample in this case will be vibrating at its maximum displacement. However, in this case, results imply that the sample appears to be damped (see figure 3.5). A variation of  $\pm 3$   $\mu\epsilon$  in peak-peak magnetostriction at  $f_{mag} = 2$  kHz and 6.5 kHz was observed for tests 1-5 at  $B_{max}$  0.5 T – 1.0 T.

Excluding the resonance frequency, peak-peak magnetostriction from  $f_{mag} = 0.5$  kHz - 7 kHz varies about  $\pm 0.5$   $\mu\epsilon$  between each test for  $B_{max} = 0.5$  T - 1.0 T. However, above  $f_{mag} = 7$  kHz up to  $f_{mag} = 8$  kHz, peak-peak magnetostriction varies about  $\pm 2.5$   $\mu\epsilon$  between each test for  $B_{max} = 0.5$  T - 1.0 T.

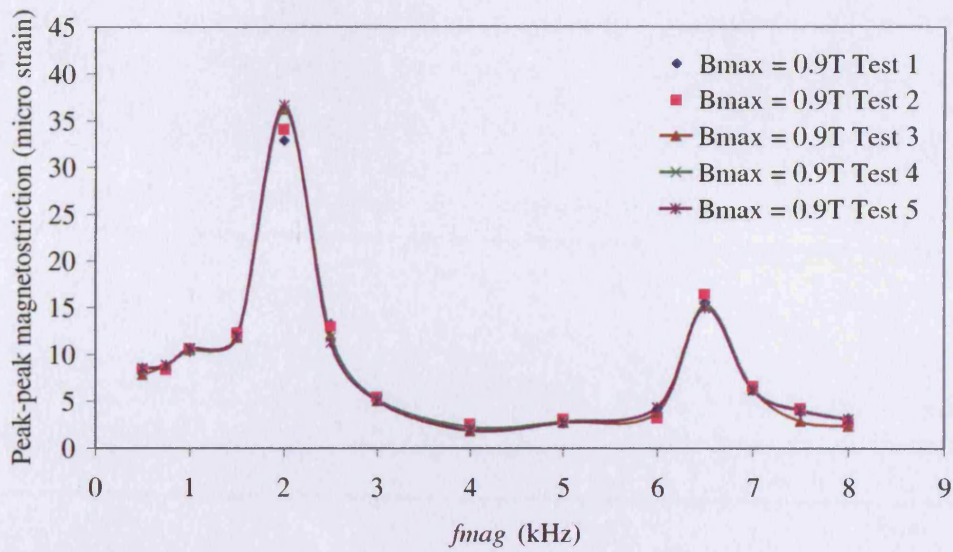


Figure 5.20 Repeatability of peak-peak magnetostriction,  $\lambda_{pp}$  against magnetising frequency,  $f_{mag}$  for GO90° at  $B_{max} = 0.9$  T.

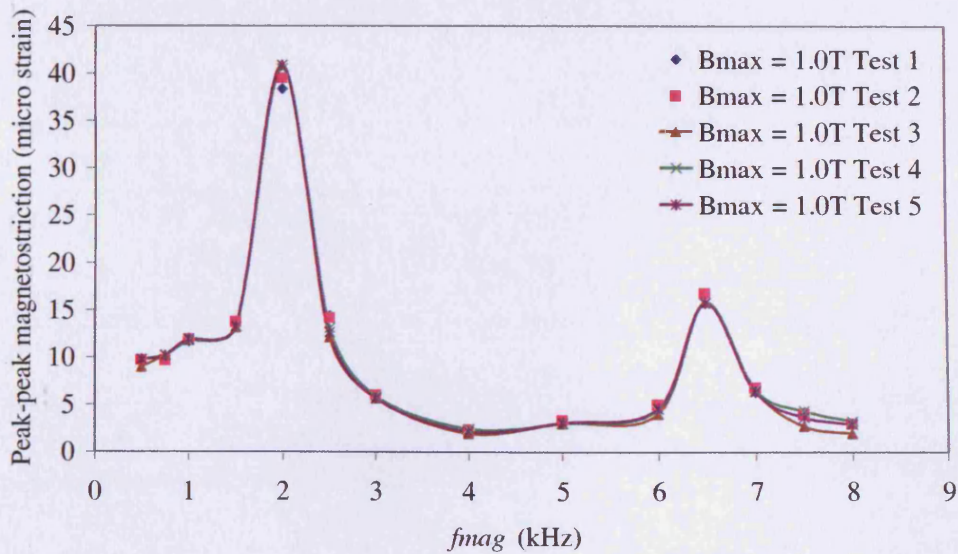


Figure 5.21 Repeatability of peak-peak magnetostriction,  $\lambda_{pp}$  against magnetising frequency,  $f_{mag}$  for GO90° at  $B_{max} = 1.0$  T.

### 5.11. Uncertainty of Calculated Resonance Frequency $f_m$

Uncertainty is needed to be calculated for measured resonance frequency  $f_m$  of each sample and calculated values using equation 3.9 separately. All measurements were repeated 5 times on seven samples, GO90°, GO0°, GO55°, 3% Si NO, 6.5% Si NO0°,

6.5% NO90° and 45% Ni-Fe. The samples were magnetised from  $f_{mag}$  of 0.5 kHz to 8 kHz in steps of 0.5 kHz at  $B_{max}$  0.5 T to 1.0 T.

According to British Measurement and Testing Association [5.9], uncertainties can be considered separately concerning their random and systematic contribution, but both of them should be combined and treated as if they were equivalent.

The estimated standard deviation (in percentage),  $S$ , of the measured and calculated resonance frequency  $f_m$  were calculated from equation 5.12.

$$S = \frac{1}{x} \cdot \sqrt{\frac{\sum_{i=1}^{n_u} (x_i - \bar{x})^2}{(n_u - 1)}} \times 100 \quad (5.12)$$

where,  $S$  is the estimated standard deviation (in percentage),  $x_i$  is the measured value,  $\bar{x}$  is the mean of the measured value,  $n_u$  is the number of measurements made. From  $S$ , the estimated standard uncertainty,  $u$ , of the mean was calculated from equation 5.13.

$$u = \frac{S}{\sqrt{n_u}} \quad (5.13)$$

The  $S$  where measurements are repeated, were assumed to be a normal distribution with a certain level of confidence. Because the measurements were repeated only five times the total uncertainty can be underestimated. For that reason the t-student factor is used. If the confidence level is 95%, equivalent  $k = 2$ . The t-student factor corresponding to five measurements is given as 1.44 for coverage factor  $k = 2$  [5.9] (See Appendix II). Therefore, the extended uncertainty,  $U_T$  can be calculated from:

$$U_T = t \times k \times u \quad (5.14)$$

Then the total uncertainty of the system is calculated by all the uncertainties of individual components using equation 5.15.

$$U_{TOT} = \sqrt{U_1^2 + U_2^2 + \dots} \quad (5.15)$$

Table 5.5 shows the calculation of total uncertainty using equation 5.15 for the calculated resonance frequency. Percentage uncertainties of calibration of ruler, length, strain measurement system and stress system are as given in manufacturer's handbook. Total uncertainty of the calculated resonance frequency was found to be  $\pm 8.91\%$ . This means that the actual theoretically calculated resonance frequencies using equation 3.9 for the Epstein sized samples could lie between  $\pm 8.91\%$  of the calculated value with the confidence level of 95%. Therefore, 5% of the calculated value can deviate by more than  $\pm 8.91\%$ .

Table 5.5.

Calculation of total uncertainty for calculated resonance frequency  $f_m$  showing factors contributing to the total uncertainty

Source of Uncertainty	Uncertainty	x t x k
	%	2.88
<i>Sample Length Measurement</i>		
Calibration of ruler	0.20	0.20
Repeatability of length measurement	0.10	0.29
<i>Young's Modulus Measurement</i>		
Length	0.20	0.20
Repeatability of length measurement	0.10	0.29
Strain system	1.50	1.50
Stress system	1.50	1.50
Repeatability of Young's Mod measurement	3.00	8.64
	<b>Total uncertainty</b>	<b>8.91</b>

Measurements were made at discrete values of magnetising frequencies  $f_{mag}$  and these factors are major contributors to uncertainty for measured resonance frequency  $f_m$ . Magnetostriction of Epstein strip samples were measured at intervals of  $f_{mag} = 0.5$  kHz and 0.25 kHz. Hence, the uncertainty of measured resonance frequency will be individually discussed in chapter 7 according to the measurement intervals used for the particular sample.

The calibration of the arbitrary waveform generator that is given in the manufacturer's handbook also adds a minor contribution (0.01%) to the uncertainty of the measured value. However, the uncertainty from  $f_{mag}$  intervals were much larger compared to the

calibration factor of the arbitrary waveform generator. Hence, the 0.01 % contribution can be negligible.

---

**References**

- [5.1] P Anderson, J Leicht, A J Moses, 'Non-Standard Magnetic Measurement under Controlled Conditions', UK Magnetic Society Seminar, Warwick, 2000.
- [5.2] Synthesised Arbitrary Waveform Generator (TGA 1230) User Manual 48591-0510 Issue 1, Thurlby Thandar Instruments Ltd. Cambridgeshire UK.
- [5.3] Stereo Power Amplifier (218THX) User Manual, NAD Electronics Ltd., London, UK
- [5.4] N F Astbury, 'Industrial Magnetic Testing', Institute of Physics, London, 1952.
- [5.5] Polytec GmbH, 'Laser Doppler Vibrometer – User Manual'
- [5.6] LabVIEW User Manual, Software Revision Version 7.0 7.1, Part No. 320999E-01, National Instruments, 2003
- [5.7] A J Moses, 'Electrical Steels: Past, Present and Future Development', IEE Proceedings A: Science, Measurement and Technology, Vol 137. Issue 5, pages 233-245, 1990.
- [5.8] A J Moses, 'The Effects of Various Heat Treatments and Magnetic Annealing on the Magnetic Properties of Grain-oriented Silicon-iron', PhD Thesis, 1970.
- [5.9] K Birch, 'Estimating uncertainties in testing', Measurement good practice guide n36, British Measurement and Testing Association, 2001.

---

## CHAPTER 6

### EXPERIMENTAL RESULTS

---

#### 6.1. Introduction

The magnetisation induced mechanical resonance measurements were mainly carried out on Epstein strips of grain-oriented and non-oriented electrical steels. The sample of grain-oriented electrical steel comprised of two types of 0.27 mm thick materials with 3% Si. The samples of non-oriented electrical steel comprised two types of 0.1 mm thick material with 6.5% Si and one 0.5 mm thick material with 3% Si. In addition, samples of 0.36 mm thick 45% Ni-Fe and Fe based 0.018 mm thick amorphous Metglas 2605SC were tested. These samples were excited with sinusoidal voltage waveforms from a range of  $f_{mag} = 0.5$  kHz to 8 kHz at  $B_{peak} = 0.3$  T to 1.0 T. Measurements were focused only on flux densities below saturation in order to maintain sinusoidal flux waveform since in practice, well designed transformers saturate only during abnormal operation, if at all. Results presented in this chapter will be followed by discussion and analysis in chapter 7.

#### 6.2. Magnetisation induced mechanical resonance of GO90°

GO90° refers to strips of grain-oriented electrical steel cut at 90° to the rolling direction. A single Epstein strip of GO90° was used to measure magnetostriction at  $f_{mag} = 0.5$  kHz to 8 kHz at  $B_{peak} = 0.5$  T to 1.0 T to obtain the magnetisation induced mechanical resonance (figure 6.1). In order to confirm the predicted mechanical resonance, the magnetostriction of same sample was measured at  $f_{mag} = 0.5$  kHz to 8 kHz at  $H = 200, 240$  and 320 A/m as described in section 6.2.1. The temperature rise of the sample during magnetisation was also measured at  $f_{mag} = 0.5$  kHz to 4 kHz for a period of 300 seconds magnetizing time as described in section 6.2.2. A stack of 5 strips GO90° from the same batch as the single strip of GO90° were used to measure magnetostriction at  $f_{mag} = 0.5$  kHz to 8 kHz at  $B_{peak} = 0.5$  T and 0.7 T and at  $f_{mag} = 0.5$  kHz to 6.5 kHz at  $B_{peak} = 0.9$  T and 1.0 T, results of which will be shown later in section 6.2.3.

Figure 6.1 shows variation in magnitude of peak-to-peak magnetostriction with magnetising frequency for GO90° at various values of  $B_{peak}$ . Resonance peaks were found in the material at 2 kHz resonant point 6.5 kHz.

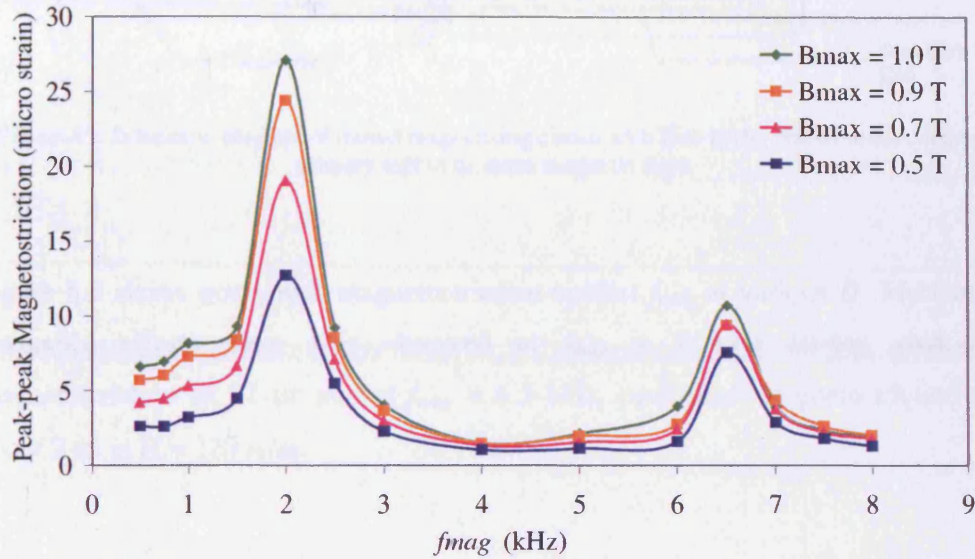


Figure 6.1. Peak-peak magnetostriction,  $\lambda_{pp}$  against magnetising frequency,  $f_{mag}$  for GO90° at  $B_{max}$  = 0.5 T, 0.7 T, 0.9 T and 1.0 T.

### 6.2.1. Magnetostriction versus Magnetising Frequency at Various Magnetic Fields

Figure 6.2 shows schematic diagram of magnetising setup to measure magnetostriction of single strip of GO90° against  $f_{mag}$  at various magnetic field,  $H$  (A/m). A LakeShore Gaussmeter (Model: 450) was used to measure  $H$ . The axial hall probe (Model: H07858) was placed at the centre of the primary coil and attached on the sample with an adhesive tape. Sinusoidal  $H$  was increased to rms of 200, 240 and 320 A/m for each  $f_{mag}$  and magnetostriction was measured.



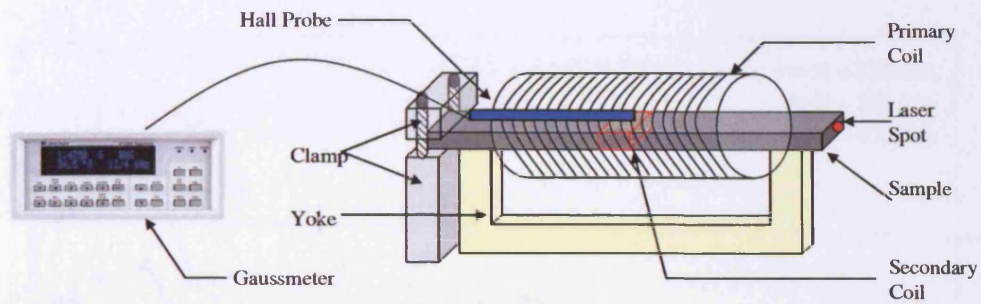


Figure 6.2. Schematic diagram of closed magnetising circuit with Hall probe placed in the centre of primary coil to measure magnetic field.

Figure 6.3 shows peak-peak magnetostriction against  $f_{mag}$  at various  $H$ . Mechanical resonance effects were also observed at  $f_{mag} = 2$  kHz having peak-peak magnetostriction of  $12 \mu\epsilon$  and at  $f_{mag} = 6.5$  kHz, peak-peak magnetostriction was about  $2 \mu\epsilon$  at  $H = 320$  A/m.

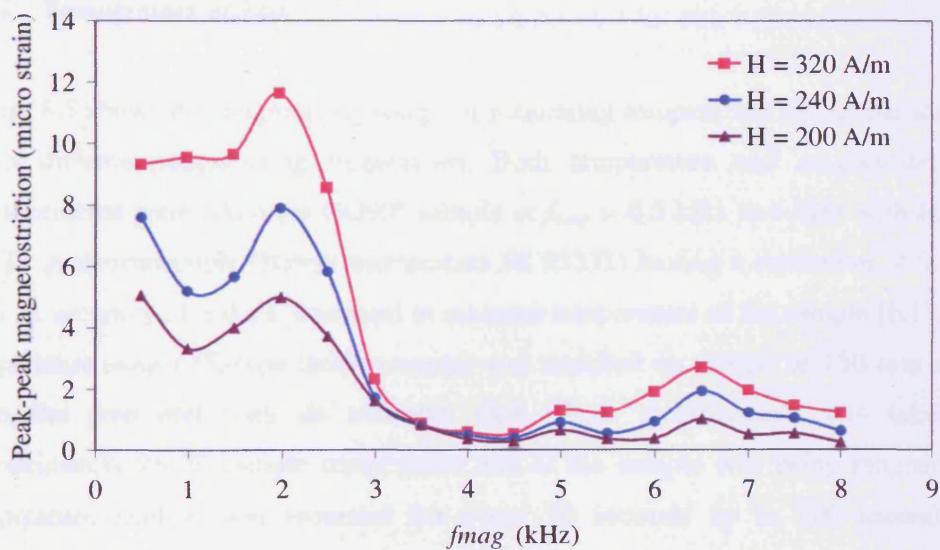


Figure 6.3. Peak-peak magnetostriction,  $\lambda_{pp}$  against magnetising frequency,  $f_{mag}$  for  $GO90^\circ$  at magnetic field,  $H = 200, 240$  and  $320$  A/m.

Figure 6.4 shows peak-peak flux density,  $B$  against  $f_{mag}$  at various  $H$ . It was observed that  $B$  increases with increasing  $H$  and  $B$  decreases with increasing  $f_{mag}$  at the same  $H$ .

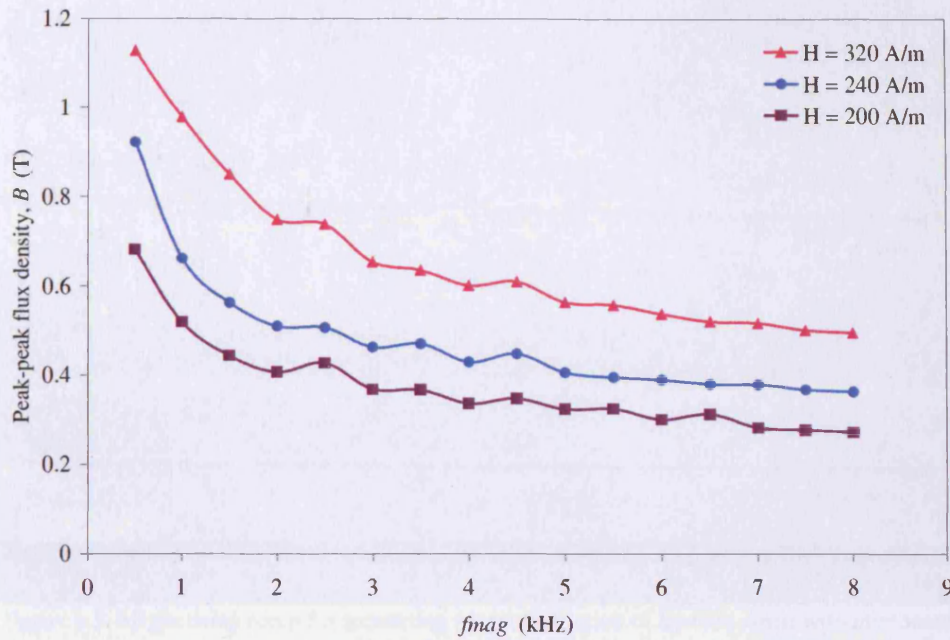


Figure 6.4. Peak-peak flux density,  $B$  against magnetising frequency,  $f_{mag}$  for GO90° at magnetic field,  $H = 200, 240$  and  $320$  A/m.

### 6.2.2. Temperature effects

Figure 6.5 shows the magnetising setup for measuring temperature rise of the sample under different magnetising frequencies. Both temperature and magnetostriction measurements were taken for GO90° sample at  $f_{mag} = 0.5$  kHz to 4 kHz with  $B_{max} = 1.0$  T. A thermocouple (Hanna Instruments HI 93531) having a resolution of  $0.1$  °C with an accuracy of  $\pm 0.2\%$  was used to measure temperature of the sample [6.1]. The temperature sensor (K-type thermocouple) was attached on sample at 150 mm away from the free end with an adhesive tape. Each measurement was taken at approximately 26 °C sample temperature and as the sample was being magnetised, temperature reading was recorded for every 30 seconds up to 300 seconds of magnetising time.

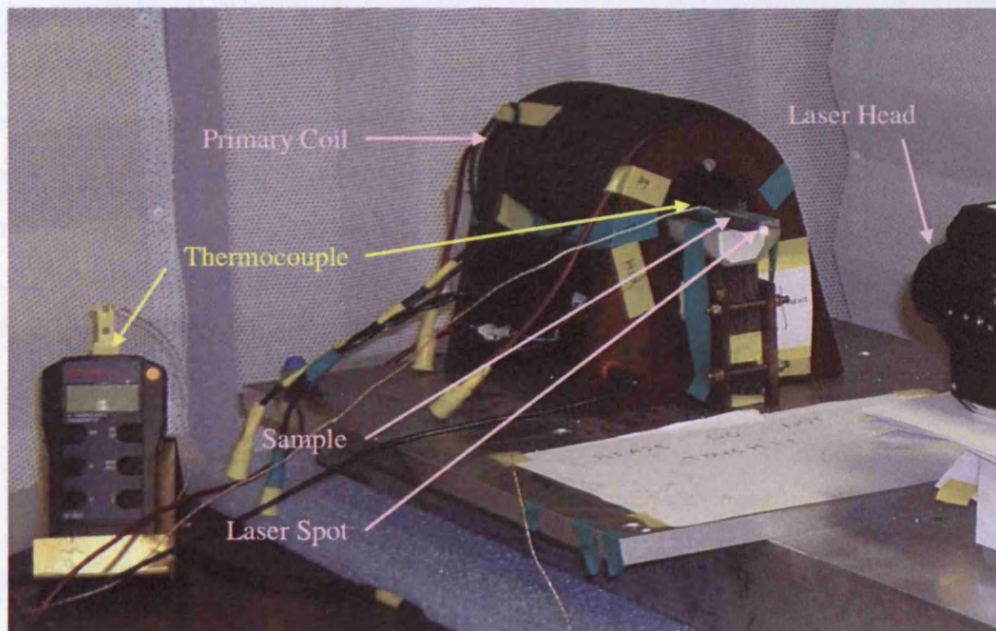


Figure 6.5. Magnetising setup for measuring magnetostriction of Epstein strips with thermocouple attached on the sample.

Figure 6.6 shows the temperature rise during magnetisation of the  $GO90^\circ$  sample at  $f_{mag} = 0.5$  kHz to 4 kHz at  $B_{max} = 1.0$  T. Initial temperature of the sample was about  $\pm 5.0$  of  $26.0$  °C for each measurement since the temperature of the sample at the start of each measurement can not be the same as it is dependant on room temperature. The temperature of the sample increases sharply during the first 60 seconds of magnetising time and it stabilised. The highest sample temperature at  $f_{mag} = 4$  kHz was  $71.3$  °C.

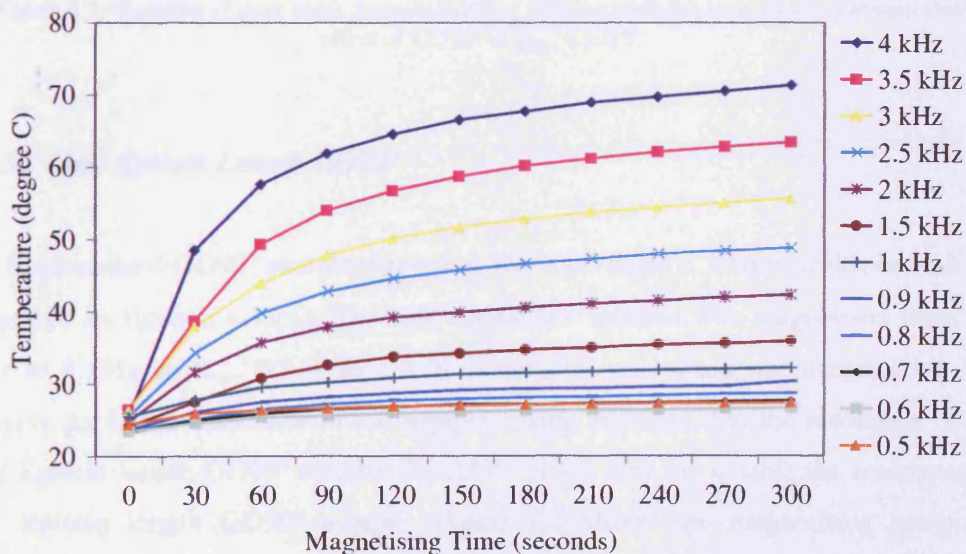


Figure 6.6. Temperature of  $GO90^\circ$  at various magnetising frequencies against magnetising time up to 300 seconds with initial temperature at approximately  $\pm 5.0$  °C of  $26.0$  °C at  $B_{peak} = 1.0$  T

This temperature rise during magnetisation has little effect on the peak-peak magnetostriction as seen from figure 6.7. Peak-peak magnetostriction has been obtained for different time intervals during 300 seconds magnetisation for  $f_{mag} = 1, 2$  and 3 kHz. Peak-peak magnetostriction varies from 38.8  $\mu\epsilon$  at 60 seconds magnetising time to 40.8  $\mu\epsilon$  at 300 seconds magnetising time at resonant point  $f_{mag} = 2$  kHz having temperature of the sample increasing from 35.7 °C at 60 seconds up to 42.3 °C at 300 seconds.

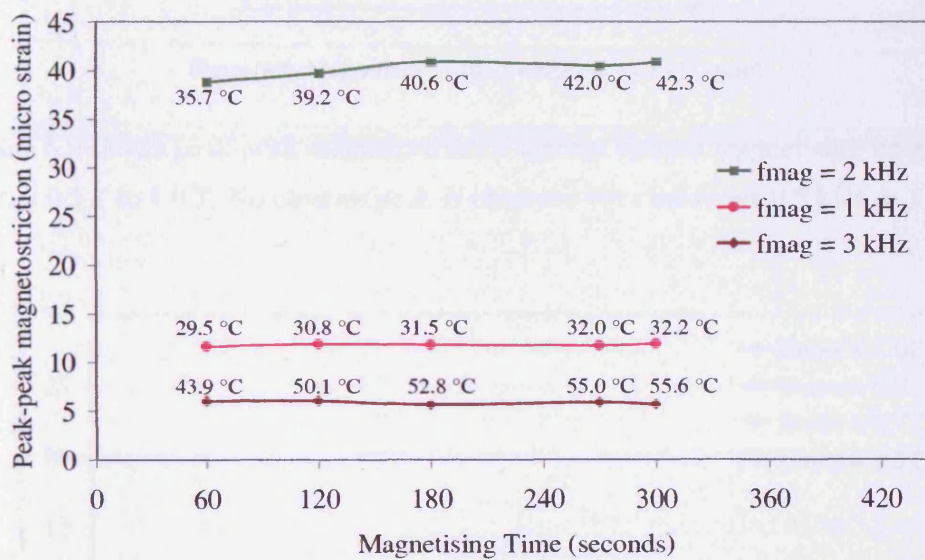


Figure 6.7. Variation of peak-peak magnetostriction with magnetising time showing temperature effect of  $GO90^\circ$  at  $B_{max} = 1.0$  T.

### 6.2.3. Half Epstein Length $GO90^\circ$

An Epstein sized  $GO90^\circ$  sample was cut at 150 mm length x 30 mm width i.e. half the length of an Epstein sample. The half cut  $GO90^\circ$  sample was magnetised from 0.5 kHz to 3 kHz at  $B_{max}$  0.5 T to 1.0 T to measure peak-peak magnetostriction and observe predicted resonance of the sample. Using equation 3.9, the resonance of the half Epstein length  $GO90^\circ$  sample should be at 4.2 kHz i.e. double the resonance of full Epstein length  $GO90^\circ$  sample. Figure 6.8 shows the magnetising setup for measuring magnetostriction of half-cut  $GO90^\circ$  sample. The half-cut sample was

placed in the centre of the primary coil on a temperature resistant nylon carrier. The sample then clamped down on the carrier with nylon bolts.

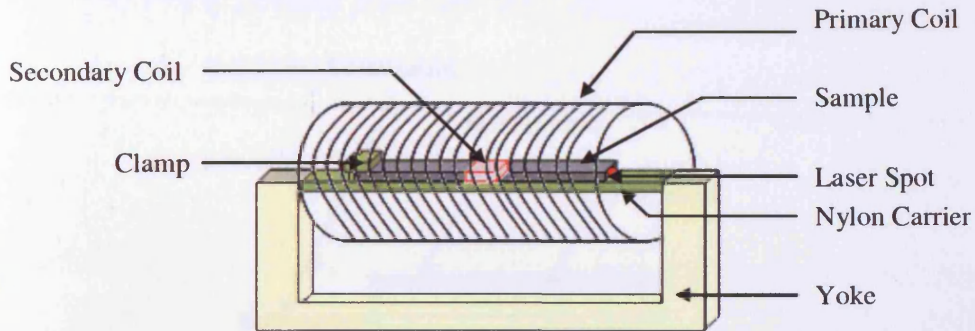


Figure 6.8. Magnetising setup for half-cut  $GO90^\circ$  sample

Figure 6.9 shows peak-peak magnetostriction against various magnetising frequencies at  $B_{max}$  0.5 T to 1.0 T. No obvious peak is observed over the range 0.5 kHz to 3 kHz.

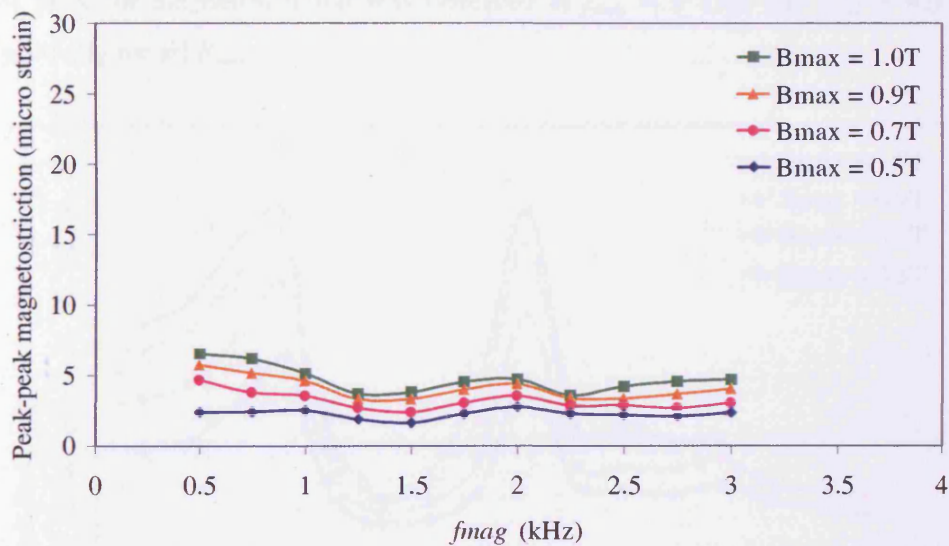


Figure 6.9. Peak-peak magnetostriction,  $\lambda_{pp}$  against magnetising frequency,  $f_{mag}$  for half-cut  $GO90^\circ$  at  $B_{max} = 0.5$  T, 0.7 T, 0.9 T and 1.0 T.

#### 6.2.4. Stack of $GO90^\circ$

Five Epstein strips of  $GO90^\circ$  were bonded together with an adhesive tape having the flux density coil wound at the centre of the length of the stack. The samples for stack were chosen from the same batch as the single strip sample. The laser spot was

pointed at the centre of the free end of stack to measure average displacement of all five strips under magnetisation (figure 6.10).

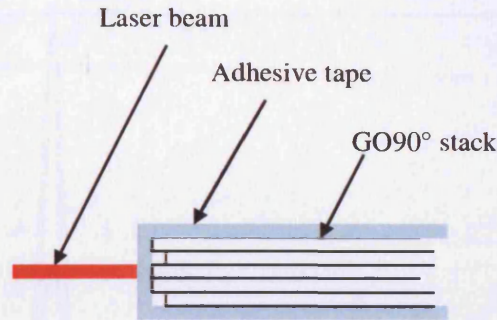


Figure 6.10. Laser spot pointed at the centre of the stack to obtain average displacement.

Figure 6.11 shows peak-peak magnetostriction of GO90° stack at  $f_{mag} = 0.5$  kHz to 8 kHz at  $B_{max} = 0.5$  T to 0.7 T and  $f_{mag} = 0.5$  kHz to 6.5 kHz at  $B_{max} = 0.9$  T to 1.0 T. Two peaks of magnetostriction was observed at  $f_{mag} = 2$  kHz and  $f_{mag} = 4.5$  kHz respectively for all  $B_{max}$ .

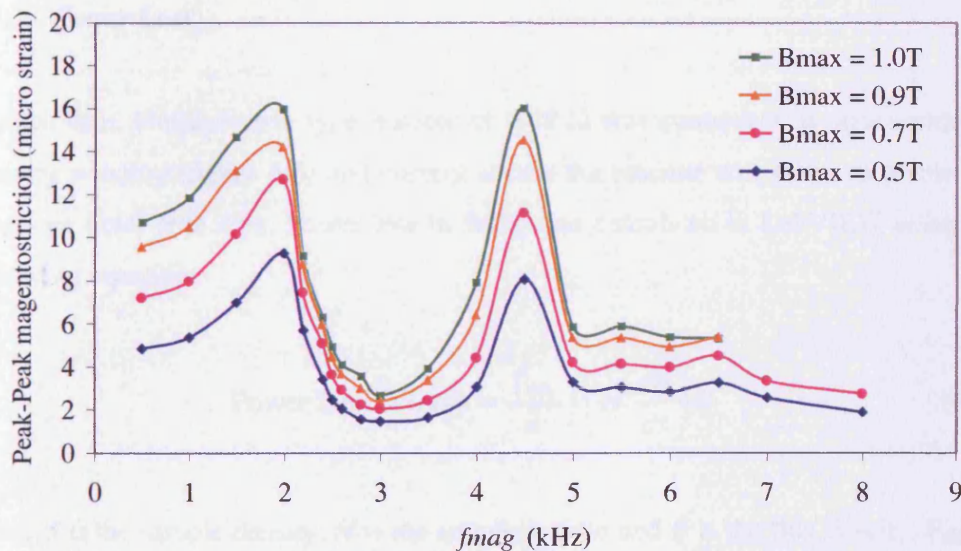


Figure 6.11. Peak-peak magnetostriction,  $\lambda_{pp}$  against magnetising frequency,  $f_{mag}$  for a stack of 5 strips of GO90° at  $B_{max} = 0.5$  T, 0.7 T, 0.9 T and 1.0 T.

### 6.3. Magnetisation induced mechanical resonance of GO0°

Figure 6.12 shows peak-peak magnetostriction against magnetising frequency for single strip GO0° sample at  $B_{max} = 0.5$  T to 1.0 T. It was observed that peak-peak

magnetostriction for  $GO0^\circ$  is much smaller than that of  $GO90^\circ$  and peaks first, second and third mode of resonances were found at  $f_{mag} = 1.75$  kHz, 5 kHz and 7.75 kHz for respectively for all  $B_{max}$ .

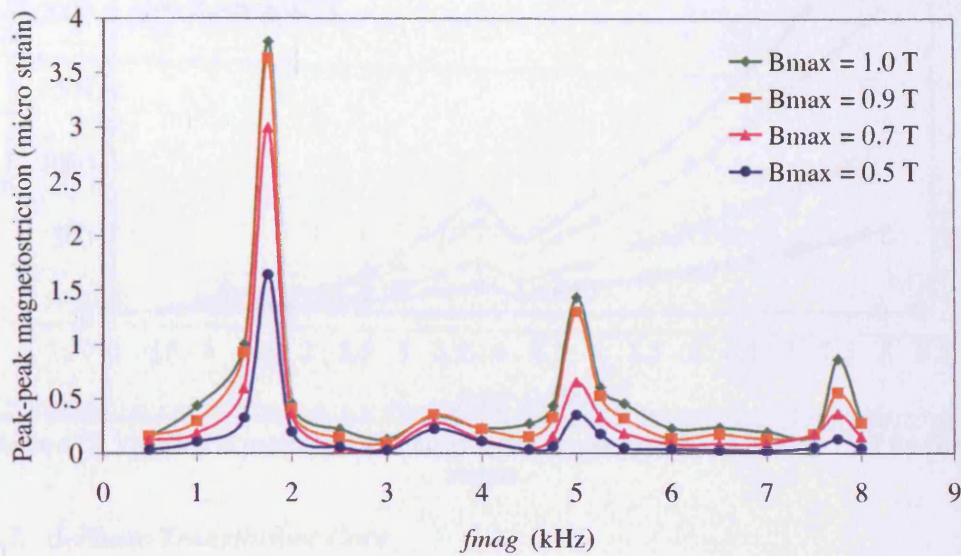


Figure 6.12. Peak-peak magnetostriction,  $\lambda_{pp}$  against magnetising frequency,  $f_{mag}$  for  $GO0^\circ$  at  $B_{max} = 0.5$  T, 0.7 T, 0.9 T and 1.0 T.

### 6.3.1. Power Loss

A thick film, non-inductive type resistor of  $0.48 \Omega$  was connected in series with the primary winding (figure 6.5) and current across the resistor was taken to obtain the magnetic field,  $H$  in A/m. Power loss in W/kg was calculated in LabVIEW using the following equation:

$$\text{Power Loss (W/kg)} = \frac{f_{mag}}{d} \int \left( H \cdot \frac{dB}{dt} \right) dt \quad (6.1)$$

where  $d$  is the sample density,  $H$  is the magnetic field and  $B$  is the flux density. Figure 6.13 shows power loss curve of  $GO0^\circ$  sample at  $f_{mag} = 0.5$  kHz to 8 kHz at  $B_{max} = 0.5$  T to 1.0 T. It was observed that power loss decreased from 140 W/kg at  $f_{mag} = 1$  kHz to 96 W/kg at  $f_{mag} = 1.5$  kHz and 739 W/kg at  $f_{mag} = 3.75$  kHz to 482 W/kg at  $f_{mag} = 4.25$  kHz for  $B_{max} = 1.0$  T.

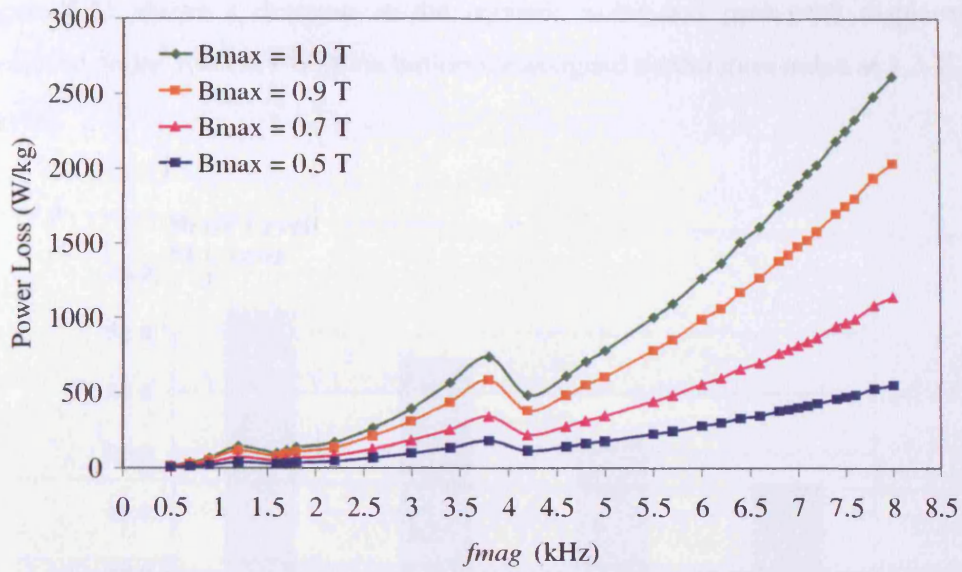


Figure 6.13. Variation of power loss with magnetising frequency at  $B_{max} = 0.5$  T to 1.0 T for GO0° sample.

6.3.2. 3-Phase Transformer Core

6.3.2.1. Displacement and acoustic noise measurements at Point 1

Figure 6.14 shows the variation of both the peak-peak displacement above point 1 and the acoustic noise measure in sound pressure level (SPL) with different modulation index at  $B_{max}$  of 1.3 T.

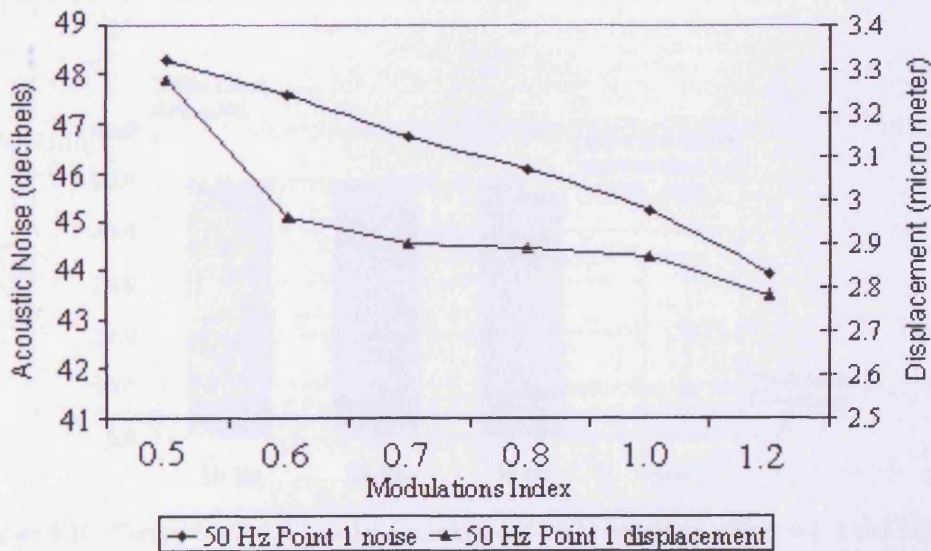


Figure 6.14. Acoustic noise and corresponding peak-peak displacement at point 1 under 50 Hz PWM excitation,  $f_s = 3$  kHz,  $B_{max} = 1.3$  T,  $m_i = 0.5$



Figure 6.15 shows a decrease in the acoustic noise and peak-peak displacement measured under 100 Hz PWM excitation for assigned modulation index at 1.3 T,  $f_s = 3$  kHz.

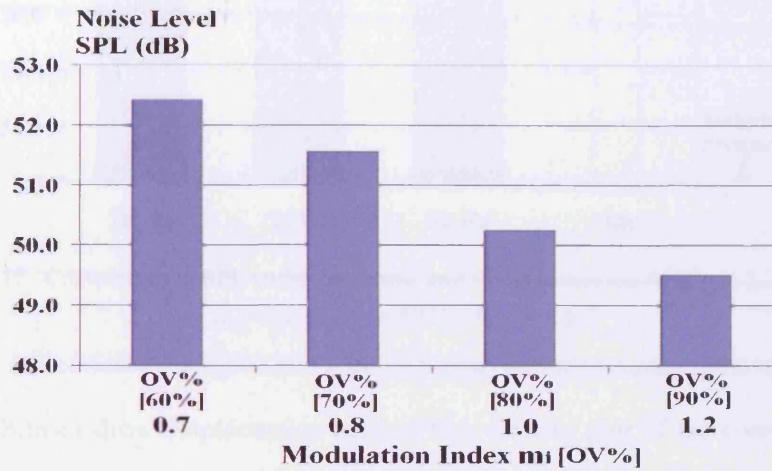


Figure 6.15. Average acoustic noise SPL under PWM excitation at point 1,  $m_i = 0.7 - 1.2$ ,  $f = 100$  Hz,  $f_s = 3$  kHz,  $B_{max} = 1.3$ T

Figure 6.16 and Figure 6.17 show average acoustic noise of the core above point 1 under sinusoidal and PWM excitation,  $f = 50$  Hz,  $m_i$  was 0.5 and 0.6,  $B_{max}$  was set to 1.3 T and 1.5T, and  $f_s$  was varied from 1 kHz to 3 kHz respectively.

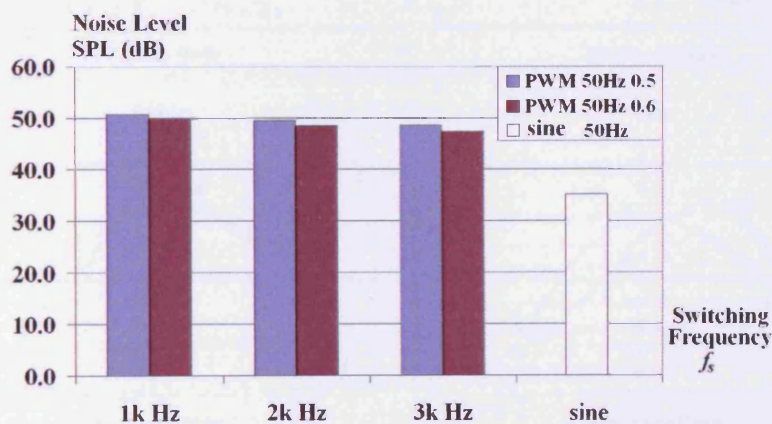


Figure 6.16. Comparison of SPL under sinusoidal and PWM excitation with  $f_s = 1, 2$  and 3 kHz,  $m_i = 0.5, 0.6$ ,  $f = 50$  Hz,  $B_{max} = 1.3$  T

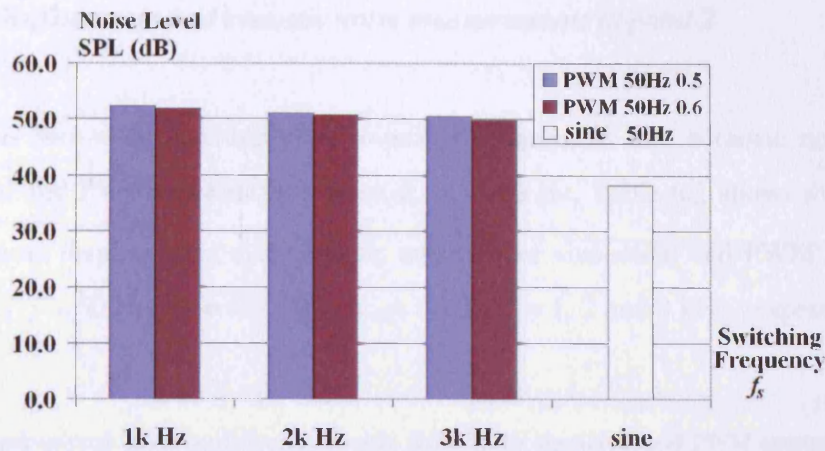


Figure 6.17. Comparison of SPL under sinusoidal and PWM excitation with  $f_s = 1, 2$  and  $3$  kHz,  $m_i = 0.5, 0.6$ ,  $f = 50$  Hz,  $B_{max} = 1.5$  T

Figure 6.18 (a-c) show displacement against flux density plot of the core under PWM excitation above point 1,  $f = 50$  Hz,  $m_i = 0.5$ ,  $B_{max} = 1.5$  T and  $f_s = 1, 2$  and  $3$  kHz, respectively and under  $50$  Hz sinusoidal excitation is shown in figure 6.18 (d).

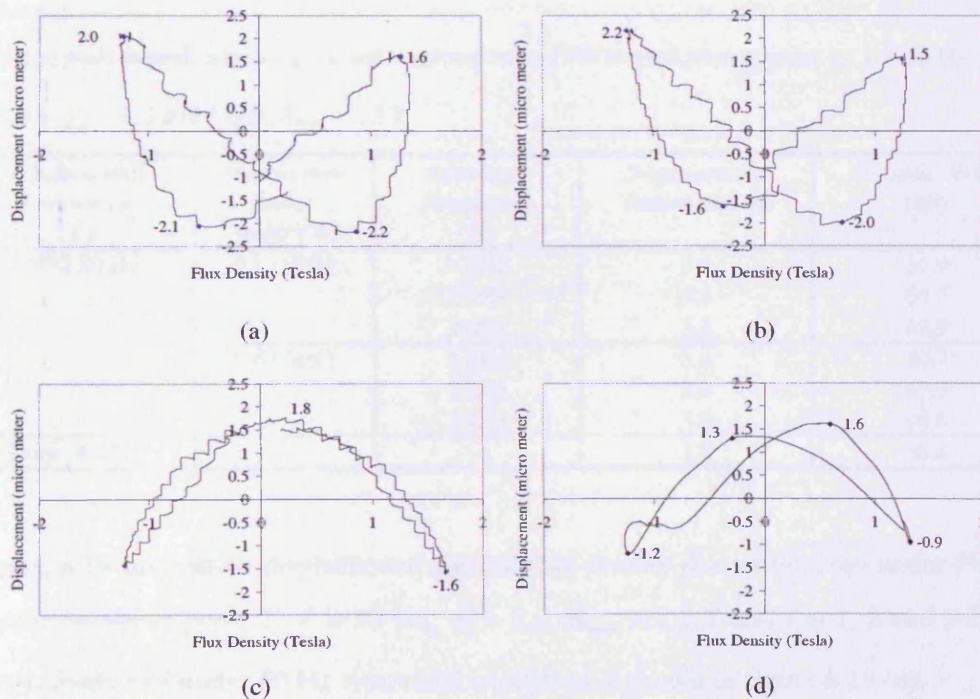


Figure 6.18. Displacement at **point 1** under  $50$  Hz PWM excitation at,  $m_i = 0.5$  and  $B_{max} = 1.5$  T (a)  $f_s = 1$  kHz (b)  $f_s = 2$  kHz (c)  $f_s = 3$  kHz and (d)  $50$  Hz sinusoidal excitation.

### 6.3.2.2. Displacement and acoustic noise measurements at point 2

Table 6.1. shows the average peak-to-peak displacement and acoustic noise under sinusoidal and PWM excitation at point 2,  $f = 50$  Hz. Table 6.2 shows the average peak-to-peak displacement and acoustic noise under sinusoidal and PWM excitation at point 2,  $f = 50$  Hz,  $m_i = 0.5, 0.6$ ,  $B_{max} = 1.3$  T,  $f_s = 1, 2$  and  $3$  kHz, respectively.

Table 6.1.

Average peak-to-peak displacement and acoustic noise under sinusoidal and PWM excitation at point 2,  $f = 50$  Hz,  $m_i = 0.5 - 1.2$ ,  $f_s = 3$  kHz,  $B_{max} = 1.3$  T.

Fundamental Frequency ( $f$ )	Modulation Index $m_i$ [OV%]	Displacement (micro meter)	Acoustic Noise (dB)
PWM 50 Hz	0.5 [40%]	3.2	49.9
	0.6 [50%]	3.0	48.6
	0.7 [60%]	2.9	47.5
	0.8 [70%]	2.8	46.8
	1.0 [80%]	2.7	45.5
	1.2 [90%]	2.5	45.0
Sine 50 Hz	-	1.9	36.8

Table 6.2.

Average peak-to-peak displacement under sinusoidal and PWM excitation at point 2,  $f = 50$  Hz,  $m_i = 0.5, 0.6$ ,  $f_s = 1, 2$  and  $3$  kHz,  $B_{max} = 1.3$  T.

Fundamental Frequency ( $f$ )	Modulation Index $m_i$ [OV%]	Switching Frequency ( $f_s$ )	Displacement (micro meter)	Acoustic Noise (dB)
PWM 50 Hz	0.5 [40%]	1 kHz	3.6	51.9
		2 kHz	3.4	50.7
		3 kHz	3.2	49.9
	0.6 [50%]	1 kHz	3.4	50.7
		2 kHz	3.2	49.3
		3 kHz	3.0	48.6
sine 50 Hz	--	--	1.9	36.8

Figure 6.19 (a-c) show displacement against flux density plot of the core under PWM excitation above point 2,  $f = 50$  Hz,  $m_i = 0.6$ ,  $B_{max} = 1.3$  T and  $f_s = 1, 2$  and  $3$  kHz, respectively and under 50 Hz sinusoidal excitation is shown in figure 6.19 (d).

Table 6.3.

Average acoustic noise SPL under sinusoidal and PWM excitation at different point,  $f = 50$  Hz,  $m_i = 0.5-1.2$ ;  $f = 100$  Hz,  $m_i = 0.7-1.2$ ;  $f_s = 3$  kHz,  $B_{max} = 1.3$  T.

Fundamental Frequency ( $f$ )	Modulation Index $m_i$ [OV%]	Acoustic Noise (dB)		
		Point 1	Point 2	Point 3
50 Hz	0.5 [40%]	48.6	49.9	50.0
	0.6 [50%]	47.3	48.6	49.0
	0.7 [60%]	46.2	47.5	47.8
	0.8 [70%]	45.5	46.8	46.3
	1.0 [80%]	44.8	45.5	45.9
	1.2 [90%]	44.2	45.0	45.2
Sine 50 Hz	-	35.1	36.8	37.0
100 Hz	0.7 [60%]	52.4	53.3	53.0
	0.8 [70%]	51.6	52.5	52.1
	1.0 [80%]	50.2	51.7	51.4
	1.2 [90%]	49.5	50.2	50.8

Table 6.4.

Average acoustic noise SPL under sinusoidal and PWM excitation at different point,  $f = 50$  Hz,  $m_i = 0.5, 0.6$ ,  $f_s = 1, 2$  and  $3$  kHz,  $B_{max} = 1.3$  T and  $1.5$  T.

Fundamental Frequency ( $f$ )	Modulation Index $m_i$ [OV%]	Switching Frequency ( $f_s$ )	Acoustic Noise (dB)					
			1.3 T			1.5 T		
			Point 1	Point 2	Point 3	Point 1	Point 2	Point 3
PWM 50 Hz	0.5 [40%]	1 kHz	50.6	51.9	51.9	52.4	54.0	53.6
		2 kHz	49.4	50.7	50.8	51.1	52.5	52.4
		3 kHz	48.6	49.9	50.0	50.5	51.7	51.5
	0.6 [50%]	1 kHz	49.7	50.7	50.8	51.9	53.0	52.8
		2 kHz	48.4	49.3	49.9	50.6	51.8	51.7
		3 kHz	47.3	48.6	49.0	49.8	50.7	50.6
sine 50 Hz	--	--	35.1	36.8	37.00	38.2	39.6	39.7

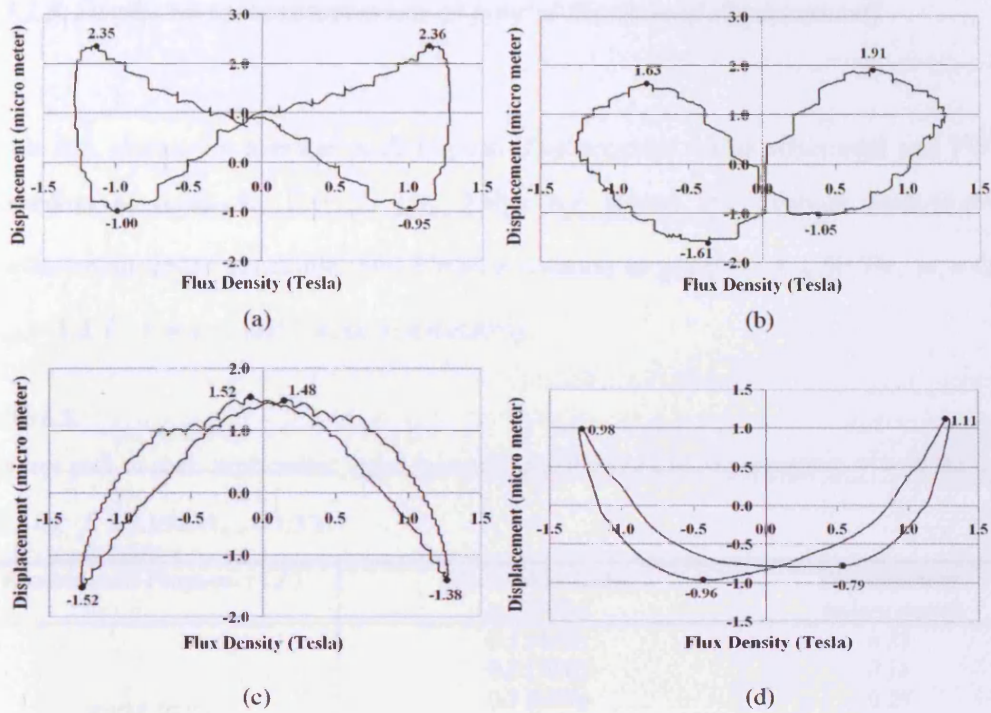


Figure 6.19. Displacement at **point 2** under 50 Hz PWM excitation at  $m_i = 0.6$  and  $B_{max} = 1.3$  T (a)  $f_s = 1$  kHz (b)  $f_s = 2$  kHz (c)  $f_s = 3$  kHz and (d) 50 Hz sinusoidal excitation.

Figure 6.20 show the harmonic components of the displacement at point 2 under sinusoidal and PWM excitation,  $f = 50$  Hz,  $m_i = 0.6$ ,  $B_{max} = 1.3$  T and 1.5 T,  $f_s = 1, 2$  and 3 kHz, respectively.

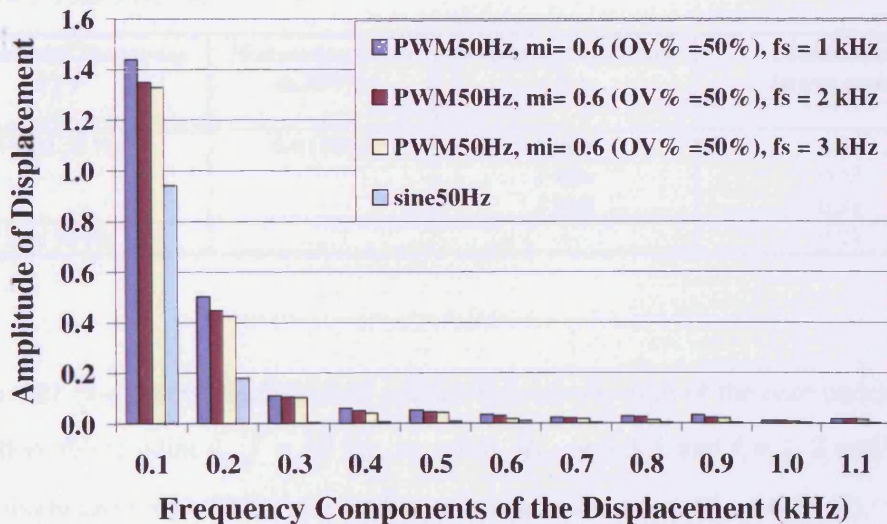


Figure 6.20. Harmonic components of displacement under sinusoidal and PWM excitation at **point 2**,  $f = 50$  Hz,  $m_i = 0.6$ ,  $f_s = 1, 2$  and 3 kHz,  $B_{max} = 1.3$  T

### 6.3.2.3. Displacement measurements at point 4 (horizontal displacement)

Table 6.5. shows the average peak-to-peak displacement under sinusoidal and PWM excitation at point 4,  $f = 50$  Hz. Table 6.6 shows the average peak-to-peak displacement under sinusoidal and PWM excitation at point 4,  $f = 50$  Hz,  $m_i = 0.6$ ,  $B_{max} = 1.3$  T,  $f_s = 1, 2$  and  $3$  kHz, respectively.

Table 6.5.

Average peak-to-peak displacement under sinusoidal and PWM excitation at point 4,  $f = 50$  Hz,  $m_i = 0.5 - 1.2$ ,  $f_s = 3$  kHz,  $B_{max} = 1.3$  T.

<b>Fundamental Frequency (<math>f</math>)</b>	<b>Modulation Index <math>m_i</math> [OV%]</b>	<b>Displacement (micro meter)</b>
PWM 50 Hz	0.5 [40%]	0.33
	0.6 [50%]	0.31
	0.7 [60%]	0.29
	0.8 [70%]	0.28
	1.0 [80%]	0.26
	1.2 [90%]	0.24
Sine 50 Hz	-	0.21

Table 6.6.

Average peak-to-peak displacement under sinusoidal and PWM excitation at point 4,  $f = 50$  Hz,  $m_i = 0.6$ ,  $f_s = 1, 2$  and  $3$  kHz,  $B_{max} = 1.3$  T.

<b>Fundamental Frequency (<math>f</math>)</b>	<b>Modulation Index <math>m_i</math> [OV%]</b>	<b>Switching Frequency (<math>f_s</math>)</b>	<b>Displacement (micro meter)</b>
PWM 50 Hz	0.6 [50%]	1 kHz	0.36
		2 kHz	0.33
		3 kHz	0.31
sine 50 Hz	--	--	0.21

Figure 6.21 (a-c) show displacement against flux density plot of the core under PWM excitation above point 4,  $f = 50$  Hz,  $m_i = 0.6$ ,  $B_{max} = 1.3$  T and  $f_s = 1, 2$  and  $3$  kHz, respectively and under 50 Hz sinusoidal excitation is shown in figure 6.21 (d).

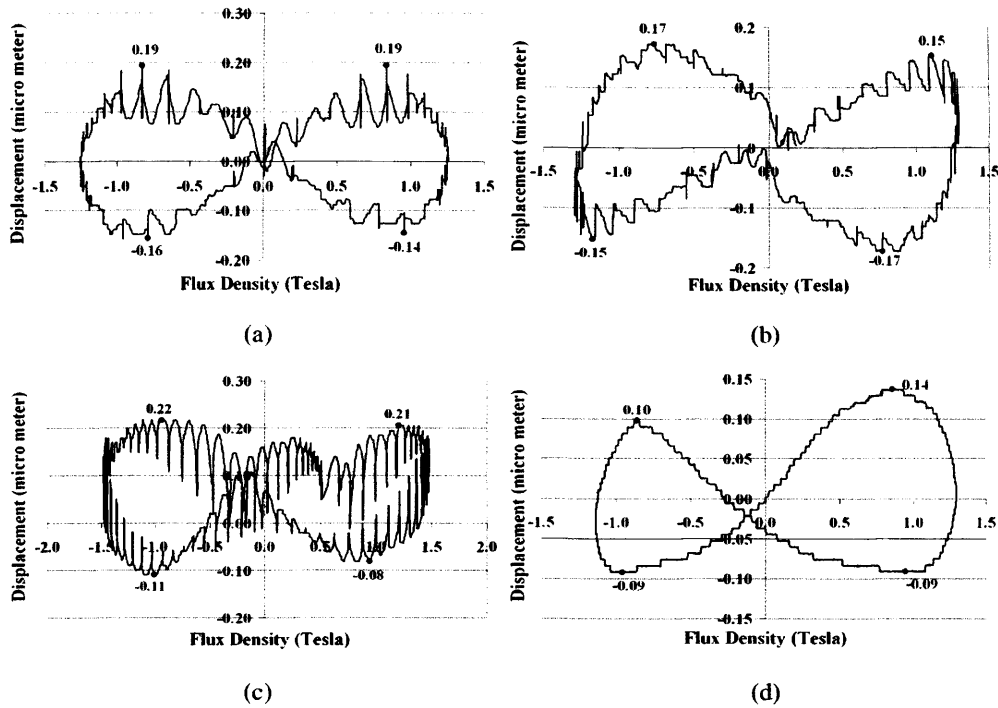


Figure 6.21. Displacement at **point 4** under 50 Hz PWM excitation at,  $m_i = 0.6$  and  $B_{max} = 1.3$  T (a)  $f_s = 1$  kHz (b)  $f_s = 2$  kHz (c)  $f_s = 3$  kHz and (d) 50 Hz sinusoidal excitation.

Figure 6.22 show the harmonic components of the displacement at point 4 under sinusoidal and PWM excitation,  $f = 50$  Hz,  $m_i = 0.6$ ,  $B_{max} = 1.3$  T,  $f_s = 1, 2$  and  $3$  kHz, respectively.

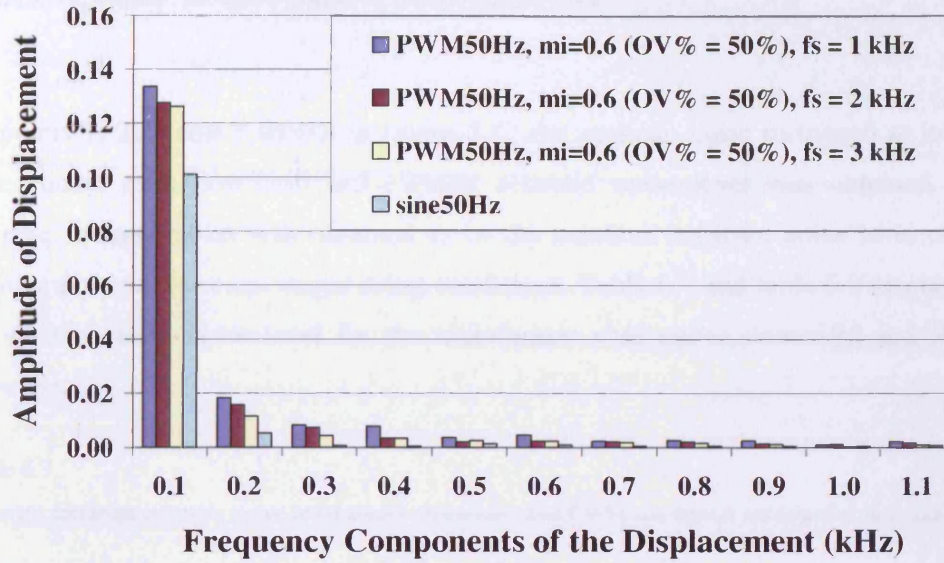


Figure 6.22. Harmonic components of displacement under sinusoidal and PWM excitation at point 4,  $f = 50$  Hz,  $m_i = 0.6$ ,  $f_s = 1, 2$  and  $3$  kHz,  $B_{max} = 1.3$  T

6.3.2.4. Acoustic noise measurements at point 5

Figures. 6.23 (a) and (b) show the noise level measured above point 5 (figure 5.12) when the core was magnetized under sinusoidal flux and under PWM excitation with two values of  $m_i$  at three different value of  $f_s$ . The noise measured under PWM excitation is around 10dB to 15 dB greater than under corresponding sinusoidal flux.

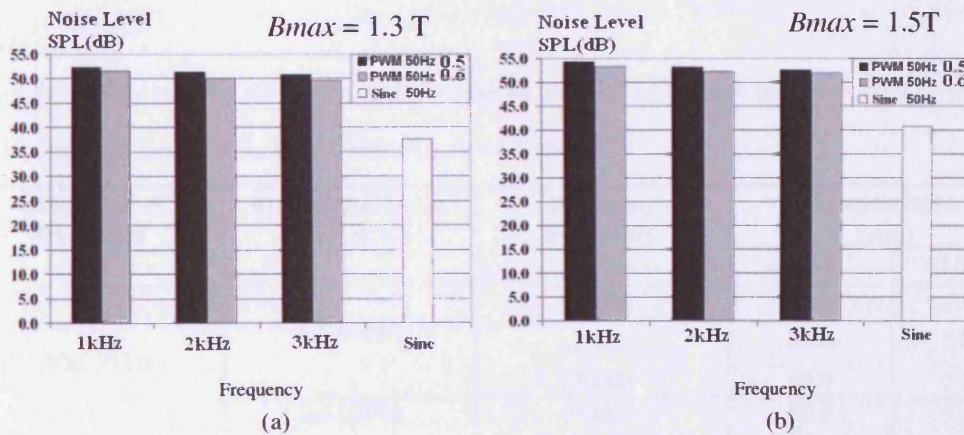


Figure 6.23. Comparison of SPL under PWM excitation with values of  $f_s = 1, 2$  and  $3$  kHz with that under sinusoidal conditions  $f_{mag} = 50$  Hz at (a)  $B_{max} = 1.3$  T and (b)  $B_{max} = 1.5$  T.



### 6.3.2.5. Resultant acoustic noise of the 3-phase core

At points 1, 2, 3 and 5 shown in figure 5.12 the acoustic noise measured at least 3 times under each condition and average acoustic noise level was obtained. The average acoustic noise was obtained to be the resultant acoustic noise level of the transformer core for each magnetising conditions. Table 6.7 and table 6.8 display the resultant acoustic noise level for the transformer core under sinusoidal and PWM excitation.

Table 6.7.

Average resultant acoustic noise level under sinusoidal and PWM excitation for transformer core,  $f = 50$  Hz,  $m_i = 0.5-1.2$ ;  $f = 100$  Hz,  $m_i = 0.7-1.2$ ,  $f_s = 3$  kHz,  $B_{max} = 1.3$  T

Fundamental Frequency ( $f$ )	Modulation Index $m_i$ [OV%]	Acoustic Noise (dB)
PWM 50 Hz	0.5 [40%]	49.8
	0.6 [50%]	48.6
	0.7 [60%]	47.4
	0.8 [70%]	46.6
	1.0 [80%]	45.8
	1.2 [90%]	45.0
Sine 50 Hz	-	36.7
PWM 100 Hz	0.7 [60%]	53.2
	0.8 [70%]	52.4
	1.0 [80%]	51.3
	1.2 [90%]	50.5

Table 6.8.

Average resultant acoustic noise level under sinusoidal and PWM excitation for transformer core,  $f = 50$  Hz,  $m_i = 0.5, 0.6$ ,  $f_s = 1, 2$  and  $3$  kHz,  $B_{max} = 1.3$  T and  $1.5$ T.

Fundamental Frequency ( $f$ )	Modulation Index $m_i$ [OV%]	Switching Frequency ( $f_s$ )	Acoustic Noise (dB)	
			1.3 T	1.5 T
PWM 50 Hz	0.5 [40%]	1 kHz	51.7	53.6
		2 kHz	50.6	52.3
		3 kHz	49.8	51.5
	0.6 [50%]	1 kHz	50.7	52.8
		2 kHz	49.4	51.6
		3 kHz	48.6	50.8
Sine 50 Hz	--	--	36.7	39.5

#### 6.4. Magnetisation induced mechanical resonance of GO55°

Figure 6.24 shows peak-peak magnetostriction against various  $f_{mag}$  and  $B_{max}$  from 0.5 T to 1.0 T for GO55° sample. The sample was magnetised from  $f_{mag} = 0.5$  kHz to 8 kHz for  $B_{max} = 0.5$  T and only magnetised up to  $f_{mag} = 5$  kHz for  $B_{max} = 0.7$  T, 0.9 T and 1.0 T.

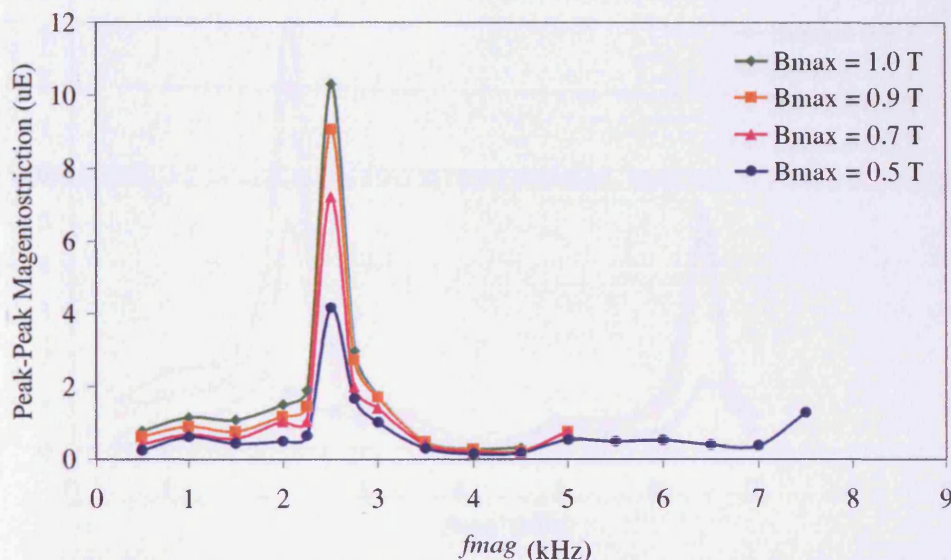


Figure 6.24. Peak-peak magnetostriction,  $\lambda_{pp}$  against magnetising frequency,  $f_{mag}$  for GO55° at  $B_{max} = 0.5$  T, 0.7 T, 0.9 T and 1.0 T.

#### 6.5. Magnetisation induced mechanical resonance of NO

Magnetostriction of three Epstein strips of NO steel was measured to obtain the magnetisation induced mechanical resonance of the materials. One of the three samples was the 3% Si NO sample with 0.5 mm thickness, which was magnetised from 0.5 kHz to 8 kHz at  $B_{max} = 0.3$  T to 0.9 T. The other two samples were 6.5% Si NO samples with 0.1 mm thickness cut at 0° and 90° to rolling direction, which were magnetised from 0.5 kHz to 6 kHz and 0.5 kHz to 7 kHz respectively at  $B_{max} = 0.5$  T to 1.0 T.

### 6.5.1. 3% Si NO

Figure 6.25 shows peak-peak magnetostriction against  $f_{mag}$  at  $B_{max}$  0.3 T to 0.9 T for 3% Si L800-50 NO sample. Resonance peaks were observed at  $f_{mag} = 2.25$  kHz and 6.4 kHz for all  $B_{max}$ .

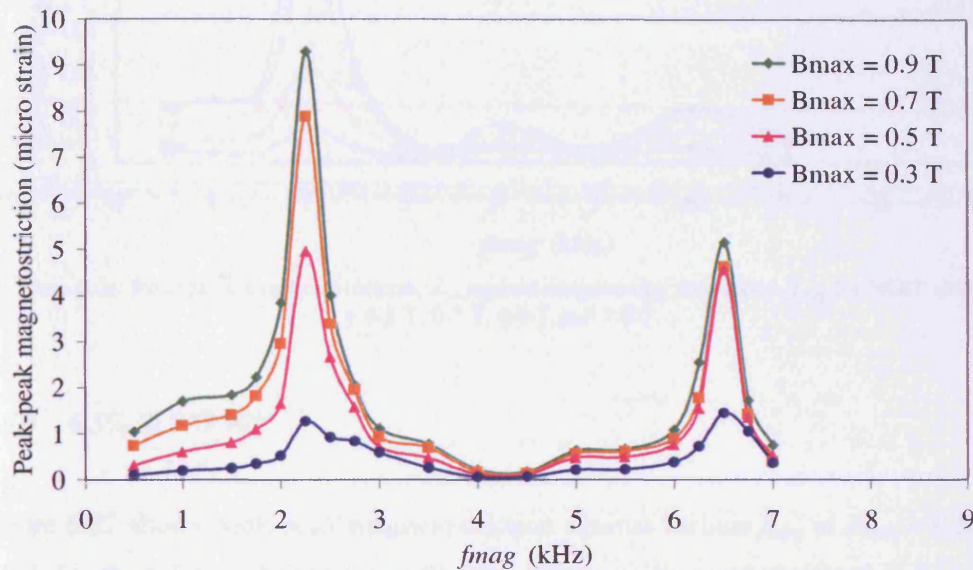


Figure 6.25. Peak-peak magnetostriction,  $\lambda_{pp}$  against magnetising frequency,  $f_{mag}$  for 3% Si NO at  $B_{max} = 0.3$  T, 0.5 T, 0.7 T and 0.9 T.

### 6.5.2. 6.5% Si NO 0°

Figure 6.26 shows peak-peak magnetostriction against various  $f_{mag}$  at  $B_{max} = 0.5$  T to 1.0 T for the 6.5% Si NO 0° sample. Resonance peaks were observed at  $f_{mag} = 2$  kHz and 6 kHz for all  $B_{max}$ .

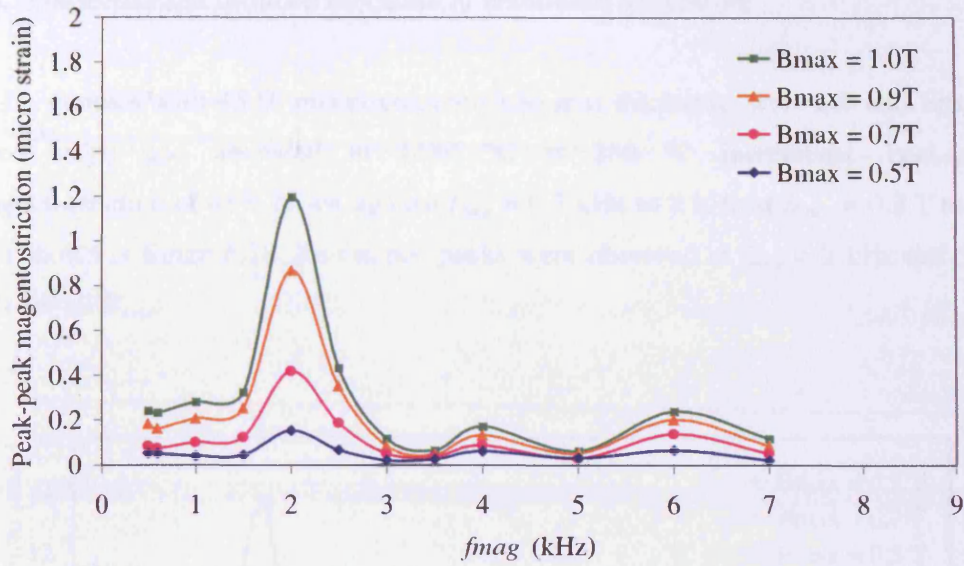


Figure 6.26. Peak-peak magnetostriction,  $\lambda_{pp}$  against magnetising frequency,  $f_{mag}$  for  $\text{NO}0^\circ$  at  $B_{max} = 0.5$  T, 0.7 T, 0.9 T and 1.0 T.

### 6.5.3. 6.5% Si NO 90°

Figure 6.27 shows peak-peak magnetostriction against various  $f_{mag}$  at  $B_{max} = 0.5$  T to 1.0 T for the 6.5% Si NO 90° sample. Resonance peaks were observed at  $f_{mag} = 2.5$  kHz and 7 kHz for all  $B_{max}$ .

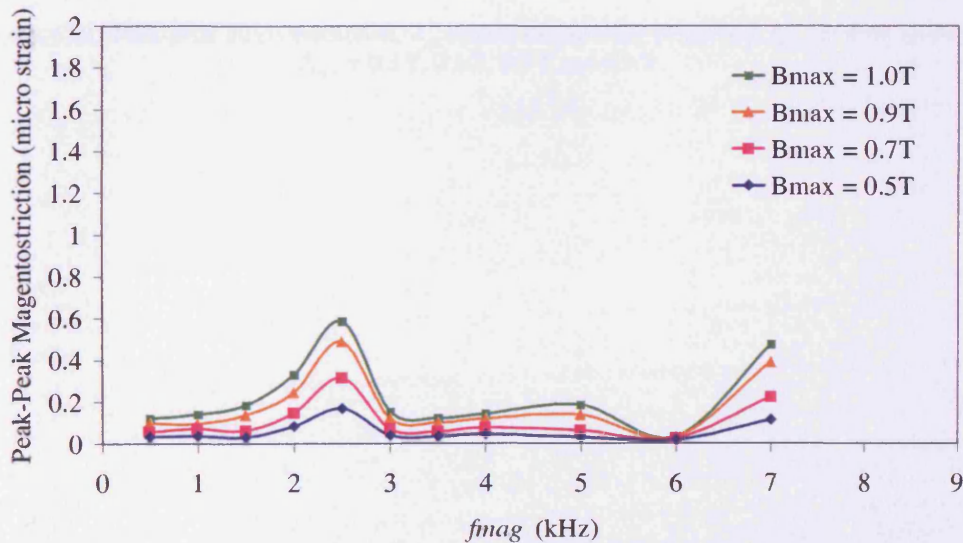


Figure 6.27. Peak-peak magnetostriction,  $\lambda_{pp}$  against magnetising frequency,  $f_{mag}$  for  $\text{NO}90^\circ$  at  $B_{max} = 0.5$  T, 0.7 T, 0.9 T and 1.0 T.

### 6.6. Magnetisation induced mechanical resonance 45% Ni-Fe

Ni-Fe samples with 45 % nickel content (0.36 mm thickness) were cut into Epstein sized strips and annealed at 1180 °C at 250 °C increments. Peak-peak magnetostriction of 45% Ni-Fe against  $f_{mag} = 0.5$  kHz to 8 kHz at  $B_{max} = 0.3$  T to 0.9 T is shown in figure 6.28. Resonance peaks were observed at  $f_{mag} = 2$  kHz and 5.25 kHz for all  $B_{max}$ .

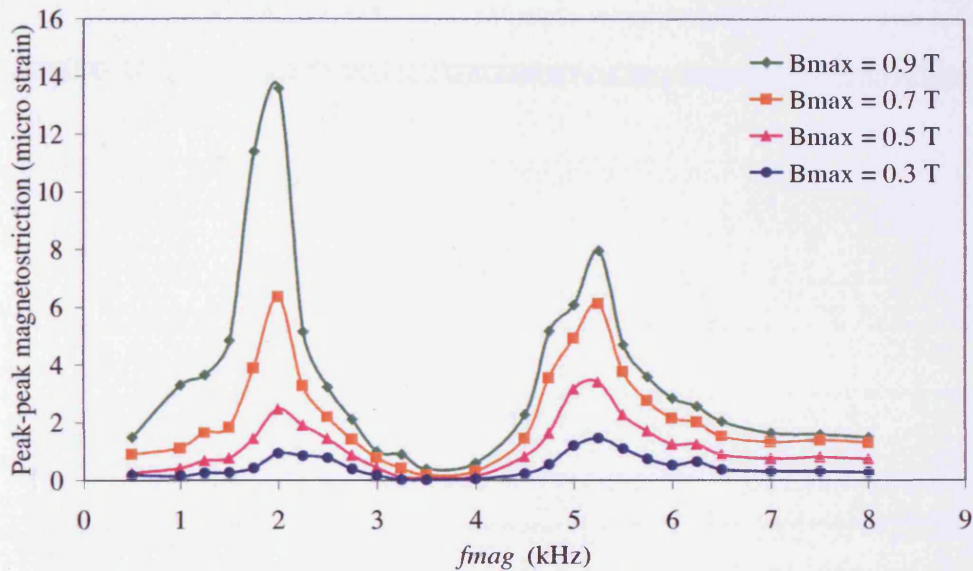


Figure 6.28. Peak-peak magnetostriction,  $\lambda_{pp}$  against magnetising frequency,  $f_{mag}$  for 45% Ni-Fe at  $B_{max} = 0.3$  T, 0.5 T, 0.7 T and 0.9 T.

**References**

- [6.1] Hanna Instruments, 'Instruction Manual', MANK93R3, 1998.

---

## CHAPTER 7

### DISCUSSION OF RESULTS

---

#### 7.1. Introduction

Magnetostriction of various Epstein sized electrical steel strips commonly used in electromagnetic cores were measured over  $f_{mag}$  range from 0.5 kHz to 8 kHz at  $B_{max}$  0.5 T to 1.0 T, which gives an important new understanding of the phenomenon. Magnetisation induced mechanical resonance was observed when peak-peak magnetostriction was plotted against the magnetising frequency. Large increase in peak-peak magnetostriction was observed at certain  $f_{mag}$  suggesting that the sample under test was resonating. The measured resonance peaks were then compared with theoretical resonance frequency of the sample using the following equation.

$$f_m = \frac{n}{8l} \sqrt{\frac{E}{d}} \quad (7.1)$$

#### 7.2. Magnetisation Induced Mechanical Resonance of 3% Si-Fe Grain Oriented Materials

##### 7.2.1. 3%Si-Fe GO90°

Young's modulus  $E$  was determined by means of linear regression method and  $E$  of GO90° was measured to be 202 GPa as shown in figure 7.1. The coefficient of determination,  $R^2$  was calculated with least square method and was approximately equal to 1 for the curve shown in figure 7.1. When clamping the sample in the stressing system (see figure 5.10), since the sample is a thin long strip, it is possible that the sample is not clamped completely vertical to the clamps. Some amount of bending contributes to the strain value when the sample is initially stressed. However, once more stress is applied, the stress-strain curve increases linearly as expected. Therefore, the slope of the stress-strain curve was calculated from stress of 20 MPa or pass the region of possible bending strain from occurring. However, the non-linear

region below 20 MPa can be avoided if an additional strain gauge was placed at the opposite side of the sample to compensate for any bending strain measured.

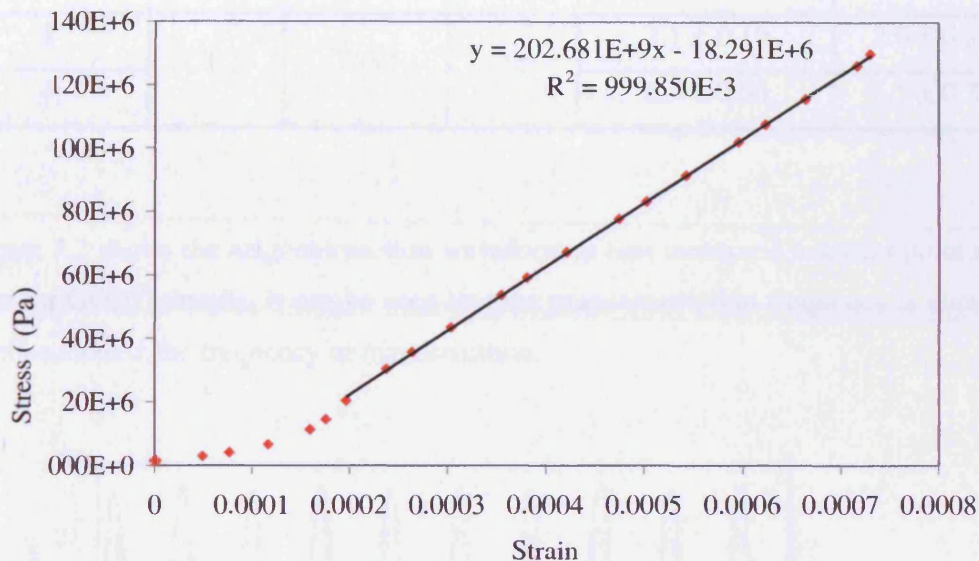


Figure 7.1. Stress-strain curve of GO90° sample used to obtain Young's modulus,  $E$  of the sample.

Resonance characteristics were found in the GO90° material at 2 kHz. At resonant point, vibration caused by magnetostriction increased 400 % and 150 % at 6.5 kHz for  $B_{max} = 1.0$  T. Although the GO90° material is of no practical importance, results confirm the predicted effect of material parameters on resonance. Table 7.1 shows a comparison of calculated  $f_m$  using equation 7.1 and measured value of  $f_m$  from figure 6.1 for GO90° sample. Magnetostriction measurements were taken at  $f_{mag} = 0.5$  kHz intervals and corresponding  $f_{mag}$  when rise in amplitude of peak-peak magnetostriction occurs was regarded as point where resonance occurs. Measurements could have been taken at 0.05 kHz intervals to have more accurate value of measured resonance frequency. However, from table 7.1, the first resonant point and its harmonic correspond well with the calculated theoretical value. Calculated resonance frequency was  $2.1 \pm 0.19$  kHz and the measured value was 2 kHz. Hence, the measured resonance lies well within the expected resonance frequency.



Table 7.1

Comparison of calculated and measured  $f_m$  for GO90°

$n^{\text{th}}$ Harmonic	$E$ (GPa)	$d$ (kg/m <sup>3</sup> )	$l$ (mm)	$f_m$ (kHz)	
				Calculated	Measured
1	202	7650	305	2.1 ± 0.19	2.0 ± 0.25
3				6.3 ± 0.56	6.5 ± 0.25

Figure 7.2 shows the magnetostriction waveform at first measured resonant point at 2 kHz for GO90° sample. It can be seen that the magnetostriction frequency is about 4 kHz i.e. double the frequency of magnetisation.

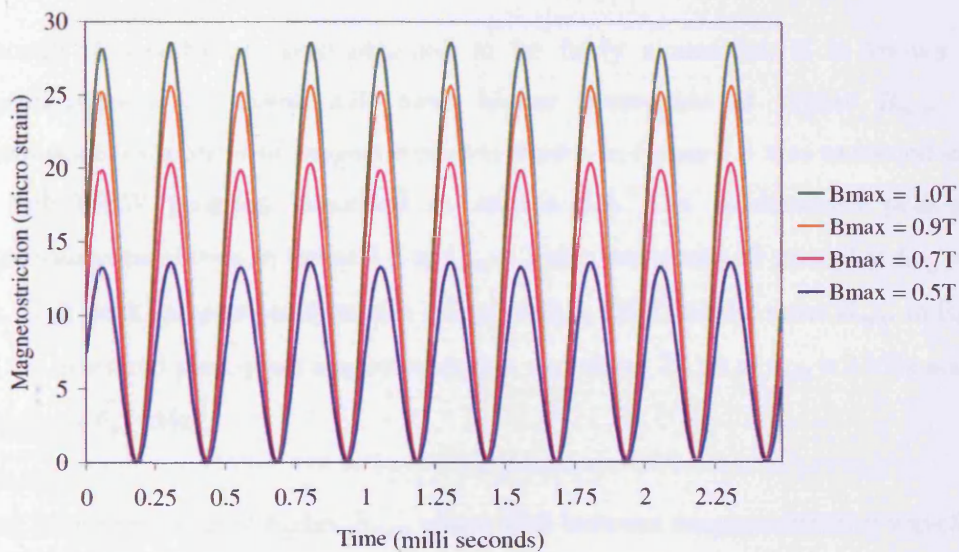
Figure 7.2. Magnetostriction waveform at  $f_{mag} = 2$  kHz for GO90°

Figure 7.3 shows the flux density waveform at the first measured resonant point for GO90° sample. The waveform is fairly sinusoidal and as mentioned in section 5.6, measured flux density waveforms are sinusoidal within 1% error of the form factor,  $FF$ .

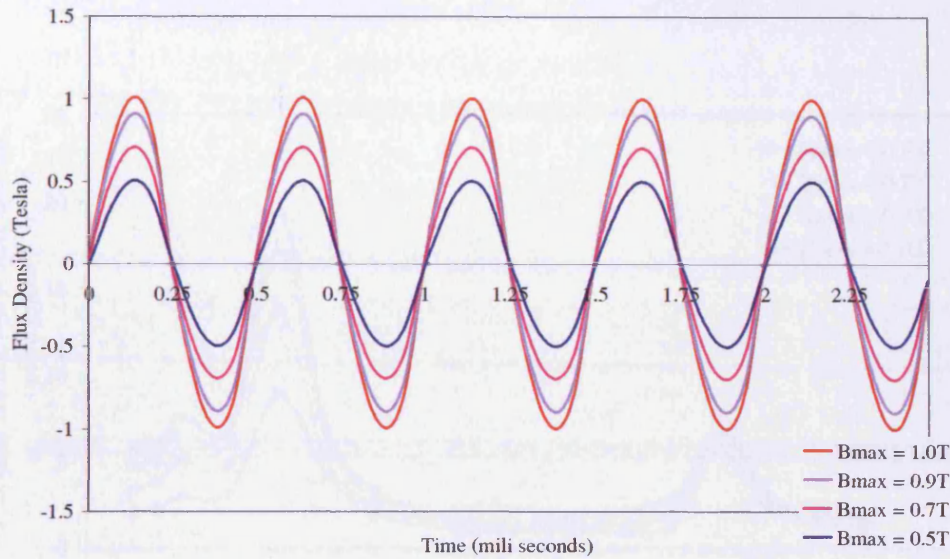


Figure 7.3. Flux density,  $B$  waveform at  $f_{mag} = 2$  kHz for  $GO90^\circ$

Although  $B$  waveforms were obtained to be fairly sinusoidal, it is known that magnetostriction waveform will have higher harmonics at higher  $B_{max}$ . The fundamental component of magnetostriction shown in figure 7.4 was extracted using the LabVIEW program described in section 5.4. The fundamental peak-peak magnetostriction shown in figure 7.4 at  $f_{mag} = 2$  kHz was about  $19 \mu\epsilon$  and at  $f_{mag} = 6.5$  kHz, peak-peak magnetostriction was  $7.7 \mu\epsilon$  at  $B_{max} 1.0$  T. At the same  $B_{max}$ , in figure 6.1, the measured peak-peak magnetostriction was about  $27 \mu\epsilon$  at  $f_{mag} = 2$  kHz and  $11 \mu\epsilon$  at  $f_{mag} = 6.5$  kHz.

Apart from harmonics at higher  $B_{max}$ , phase shift between magnetostriction waveform and  $B$  waveform was also observed. Figure 7.5 shows the plot of magnetostriction against flux density,  $B$  of  $GO90^\circ$  at  $f_{mag} = 1.5, 2$  and  $2.5$  kHz. It is observed that magnetostriction and shape of the butterfly loop is the same before resonance at  $f_{mag} = 1.5$  kHz and after resonance at  $f_{mag} = 2.5$  kHz. However at measured resonant point of  $2$  kHz, a phase shift between magnetostriction and flux density was observed, confirming the characteristics of passing through a resonant point. Similar behaviour is also observed in figure 7.6 at 3<sup>rd</sup> harmonic of the resonant point,  $f_{mag} = 6.5$  kHz, a phase shift occurred. However, peak-peak magnetostriction at  $f_{mag} = 6$  kHz and  $7$  kHz have a difference of approximately  $1 \mu\epsilon$ .

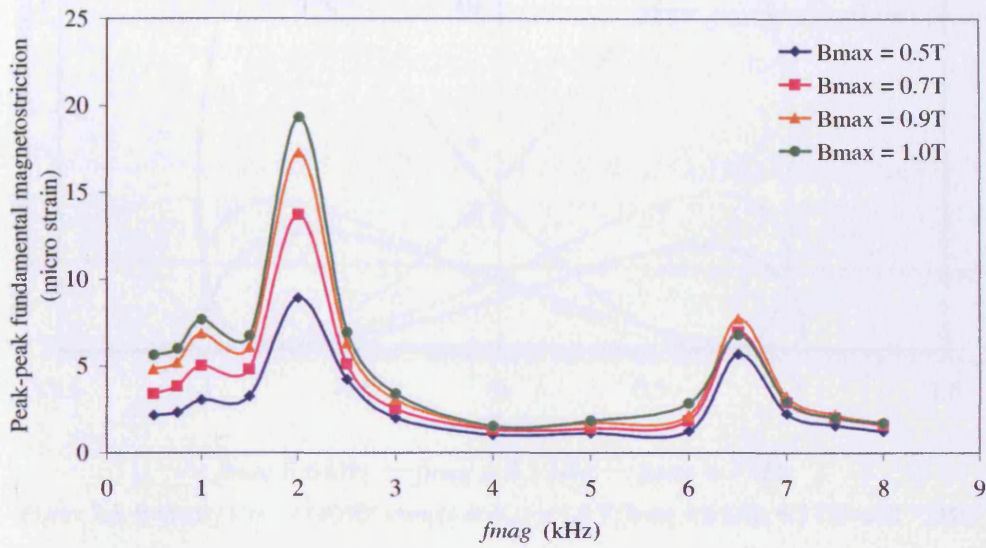


Figure 7.4. Average of fundamental peak-peak magnetostriction against various  $f_{mag}$  for  $B_{max}$  0.5 T to 1.0 T of GO90°

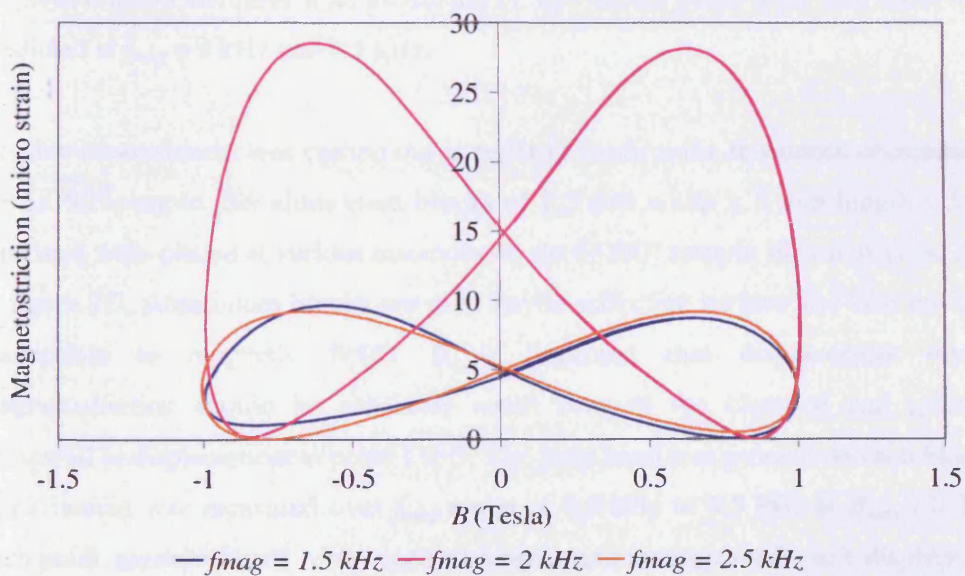


Figure 7.5. Butterfly loop of GO90° sample at  $B_{max} = 1.0$  T,  $f_{mag} = 1.5$  kHz, 2 kHz and 2.5 kHz.

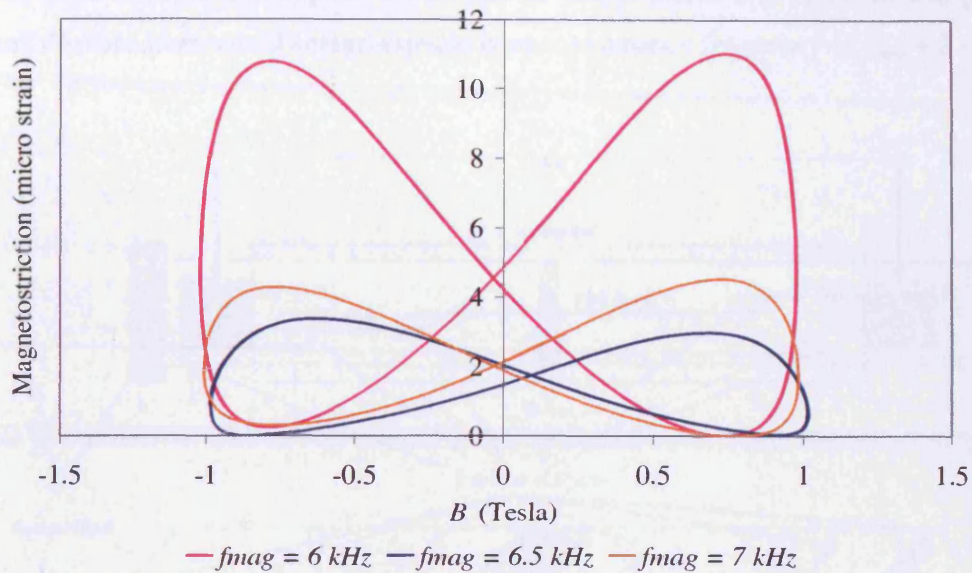


Figure 7.6. Butterfly loop of GO90° sample at  $B_{max} = 1.0 \text{ T}$ ,  $f_{mag} = 6 \text{ kHz}$ ,  $6.5 \text{ kHz}$  and  $7 \text{ kHz}$ .

In order to confirm the predicted mechanical resonance, the same sample was also used to measure magnetostriction at  $f_{mag} = 0.5 \text{ kHz}$  to  $8 \text{ kHz}$  at magnetic field,  $H = 200, 240$  and  $320 \text{ A/m}$  (figure 6.3). It was observed that vibration caused by magnetostriction increases with increasing  $H$ . Resonance peaks were also observed as predicted at  $f_{mag} = 2 \text{ kHz}$  and  $6.5 \text{ kHz}$ .

Another measurement was carried out in order to confirm the resonance occurrence in the GO90° sample. Six aluminium blocks of  $2.5 \text{ mm}$  width  $\times$   $5 \text{ mm}$  length  $\times$   $1 \text{ mm}$  thickness were placed at various distances on the GO90° sample shown as point 1 to 6 in figure 7.7. Aluminium blocks are used for its reflective surface and also not being susceptible to magnetic fields. It is expected that displacement due to magnetostriction should be relatively small near to the clamped end (point 6) compared to displacement at point 1 to 5. The laser head was pointed on each block as displacement was measured over  $f_{mag}$  range of  $0.5 \text{ kHz}$  to  $4.5 \text{ kHz}$  at  $B_{max} 1.0 \text{ T}$ . At each point, measurements were repeated 3 times and average peak-peak displacement was plotted against  $f_{mag}$  as shown in figure 7.8. As observed in figure 7.8 that first measured resonant point does occur at  $f_{mag} = 2 \text{ kHz}$  for GO90° sample. As expected, peak-peak displacement at point 6 is lower than that of points 1 to 5, where average

peak-peak displacement at point 6 was  $1.09 \mu\epsilon$  and at points 1 to 5, increase in peak-peak displacement was observed especially near resonance frequency of  $f_{mag} = 2 \text{ kHz}$ .

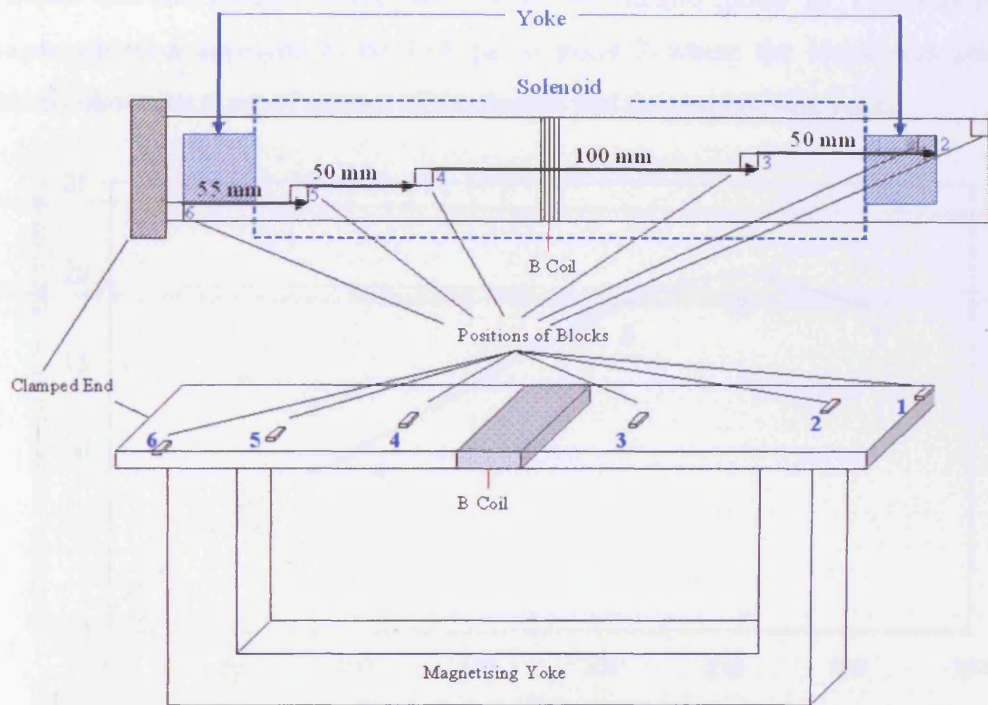


Figure 7.7. Schematic diagram of aluminium blocks placed at various distances on the sample to measure magnetostriction at various  $f_{mag}$ .

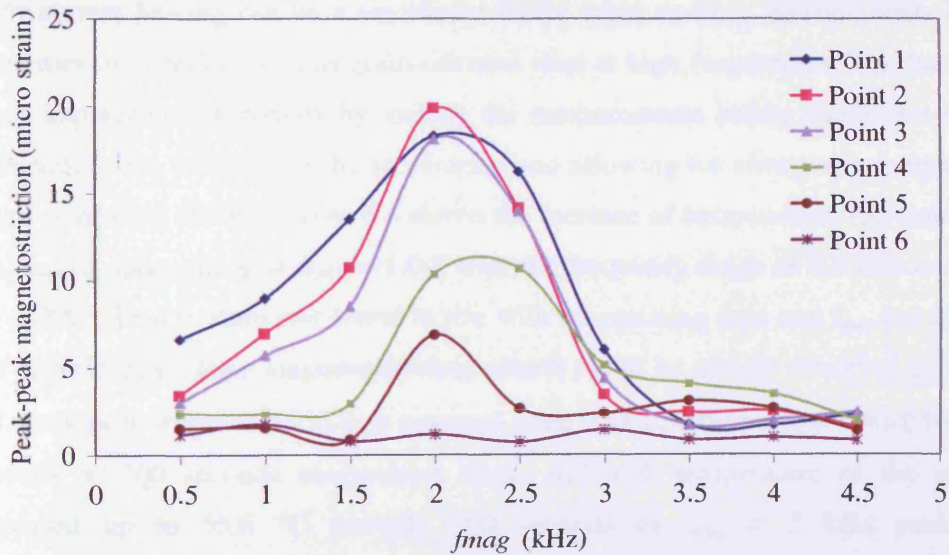


Figure 7.8. GO90° positioning at  $B_{max} = 1.0 \text{ T}$  using position aluminium blocks 2.5 mm(h) by 5 mm

Figure 7.9 shows a variation of peak-peak magnetostriction at each block along the GO90° sample at  $f_{mag} = 2$  kHz  $B_{max} = 1.0$  T. It was observed that peak-peak magnetostriction or the longitudinal displacement increases further away from the clamped end and reduces at the free end of the sample (point 1). The peak-peak magnetostriction appeared to be  $19.8 \mu\epsilon$  at point 2 where the block was placed directly above the point of contact of the sample and the magnetising yoke.

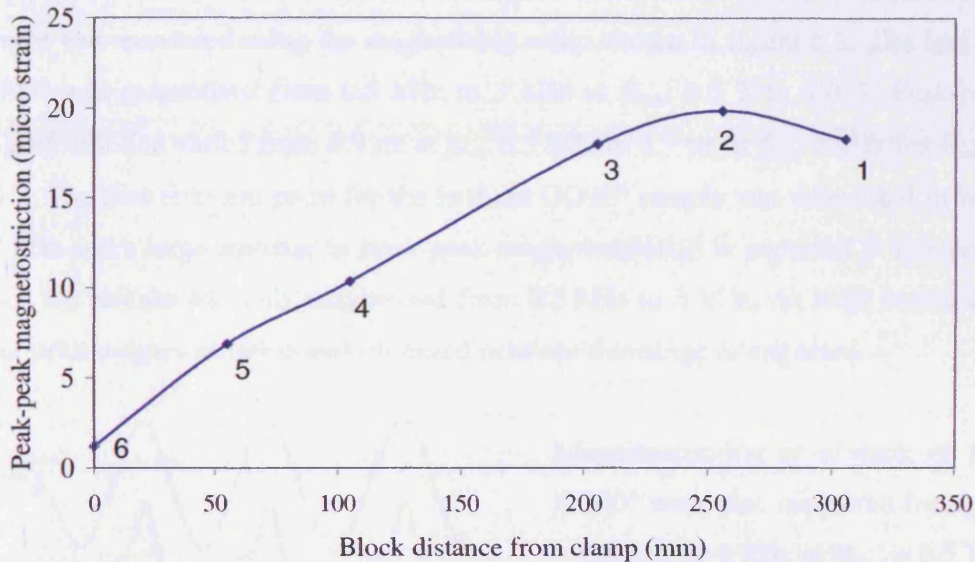


Figure 7.9. Peak-peak magnetostriction against distance of blocks (numbered 1 – 6) measured from clamped end for GO90° at  $f_{mag} = 2$  kHz  $B_{max} = 1.0$  T

Eddy current heating can be a significant factor when making measurements of the properties of materials such as grain-oriented steel at high frequencies. This has to be taken into account preferably by making the measurements before significant rise in temperature has occurred, or by monitoring and allowing for changes in temperature when comparing results. Figure 6.6 shows the increase of temperature with time from the start of magnetizing at  $B_{max} = 1.0$  T over the frequency range of 0.5 kHz to 4 kHz for GO90°. Temperature was found to rise with magnetising time and  $f_{mag}$  but this did not significantly affect magnetostriction, which could be clearly observed in figure 6.7. Peak-peak magnetostriction at resonant point 2 kHz, differs about  $6.6 \mu\epsilon$  from 60 seconds to 300 seconds magnetising time. Although temperature of the sample increased up to  $55.6$  °C towards 300 seconds of  $f_{mag} = 3$  kHz peak-peak

magnetostriction difference was only  $2.7 \mu\epsilon$  from 60 seconds magnetising time to 300 seconds.

The theoretical resonance frequency is inversely proportional to the sample length, which suggests that if sample length is double the Epstein length, resonance frequency will be halved or if the sample length is half the Epstein length, resonance frequency should be doubled. Therefore, magnetostriction of a 150 mm length  $GO90^\circ$  sample was measured using the magnetising setup shown in figure 6.8. The half cut  $GO90^\circ$  was magnetised from 0.5 kHz to 3 kHz at  $B_{max}$  0.5 T to 1.0 T. Peak-peak magnetostriction varied from  $6.9 \mu\epsilon$  at  $f_{mag}$  0.5 kHz to  $4.7 \mu\epsilon$  at  $f_{mag}$  3 kHz for  $B_{max} = 1.0$  T. The first resonant point for the half cut  $GO90^\circ$  sample was calculated to be at 4.2 kHz and a large increase in peak-peak magnetostriction is expected at this point. Since the sample was only magnetised from 0.5 kHz to 3 kHz, no large increase in peak-peak magnetostriction was observed between this range as expected.

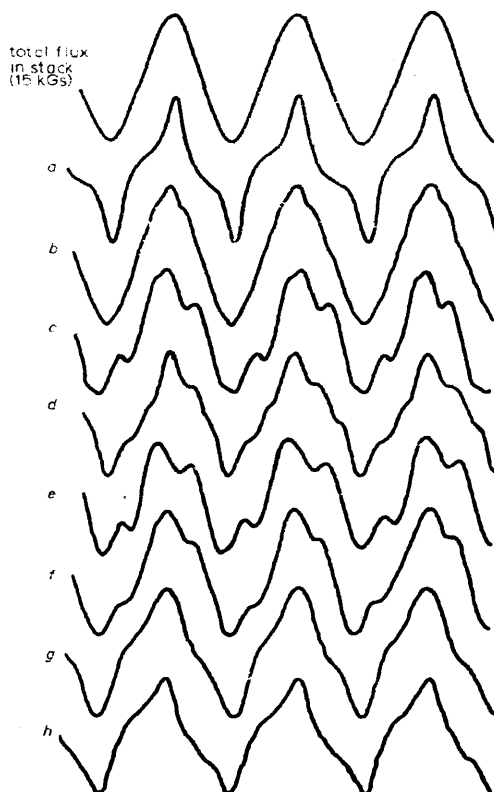


Figure 7.10. Waveforms of the total flux density for stack of 8 Epstein strips and the individual waveform for each sample in the stack where  $a - h$  represent in order the position of the samples in the stack [7.1]

Magnetostriction of a stack of five  $GO90^\circ$  were also measured from  $f_{mag} = 0.5$  kHz to 8 kHz at  $B_{max} = 0.5$  T to 0.7 T and  $f_{mag} = 0.5$  kHz to 6.5 kHz at  $B_{max} = 0.9$  T to 1.0 T. It is expected that the resonance point of a stack of  $GO90^\circ$  of the same geometry as the single strip  $GO90^\circ$  would be the same. However, sharp rise in peak-peak magnetostriction of the stack was observed at 2 kHz and 4.5 kHz (figure 6.11) rather than the expected first resonance at 2.1 kHz and 3<sup>rd</sup> harmonic of resonance at 6.3 kHz.

It is well known that the flux density distribution in a stack of strips is not uniform and rather distorted even

when the overall flux density is sinusoidal as seen in figure 7.10 [7.1]. Also in [7.1], it is said that magnetostrictive vibration of the stack does depend on the method of bonding of the strips.

In the case of GO90° stack, the strips were bonded together with adhesive tape and magnetostriction was measured on the surface of the cross-sectional area of the stack as an average magnetostriction at the point (see figure 6.10). The amplitude of peak-peak magnetostriction of the stack is 16  $\mu\epsilon$  at  $f_{mag}$  2 kHz for  $B_{max}$  1.0 T compared to 27  $\mu\epsilon$  at the same magnetising conditions for the single strip of GO90°. Although, factors such as flux density distortion and bonding of the stack could be affecting the 3<sup>rd</sup> harmonic of resonance frequency occurring at 4 kHz, large increase in peak-peak magnetostriction or resonance still occurs in a stack of GO90° material. Hence, when predicting resonance for transformer cores, it is necessary to consider the effects of flux density distribution in the laminations. This experiment also found to be in agreement with large number of previous research reported that bonding of laminations tend to reduce amplitude of magnetostriction or vibration.

Findings presented in this section are relevant to all samples that will be discussed in the following sections. Above discussed results is to verify that resonance does occur in the samples tested for this project.

### 7.2.2. 3%Si-Fe GO0°

GO0° material is a much more practical material compared to GO90° material since GO0° is widely used for magnetic cores of transformers and motors. GO0° has good magnetic properties such as high permeability and low losses as well as has much lower magnetostriction than GO90°. In section 6.3, figure 6.12, resonance peak are observed for GO0° sample although peak-peak magnetostriction is much smaller than GO90°. With the magnetising frequency range of 0.5 kHz to 8 kHz, resonance peaks were detected up to 5<sup>th</sup> harmonic. Young's modulus of GO0° was measured to be 111 GPa (figure 7.11) which is comparable to the Young's modulus value of 110 GPa obtained in [7.2] of the same sample. Calculated resonance at magnetising frequencies



were 1.6 kHz, 4.7 kHz and 7.8 kHz for 1<sup>st</sup> resonant, 3<sup>rd</sup> harmonic and 5<sup>th</sup> harmonic of resonance respectively (table 7.2).

For  $GO0^\circ$ , the magnetostriction was measured at every  $f_{mag} = 0.25$  kHz increments. The calculated first harmonic of resonance was 1.6 kHz and with uncertainty of  $\pm 8.91\%$ , calculated value could be between 1.46 kHz to 1.74 kHz. The measured value was 1.75 kHz and with 0.25 kHz increments. Hence, the measured value could lie between 1.5 kHz and 1.75 kHz. Taking into account of the uncertainty range, measured first harmonic corresponds to the calculated value. Similar to first harmonic, the measured third and fifth harmonic of resonance was found to lie between expected values.

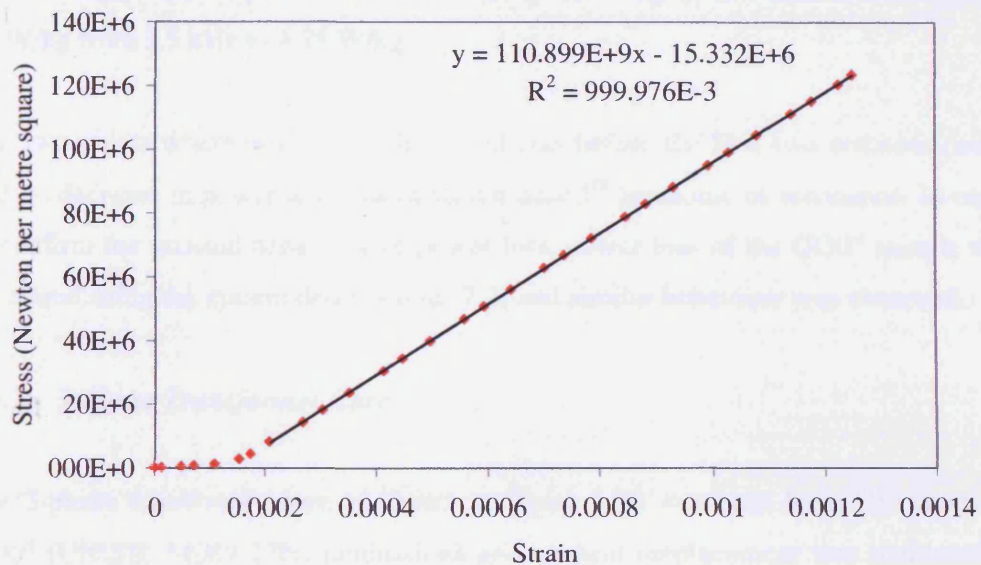


Figure 7.11. Stress-strain curve of  $GO0^\circ$  sample.

Table 7.2

Comparison of calculated and measured  $f_m$  for  $GO0^\circ$

$n^{th}$ Harmonic	$E$ (GPa)	$d$ ( $kg/m^3$ )	$l$ (mm)	$f_m$ (kHz)	
				Calculated	Measured
1	111	7650	305	$1.6 \pm 0.14$	$1.75 \pm 0.13$
3				$4.7 \pm 0.42$	$5.0 \pm 0.13$
5				$7.8 \pm 0.69$	$7.75 \pm 0.13$

Power loss measurements were taken for  $GO0^\circ$  to observe the power loss curve at resonant points. As mentioned in section 3.3.1, Thottuvelil et al reported an unusual behaviour of energy loss curves near resonance point for tape wound amorphous cores (figure 3.8) [7.3].

As shown in figure 6.13 and briefly discussed in section 6.3.1, similar unusual behaviour of power loss was observed for  $GO0^\circ$  sample. Power loss increases with  $f_{mag}$  up to 1 kHz and decrease by 44 W/kg at 1.5 kHz and increases again up to 3.5 kHz and decreases by 257 W/kg at 4.25 kHz and continued to increase as a smooth curve up to 8 kHz for  $B_{max}$  of 1.0 T. It is also reported in [7.3] that changes in core loss increases with increasing  $B_{max}$  which also agrees to what is suggested in figure 6.13. At  $B_{max} = 0.5$  T, power loss decreased by 12 W/kg from 1 kHz to 1.5 kHz and 66 W/kg from 3.5 kHz to 4.25 W/kg.

The two points where power loss decreased was before the first two resonant points and no decrease in power loss was observed near 5<sup>th</sup> harmonic of resonance. In order to confirm the unusual behaviour of power loss, power loss of the  $GO0^\circ$  sample was measured using the system described in [7.2] and similar behaviour was observed.

### 7.2.3. 3-Phase Transformer Core

The 3-phase transformer core as shown in figure 5.10 was built from 200 layers of  $GO0^\circ$  (UNISIL M089-27N) laminations and vertical displacement was measured at point 1, 2 and 3 and magnetostriction was measured at point 4. Corresponding acoustic noise was measured at point 1, 2, 3 and 5 respectively. This experiment was conducted to investigate different length laminations leading to the variability of noise output under PWM and sinusoidal excitation and predominant harmonics that exist near predicted resonant frequency of the core.

The 3-phase core was magnetized under sinusoidal and PWM voltage and the primary currents were independently adjusted to obtain balanced peak flux density,  $B_{peak}$  1.3 T and 1.5 T in the limbs. Under PWM condition  $f_s$  was varied between 1 kHz and 3 kHz. The noise was measured in turn directly above point 1 to 5 and the

corresponding core vibration was recorded.

Similar trends to figure 6.14 were found above the other points on the core surface at switching frequencies from 1 kHz to 3 kHz. In figure 6.14, the average values of acoustic noise and peak-to-peak displacement under sinusoidal excitation were 35.1 dB and  $2.0 \mu\text{m}$  at 1.3 T. So as expected, maximum values of average acoustic noise and peak-to-peak displacement were found at  $m_i = 0.5$  (around 38.5% and 63.0% respectively more than under sinusoidal excitation). At  $m_i = 1.2$ , the acoustic noise and displacements were around 25.9% and 39.0% respectively larger than under sinusoidal excitation because of over-modulation index reducing harmonic distortion in the kilohertz range in voltage waveforms. The decrease in peak-to-peak displacement and corresponding acoustic noise output with increasing modulation index was due to the lower harmonic content of the core flux density. It was also found that the noise and displacement fall with increasing fundamental frequency to 100 Hz for the same reason. At 100 Hz, the average acoustic noise and peak-to-peak displacement were measured under PWM excitation for assigned modulation index, at 1.3 T,  $f_s = 3 \text{ kHz}$ , the drop is more significant as shown in figure 6.15.

In figure 6.16, it was found that the average acoustic noise measured under PWM excitation was around 10-15 dB greater than under corresponding sinusoidal flux due to higher harmonics in the core vibration. It was also observed that an increase in switching frequency  $f_s$  lead, under all conditions, to a reduction in the acoustic noise. At 1.3 T, it was found that around 2.0 dB ( $m_i = 0.5$ ) and around 2.5 dB ( $m_i = 0.6$ ) at lowest switching frequency (1 kHz) higher than at highest switching frequency (3 kHz) respectively. In figure 6.17, it was found that around 1.9 dB ( $m_i = 0.5$ ) and around 2.0 dB ( $m_i = 0.6$ ) at lowest switching frequency 1 kHz higher than at highest switching frequency 3 kHz respectively. So under all conditions, if switching frequency was varied from 1 kHz to 3 kHz, the maximal reduction of acoustic noise was around 2.5 dB. These results enhance the benefit on the performance of the transformer core at high value of switching frequency  $f_s$ .

It is suggested in figures 6.18 (a – d) that displacement decreases with increasing  $f_s$ , where average peak-peak displacement for  $f_s = 1$  kHz is  $3.9 \mu m$ ,  $f_s = 2$  kHz is  $3.7 \mu m$ ,  $f_s = 3$  kHz is  $3.3 \mu m$ . Displacement results for both PWM and ac excitations correspond with acoustic noise results shown in figure. 6.14 where acoustic noise reduces with increasing  $f_s$ .

From table 7.1, it can be observed that at point 2, both displacement and acoustic noise decrease with increasing modulation index. Also from table 7.2, it was observed that both displacement and acoustic noise decrease with increasing switching frequency. It was also observed that displacement and acoustic noise is much lower under sinusoidal excitation compared to PWM excitation. However, the displacement and acoustic noise produced at point 2 is higher than those produced in point 1. It was also observed in table 7.3 and 7.4 that at the corner regions of the limb, the displacement and acoustic noise at point 2 and point 3 were about 1 – 2 dB higher than those in point 1. Displacement and acoustic noise behavior at point 2 and point 3 are similar and therefore only data from point 2 was used for analyzing.

Figure 6.19 (a - d) shows plots of displacement against flux density at point 2 and it can be seen that the displacement decreases with increasing switching frequency. It was observed in figure 6.20 that at lowest switching frequency  $f_s = 1$  kHz, the higher harmonic contents of the displacement than at highest switching frequency  $f_s = 3$  kHz, this was due to higher harmonic contents in the flux density waveform at lowest switching frequency  $f_s = 1$  kHz. Also, under all the PWM conditions, the harmonic contents of the displacement were much higher than under sinusoidal excitation.

The horizontal displacement on the side of the core at point 4 (see figure 5.12) was also measured and analyzed under sinusoidal and PWM excitation at 50 Hz and 100 Hz respectively. From table 7.5, it was found that at low modulation index,  $m_i = 0.5$ , average peak-to-peak displacement was 57.1% more than under sinusoidal excitation; at high modulation index,  $m_i = 1.2$ , average peak-to-peak displacement was 14.3% more than under sinusoidal excitation.

Table 7.6 shows that displacement decreases with increasing switching frequency. Compared with under sinusoidal excitation, it was found that the average peak-to-peak displacement was highest 71.4% at lowest switching frequency 1 kHz for  $B_{peak}$  at 1.3T; and lowest 47.6% at highest switching frequency 3 kHz for  $B_{peak}$  at 1.3T. This was due to the highest harmonic components of displacement at lowest switching frequency 1 kHz, and lowest harmonic components of displacement under sinusoidal excitation (figure 6.22).

Figure 6.23 (a) and (b) show the noise level measured above point 5 when the core was magnetized under sinusoidal flux and under PWM excitation with modulation indices of apparent 0.5 and 0.6 at three different  $f_s$ . The noise measured under PWM excitation is around 10-15 dB greater than under corresponding sinusoidal flux.

As for magnetization under 100 Hz fundamental voltage, if  $m_i$  was 0.5 and 0.6, the excitation voltage was not enough to magnetise the core to peak flux density of 1.3T. This is because of the limitation of variacs output range. Also, there was no 100 Hz (3-phase sinusoidal) power supply available and that is the reason why no 100 Hz sinusoidal excitation measurements were taken for all points.

Resultant acoustic noise level for the 3-phase transformer core under sinusoidal and PWM excitation was obtained from the average acoustic noise level of points 1, 2, 3 and 5. It was found that the resultant acoustic noise measured under 50 Hz PWM excitation was around 8-13 dB greater than under corresponding sinusoidal flux due to higher harmonics in the core vibration. The resultant acoustic noise measured at low modulation,  $m_i = 0.7$  was around 3 dB greater than high modulation index,  $m_i = 1.2$  at  $f = 100$  Hz (table 7.7). From table 7.8, it was observed that at worst condition ( $m_i = 0.5, 0.6, f_s = 1$  kHz), acoustic noise was around 14-15 dB and 13-14 dB greater than under corresponding sinusoidal flux at 1.3 T and 1.5 T respectively and the acoustic noise level decreased around 2 dB when the switching frequency was changed from 1 kHz to 3 kHz.

Results presented in section 6.3.2. indicate that a transformer core vibrates in a complex manner and it is difficult to relate core vibration to the longitudinal

magnetostriction in any quantitative fashion. Due to inhomogeneities in the steel, the core vibrates not only in the plane of the laminations, but also perpendicular to them and it is this vibration which produces most noise [7.4].

Extrapolation of the results to larger cores infer that the phenomenon can possibly occur in cores with different length laminations (see figure 3.7) leading to variability of noise output according to how close the magnetising frequency or predominant harmonics are to the resonant frequency.

#### 7.2.4. 3%Si-Fe GO55°

GO55° sample is known as the hard to magnetise material compared to GO90° and GO0° samples since the sample is magnetised along [111] directions. Magnetic domain in GO55° needs more energy to align towards the magnetising direction whereas, in GO0° sample, magnetic domains are more or less aligned towards to rolling direction, which is the magnetising direction. Although magnetostriction is near zero, GO55° sample is not of practical importance since it produces high losses. Magnetostriction of the Epstein sized GO55° sample was measured not only to observe the amplitude of magnetostriction is near zero, but also to confirm mechanical resonance of such sample.

A large increase in peak-peak magnetostriction or the first resonant point was observed at  $f_{mag} = 2.5$  kHz for all  $B_{max}$  (figure 6.24). At the first resonant point, magnetostriction increased up to 500% of magnetostriction at  $f_{mag} = 2.25$  kHz for  $B_{max} = 1.0$  T. It was only possible to magnetise up to  $f_{mag} = 7.5$  kHz for  $B_{max} = 0.5$  T and at this point, another increase in peak-peak magnetostriction was observed. This second increase at 7.5 kHz can be regarded as the 3<sup>rd</sup> harmonic of resonance assuming if Young's modulus  $E$  was not known.

From equation 7.1, assuming the 1<sup>st</sup> resonant point was at 2.5 kHz,  $E$  can be calculated as below.

$$f_m = \frac{n}{8l} \sqrt{\frac{E}{d}}$$

$$2.5 \times 10^3 = \frac{1}{8 \times 0.303} \sqrt{\frac{E}{7650}}$$

$$E = 281 \text{ GPa}$$

$E$  of GO55° was measured to be 266 GPa as observed in figure 7.12. Measured value of  $E$  from the stress-strain test was about 15 GPa difference from the  $E$  that is obtained from measured resonance peaks. Table 7.3 shows the comparison of calculated resonance frequency from measured  $E = 266$  GPa with measured resonance frequency.

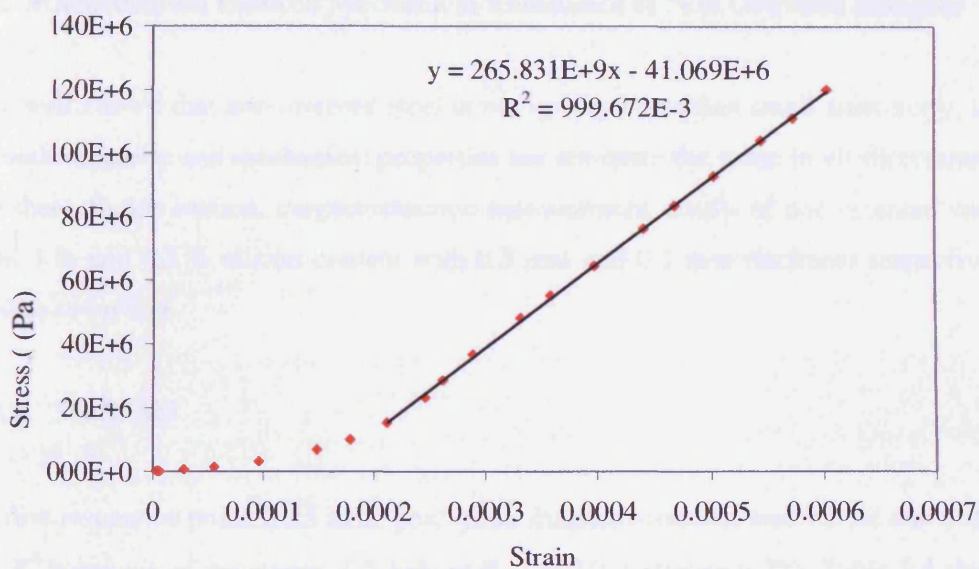


Figure 7.12. Stress-strain curve of GO55° sample.

The calculated value of first resonance was 0.1 kHz less than the measured value and the 3<sup>rd</sup> harmonic of resonance was calculated to be 0.3 kHz less than the measured value. Here, the measurement interval at first harmonic of resonance was 0.25 kHz and 0.5 kHz at third harmonic. However, for both first and third harmonic, the measured value was found to be within the expected calculated value.

Table 7.3  
Comparison of calculated and measured  $f_m$  for GO55°

$n^{\text{th}}$ Harmonic	$E$ (GPa)	$d$ (kg/m <sup>3</sup> )	$l$ (mm)	$f_m$ (kHz)	
				Calculated	Measured
1	266	7650	305	2.4 ± 0.21	2.5 ± 0.13
3				7.2 ± 0.64	7.5 ± 0.25

It can be clearly seen in figure 6.24 that even in a material known to have near zero magnetostriction as the GO55°, mechanical resonance does exist and at first resonant point, peak-peak magnetostriction increases more than 10 times higher than other magnetising frequencies at  $B_{max} = 1.0$  T.

### 7.3. Magnetisation Induced Mechanical Resonance of Non Oriented Samples

It is well known that non oriented steel is not isotropic and has small anisotropy, that is, both magnetic and mechanical properties are not quite the same in all directions in the sheet. In this section, magnetostriction measurement results of non oriented steels with 3 % and 6.5 % silicon content with 0.5 mm and 0.1 mm thickness respectively will be discussed.

#### 7.3.1. 3% Si NO

At first resonance point, 2.25 kHz, peak-peak magnetostriction was 9.3  $\mu\epsilon$  and 5.2  $\mu\epsilon$  for 3<sup>rd</sup> harmonic of resonance, 6.5 kHz at  $B_{max} = 0.9$  T (figure 6.25). Table 7.4 shows the comparison of calculated resonance frequency using the  $E = 191$  GPa obtained from figure 7.13 with measured resonance frequency.

Similar to GO0° sample, the magnetostriction was measured at every  $f_{mag}$  0.25 kHz increments. Hence, the calculated value could be between 1.8 kHz and 2.2 kHz whereas the measured value could be between 2 kHz and 2.25 kHz. Hence, the measured first harmonic corresponds to the calculated value. As for third harmonic of resonance, the calculated resonance frequency was  $6.06 \pm 0.54$  kHz while the measured value of 6.5 kHz lies within the expected value.



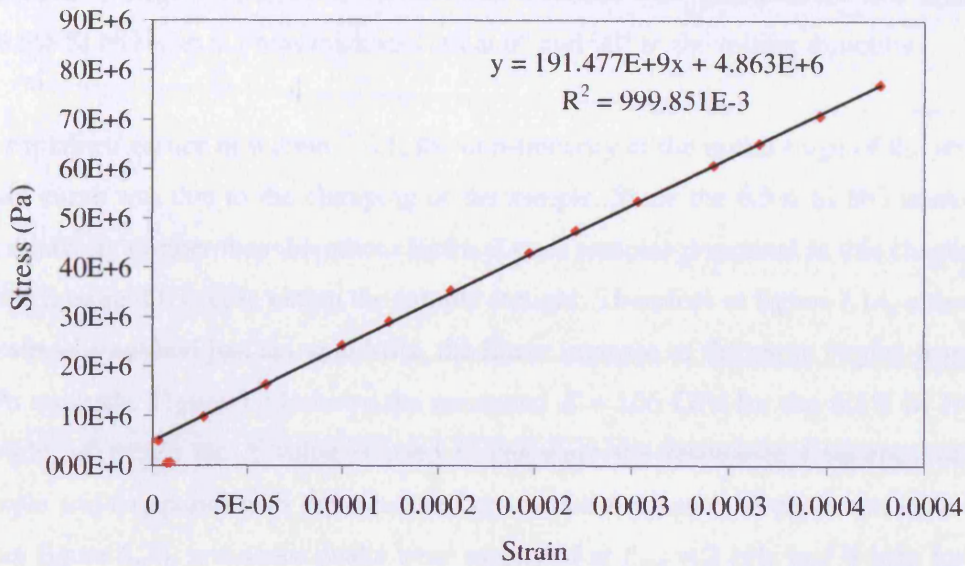


Figure 7.13. Stress-strain curve of 3% Si NO sample.

Table 7.4

Comparison of calculated and measured  $f_m$  for 3% Si NO

$n^{\text{th}}$ Harmonic	$E$ (GPa)	$d$ ( $\text{kg}/\text{m}^3$ )	$l$ (mm)	$f_m$ (kHz)	
				Calculated	Measured
1	191	7850	305	$2.02 \pm 0.18$	$2.25 \pm 0.13$
3				$6.06 \pm 0.54$	$6.5 \pm 0.13$

### 7.3.2. 6.5% Si NO

Recently, a few electrical steel companies has produced a state-of-the-art flat-rolled non-oriented steel that is 0.1 mm thick with 6.5 % Si-Fe composition. This 6.5 % non-oriented steel can be used in applications of high frequency transformer with its improved electrical resistance, low core losses, near zero magnetostriction, and high permeability. However, since mechanical resonance is a function of sample length ( $l$ ), small high frequency transformers will exhibit a high resonance frequency. Although the material is said to have 'zero' magnetostriction, in practice, the right term for this material should be 'near zero' magnetostriction since very small magnetostriction is still measured. Hence, at point of resonance, noise and vibration will still be a major concern.

Variation of magnetostriction at various flux densities was measured for two samples of 6.5% Si NO with 0.1 mm thickness cut at  $0^\circ$  and  $90^\circ$  to the rolling direction.

As explained earlier in section 7.2.1, the non-linearity at the initial stage of the stress-strain curve was due to the clamping of the sample. Since the 6.5% Si NO materials are relatively thinner than the other electrical steel samples presented in this chapter, it is much more difficult to clamp the sample straight. Therefore in figure 7.14, although the stress is applied just above 0 MPa, the linear increase of the curve begins from 15 MPa onwards. Figure 7.14 shows the measured  $E = 166$  GPa for the 6.5% Si NO $0^\circ$  sample, of which the  $E$  value is used to calculate the resonance frequency of the sample and compared with the measured resonance frequency as shown in table 7.5. From figure 6.26, resonance peaks were measured at  $f_{mag} = 2$  kHz and 6 kHz for the 6.5% Si NO $0^\circ$  sample whereas, resonance frequencies were calculated to be at 2.1 kHz and 6.3 kHz for the 1<sup>st</sup> and 3<sup>rd</sup> harmonic respectively. Magnetostriction was measured at 0.5 kHz intervals and both first and third harmonic of measure resonance frequency was found to be within the expected range of calculated value.

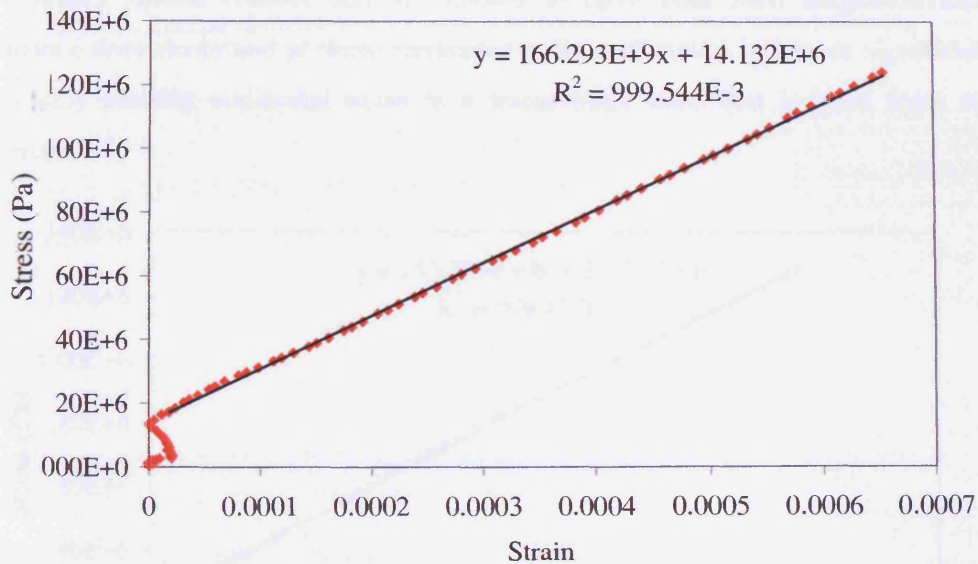


Figure 7.14. Stress-strain curve of 6.5% Si NO $0^\circ$  sample.

Table 7.5

Comparison of calculated and measured  $f_m$  for 6.5% Si NO0°

$n^{\text{th}}$ Harmonic	$E$ (GPa)	$d$ (kg/m <sup>3</sup> )	$l$ (mm)	$f_m$ (kHz)	
				Calculated	Measured
1	166	7430	280	2.1 ± 0.19	2 ± 0.25 kHz
3				6.3 ± 0.56	6 ± 0.25 kHz

Figure 7.15 shows the stress-strain curve of 6.5% Si NO90° sample from which  $E$  is 213 GPa which is about 28% higher than  $E$  of 6.5% Si NO0° sample. Resonance peaks for 6.5% Si NO90° sample were measured at 2.5 kHz and 7 kHz. Table 7.6 shows the comparison of calculated resonance frequencies with measured values of 6.5% Si NO90° sample. Resonance frequencies were calculated to be 2.4 kHz and 7.2 kHz for 1<sup>st</sup> and 3<sup>rd</sup> harmonics. The calculated resonance frequency was  $2.4 \pm 0.21$  kHz and  $7.2 \pm 0.64$  kHz for first and third harmonic respectively. Measured resonance frequency was found to agree within the uncertainty of the calculated value.

As mentioned in section 7.2.4, it is also shown in this section that although materials with higher silicon content that are known to have near zero magnetostriction, resonance does occur and at these resonance points, vibration increases significantly potentially causing additional noise to a transformer core that is built from such materials.

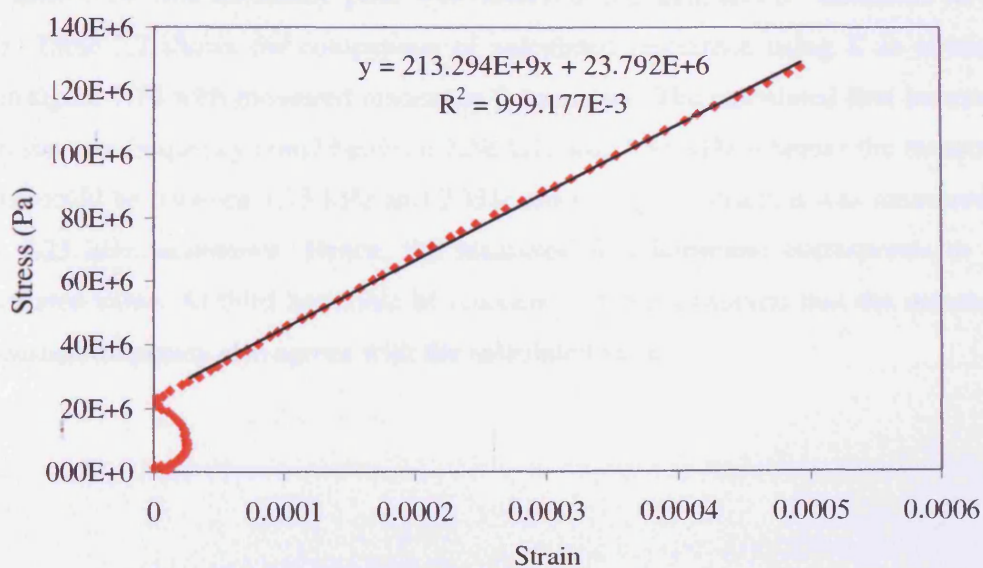


Figure 7.15. Stress-strain curve of 6.5% Si NO90° sample.

Table 7.6  
Comparison of calculated and measured  $f_m$  for 6.5% Si NO90°

$n^{th}$ Harmonic	$E$ (GPa)	$d$ (kg/m <sup>3</sup> )	$l$ (mm)	$f_m$ (kHz)	
				Calculated	Measured
1	213	7430	280	2.4 ± 0.21	2.5 ± 0.25
3				7.2 ± 0.64	7.0 ± 0.25

#### 7.4. Magnetisation Induced Mechanical Resonance of Ni-Fe Sample

Nickel is a very expensive material but when alloyed with iron in percentages of 30 – 80%, nickel-iron (Ni-Fe) alloys having better magnetic properties than electrical steels such as high permeability and low coercivity. With very high relative permeability, low power loss and high electrical resistivity, Ni-Fe are much in demand for pulse transformers and like devices [7.5]. A sheet of 45% Ni-Fe was cut into 0.303 mm by 30 mm Epstein strips and since there might be stresses induced from cutting edges, the strips were then annealed. The Ni-Fe strips were annealed at 1180 °C with 250 °C increments and cooled at the same rate to produced ideal magnetic properties of the samples. For 45% Ni composition, the saturation induction is about 1.6 T [7.6], the sample was magnetised from  $B_{max} = 0.3$  T to 0.9 T to have a sinusoidal flux without any feedback control.

In figure 6.28, first resonance peak was observed at 2 kHz and 3<sup>rd</sup> harmonic at 5.2 kHz. Table 7.7 shows the comparison of calculated resonance using  $E$  as obtained from figure 7.16 with measured resonance frequencies. The calculated first harmonic of resonance frequency could be between 1.58 kHz and 1.88 kHz whereas the measured value could be between 1.75 kHz and 2 kHz since magnetostriction was measured at  $f_{mag}$  0.25 kHz increments. Hence, the measured first harmonic corresponds to the calculated value. At third harmonic of resonance, it was observed that the measured resonance frequency also agrees with the calculated value.

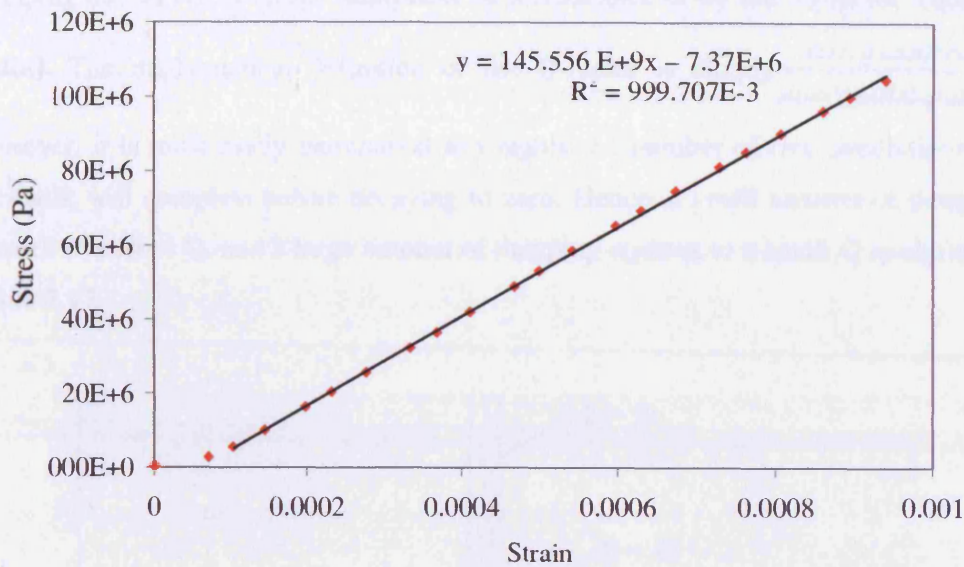


Figure 7.16. Stress-strain curve of 45% Ni-Fe sample.

Table 7.7

Comparison of calculated and measured  $f_m$  for 45% Ni-Fe.

$n^{\text{th}}$ Harmonic	$E$ (GPa)	$d$ ( $\text{kg/m}^3$ )	$l$ (mm)	$f_m$ (kHz)	
				Calculated	Measured
1	120	8071	305	$1.73 \pm 0.15$	$2.0 \pm 0.13$
3				$5.21 \pm 0.46$	$5.25 \pm 0.13$

### 7.5. Damping

All matter such as solid, liquid and gaseous matter, is capable of vibration. Such vibration can be natural vibration or forced vibration. From the results shown in chapter 6 and the discussion in the previous sections, resonance can be described as the condition of maximum amplitude when the frequency of magnetostriction coincides with or when it is near the natural frequency of the electrical steel strips. In the absence of damping or other amplitude limiting devices, resonance is the condition at which a system gives an infinite response to a finite excitation. However, this is not the case for the results shown in this thesis. The resonance peaks are observed to be damped through dissipation of energy. At resonance the amount of energy lost due to damping is equal to the rate of energy supplied by magnetostriction.

Damping has an effect on the 'sharpness' of a resonance or by the 'Q-factor' (quality factor). The mathematical definition of the Q-factor is simply  $\frac{\text{energy.stored}}{\text{energy.dissipated}}$ . However, it is most easily understood as roughly the number of free oscillations the oscillator will complete before decaying to zero. Hence, a small amount of damping equates to a large Q, and a large amount of damping equates to a small Q as shown in figure 7.17.

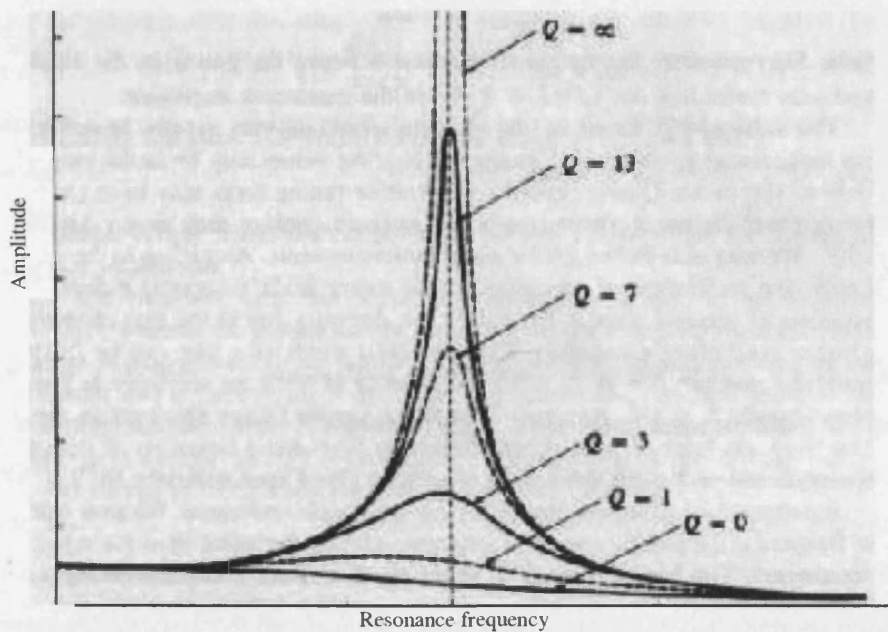


Figure 7.17. Damping of resonance peaks in terms of Q

In the case of the electrical steel strips, damping is not localised and viscous but is usually distributed and mostly non-linear i.e. not simply proportional to velocity. Hence, other assumptions will have to be made and predictions regarding its behaviour damping can only be approximate.

## 7.6. Summary

A thorough investigation was carried out on Epstein sized GO90° sample to show that resonance occurs at the predicted resonance frequency of  $f_{mag} = 2$  kHz. In addition, 2<sup>nd</sup> resonance mode (3<sup>rd</sup> harmonics of resonance) of the sample was also observed at  $f_{mag} = 6.5$  kHz during the investigation. Magnetostriction of GO90° strip was measured at

$f_{mag}$  0.5 – 8 kHz under flux densities of 0.5, 0.7, 0.9 and 1.0 T. An increase in magnetostriction was found at resonance and this increase was also seen when measuring magnetostriction under magnetic fields of 200, 240 and 320 A/m. Magnetostriction was also measured at 6 various points along the sample to observe resonance at these points where increase in magnetostriction was found at  $f_{mag} = 2$  kHz. The GO90° sample was then cut half in length (150 mm) and similar experiment was carried out to confirm predicted resonance at  $f_{mag} = 4.2$  kHz. Although the half cut sample was not magnetised up to  $f_{mag} = 4.2$  kHz, no significant increase in magnetostriction was observed between  $f_{mag} = 0.5 - 3$  kHz. However, when a stack of five Epstein sized GO90° samples were bonded with adhesive tape and similar experiment was carried out, the 3<sup>rd</sup> harmonic of resonance was observed at  $f_{mag} = 4.5$  kHz; different from predicted 3<sup>rd</sup> harmonic at  $f_{mag} = 6.3$  kHz. The results from GO90° stack shows that the flux density distortion can affect the resonance mode of the sample or a transformer core.

As for the GO0° sample, 3 resonance modes were observed at  $f_{mag} = 1.75, 5.00$  and  $7.75$  kHz for 1<sup>st</sup>, 2<sup>nd</sup> and 3<sup>rd</sup> harmonic of resonance respectively. An unusual behaviour of power loss curve was observed near resonance frequency where power loss increases with  $f_{mag}$  up to 1 kHz and decrease by 44 W/kg at 1.5 kHz and increases again up to 3.5 kHz and decreases by 257 W/kg at 4.25 kHz. Acoustic noise and displacement results from the 3-phase transformer core show that both acoustic noise and displacement increases with increasing flux densities and magnetising frequencies. Acoustic noise output of a 3-phase transformer operating under PWM were around 10-15 dB higher than under sinusoidal flux showing the effect of the higher harmonics of the core vibration due to excitation waveform.

Results from near zero magnetostriction materials such as GO55° and 6.5% Si NO also show that magnetostriction increases at predicted resonance frequencies and at least 2 resonance modes were observed for each material. Although higher silicon content and cut direction along the hard direction [111] produces low magnetostriction, at resonance point, magnetostriction is found to increase significantly. As for non oriented materials having very small anisotropy, mechanical resonance is found to be different for different cut directions of the samples where

resonance modes occur at different  $f_{mag}$ . Resonance frequency was also observed in 45% Ni-Fe alloy with better magnetic properties than electrical steels. Again, two resonance modes were observed for 45% Ni-Fe.



**References**

- [7.1] S A Majed and J E Thompson, 'Magnetic Properties of Grain-oriented Silicon Iron, Part 3 – Magnetostrictive Stress Sensitivity of Simple Assemblies of Strips', Proceedings of IEE, Vol. 117, No. 1, pages 243-248, 1970.
- [7.2] P I Anderson, 'Evaluation of Magnetostriction Measurement Techniques', MSc Dissertation, University of Wales, 1996.
- [7.3] A J Thottuvelil, T G Wilson and H A Owen Jr, 'Unusual High-Frequency Behaviour of Some Amorphous Metallic-Alloy Tape-Wound Magnetic Cores', IEEE Transactions on Magnetics, Vol. Mag-20, No. 4, pages 570-578, 1984
- [7.4] A J Moses, 'Measurement of Magnetostriction and Vibration with Regard to Transformer Noise', IEEE Transactions on Magnetics, Vol Mag-10, No. 2, pages 154-156, 1974.
- [7.5] P Beckley, 'Electrical Steels', European Electrical Steels, Orb Works, 2000.
- [7.6] D Jiles, 'Introduction to Magnetism and Magnetic Materials' Chapman & Hall, 1991.

---

## CHAPTER 8

### CONCLUSIONS AND FUTURE WORK

---

#### 8.1. Conclusions

It is clearly shown in this thesis that materials that are used to make transformer cores, in particular, grain oriented, non oriented and nickel-iron alloys resonate at certain frequencies and at this point, the amplitude of vibration increases significantly; potentially adding to noise produced by transformer cores which already are a major environmental concern.

It can be concluded that there are five major factors to consider when designing a transformer core;

##### 1) *Dimensions*

Equation 7.1 shows that the resonance frequencies are dependent on the length of the core. The smaller the transformer core is, the higher the resonance frequency will be. Hence, the length of the core where longitudinal vibration or magnetostriction occurs should be taken into consideration in particular small high frequency transformer core to avoid core being magnetised close to resonant frequency or its predominant harmonics.

##### 2) *Material selection*

Having better magnetic properties by increasing silicon content in electrical steels not necessarily reduces the risk of a transformer core built from such material producing excessive vibration and acoustic noise. It was shown that near zero magnetostriction materials increases vibration at predicted resonance frequencies

##### 3) *Bonding method*

Vibration and resultant acoustic noise output at clamped end was found to be smaller than free end. However, in a stack of bonded laminations, it was shown that flux density distortion can affect the resonance mode of a core. Although

vibration and acoustic noise reduces at point of bonding, at resonance, vibration increases considerably. This is shown to imply that the phenomenon is indeed the cause of excessive noise found in some medium or high frequency power transformers and in transformers operating under distorted flux conditions. Hence, clamping or bolting a transformer core should be considered when designing a transformer core.

#### 4) *Excitation frequency*

The resultant acoustic noise measured under PWM voltage was found to be greater than under corresponding sinusoidal condition due to higher harmonic contents in the core vibration. It was understood that care should be taken when selecting PWM magnetising frequencies especially in the case of inverters where the higher harmonic contents of vibration could indicate mechanical resonance phenomenon that is a possible cause of deterioration of a core performance by increasing vibration and acoustic noise.

Transformer cores having sinusoidal excitation such as power transformers operate at much lower frequencies (eg 50 Hz, 60 Hz) compared to PWM (eg 1 kHz, 2 kHz etc) excitation. However, such power transformers can be larger in dimensions and as stated in 1), larger length of core will result in resonance occurring at much lower magnetising frequency.

Therefore, design of a transformer at desired excitation frequency should be careful selected to avoid excitation at or near resonance.

#### 5) *Harmonics of vibration*

Using equation 7.1, it can be calculated that a transformer core made from grain oriented material cut along rolling direction with length of 0.5 m would resonate at 0.95 kHz magnetisation. Although a transformer core of length 0.5 m may not be designed to operate at 0.95 kHz magnetisation, harmonics of vibration can coincide with the resonance frequency. It was shown that harmonics of vibration

under PWM excitation can increase vibration and noise output of a transformer core.

Since, there are increasing numbers of renewable energy plants (e.g. wind turbines) the electrical energy is processed by means of PWM, there is a tendency to use the transformer as a "self-filtering" electromagnetic device. In such a case there are far more higher harmonics which can be dangerous if the natural frequency coincides with any of the higher harmonics. Hence harmonics of vibration should be taken into consideration when designing a transformer core.

## 8.2. Future Work

Harmonic analysis of the transformer vibration at different points on the core can be carried out at the normal operating frequency of such transformers. This can be followed by vibration measurement on the same points of the core but excited at expected mechanical resonance frequencies. Flux distortion of laminations should also be considered. Harmonics of transformer vibration can be quantified at the resonance frequencies and acoustic noise input from such harmonics can be analysed. It will also be useful to quantify long term transformer efficiency affected by such harmonics of vibration that coincide with the mechanical resonance of the transformer itself.

The present investigation has also given rise to extend mathematical approach in predicting mechanical resonance for cores made from materials used in this investigation but different geometries such as toroidal cores. Although the laser Doppler vibrometer has an advantage in ease of use to measure magnetostrictive vibration, in the case of toroidal cores, resistance strain gauges will be more advantageous. The Laser vibrometer can only measure vibration at a surface whereas strain gauges can measure displacement between the laminations of a toroidal core.

A further development to the current magnetostriction measurement system to an automated computer controlled system would be an added advantage. This can be done by using a high performance GPIB interface such as the NI-PCI-GPIB or a data

acquisition card (DAQ) such as the NI-PXI-5922. Such interface or DAQ have only become commercially available in the last three years but the cost of the interface can be considerably high. LabVIEW can be used to communicate with signal generator, laser vibrometer and the oscilloscope. In addition, a digital feedback system can be integrated in the LabVIEW program in order to magnetise to higher than 1.7 T while maintaining a sinusoidal  $B$  waveform. The computer controlled system would be able to produce more data points on the frequency against magnetostriction characteristic around the resonance points to improve the measurement accuracy.

**APPENDIX I – PUBLISHED WORK**

---

1. X G Yao, **Thant P P Phway**, A J Moses, F Anayi, “Magneto-mechanical resonance in a 3-Phase transformer core under PWM voltage excitation”, Abstract submitted for poster contribution to IEEE International Magnetics Conference, January 2008, Madrid, Spain.
2. **Thant P P Phway**, A J Moses, “Magnetostriction trend of non-oriented 6.5% Si-Fe”, Contributed for poster presentation at 18<sup>th</sup> Soft Magnetic Materials, September 2007, Cardiff, UK. Paper to be published in Journal of Magnetism and Magnetic Materials.
3. **Thant P P Phway**, A J Moses, “Magnetisation induced mechanical resonance in electrical steels”, Journal of Magnetism and Magnetic Materials, Vol. 316, pages 468-471, 2007. Contributed oral presentation for 3<sup>rd</sup> Joint European Magnetics Symposia, June 2006, San Sebastian, Spain.
4. Yao X Guang, **Thant P P Phway**, A J Moses, F Anayi, “Acoustic noise and displacement analysis of a 3-phase transformer core under sinusoidal and PWM excitations”, XVII International Conference on Electrical Machines, 2006. Contributed oral presentation for XVII International Conference on Electrical Machines 514 OTM4-4, September 2006, Crete, Greece.
5. **Thant P P Phway**, S Zurek, T Meydan, D Walmsley, “Control tip oscillation in magnetostrictive dental scalers”, Journal of Sensors and Actuators A: Physical, vol 129/1-2, pages 167-171, 2006. Contributed oral presentation for 5<sup>th</sup> European Magnetic Sensors and Actuators Conference, July 2004, Cardiff, United Kingdom.
6. **Thant P P Phway**, A J Moses, D C Jiles, “Frequency dependence of magnetostriction for magnetic actuators”, Journal of Electrical Engineering, vol 55, No 10/S, pages 7-10, 2004. Contributed oral presentation for Magnetic Measurements, June 2004, Prague, Czech Republic.

# Magneto-mechanical resonance in a model 3-phase 3-limb transformer core under sinusoidal and PWM voltage excitation

Xiao Guang Yao<sup>1</sup>, Thant. P. P. Phway<sup>2</sup>, A. J. Moses<sup>1</sup> and F. Anayi<sup>1</sup>

<sup>1</sup>Wolfson Centre for Magnetics, School of Engineering, Cardiff University, Queen's Building, The Parade, Newport Road, Cardiff CF24 3AA, Wales, UK

<sup>2</sup>Schlumberger Drilling & Measurements, Unit 8, Kirkton Avenue, Pitmedden Industrial Estate, Dyce, Aberdeen AB21 0UB, Scotland, UK

This investigation presents the measurement results of acoustic noise and vibration for a model three-phase three-limb transformer core under sinusoidal and PWM voltage excitation for assigned value of modulation index with increasing switch frequency from 1 kHz to 3 kHz at no-load condition. Results imply that the acoustic noise decreased around 2 dBA with increasing switch frequency. However, the magneto-mechanical resonance phenomenon was observed at 1.5 kHz excitation frequency, which could cause excess acoustic noise under some excited conditions as well as affecting efficiency of the transformer core.

*Index Terms*—Acoustic noise, Magneto-mechanical resonance, PWM, Vibration

## I. INTRODUCTION

Increased environmental consciousness has given rise to further reduce the acoustic noise level of transformer core. The causes and reduction of transformer noise has been the subject of extensive research articles even before discovering that magnetostriction was the main source of noise in transformer cores. However, only sinusoidal voltage supplies were considered in all these studies [1] [2].

Transformers subjected to PWM voltage excitation are becoming more common in industrial applications and renewable energy supply systems, such as active power line conditioning and wind turbine system [3] [4]. Therefore, improvement in the performance of transformer cores under PWM voltage excitation has become prominent. Very limited research work has been reported on acoustic noise level for transformer core under PWM voltage excitation [5], and also almost no study has been reported on magneto-mechanical resonance in transformer cores. If a transformer core is subjected to resonance under magnetisation, the vibration of the core can enhance the output acoustic noise of the core as well as flapping of laminations which could affect the efficiency of the transformer core.

In this investigation, acoustic noise and vibration behaviour of a model 3-phase 3-limb transformer core under sinusoidal and PWM voltage excitation for assigned value of modulation index with increasing switching frequency at no-load condition were analysed.

## II. DEFINITIONS

### A. Modulation Index and Switching Frequency

A PWM voltage waveform is obtained by comparing a

reference voltage waveform (modulating signal, usually sinusoidal) with a carrier voltage waveform (usually triangular). That is, the PWM waveform is a synthesis of a reference voltage waveform (amplitude  $A_{ref}$ , frequency  $f$ ) and carrier voltage waveform (amplitude  $A_c$ , frequency  $f_c$ ) at different frequencies. The PWM output voltage waveform synthesis is illustrated in fig. 1.

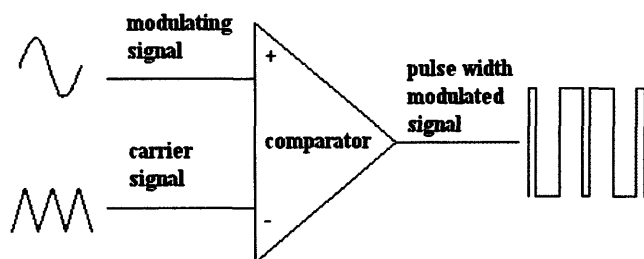


Fig. 1. Pulse width modulating PWM waveform generated by comparison between sinusoidal control signal and carrier (triangular) signal.

Two key parameters which determine the performance of PWM inverters are modulation index  $m_a$  and switching frequency  $f_s$  (frequency of the carrier voltage waveform  $f_c$ ). The modulation index  $m_a$  is given by (1).

$$m_a = \frac{A_{ref}}{A_c} \quad (1)$$

### B. Sound Pressure Level

The acoustic A-weighted Sound Pressure Level (SPL) is given by (2):

$$SPL(dBA) = 20 \log_{10} \frac{n_{mea}}{n_{ref}} \quad (2)$$

where  $n_{mea}$  is the measured pressure level,  $n_{ref}$  is the reference pressure level. The scale in (2) uses the hearing threshold of 20  $\mu$ Pa as the reference level of 0 dB.

### C. Total Harmonic Distortion

The harmonic content of a periodic waveform  $v(t)$  is described by the Total Harmonic Distortion  $THD[\%]$  given by

$$THD[\%] = \frac{\sqrt{\sum_{n=2} v_n^2}}{v_1} \times 100 \quad (3)$$

where  $v(t)$  and  $v_1$  are the amplitude of the fundamental and harmonic component of order  $n$ , respectively.

## III. EXPERIMENTAL SETUP

### A. Model Transformer Core Construction

A model 3-phase 3-limb transformer core was assembled by 1000 laminations each of 0.27 mm thick grain-oriented 3% silicon electrical steel which is believed to resonate when magnetised at approximately 1.5 kHz in the form of Epstein strips [6]. The core dimensions and positions at which acoustic noise and vibration were measured are shown in fig. 2. Since the transformer core is not necessarily symmetrical, an average noise should be measured instead of just one point of the transformer core. Therefore, noise level was measured at 4 different point of the core and acoustic noise level of the core was presented as an average value of the noise obtained at point 1, 2, 3, 5 shown in fig 2.

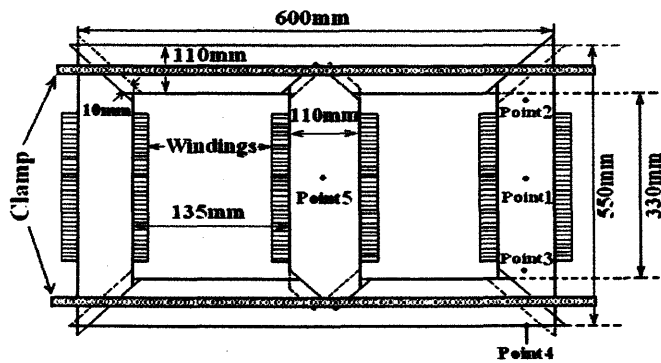


Fig. 2. Layout of the core showing positions of measuring points.

### B. Magnetising System

A 3-phase PWM inverter (Toshiba inverter TOSVERT VF-A3) was connected to three individual variacs, which supplied the three primary windings of the core and enabled the core to be magnetised at peak flux density value up to  $1.5 \pm 0.015$  T at no-load condition. The primary and secondary windings, all

connected in delta configurations, had 50 turns of copper wire each. The primary phase voltages could be adjusted by means of three individual variacs to produce equal flux densities in the three limbs. The magnetising system is shown in fig. 3.

Output voltage regulation function (OV %) is an important function in the PWM inverter, which controls the modulation index and is varied over the range of 40 % – 90 %, which corresponds approximately to modulation index  $m_a$  from 0.5 to 1.2. In this investigation work, OV % was selected 50 %, which corresponds approximately to modulation index  $m_a = 0.6$  with switching frequency  $f_s$  varied from 1 kHz to 3 kHz.

The fundamental magnetisation frequency was 50 Hz and the peak flux density was set to 1.5 T.

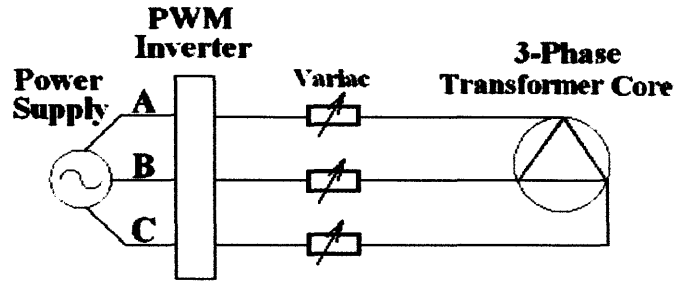


Fig. 3. Magnetising circuit for the core under PWM voltage excitation.

### C. Experimental Procedure

The sound pressure level was recorded using a microphone (Brüel & Kjaer type 4231), which was placed 0.5 m vertically above points 1, 2, 3 and 5 in turn; the corresponding core vibration, which the vertical vibration of the core surface at points 1, 2, 3 and horizontal displacement on the side of the core at point 4 were measured using a single-point laser vibrometer (SPLV) [6]. The uncertainty of Sound Pressure Level measurement system  $u(dB)$  is  $\pm 0.2$  dBA when 20  $\mu$ Pa is at reference condition [2]. SPLV is a non-contact vibration measurement technique that allows direct measurement of velocity or displacement to an accuracy of  $\pm 2$  nm. The sound pressure signal from microphone and vibration signal from SPLV were recorded by a digital oscilloscope (YOKOGAWA DL716 - 16CH), which displays and saves data in 16-bit resolution at 16 Ms/s (sampling rate). The saved data was analysed using algorithms embedded in National Instrument LabVIEW and Simpler Simulation Centre software.

The core was assembled and dismantled twice. At each time, the measurement was taken three times at each measuring point under each excitation condition. The repeatability of the resultant acoustic noise results was found to be around  $\pm 1\%$  and the vibration results was around  $\pm 2\%$ .



In order to measure the true acoustic noise and vibration produced only by the transformer core, the transformer core is isolated from the ambient noise, such as the noise generated by variacs, which could interfere with the measurement results. The transformer core, laser head and microphone was placed in the anechoic chamber (fig 4) while the magnetising system was placed outside the chamber. The anechoic chamber (width  $\times$  length  $\times$  height = 3.3 m  $\times$  2.1 m  $\times$  2.1 m) is insulated on all surrounding walls, including the ceiling with acoustically damped material.

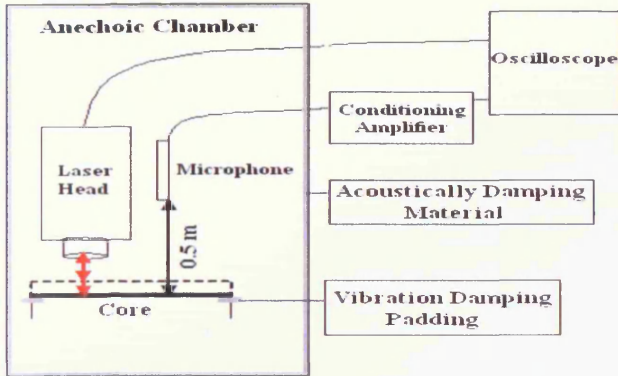


Fig. 4. Vibration and acoustic noise measurement setup placed in an anechoic chamber.

IV. RESULTS AND DISCUSSION

Table 1 shows the resultant results of acoustic noise of the core, the average peak-to-peak vertical displacement at point 2 and horizontal displacement at point 4 under sinusoidal and PWM voltage excitation for assigned value of modulation index  $m_a = 0.6$  with increasing switching frequency  $f_s$  from 1 kHz to 3 kHz, at  $f = 50$  Hz,  $B_{peak} = 1.5$  T.

TABLE 1  
RESULTANT ACOUSTIC NOISE AND AVERAGE DISPLACEMENT UNDER SINUSOIDAL AND PWM VOLTAGE EXCITATION

Waveform	Modulation index	Switching frequency	Resultant acoustic noise (dBA)	Displacement (micro meter)	
				Point 2	Point 4
sine 50 Hz	--	--	39.5	2.3	0.48
		1 kHz	52.8	3.8	0.59
PWM 50 Hz	0.6	2 kHz	51.6	3.5	0.56
		3 kHz	50.8	3.4	0.54

TABLE 2  
THD[%] OF DISPLACEMENT UNDER SINUSOIDAL AND PWM VOLTAGE EXCITATION

Waveform	Modulation index	Switching frequency	THD[%]	
			Point 2	Point 4
sine 50 Hz	--	--	27.5	11.1
		1 kHz	42.4	43.2
PWM 50 Hz	0.6	2 kHz	39.7	40.4
		3 kHz	38.4	37.2

The harmonic components of vibration at point 2 and point 4 were obtained by Fast Fourier Transform (FFT) method, performed with Day Post Processor in the Ansoft Simplorer environment. Fig. 5 to fig. 8 display the harmonic components of vertical displacement at point 2, fig. 9 to fig. 12 display the harmonic components of horizontal displacement at point 4 under sinusoidal and PWM voltage excitation for assigned value of modulation index  $m_a = 0.6$  with switching frequency  $f_s$  varied from 1 kHz to 3 kHz, at magnetising frequency  $f = 50$  Hz,  $B_{peak} = 1.5$  T. The THD[%] of vibration at point 2 and point 4 were also calculated using FFT analysis, which is shown in table 2.

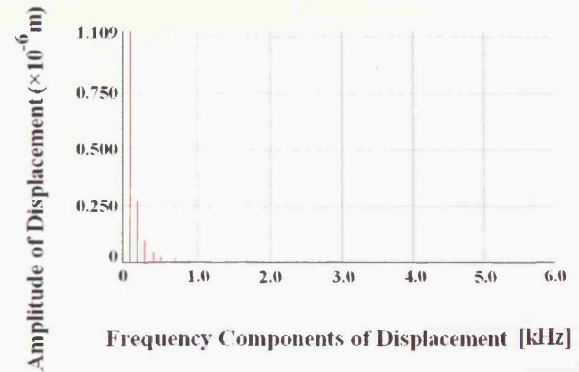


Fig. 5. Harmonic components of vertical displacement at point 2 under sinusoidal voltage excitation,  $f = 50$  Hz,  $B_{peak} = 1.5$  T.

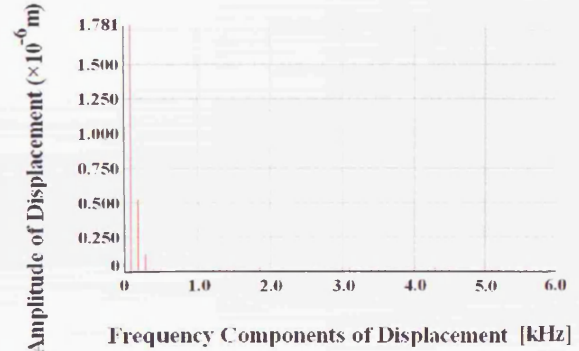


Fig. 6. Harmonic components of vertical displacement at point 2 under PWM voltage excitation,  $f = 50$  Hz,  $m_a = 0.6$ ,  $f_s = 1$  kHz,  $B_{peak} = 1.5$  T.

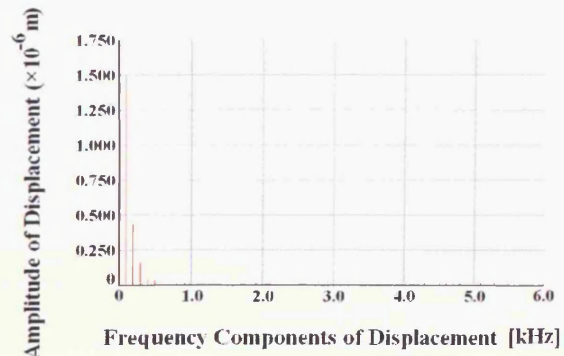


Fig. 7. Harmonic components of vertical displacement at point 2 under PWM voltage excitation,  $f = 50$  Hz,  $m_a = 0.6$ ,  $f_s = 2$  kHz,  $B_{peak} = 1.5$  T.

It is clearly noticed that the displacement decreases with increasing  $f_s$  (see table 1). However, at  $f_s = 3$  kHz (fig. 8 and fig. 12), the amplitude of harmonic component at around 3 kHz is higher than at  $f_s = 1$  kHz and 2 kHz, indicating magneto-mechanical resonance.

The resultant acoustic noise measured under PWM voltage excitation is around 11-13 dBA greater than under corresponding sinusoidal condition due to higher harmonic contents in the core vibration (see table 2). The average vertical and horizontal displacement decreases by around  $0.4 \mu\text{m}$  and  $0.05 \mu\text{m}$  with increasing switching frequency from 1 kHz to 3 kHz is due to lower amplitude harmonic content of the displacement. Similar trends were found for other points.

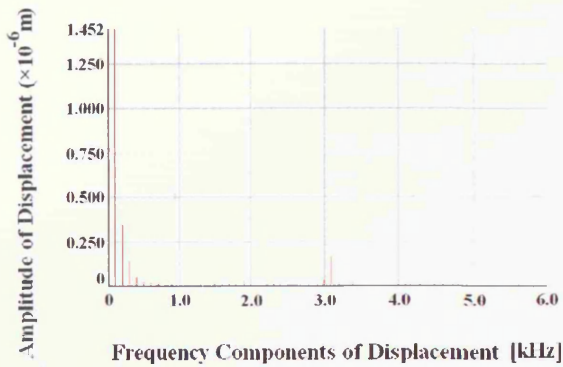


Fig. 8. Harmonic components of vertical displacement at point 2 under PWM voltage excitation,  $f = 50$  Hz,  $m_a = 0.6$ ,  $f_s = 3$  kHz,  $B_{peak} = 1.5$  T.

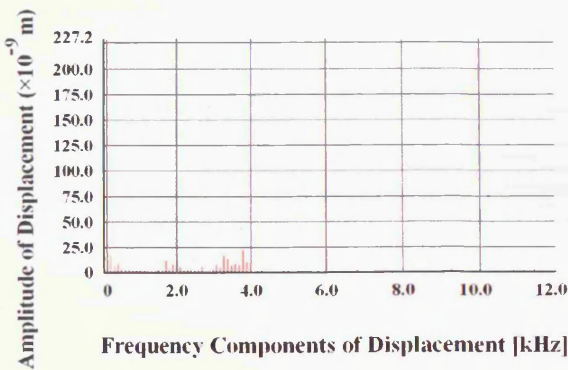


Fig. 11. Harmonic components of horizontal displacement at point 4 under PWM voltage excitation,  $f = 50$  Hz,  $m_a = 0.6$ ,  $f_s = 2$  kHz,  $B_{peak} = 1.5$  T.

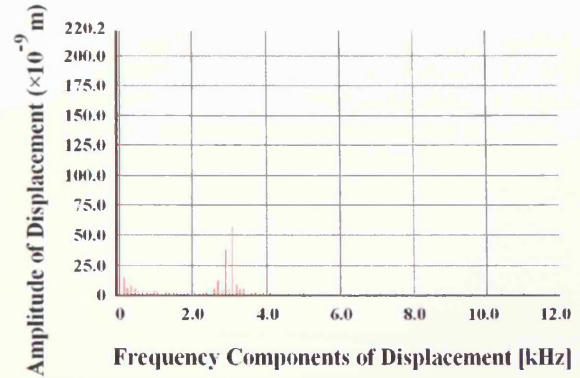


Fig. 12. Harmonic components of horizontal displacement at point 4 under PWM voltage excitation,  $f = 50$  Hz,  $m_a = 0.6$ ,  $f_s = 3$  kHz,  $B_{peak} = 1.5$  T.

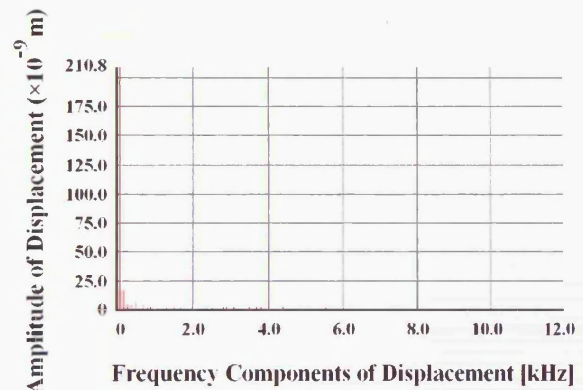


Fig. 9. Harmonic components of horizontal displacement at point 4 under sinusoidal voltage excitation,  $f = 50$  Hz,  $B_{peak} = 1.5$  T.

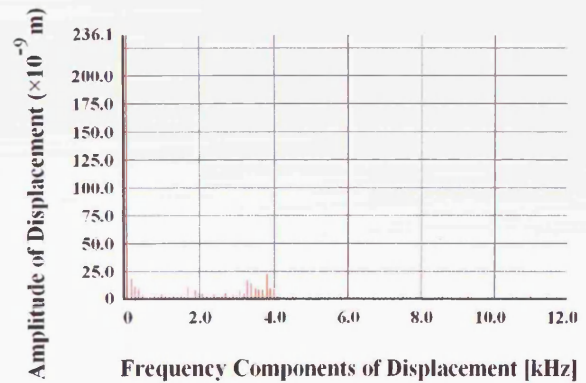


Fig. 10. Harmonic components of horizontal displacement at point 4 under PWM voltage excitation,  $f = 50$  Hz,  $m_a = 0.6$ ,  $f_s = 1$  kHz,  $B_{peak} = 1.5$  T.

## V. CONCLUSIONS

Results shows that acoustic noise and displacement decrease with increasing switching frequency for the 3-phase core excited under PWM waveform. However, near the resonance frequency at  $f_s = 3$  kHz, amplitude of harmonic component at around 3 kHz increases. The observed magneto-mechanical resonance phenomenon is a possible cause of

deterioration of a transformer core performance by increasing vibration and acoustic noise.

#### REFERENCES

- [1] Z. Valkovic, "Effects of transformer core design on noise level", *J. Phys. IV. France*, pp. 603-606, 1998.
- [2] B. Weiser, H. Pfützner and J. Anger, "Relevance of magnetostriction and forces for the generation of audible noise of transformer cores", *IEEE Trans. Magn.*, vol. 36, no. 5, pp. 3759-3777, September 2000.
- [3] C. A. Petry, J. C. Fagundes and I. Barbi, "Study of an ac-ac indirect converter for application as line conditioner", *IEEE International Symposium on Industrial Electronics*, pp. 757-762, June 20-23, 2005.
- [4] Z. Chen, F. Blaabjerg, "Wind energy-the world's fastest growing energy source", *IEEE Power Electronics Society Newsletter*, vol. 18, no. 3, pp. 15-18, Third Quarter 2006.
- [5] Yao X. Guang, Thant P. P. Phway, A. J. Moses and Fatih Anayi, "Acoustic noise and displacement analysis of a 3-phase transformer core under sinusoidal and PWM excitation", *17<sup>th</sup> Int. Conf. on Electrical Machines (ICEM 2006) Chania, Crete, 2-5 September 2006*, (2006) 514 OTM4-4.
- [6] Thant P. P. Phway, A. J. Moses, "Magnetisation-induced mechanical resonance in electrical steel", *JMMM*, 316 (2007) 468-471.

# Magnetostriction trend of non-oriented 6.5% Si-Fe

Thant P. P. Phway<sup>a\*</sup>, Anthony J. Moses<sup>b</sup>

<sup>a</sup> Anadrill Schlumberger, Unit 8, Kirkton Avenue, Pitmedden Industrial Estate, Dyce, Aberdeen AB21 0UB, Scotland.

<sup>b</sup> Wolfson Centre for Magnetism, Cardiff School of Engineering, Newport Road, Cardiff CF24 3AA, Wales.

Elsevier use only: Received date here; revised date here; accepted date here

## Abstract

Non-oriented electrical steel is produced in strip form typically 0.35 mm to 1.0 mm thick and containing 0 % to 3 % (wt) silicon. It is well known that non-oriented electrical steel is not quite isotropic but has small anisotropy. In the last decade NKK produced 0.1mm thick, non-oriented steel 6.5 % Si which has applications such as in high frequency transformer due to its high electrical resistivity, low core losses, near zero magnetostriction, and high permeability. The magnetostriction of 6.5% silicon steel samples with dimensions 280 mm x 30 mm x 0.1 mm was measured when magnetized sinusoidally between 0.5 T and 1.0 T at frequencies between 0.5 kHz and 6 kHz. Test samples were clamped at one end and the peak to peak displacement of the free end was measured with the aid of the Single Point Laser Vibrometer. The average peak-peak magnetostriction was 0.2 – 0.25  $\mu\epsilon$  apart from a sharp rise to 1.2  $\mu\epsilon$  at 2 kHz magnetizing frequency. This agrees well with the predicted value of 2 kHz for  $l = 0.28$  m,  $d = 7430$  kg/m<sup>3</sup> and  $E = 166$  GPa. This shows that although the 6.5 % silicon steel is often thought of as having near zero magnetostriction, care is needed to avoid lamination lengths corresponding to resonance points which could induce higher noise in laminated cores.

© 2008 Elsevier B.V. All rights reserved

PACS: 43.35.+d; 42.79.Qx

Keywords: magnetostriction; non-oriented; mechanical resonance; transformer noise

## 1. Introduction

NKK has produced a state-of-the-art flat-rolled non-oriented steel that is 0.1 mm thick with 6.5 % Si-Fe composition [1, 2]. This steel can be used in applications such as high frequency transformers due to its improved electrical resistance, low core losses, near zero magnetostriction, and high permeability.

Recently, the two most significant characteristics of transformer cores, i.e. power loss and noise, have been reduced considerably with improved material and core design. However, the base value of noise that results from magnetostriction is still a major environmental noise concern of the now highly industrialised world since noise is unwanted sound, a mellow sound to some, can be completely unacceptable to others. In addition to the noise caused by magnetostriction, all materials or bodies possessing mass and

elasticity are subject to vibration in the presence of external excitation [3]. Thus, transformer core materials generally require consideration of their oscillatory behavior especially at resonant frequency.

Magnetising frequency at resonance,  $f_m$  is described as the following in [4].

$$f_m = \frac{n}{8l} \sqrt{\frac{E}{d}} \quad (1)$$

where  $E$  is the modulus of elasticity measured along the longitudinal direction of the sample,  $d$  is its density,  $l$  is the sample length and  $n$  is the  $n^{\text{th}}$  harmonic order.

From equation 1, it can be seen that the resonance frequencies are dependent on the length of the core where the

\* Corresponding author. Tel.: +447825588379.

E-mail address: tphway@slb.com

smaller the transformer core is, the higher the resonance frequency will be. Although the 6.5% Si-Fe material is said to have near zero magnetostriction, at point of resonance, noise and vibration may be a major concern.

Variation of magnetostriction at various flux densities was measured for two samples of NO 6.5% Si-Fe 0.1 mm thick cut at 0° and 90° to the rolling direction.

## 2. Experimental Procedure

The purpose of measuring magnetostriction was to identify the magnetising frequency at resonance of the single strips of 6.5% Si-Fe cut at 0° and 90° to the rolling direction. At resonance, displacement due to magnetostriction of the sample is expected to be high compared to the magnetostriction at non-resonance frequencies.

The measurement system was assembled from instruments, which were individually calibrated, where applicable. The system comprises two parts; the Single Point Laser Vibrometer [4] and a magnetising system. All measurements took place in an acoustically insulated room to help reduce external noise. The laser head and measured object was placed in a acoustic chamber (fig. 1) and the rest of the system was placed outside the chamber to ensure that noise and vibration from the equipments did not affect the measurement.

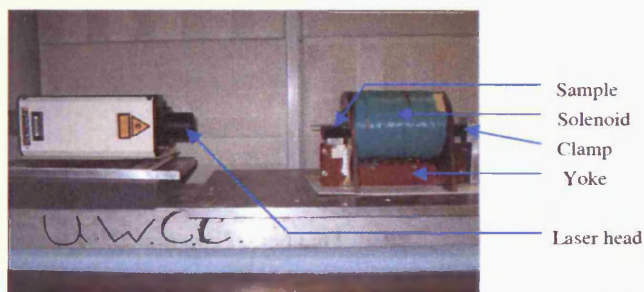


Fig 1. Laser head, sample and magnetising setup located in the acoustic chamber

The magnetizing system was connected as shown in Fig. 2 to study vibration modes of the single laminations. A 40 MHz arbitrary waveform generator is used for ac signal generation. A pre-amplifier is connected in parallel with a power amplifier and it is used for the coarse and fine control of the audio power amplifier. The peak flux density was deduced from the emf induced in a secondary coil wound around the test sample. Displacement output from the SPLV, the voltage signal in the secondary coil and the magnetising signal in the primary coil were saved on a floppy disk using a digital oscilloscope (10 Ms/s sampling rate). National Instrument Software LabVIEW 7.0 was used for data collection and analysis.

The non-oriented samples (table 1) were sinusoidally magnetised at peak flux densities,  $B_{max}$  of 0.5 T to 1.0 T at frequencies between 0.5 kHz and 7 kHz. The instantaneous magnetic flux density,  $b$  of the sample was measured using a secondary coil wound on the sample. Under sinusoidal ac conditions, source voltage is adjusted using the pre-amplifier to give an average value of the secondary rectified voltage  $V_{avg}$ ,

which can be related to the amplitude of the maximum value of the intrinsic magnetic flux density,  $B_{max}$  by the equation:

$$V_{avg} = 4N_2 A f_{mag} B_{max} \quad (2)$$

where  $N_2$  is the number of turns of the search coil,  $f_{mag}$  is the magnetising frequency and  $A$  is the cross sectional area of the test sample.

Each measurement was repeated 5 times and the average of peak-to-peak magnetostriction was found. To ensure good repeatability, each set of measurements was taken at different times between each sample being removed and re-clamped. The system had an uncertainty of 8.4% for 5 repeated measurements.

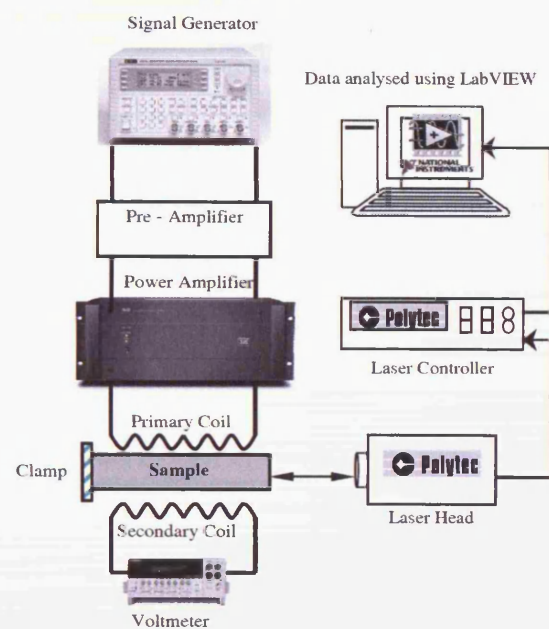


Fig 2. Schematic diagram of the magnetising system.

Table 1  
Properties of the non-oriented samples.

Sample	Cut Direction to rolling direction	Silicon Content (%)	Density, $d$ (kg/m <sup>3</sup> )	Width (mm)	Length, $l$ (mm)	Thickness (mm)
NO	0°	6.5	7430	30.0	280	0.10
NO	90°	6.5	7430	30.0	280	0.10

Young's modulus of each sample was measured to calculate the magnetising frequency at resonance of the samples (equation 1). Each sample was clamped at both end and tensile load was applied continuously up to 1 kN. The load values were then divided by cross-sectional area of the sample to obtain stress in N/m<sup>2</sup> and plotted against corresponding strain. Young's Modulus of each sample was obtained from the slope of the stress-strain curve.

### 3. Results and Discussion

Fig 3. and fig. 4 show the peak-peak magnetostriction against various  $f_{mag}$  at  $B_{max} = 0.5$  T to 1.0 T for the  $NO0^\circ$  and  $NO90^\circ$  sample respectively. Resonance peaks were observed at  $f_{mag} = 2$  kHz for  $NO0^\circ$  sample. For the same material, another rise in peak-peak magnetostriction was observed from 5 kHz to 6 kHz. Hence, vibration at 6 kHz could be regarded as the 3<sup>rd</sup> harmonic of resonance for the  $NO0^\circ$  sample. As for  $NO90^\circ$  sample, resonance peaks were observed at 2.5 kHz and 7 kHz for all values of  $B_{max}$ .

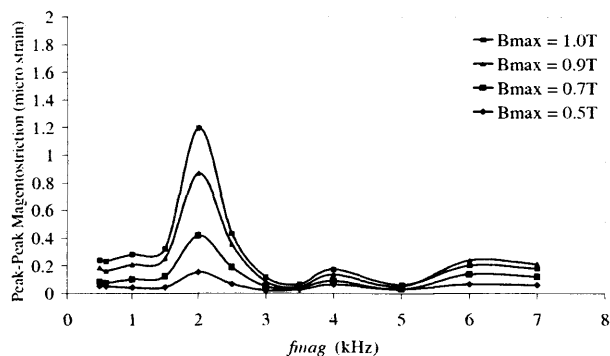


Fig 3. Peak-peak magnetostriction,  $\lambda_{pp}$  against magnetising frequency,  $f_{mag}$  for  $NO0^\circ$  at  $B_{max} = 0.5$  T, 0.7 T, 0.9 T and 1.0 T.

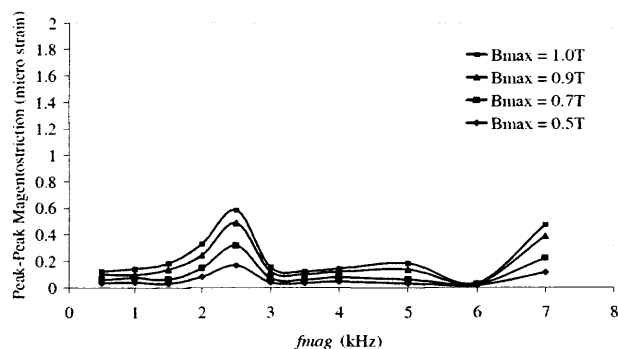


Fig 4. Peak-peak magnetostriction,  $\lambda_{pp}$  against magnetising frequency,  $f_{mag}$  for  $NO90^\circ$  at  $B_{max} = 0.5$  T, 0.7 T, 0.9 T and 1.0 T.

Table 2 shows the comparison of calculated resonance frequencies with measured values of both samples. In each case, the fundamental resonant point and its 3<sup>rd</sup> harmonic correspond well with the calculated theoretical value. Resonance frequencies were calculated to be at 2.1 kHz and 6.3 kHz for the 1<sup>st</sup> and 3<sup>rd</sup> harmonic respectively for  $NO0^\circ$  and 2.4 kHz and 7.2 kHz for 1<sup>st</sup> and 3<sup>rd</sup> harmonics respectively for  $NO90^\circ$ . Non-oriented steels have very small anisotropy and it was observed that resonant point of  $NO0^\circ$  and  $NO90^\circ$  samples occur at different magnetising frequencies.

Similar resonance behavior has been found in Epstein sized 3% Si-Fe grain-oriented strips cut at  $0^\circ$  and  $90^\circ$  to rolling direction [4].

The measurements were carried out on single strips but similar effects would be expected in longer laminations of stacked transformer cores. However, some small differences in actual values of resonant frequencies would occur due to non-

uniform flux density exists in stacks.

The results show that the magnetostriction can increase from close to zero to over 1 micro-strain if the core is magnetized or has significant harmonic flux corresponding to resonance frequency. So although a core made from such near zero magnetostriction material will have low noise, it can be much higher than expected from some dimension/frequency combinations which need to be avoided.

Table 2

Test sample parameters and comparison of calculated and measured resonance frequencies.

Sample	$E$ (GPa)	$d$ (kg/m <sup>3</sup> )	$l$ (m)	$N$ (harmonic number)	$f_m$ (kHz)	
					Calculated	Measured
$NO0^\circ$ (Fig 3.)	166	7430	0.28	1	2.1	2
				3	6.3	6
$NO90^\circ$ (Fig 4.)	213	7430	0.28	1	2.4	2.5
				3	7.2	7.0

### 4. Conclusions

The measured ac magnetostriction of 6.5% Si-Fe strips was confirmed to be close to zero provided mechanical resonance did not occur. If operated close to such resonance points, the magnetostriction is amplified and can lead to unexpectedly high acoustic noise from low magnetostriction transformer cores.

### References

- [1] Cogent Power Ltd, SIR-Gruppen Sweden, 2002.
- [2] M. Jitsukawa, Y. Hosoya, NKK Technical Review, No. 88, 2003.
- [3] W. T. Thomson, Prentice Hall, 1993.
- [4] T. Phway, A. J. Moses, J. Mag Mag. Mat., Vol 316, pp 468-471, 2007.

# Magnetisation-induced mechanical resonance in electrical steels

T.P.P. Phway\*, A.J. Moses

*Wolfson Centre for Magnetics, School of Engineering, Cardiff University, Newport Road, Cardiff CF24 3AA, UK*

Available online 19 March 2007

## Abstract

Extensive research has been carried out over the years to reduce the acoustic noise resulting from vibration of electromagnetic cores mainly caused by magnetostriction. This paper presents the results of a basic experimental study of magnetostriction in strips of grain oriented electrical steel commonly used in electromagnetic cores which gives an important new understanding of the phenomenon. Results suggest that a transformer core assembled from laminations of grain-oriented electrical steel around 0.3 m long would resonate at a magnetising frequency of 1.5 kHz which could result in excessive vibration and noise.

© 2007 Elsevier B.V. All rights reserved.

PACS: 43.35.+d; 42.79.Qx

Keywords: Mechanical resonance; Magnetostriction; Electrical steel; Transformer core; Laser vibrometer

## 1. Introduction

Grain-oriented 3% Si–Fe electrical steels are widely used for magnetic cores of transformers and motors. Extensive research has been carried out over many years to reduce transformer acoustic noise resulting from core vibration partly caused by magnetostriction of the core steel. However, not many researchers highlight the importance of mechanical resonance in the materials.

Recently, the two most significant characteristics of power transformer cores, i.e. loss and noise, have been reduced considerably with improved material and core design. However, the base value of noise that results from magnetostriction is still an environmental noise concern of the highly industrialised world.

Moses et al. [1], measured the variation of magnetostriction with mechanical stress and magnetising frequency of fully processed non-oriented electrical steels of different textures. They found that magnetostriction reduces with increasing magnetising frequency and that stress sensitivity of magnetostriction was dependent on the degree of texture.

Moses and Pegler [2], demonstrated the possibility of producing improved transformers by bonding stacks of silicon iron laminations together with flexible adhesive thereby reducing magnetostrictive vibrations of the laminations. They showed that although the pattern of vibration of certain lower frequencies and total noise output of a 100 kVA transformer core at the same magnetising frequencies was reduced only by 3 dB (A-weighted noise) below that of a bolted core. It was assumed that other factors such as resonance of external parts of yoke clamps, tie rods etc. were contributing to noise in transformer cores although the core vibration itself fell up to 10-fold.

When a sample is clamped at one end and magnetised, resonance occurs as a function of magnetising frequency and velocity of magnetostrictively-induced velocity of sound waves,  $v$  in the material as given in Eq. (1). The resonant condition occurs when the length of the sample is one quarter of the wavelength of the sound,  $\lambda$ . Higher harmonics arise when the frequency is high enough to cause the waves to traverse the length an integer number of times. Therefore, the  $n$ th harmonic of resonant frequency,  $f_n$ , can be obtained as a function of sample length as in Eq. (2):

$$v = \lambda f = \sqrt{\frac{E}{d}} \quad (1)$$

\*Corresponding author. Tel.: +44 2920876729; fax: +44 2920879538.  
E-mail address: [thantp@cf.ac.uk](mailto:thantp@cf.ac.uk) (T.P.P. Phway).

$$f_n = \frac{n}{4l} \sqrt{\frac{E}{d}} \quad (2)$$

where  $E$  is the modulus of elasticity measured along the longitudinal direction of the sample,  $d$  is its density,  $l$  is the sample length and  $n$  is the  $n$ th harmonic order. Magnetostriction is simply defined as the change in length of the strip under magnetisation. The change in length is independent of the sign of the magnetising waveform and therefore, the magnetising waveform is half of the magnetostriction frequency. Therefore, the magnetising frequency at resonance,  $f_m$ , can be described as

$$f_m = \frac{n}{8l} \sqrt{\frac{E}{d}} \quad (3)$$

Fig. 1 shows calculated  $f_m$  in the fundamental mode of vibration with corresponding core length using Eq. (3) for 3% Si-Fe grain-oriented steel cut at  $0^\circ$  to the rolling direction. This suggests that a transformer core having length of approximately 0.30 m would resonate under 1.5 kHz magnetisation. In reality, a transformer core of 0.30 m length is not magnetised at 1.5 kHz, however, harmonics of induced flux can coincide with the resonance frequency. Also, vibration modes of practical transformers would be different from those of single strips. However, existence of such resonance in single strips implies that similar resonance could exist in laminations of practical transformer cores. Such resonance may produce excessive core vibration and noise as well as possible failure in transformer cores due to coating damage by laminations rubbing against each other. Hence, it is important to understand the vibration modes of laminations in order to avoid this situation particularly in high-frequency cores. The noise problem is becoming of increasing industrial importance particularly in equipment subjected to high frequency and harmonic magnetisation.

## 2. Experimental approach

Hirano et al. [3] compared measurement of magnetostriction of silicon steel sheets using laser displacement

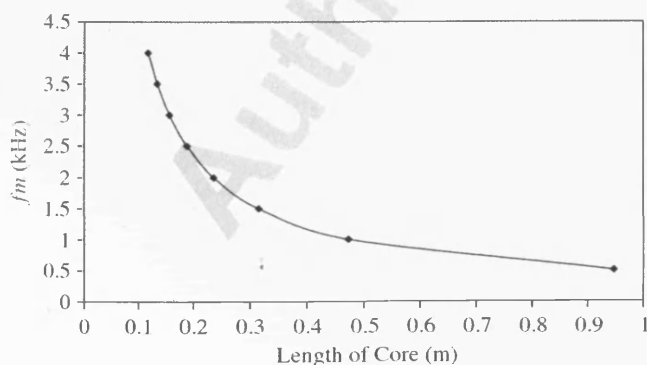


Fig. 1.  $f_m$  as a function of length of core,  $l$  for single-phase transformer core assembled from 3% Si-Fe grain-oriented cut at  $0^\circ$  to rolling direction.

metre and a laser vibrometer. The silicon steel sheet was 500 mm  $\times$  100 mm and 50 Hz magnetisation was excited along  $90^\circ$  to the rolling direction of the sheet. They found that the characteristics of peak-peak magnetostriction measured by laser displacement metre agreed well with that obtained using the laser vibrometer. Such optical techniques open the possibility of measuring magnetostriction in instances where it is not practical to attach strain gauges. Although optical techniques have much higher resolution than traditional resistance strain gauges or accelerometers in measuring magnetostriction, one must consider the cost and specifications that will suit individual applications.

In this investigation, magnetostriction of 3% Si-Fe grain-oriented steel strips cut at  $0^\circ$  and  $90^\circ$  to rolling direction with dimensions 303 mm  $\times$  30 mm  $\times$  0.27 mm was measured over the frequency range of 0.5 kHz–8 kHz. One end of each test sample was clamped and the displacement amplitude of the free end was measured with the aid of the single-point laser vibrometer (SPLV) from which peak-to-peak magnetostriction was determined. The SPLV (Polytec OFV-3001/303) has a resolution of 0.002  $\mu$ m and focuses sample surfaces as small as 25  $\mu$ m.

A magnetising system was connected as shown in Fig. 2 to study vibration modes of the single laminations. A 40 MHz arbitrary waveform generator is used for AC signal generation. A pre-amplifier is connected in parallel with a power amplifier and it is used for the coarse and fine control of the audio power amplifier. The peak flux density

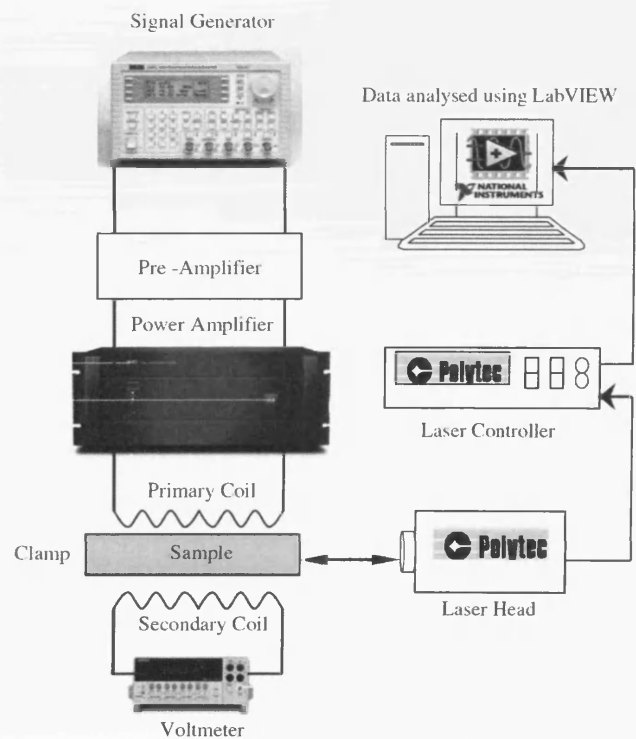


Fig. 2. Schematic diagram of the magnetising system.



was deduced from the EMF induced in a secondary coil wound around the sample. A flux closure yoke was used to compensate for air flux.

Displacement output from the SPLV, the voltage signal in the secondary coil and the magnetising signal in the primary coil were saved on a floppy disk using a digital oscilloscope (10 Ms/s sampling rate). National Instrument Software LabVIEW 7.0 was used for data collection and analysis.

The samples were sinusoidally magnetised at peak flux densities,  $B_{\max}$  of 0.5–1.0 T. The instantaneous magnetic flux density,  $B$  of the sample was measured using a secondary coil wound on the sample. Under sinusoidal AC conditions this gave an average output voltage,  $V_{\text{avg}}$  which can be related to the amplitude of the magnetic flux density  $B_{\max}$  by

$$V_{\text{avg}} = 4NAfB_{\max}, \quad (4)$$

where  $N$  is the number of turns on the search coil ( $= 10$ ),  $f$  is the magnetising frequency and  $A$  is the cross sectional area of the sample ( $= 8.1 \times 10^{-6}$ ). Each measurement was repeated five times and the average of peak-to-peak magnetostriction was found. To have a good repeatability, each set of measurements was taken at different times having the samples removed and re-clamped. The peak-to-peak magnetostriction values have uncertainty of 3.5% for five repeated measurements.

### 3. Results and discussion

Table 1 shows a comparison between calculated and measured  $f_m$  of both  $0^\circ$  and  $90^\circ$  grain-oriented material. In each case, the first resonant point and its harmonics correspond well with the calculated theoretical value.

Figs. 3 and 4 show the variation in magnitude of peak-to-peak magnetostriction with magnetising frequency for  $0^\circ$  and  $90^\circ$  samples, respectively. At 1.56 kHz the vibration increased by a factor of around 320% due to resonance followed by an increase of 200% and 160% at 4.5 and 7.5 kHz, respectively. These correspond to the mechanical resonance modes of the  $0^\circ$  grain-oriented steel under test.

Similar resonance characteristics were found in the  $90^\circ$  material where at 2 kHz resonant point occurred, vibration

caused by magnetostriction increased 400% and 150% at 6.5 kHz. Although the  $90^\circ$  material is of no practical importance, results confirm the predicted effect of material parameters on resonance.

Although the measurements were carried out on single strips, similar effects would be expected in stacks of transformer laminations of the same dimensions as the strips. Therefore, some differences would occur due to non-uniform flux density which is known to exist in stacks.

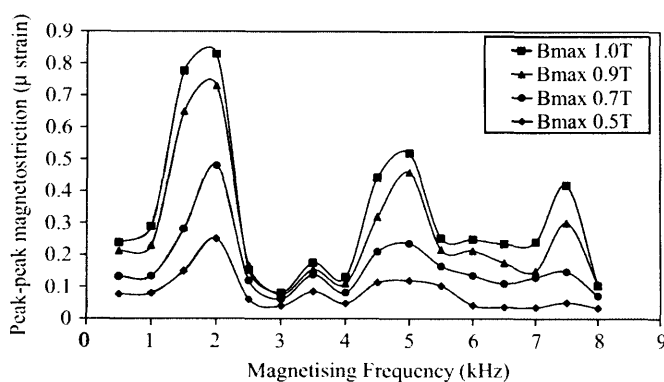


Fig. 3. Magnetostriction as a function of magnetising frequency of 3% Si-Fe grain-oriented  $0^\circ$  sample at  $B_{\max} = 0.5, 0.7, 0.9$  and 1.0 T.

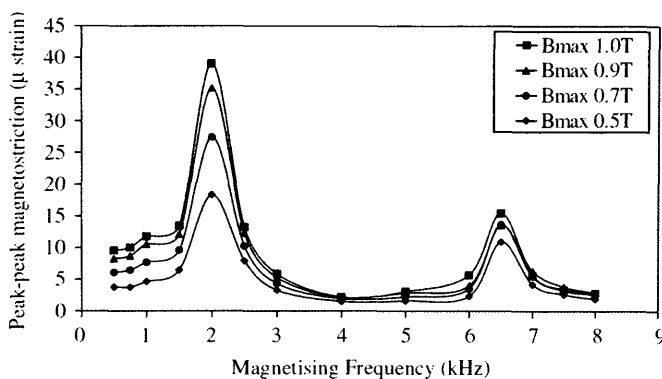


Fig. 4. Magnetostriction as a function of magnetising frequency of 3% Si-Fe grain-oriented  $90^\circ$  sample at  $B_{\max} = 0.5, 0.7, 0.9$  and 1.0 T.

Table 1  
Test sample parameters and comparison of calculated and measured resonance frequencies

Sample	$E$ (GPa)	$\rho$ (kg m <sup>-3</sup> )	$l$ (m)	$N$ (harmonic number)	$f_m$ (kHz)	
					Calculated	Measured
$0^\circ$ (Fig. 3)	110	7650	0.303	1	1.56	1.70
				3	4.69	5.00
				5	7.82	7.50
$90^\circ$ (Fig. 4)	193			1	2.07	2.00
				3	6.20	6.50

#### **4. Conclusions**

The basic magnetostriction of similar size laminations in a stacked transformer core of 0° material, would be likely to resonate if magnetised at 1.56 kHz resulting in excessive vibration and acoustic noise unless it was naturally damped. Extrapolation of the results predict possible resonance effects in larger cores. This is shown to imply that the phenomenon can be the cause of excessive noise found in some medium frequency power transformers and in transformers operating under distorted flux conditions. The high vibration in the resonant state could also lead to long term deterioration of lamination coating and possible core failure. Therefore, more care should be taken in such cases to control or avoid the phenomenon.

#### **Acknowledgement**

The authors wish to thank EPSRC for partial support towards this project (GR/T22568).

#### **References**

- [1] A.J. Moses, A. Ntasis, T. Kochmann, J. Schneider, *J. Magn. Magn. Mater.* 215–216 (2000) 669.
- [2] A.J. Moses, S.M. Pegler, *J. Sound Vib.* 29 (1) (1973) 103.
- [3] M. Hirano, Y. Ishihara, K. Harada, T. Tokada, *J. Magn. Magn. Mater.* 254–255 (2003) 43.

# Acoustic Noise and Displacement Analysis of a 3-Phase Transformer Core under Sinusoidal and PWM excitation

Yao X. Guang, Thant P. P. Phway, Anthony J. Moses and Fatih Anayi

**Abstract**—Transformers are key elements in power generation, transmission and distribution. In industrial applications such as line conditioning, electrified railway power systems, PWM dc-dc power converters, transformers subjected to PWM voltage excitation are becoming more common. Recently, increased attempts are being made to attain a better understanding of transformer core noise which is partly generated by core vibration due to magnetostrictive properties of the core lamination. The variation of the acoustic noise in a three-phase transformer core under no-load condition with switching frequency in the range 1 kHz - 3 kHz and different modulation indices were measured (magnetization frequency 50 Hz-100 Hz; induction 1.3 T-1.5 T). The noise under PWM excitation was around 10-15 dB more than under sinusoidal flux. The core surface vibration causes higher sound pressure level.

**Index Terms**—Acoustic noise, Laser vibrometer, PWM, Switching frequency.

## I. INTRODUCTION

Pulsating forms of voltage excitation produced by PWM (Pulse Width Modulation) frequency converters result in an increase in losses in soft magnetic materials compared to a sinusoidal supply [1]. Now, more and more applications such as electrified railway power system, active power line conditioning, ac-ac converter and PWM dc-dc power converter are based upon classical rectifiers to store electrostatic energy by means of a dc-link while the inverter in active mode is used to inject power to the grid network [2-3]. In these applications, transformers are therefore subjected to PWM voltage excitation, due to PWM control of the converter [4-7]. So tight regulations on energy management in the context of distributed generation and renewable sources will strengthen the position in the market of active power line

conditioners, of which transformers under PWM supply are essential elements [8]. Therefore, improvement in the performance of transformers under PWM supply is relevant.

Recently, increased attempts have been made to attain a better understanding of transformer core noise generated by core vibration. This has been prompted by the increased environmental importance of such noise.

In order to reduce the acoustic noise level, much extensive research has been carried out over the years. The magnetostriction in T-joints and corners had already been analyzed in [9-12] and acoustic noise for the cores had been analyzed under different configuration such as SSL (single-step lap joint assembling) and MSL (multi-step lap joint assembly) [13-17]. However, only sinusoidal voltage supplies were considered in all these studies.

In this paper, vibration and its resulting no-load noise of a 3-phase transformer core have been measured under sinusoidal and PWM excitation, the results of acoustic noise and corresponding vibration had been analyzed, and contribute towards a better understanding for the influence of modulation index and switching frequency on the performance of the core.

## II. THEORETICAL BASIS

A PWM voltage waveform is obtained by comparing a reference voltage waveform (modulating signal, usually sinusoidal) with a carrier voltage waveform (usually triangular). That is, the PWM waveform is a synthesis of a reference voltage waveform (amplitude  $A_{ref}$ , frequency  $f$ ) and carrier voltage waveform (amplitude  $A_c$ , frequency  $f_c$ ) at different frequencies. The modulation index  $m_i$  and frequency ratio  $m_f$  are given by (1) and (2) respectively.

$$m_i = \frac{A_{ref}}{A_c} \quad (1)$$

$$m_f = \frac{f_c}{f} \quad (2)$$

The PWM output voltage waveform synthesis is illustrated in Fig. 1.

Manuscript received June 30, 2006.

Yao Xiao Guang is a Ph.D. student with the Wolfson Centre for Magnetics, School of Engineering, Cardiff University, Newport Road, Cardiff CF24 3AA, Wales, UK (phone: +44--29--20876046; fax: +44--29--20879538; e-mail: yaoxg@cf.ac.uk).

Thant P. P. Phway is a Ph.D. student with the Wolfson Centre for Magnetics. (e-mail: thantp@cf.ac.uk).

Anthony J. Moses is Associate Director of Wolfson Centre for Magnetics. (e-mail: mosesaj@cf.ac.uk).

Fatih Anayi is a Senior Research Associate at the Wolfson Centre for Magnetics. (e-mail: anayif@cf.ac.uk).

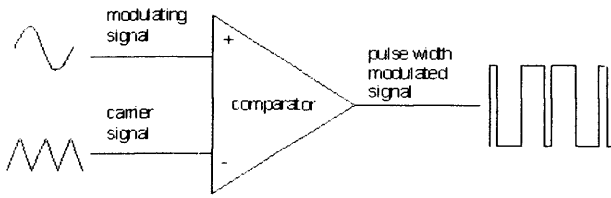


Fig. 1. Generation of PWM voltage waveform

The three significant parameters which determine the performance of PWM inverters are modulation index  $m_i$ , carrier index (frequency ratio)  $m_f$  and the frequency of the carrier voltage waveform or switching frequency  $f_s$ .

The acoustic Sound Pressure Level (SPL) is given by:

$$SPL(dB) = 20 \log_{10} \frac{n_{mea}}{n_{ref}} \quad (3)$$

where  $n_{mea}$  is the measured pressure level,  $n_{ref}$  is the reference pressure level. The scale in (3) uses the hearing threshold of  $20 \mu Pa$  as the reference level of 0 dB.

### III. EXPERIMENTAL PROCEDURE

A three phase, three limb laminated transformer core was assembled from 200 layers of 0.27 mm thick grain-oriented 3% silicon steel (UNISIL M089-27N). The density and resistivity of the material were  $7650 \text{ kg/m}^3$  and  $46 \mu\Omega\text{cm}$  respectively. The core mass was 96.1kg. The overall dimensions as well as position of primary and secondary coil windings are shown in Fig.2.

Epstein strips (300 mm x 30 mm) of the same batch of materials cut at parallel to the rolling direction were magnetized under sinusoidal flux density and PWM voltage waveforms in a single strip tester. The PWM waveforms were generated by a waveform generator (TGA1230 30MHz Arbitrary Waveform Generator). The single strip samples were magnetized individually at 1.3 T and 1.5 T respectively having one end clamped and magnetostriction,  $\lambda$  at the free end was measured with the aid of a single point laser vibrometer, SPLV [18]. SPLV is a non-contact vibration measurement technique that allows direct measurement of velocity or displacement to an accuracy of  $\pm 2 \text{ nm}$ .

Three single strip samples were selected, and for each sample, the magnetostriction  $\lambda$  was measured three times. Table.1 shows average peak to peak results in  $\mu\epsilon$  (micro strain). It can be observed that at low  $m_i$ ,  $\lambda$  is larger than that at high  $m_i$  and that at the same  $m_i$ ,  $\lambda$  decreases with increasing  $m_f$ .

TABLE.1

Corresponding magnetostriction of single strip under sinusoidal and PWM excitation.

Waveform	$f$ (Hz)	$m_i$	$m_f$	$\lambda \times 10^{-6}$ (m) at 1.3 T	$\lambda \times 10^{-6}$ (m) at 1.5 T
Sinusoidal	50	-	-	0.21	0.50
PWM	50	0.5	15	0.36	0.64
PWM	50	0.8	15	0.32	0.61
PWM	50	0.8	55	0.26	0.55
PWM	50	1.0	15	0.29	0.58
PWM	50	1.2	15	0.27	0.56
PWM	100	0.8	15	0.61	0.88

The 3-phase transformer core was clamped with a non-magnetic bar having bolts at each end (Fig. 2).

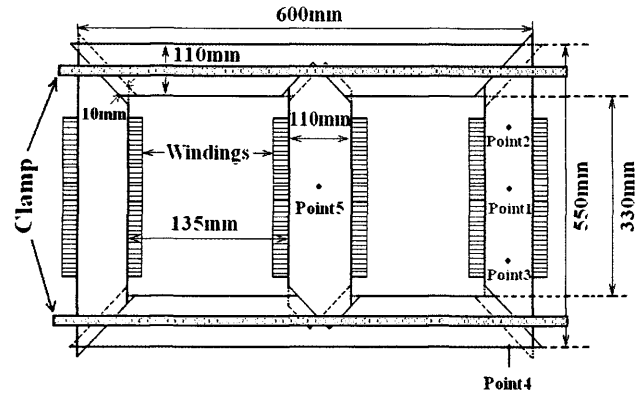


Fig. 2. Layout of experimental 3-phase transformer core showing positions of measuring points

Fig. 3. shows the magnetizing circuit of the core assembly. A 3-phase PWM inverter (Toshiba inverter TOSVERT VF-A3) was connected to three independent variacs, which supplied the three 50-turn primary windings of the delta-wound transformer core under no-load condition, and were used to keep the three winding voltages balanced. The voltage applied to the primary windings, the induced voltages in the 50-turn secondary windings, the sound pressure level was recorded using a microphone (Brüel & Kjaer type 4231) and vibration signal from SPLV were recorded by a digital oscilloscope (YOKOGAWA DL716 - 16CH Digital Scope). The digital oscilloscope has plug-in high voltage isolation modules which display and save waveforms in 12-bit resolution at 10 MS/s. All displayed waveforms are saved in a floppy disk and data is analyzed using algorithms embedded in National Instrument LabVIEW software.

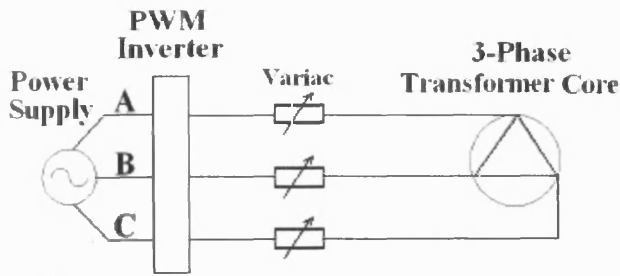


Fig. 3. Magnetizing circuit of the 3-phase transformer core

The transformer core was placed horizontally on a table in an acoustic chamber. The magnetizing system was located in a separate measurement room. Acoustic noise and vibration were measured using the setup shown in Fig.4 where amplifier is placed in the acoustic chamber and oscilloscope placed outside the anechoic chamber. The microphone was placed 0.5 m vertically above the core and moved from points 1 to 5 in turn and moved between measurements. The vibration of the core surface at the same points was measured with the SPLV.

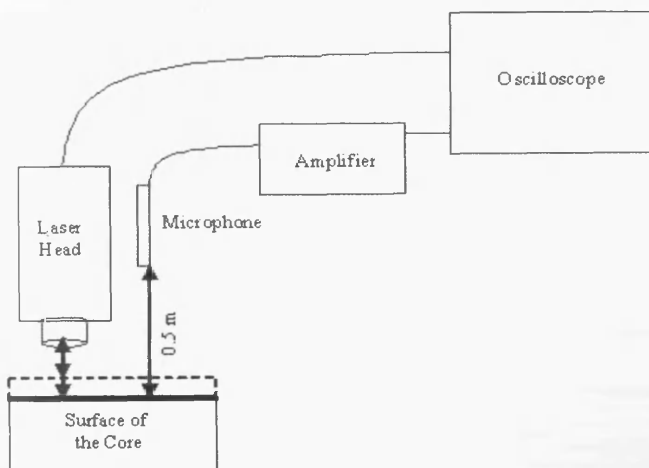


Fig. 4. Vibration and acoustic noise measurement setup placed in an anechoic chamber

Throughout the experimental work carried out, the Output Voltage Regulation Function, OV (%) in the PWM converter was varied in the range 40% - 90%, which corresponds approximately to the range of modulation indices 0.5 - 1.2. Moreover, the carrier signal frequency (switching frequency,  $f_s$ ) was varied in the range 1 kHz - 3 kHz while the reference signal frequency (fundamental frequency  $f$  of magnetization) was set to 50 Hz and 100 Hz respectively.

Vertical displacement of the core surface at points 1, 2, 3 and 5 and horizontal displacement of the side of the core at point 4 (Fig. 2) were measured using the SPLV.

#### IV. EXPERIMENTAL RESULTS AND DISCUSSIONS

The core was magnetized under sinusoidal and PWM

voltage and the primary currents were independently adjusted to obtain balanced peak flux density,  $B_{peak}$  1.3 T and 1.5 T in the limbs. Under PWM condition  $f_s$  was varied between 1 kHz and 3 kHz. The noise was measured in turn directly above point 1 to 5 and the corresponding core vibration was recorded. Figs.5 and 6 show the noise level measured above point 5 when the core was magnetized under sinusoidal flux and under PWM excitation with two values of OV (corresponding to modulation indices of apparent 0.5 and 0.6) at three different  $f_s$ . The noise measured under PWM excitation is around 10-15 dB greater than under corresponding sinusoidal flux due to higher harmonics in the core vibration.

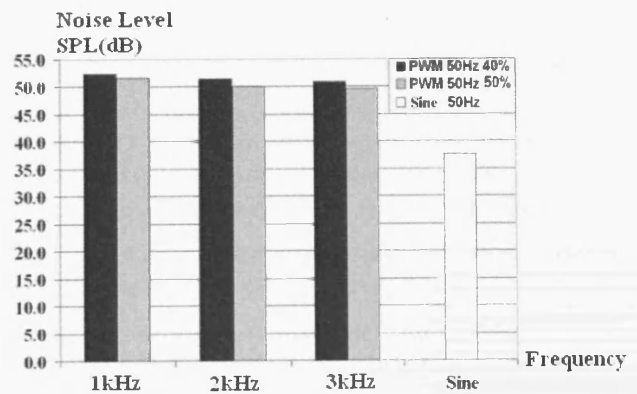


Fig.5. Comparison of SPL under PWM excitation with values of  $f_s = 1, 2$  and 3 kHz, OV%=40% and 50%, with that under sinusoidal conditions ( $f = 50$  Hz,  $B_{peak} = 1.3 T$ )

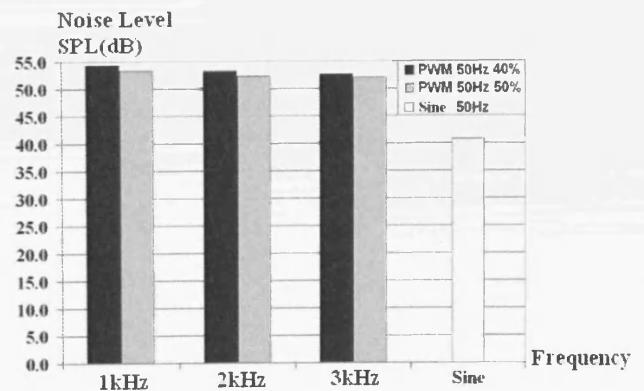


Fig.6. Comparison of SPL under PWM excitation with values of  $f_s = 1, 2$  and 3 kHz, OV%=40% and 50%, with that under sinusoidal conditions ( $f = 50$  Hz,  $B_{peak} = 1.5 T$ )

Fig. 7 shows the drop of acoustic noise above point 5 on the core as the modulation index is increased over its full range at 1.3 T, 50 Hz fundamental,  $f_s$  at 3 kHz. However, it is around 8 dB higher than the sinusoidal value even at OV of 90%

for  $f_s$  at 3 kHz.

The noise was measured at 1.3 T, 100 Hz fundamental,  $f_s$  at 3 kHz, and the drop was more significant as shown in Fig. 8.

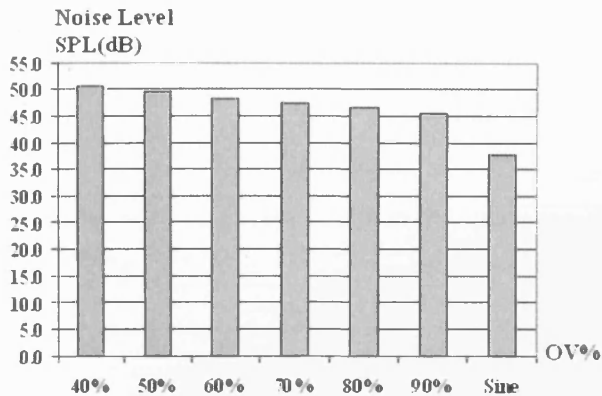


Fig. 7. Acoustic noise SPL under sinusoidal ( $f = 50$  Hz,  $B_{peak} = 1.3$  T) and PWM excitation at point 5 with  $f = 50$  Hz,  $f_s = 3$  kHz,  $B_{peak} = 1.3$  T and  $OV \% = 40\% - 90\%$

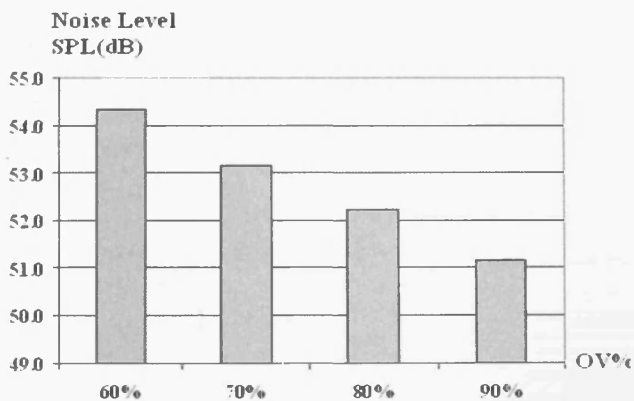


Fig. 8. Acoustic noise SPL under PWM excitation at point 5 with  $f = 100$  Hz,  $f_s = 3$  kHz,  $B_{peak} = 1.3$  T and  $OV \% = 40\% - 90\%$

Under 100 Hz fundamental voltage, if  $OV\%$  was 40% and 50%, the excitation voltage was not enough to magnetize the core to peak flux density of 1.3T. This is because of the limitation of variacs output range. Also, there was no 100 Hz (3-phase sinusoidal) power supply available and that is the reason why no measurement of 100 Hz was taken.

Fig. 9 shows the variation of both the peak-peak displacement above point 1 and the acoustic noise with modulation index at a fixed peak flux density,  $B_{peak}$  of 1.3 T. The similar trends were found above the other points on the core surface at switching frequencies from 1 kHz to 3 kHz. The decrease in displacement and corresponding noise output with increasing modulation index is due to the lower harmonic

content of the core flux density. It was also found that the noise and displacement fall with increasing fundamental frequency for the same reason.

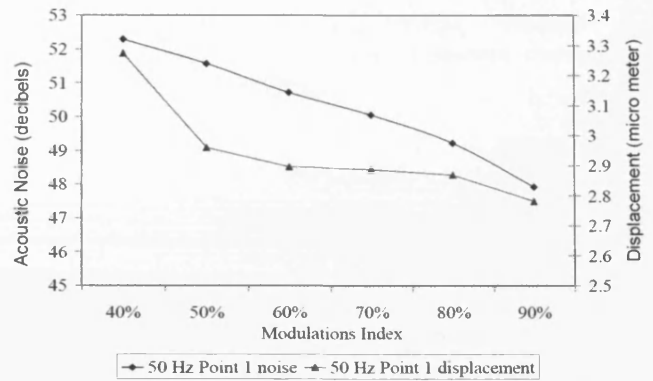


Fig. 9. Acoustic noise SPL and corresponding peak-peak displacement at point 1 under 50 Hz PWM excitation,  $f_s = 3$  kHz,  $B_{peak} = 1.3$  T,  $OV\% = 40\% - 90\%$

Fig. 10 to 12 show displacement against flux density plot of the core under 50 Hz PWM excitation above point 1 at  $OV = 40\%$ ,  $B_{peak} = 1.5$  T and  $f_s = 1, 2$  and 3 kHz respectively whereas Fig. 13 shows the displacement against flux density plot of the core under 50 Hz ac excitation at  $B_{peak} = 1.5$  T. It is suggested in Fig. 10 to 12 that displacement decreases with increasing  $f_s$  where average peak-peak displacement for  $f_s = 1$  kHz is  $3.9 \mu m$ ,  $f_s = 2$  kHz is  $3.7 \mu m$ ,  $f_s = 3$  kHz is  $3.3 \mu m$ . Under sinusoidal 50Hz the average peak-peak displacement is  $2.5 \mu m$ . Displacement results for both PWM and ac excitations correspond with acoustic noise results shown in Fig.6 where acoustic noise reduces with increasing  $f_s$ .

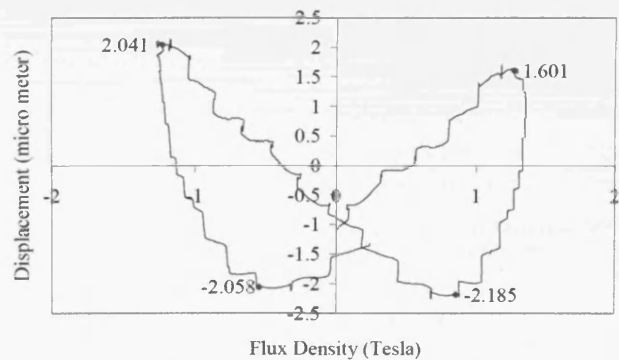


Fig. 10. Displacement at point 1 under 50 Hz PWM excitation at  $f_s = 1$  kHz  $OV = 40\%$  and  $B_{peak} = 1.5$  T.

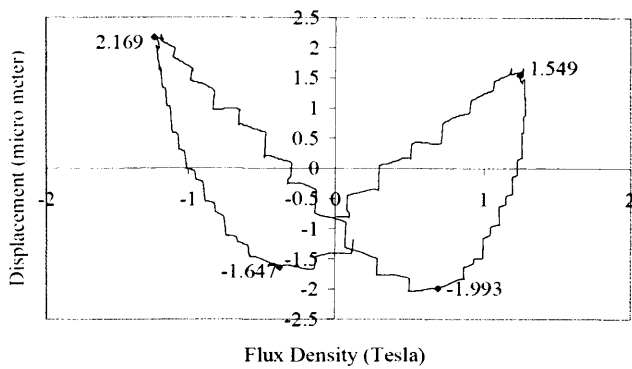


Fig. 11. Displacement at point 1 under 50 Hz PWM excitation at  $f_s = 2$  kHz,  $OV = 40\%$  and  $B_{peak} = 1.5$  T.

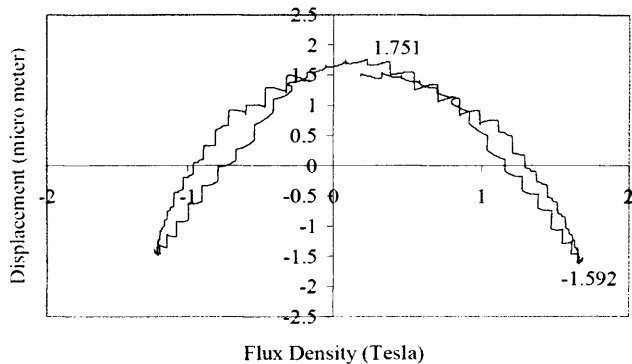


Fig. 12. Displacement at point 1 under 50 Hz PWM excitation at  $f_s = 3$  kHz,  $OV = 40\%$  and  $B_{peak} = 1.5$  T.

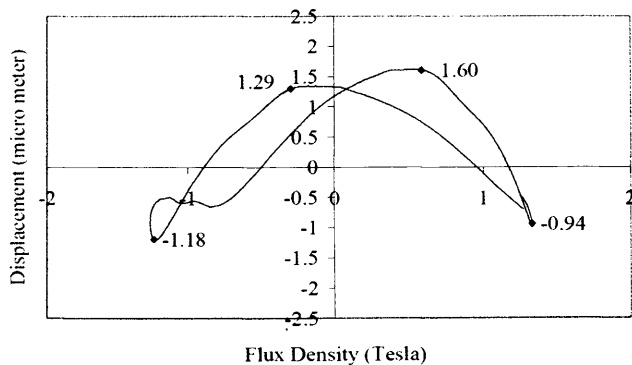


Fig. 13. Displacement at point 1 under 50 Hz ac excitation at  $B_{peak} = 1.5$  T.

### V. CONCLUSIONS

The results implied that acoustic noise output of 3-phase transformer operating under PWM is far higher than under corresponding sinusoidal excitation. The noise under PWM excitation was around 10-15 dB more than under sinusoidal flux showed the effect of the harmonics in the core vibration. Under PWM conditions, it was found that an increase of  $f_s$  from 1 kHz to 3 kHz resulted in acoustic noise maximal reduction of 2 dB and 3 dB at 1.3 T and 1.5 T

respectively ( $f = 50$  Hz,  $OV = 40\%$ ). The beneficial impact on the reduction of noise at the highest values of  $OV = 90\%$  ( $f = 100$  Hz,  $B_{peak} = 1.3$  T) was 3 dB. From the results of material's single stripe magnetostriction along rolling direction and displacement on the core surface, it showed that surface vibration caused more sound.

### REFERENCES

- [1] T.C. Green, C.A. Hernandez-Aramburo, A.C. Smith, "Losses in grid and inverter supplied induction machines drives", in *Electric Power Applications, IEE Proceedings*, Vol 150, Issue 6, pp 712-724, 2003.
- [2] H. Akagi, "Trends in Active Power Line Conditioners", in *IEEE Transactions on Power Electronics*, Vol 9, Issue 3, pp263-268, 1994.
- [3] V. B. Bharavaju and P. N. Enjeti, "An Active Line Conditioner to Balance Voltages in a Three-Phase System", in *IEEE Transactions on Industry Applications*, Vol 32, Issue 2, pp 287-292, 1996.
- [4] T.W. Kim, J.H. Choi and B.H. Kwon, " High Performance Line Conditioner with Output Voltage Regulation and Power Factor Correction", in *IEE Proceedings Power Applications*, Vol 151, Issue 1, pp 91-97, 2004.
- [5] C.A. Petry, J.C. Fagundes and I. Barbi, "Study of an AC-AC Indirect Converter for Application as Line Conditioner, in *IEEE International Symposium on Industrial Electronics*, pp 757-762, 20-23, 2005.
- [6] F. Barrero, S. Martinez, F. Yeves, F. Mur and P.M. Martinez, "Universal and Reconfigurable to UPS Active Power Filter for Line Conditioning, in *IEEE Transactions on Power Delivery*, Vol 18, Issue 1, pp 283-290, 2003.
- [7] S. Moisseev, K. Soshin, S. Sato, L. Gamage and M. Nakaoka, "Novel soft-commutation DC-DC power converter with high-frequency transformer secondary side phase-shifted PWM active rectifier", in *IEE Proceedings Electric Power Application*, Vol. 151, No.3, 2004, pp 260-267.
- [8] G. Bertotti, "General Properties of Power Losses in Soft Ferromagnetic Materials", in *IEEE Transactions on Magnetics*, Vol 24, Issue 1, pp 621-630, 1988.
- [9] A. Hasenzagl, B. Weiser, H. Pfützner, "Magnetostriction of 3% SiFe for 2-D magnetization patterns", *Journal of Magnetism and Magnetic Materials*, 160(1996), pp. 55-56
- [10] B. Weiser, H. Pfützner, "Relevance of Magnetostriction and Forces for the Generation of Audible Noise of Transformer Cores", *IEEE Transactions on Magnetics*, Vol. 36, No. 5, 2000, pp. 3759-3777
- [11] C. Krell, N. Baumgartinger, G. Krismanic, "Relevance of multidirectional magnetostriction for the noise generation of transformer cores", *Journal of Magnetism and Magnetic Materials*, 215-216(2000), pp. 634-636
- [12] Tadashi Sasaki, Shunji Takada, "Magnetostrictive Vibration of Electrical Steel Sheets under a Non-Sinusoidal Magnetizing Condition", *IEEE Transactions on Magnetics*, Vol. 23, No. 5, 1987, pp. 3077-3079
- [13] Arthur W. Kelley, "Measurement of Spacecraft Power Transformer Acoustic Noise", *IEEE Transactions on Magnetics*, Vol. 26, No. 1, 1990, pp. 281-289.
- [14] B.Weiser, A. Hasenzagl, "Mechanisms of noise generation of model transformer cores", *Journal of Magnetism and Magnetic Materials*, 160 (1996), pp. 207-209
- [15] Z. Valkovic, "Effects of Transformer Core Design on Noise Level", *Journal of Phys. IV France* 8 (1998), pp. 603-606
- [16] Albana Ilo, "Behavior of Transformer Cores with Multi-step Lap Joints", *IEEE Power Engineering Review*, 2002, pp. 43-47
- [17] Z. Valkovic, "Investigations of core noise levels using a dry-type transformer model", *Journal of Magnetism and Magnetic Materials*, 160(1996), pp. 205-206
- [18] Thant P. P. Phway, A. J. Moses, D. C. Jiles, "Frequency Dependence of Magnetostriction for Magnetic Actuators", *Journal of Electrical Engineering*, p. 7, Vol55 No10/S, 2004.

# Control of tip oscillation in magnetostrictive dental scalers

Thant P.P. Phway<sup>a</sup>, S. Zurek<sup>a</sup>, T. Meydan<sup>a,\*</sup>, A.D. Walmsley<sup>b</sup>

<sup>a</sup> Wolfson Centre for Magnetics, School of Engineering, Cardiff University, Cardiff CF24 3AA, Wales, United Kingdom

<sup>b</sup> School of Dentistry, University of Birmingham, St. Chad's Queensway, Birmingham B4 6NN, United Kingdom

Received 5 July 2004; received in revised form 7 October 2005; accepted 23 November 2005

Available online 20 January 2006

## Abstract

Ultrasonic dental scalers are electronically powered dental cleaning tools which are commonly used by clinicians for dental cleaning. They were developed in the mid 1950s [S.C. Trenter, A.D. Walmsley, G. Landini, J.M. Shippen, Assessment of the ultrasonic dental scaler insert, *Med. Eng. Phy.* 24 (2002) 139–144]. Ultrasonic scalers are being widely used with few studies on the correct methods and techniques that should be used to obtain their maximum efficiency. Different types of inserts/tips do not show clearly which particular designs are best suited to the task of removing dental calculus to combat periodontal disease. The aim of this study is to begin preliminary investigation on whether the performance of these clinical instruments may be improved if the displacement waveform of the scaler tip could be controlled.

© 2005 Elsevier B.V. All rights reserved.

**Keywords:** Ultrasonic; Magnetostrictive dental scalers; Vibration; Displacement; Control algorithm

## 1. Introduction

Ultrasonic scalers involve a power-unit box that sits on the counter and a water source must be connected to it. The difference between sonic and ultrasonic scalers is power. The sonic scaler is a low-power device therefore not very effective on heavy calculus which can be easily removed with an ultrasonic scaler [1]. However, clinical studies show that they are similar in efficacy to hand scalers with respect to preventing periodontal attachment loss, maintaining periodontal attachment levels and/or preventing tooth loss [2].

The ultrasonic scaler may result in potential hazards to both patient undergoing treatment and to the clinical operator of the equipment. These potential hazards were highlighted in a number of papers in literature by Trenter and Walmsley [3].

Trenter et al. [3] published preliminary work on assessing the natural frequency of a straight internal ultrasonic scaler insert and measured displacement observed at the tip when operated under different generator settings. From their approach of using finite element analysis and scanning laser vibrometry, they concluded that there is a large variation in the displacement observed at the scaler tip and have suggested that further research

is required on the manufacturer and clinical use of ultrasonic scalers.

Magnetostrictive dental scalers produce ultrasonic vibrations via a stack of laminated nickel placed in a coil carrying a dc signal with an ac signal of smaller magnitude imposed upon it (Fig. 1). The generator then converts the electrical energy to ultrasonic waves via magnetostriction,  $\lambda$ . Commercially available ultrasonic dental scalers oscillate at frequencies from 25 to 42 kHz.

A similar coil to the commercial dental scaler was built and scaler tip displacement was measured at 15 kHz magnetising frequency. Displacements of scaler tip (30 kHz Denstply International) were taken using Laser Doppler Vibrometer. The investigation has shown that tip scaler motion is not always sinusoidal, which may not be clinically efficient. This paper is aimed to demonstrate a control algorithm for the displacement outputs of the magnetostrictive dental scaler. The control algorithm includes a PC based data acquisition with a digital feedback control.

## 2. Experimental work

A 40 MHz arbitrary waveform generator was used for ac signal generation (Fig. 2). A pre-amplifier was connected in parallel with the power amplifier. A digital multimeter was used to monitor the average voltage induced in a secondary search coil.

\* Corresponding author. Fax: +44 29 2087 9538.

E-mail address: [meydan@cardiff.ac.uk](mailto:meydan@cardiff.ac.uk) (T. Meydan).



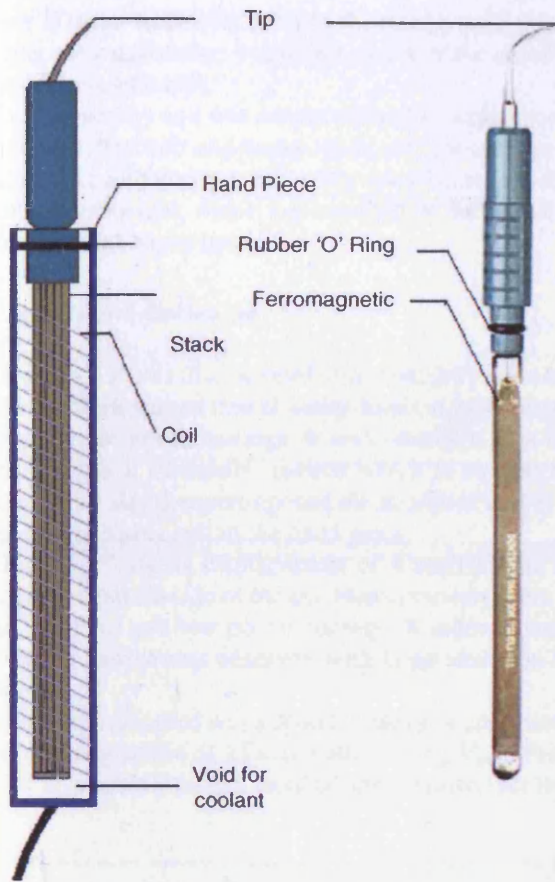


Fig. 1. A schematic diagram of 30kHz magnetostrictive dental scaler insert.

A digital oscilloscope with a high voltage isolation module (10 MS/s sampling rate) was used to display displacement output from the laser vibrometer, voltage signal in the search coil ( $V_{ind}$ ) and magnetizing signal in the primary coil. The voltage signal in the primary coil was taken as a reference signal for triggering. To improve the accuracy of measurement, National Instrument Software LabVIEW 7.0 was used for data collection and analysis purposes. In the present research a single point laser vibrometer (SPLV) was used. The SPLV has 12-bit digital resolution could resolve signal differences of 0.0039 V, which corresponds to a change in length of  $\Delta l = 1.95$  nm.

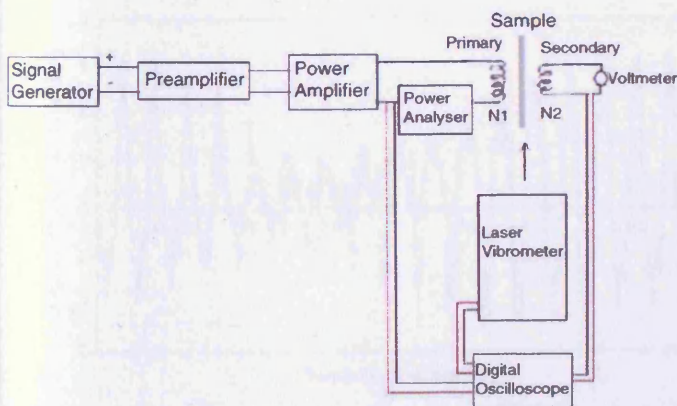


Fig. 2. Block diagram of system set up.

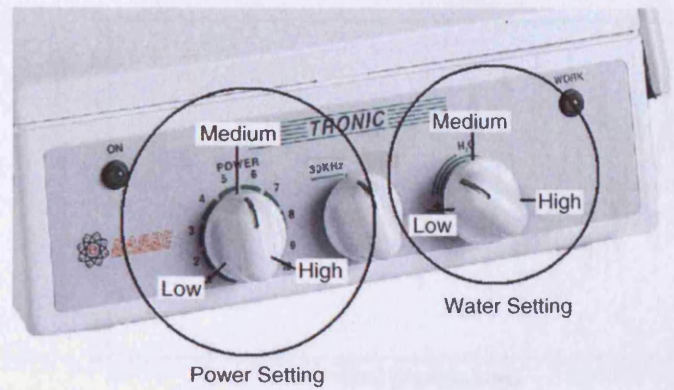


Fig. 3. Water and power settings on a magnetostrictive dental scaler.

Fig. 3 shows a diagram of 30 kHz magnetostrictive dental scaler generator at high, medium, low water and power settings. In this research, measurements were taken only at different power settings without any water supply. An unused and used 30 kHz dental scaler inserts were used for each measurement. Both inserts are of the same scaler tip design manufactured by Dentsply International.

Two sets of measurements were taken. Displacement was measured from the side and front (Fig. 4) of both unused and used scaler insert for each set. One set of measurements were taken using the commercial scaler generator and the other set was taken using a magnetising coil that operates similar to the commercial generator.

The magnetising coil carries an ac current fed from the signal generator with 25 number of turns to maintain low impedance at high frequency and a secondary search coil with 10 number of turns was also used for monitoring the flux density. Under sinusoidal ac conditions this gave an average output voltage,  $V_{avg}$  which can be related to the amplitude of the magnetic flux density  $B_{max}$  by the equation [4]

$$V_{avg} = \frac{NA\omega B_{max}}{\sqrt{2}} \approx 4NAfB_{max} \quad (1)$$

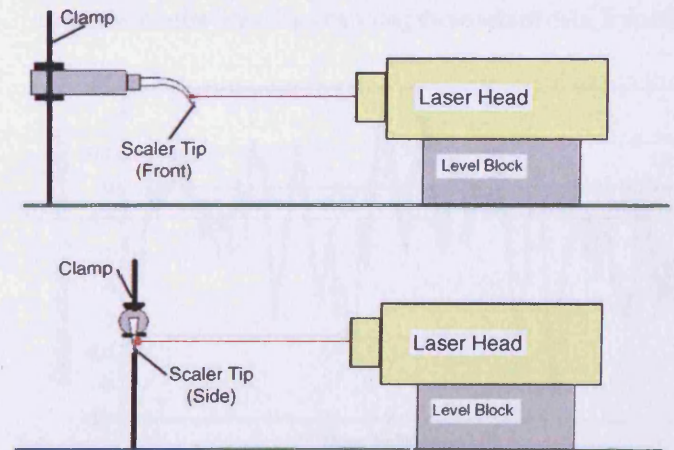


Fig. 4. Diagram showing displacement measurements from front and side of the dental scaler tip with laser vibrometer.

where  $N$  is the number of turns in the search coil,  $\omega$  is  $2\pi f$  with  $f$  being the magnetizing frequency and  $A$  is the cross-sectional area of the search coil.

The secondary coil was connected to the oscilloscope and the multimeter. The coil and scaler insert was clamped to align the scaler insert with the laser beam. The laser beam was focused on a reflective thin film, which was attached on the tip for optimum reflection back to the laser.

### 3. Results and discussion

Figs. 5–7 shows displacement (micrometer) waveform from the front of an unused dental scaler insert at high, medium and low generator power settings. It was observed that the waveform exhibits a modulated pattern which is caused by the ac magnetising signal superimposed on dc signal that is supplied to the magnetising coil in the hand piece.

Figs. 8–10 shows displacement of a used dental scaler tip measured from the side of the tip. Measurements were taken for high, medium and low power settings. Random displacement waveform pattern was observed with large variation in amplitude.

The generator used was a 30 kHz generator and therefore, the coil was magnetised at 15 kHz with varying  $V_{avg}$ . Figs. 11–14 shows displacement (from front of tip) measured for the unused

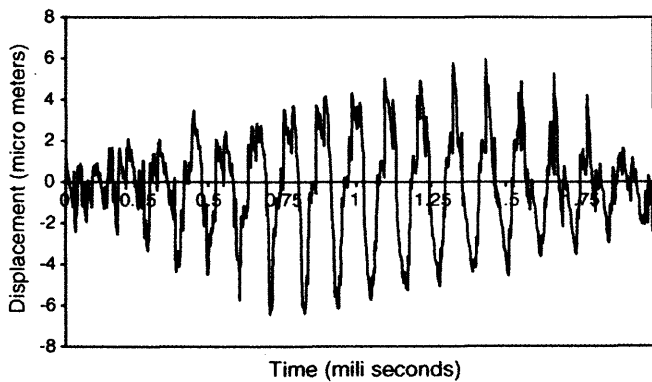


Fig. 5. Graph of unused 30 kHz scaler insert at high generator power settings of displacement from the side of scaler tip.

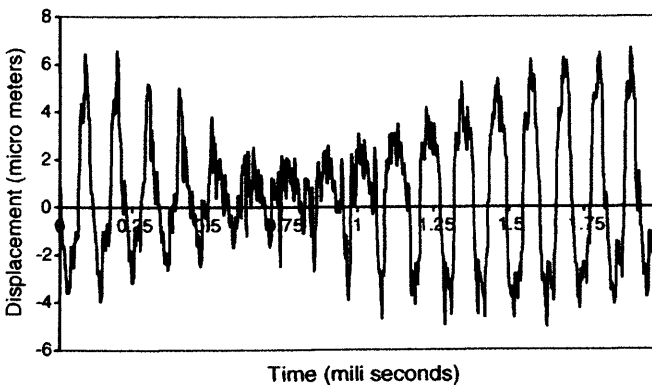


Fig. 6. Graph of unused 30 kHz scaler insert at medium generator power settings of displacement from the side of scaler tip.

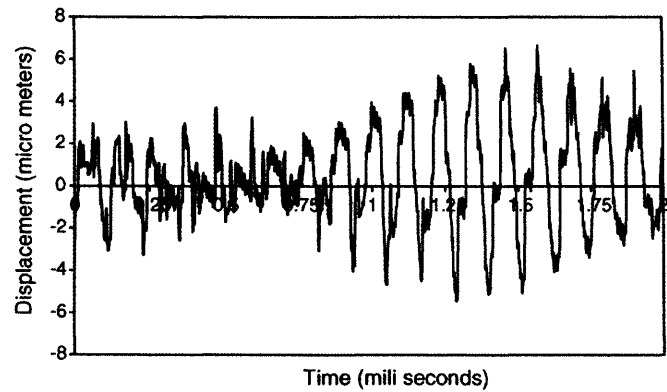


Fig. 7. Graph of unused 30 kHz scaler insert at low generator power settings of displacement from the side of scaler tip.

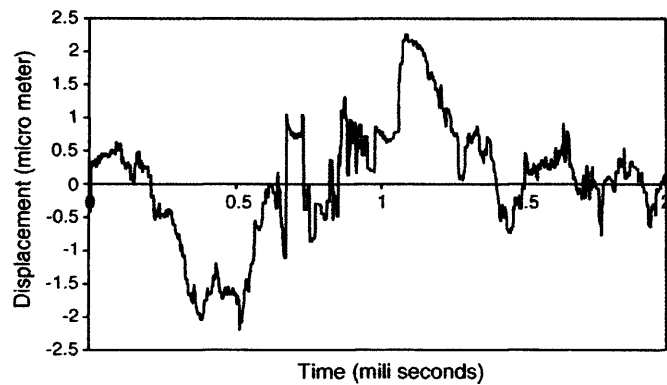


Fig. 8. Graph of used 30 kHz scaler insert at high generator power settings of displacement from the front of scaler tip.

dental scaler tip magnetised with a coil made similar to that of the generator handpiece. Here, with the aid of the secondary search coil, the average voltage,  $V_{avg}$  passing through the laminated stack of nickel was measured. It was observed that at 1–3 V (Figs. 11–13) the displacement waveform appears to be sinusoidal with amplitude remaining constant throughout magnetisation. Displacement amplitude also increases as  $V_{avg}$  was increased. However, in Fig. 13, at 4 V, the displacement exhibits a randomize behaviour. By analysing these sets of data, it could be

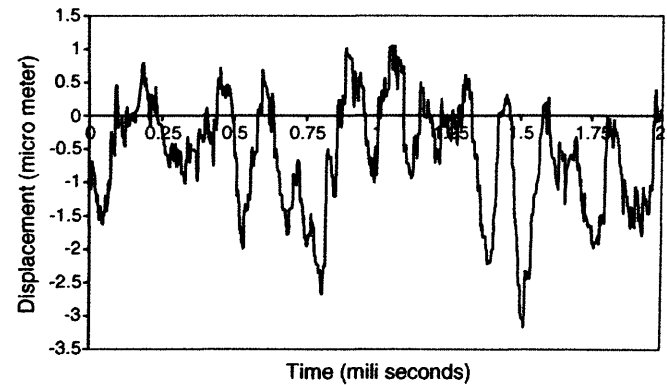


Fig. 9. Graph of used 30 kHz scaler insert at medium generator power settings of displacement from the front of scaler tip.

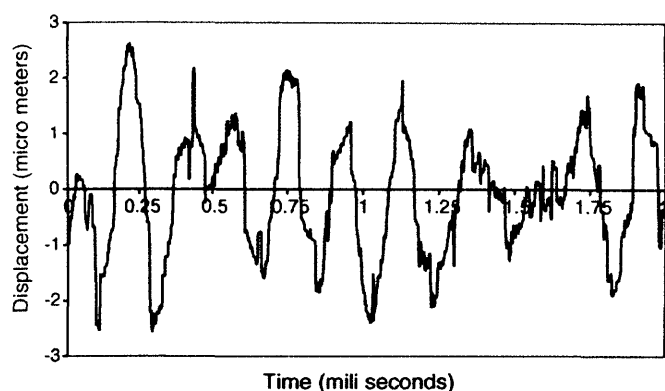


Fig. 10. Graph of *used* 30 kHz scaler insert at low generator power settings of displacement from the front of scaler tip.

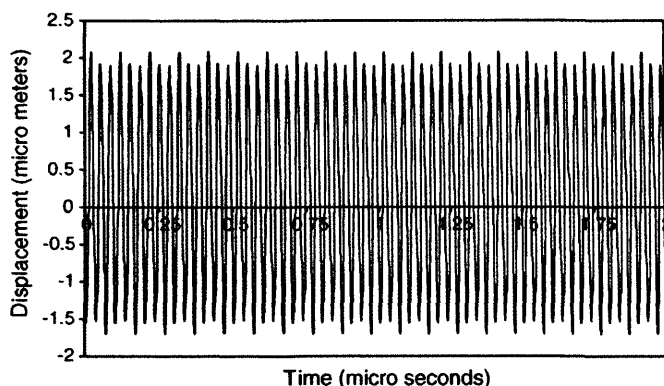


Fig. 13. Graph of *unused* 30 kHz scaler insert at 3 V of displacement from the front of scaler tip.

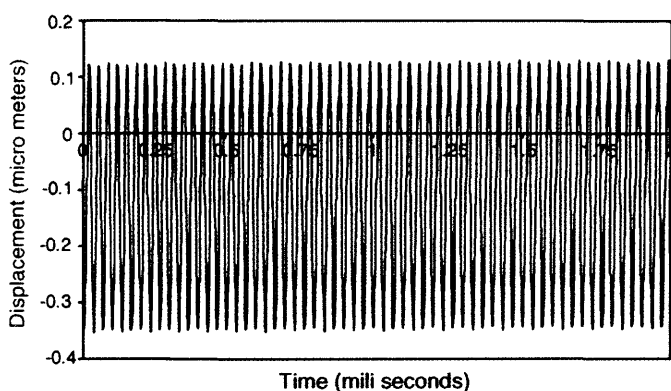


Fig. 11. Graph of *unused* 30 kHz scaler insert at 1 V of displacement from the front of scaler tip.

concluded that scaler inserts are fragile and need regular replacement to achieve its desired performance.

#### 4. Digital feedback control

Magnetostriction,  $\lambda$  is defined as  $d/l$ , where  $d$  is the displacement or change in length and  $l$  is the original length.  $\lambda$  is plotted against magnetic field (A/m) or flux density (T). Therefore, the displacement of the tip of a dental scaler can be controlled by controlling the shape of the flux density or magnetic field.

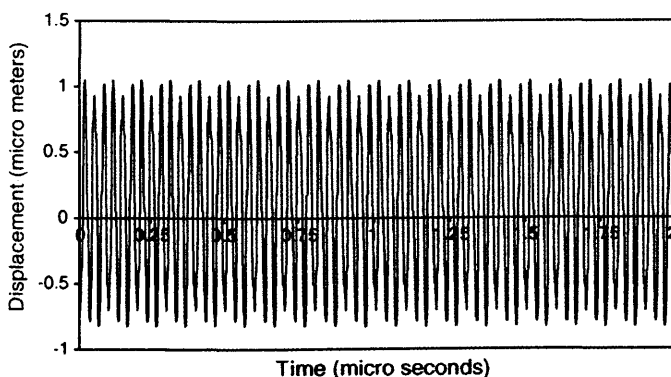


Fig. 12. Graph of *unused* 30 kHz scaler insert at 2 V of displacement from the front of scaler tip.

The control of the shape of a waveform can be achieved by means of analogue or digital feedback. Since there are digital devices already used in the system, the natural choice of method is to use a digital feedback. Recently, a new adaptive digital feedback algorithm (ADFA) has been developed, which proved to be capable of controlling the shape of flux density waveform over wide range of frequency and in various magnetising yokes [5]. The ADFA is written in LabVIEW and a simplified diagram of the program is shown in Fig. 15.

The ADFA consists of four main parts. The first is the measuring thread A (Fig. 15) in which acquired signals are used to calculate and monitor flux density, displacement and voltage in magnetizing coil. The second thread B (Fig. 15) is responsible only for digital feedback with same input data that are used for the measuring thread. These data are then fed to a proportional controller, C (Fig. 15), which calculates the correction of the shape of magnetising current, hence the shape of flux density and, in effect, the shape of displacement.

The algorithm initially assumes that the relationship between the magnetising current and the magnetostriction is linear. However, the overall non-linearity between measured displacement depends also on the shape and magnetic properties of the yoke, sample used, and the transfer function of components used such as power amplifier. In order to compensate for this, a module that calculates the phase lead/lag between the magnetising signal

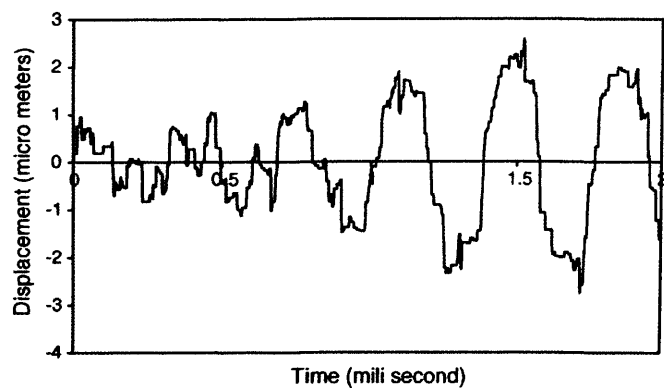


Fig. 14. Graph of *unused* 30 kHz scaler insert at 4 V of displacement from the front of scaler tip.

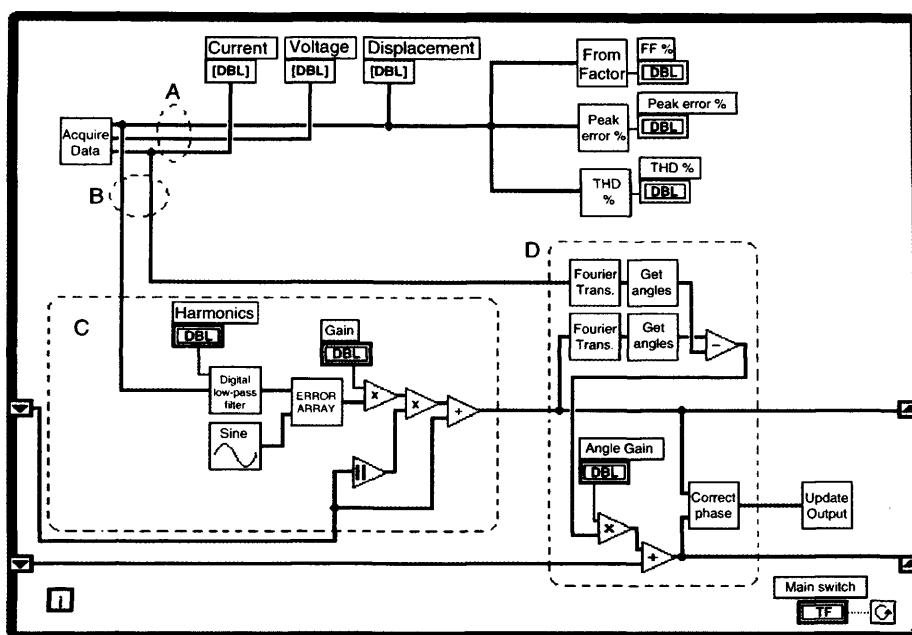


Fig. 15. Block diagram of ADFA program.

generated by the arbitrary waveform generator and actual magnetising current for each harmonic is implemented (D in Fig. 15). The array of phase shifts for all harmonics is continuously adapted in every subsequent iteration. Before the magnetising signal is generated, the waveform computed by the proportional controller (C in Fig. 15) is fed to the *correct phase* element (see D in Fig. 15), which provides a Fourier transform of the waveform, modifies the phase of each harmonic, and then calculates an inverse Fourier transform.

## 5. Conclusion

The proposed algorithm is capable of controlling the output waveform of displacement with the aid of digital feedback control. The amplitude of the waveform could also be specified to give optimum performance. This will help in improving the

design of the dental scaler inserts and both manufacturer and user will understand magnetostrictive dental scalers better.

## References

- [1] Parkell, Inc., 155 Schmitt Blvd., P.O. Box 376, Farmingdale, NY 11735 USA, [www.parkell.com](http://www.parkell.com).
- [2] J. Tunkel, A. Heinecke, T.F. Flemmig, A systematic review of efficacy of machine-driven and manual subgingival debridement in the treatment of chronic periodontitis, *J. Clin. Periodontol.* 29 (Suppl. 3) (2002) 72–81.
- [3] S.C. Trenter, A.D. Walmsley, Ultrasonic dental scaler: associated hazards, *J. Clin. Periodontol.* 30 (2003) 95–101.
- [4] D.C. Jiles, *Introduction to Magnetism and Magnetic Materials*, Chapman & Hall, 1998.
- [5] S. Zurek, P. Marketos, T. Meydan, A.J. Moses, Use of novel adaptive digital feedback for magnetic measurements under controlled magnetizing conditions, *IEEE Trans Magn.* 41 (11) (2005) 4242–4249.

## FREQUENCY DEPENDENCE OF MAGNETOSTRICTION FOR MAGNETIC ACTUATORS

Thant P. P. Phway\* — Antony J. Moses\*\* — David C. Jiles\*\*\*

The frequency dependence of magnetostriction is an important characteristic of magnetic materials when considering possible applications in sensors and actuators. In this study, magnetostriction of grain oriented silicon steel sheets, 303 mm long by 30 mm wide by 0.27 mm thick has been measured in the transverse rolling direction at frequencies in the range of 500Hz to 3000Hz. One end of a sample was clamped and displacement amplitude of the other end of the sample was measured using a "Single Point Laser Doppler Vibrometer" and from this, the magnitude of peak-to-peak magnetostriction was determined. Results show a large variation in magnitude of peak-to-peak magnetostriction between 1500Hz and 2500Hz. A sharp increase in magnitude of magnetostriction was found at 2250Hz.

Keywords: magnetostriction, frequency, resonance, laser vibrometer, electrical steels

### 1 INTRODUCTION

Magnetostriction of magnetic materials has been a subject of extensive study in recent years because its measurement and the related phenomenon of thermal expansion provide basic information on magnetoelastic coupling which is important in determining the applicability in sensors and actuators.

Distinction is drawn between the spontaneous magnetostriction that arises when a material is cooled through its Curie point and field induced or technical magnetostriction. The range of magnetic field induced changes in strain is from 5% in some magnetic shape memory alloys [1] through values of up to 2000 ppm in Terfenol [2], to 200 ppm in manganese doped cobalt ferrite [3] and as low at 10 ppm in iron [4].

When the frequency dependence of magnetostriction is measured a resonance occurs as the combination of frequency of excitation and velocity of magnetostrictively induced sound waves causes an anti-node to be set up at the free end of a sample.



Fig. 1. Resonance condition of the sample with (a) free end and (b) clamped end

If a sample is clamped at one end, as shown in Fig. 1 (b), then the resonant condition occurs when the length of the sample is one quarter of the wavelength of sound. Higher harmonics arise when the frequency is high enough to cause the waves to traverse the length an

integer number of times. The  $n^{\text{th}}$  harmonic frequency  $f_n$  occurs when

$$f_n = \frac{n}{4\ell} \sqrt{\frac{E}{\rho}} \quad (1)$$

Where the modulus of elasticity,  $E$  for the sample was 193 GPa, the density  $\rho$  was 8051 kg/m<sup>3</sup> having mass of 19.76g and volume of 303mm ( $\ell$  length)  $\times$  30mm (width)  $\times$  0.27mm (thickness) = 2.45  $\times 10^{-6}$  m<sup>3</sup>. Therefore, a resonant frequency of 4166Hz was expected.

### 2 PREVIOUS RESEARCH

Jagielski et al [5] have measured the magnetostriction coefficients  $\lambda_{111}$  and  $\lambda_{100}$  using the resonance method under the action of applied stress. The magnetoelastic coupling caused a shift in the resonance frequency under stress, so that

$$M_s \Delta H(\sigma) = \frac{3}{2} \lambda \Delta \sigma \quad (2)$$

and hence the magnetostriction can be determined from the equation

$$\lambda = \frac{2}{3} M_s \frac{\partial H_{res}}{\partial \sigma} \quad (3)$$

Where  $M_s$  is the saturation magnetization,  $H_{res}$  is field resonance and  $\sigma$  is the uniaxial stress.

Various techniques have been used to measure the displacement caused by magnetostriction. Methods such as resistance strain gauges, semiconductor strain gauges, accelerometers and laser velocimeters have been used to measure displacement at specific magnetizing frequencies. Previous researchers have investigated magnetostriction at magnetizing frequencies of 50Hz – 2000Hz. However at the higher magnetizing frequencies within this range, typically at 1000Hz and above, optical methods such as the laser displacement meter and the laser vibrometer have become more widely used. The main advantage of the

\* Wolfson Centre for Magnetics Technology, Cardiff School of Engineering, P O Box 925, Cardiff CF24 0YF, [thantp@cf.ac.uk](mailto:thantp@cf.ac.uk), [mosesaj@cf.ac.uk](mailto:mosesaj@cf.ac.uk), [jilesd@cf.ac.uk](mailto:jilesd@cf.ac.uk) \*\* Permanent Address: Ames Laboratory, Iowa State University, Ames, Iowa 50011, USA, Email: [gauss@ameslab.gov](mailto:gauss@ameslab.gov)

laser vibrometer is that it allows non-contact measurement of displacement with high spatial resolution, which is needed in the case of materials with low magnetostriction. It also has the advantage of being not susceptible to magnetic fields or extreme operating temperatures. It allows measurement of magnetostriction in any direction of anisotropic material.

Results obtained by Kakuno and Gondo [6] using the laser vibrometer method was validated using strain gauges. Nakakta et al [7] have also measured magnetostriction coefficients using the laser Doppler vibrometer method and were able to achieve resolution of displacements of  $4 \times 10^{-8}$  m. Wakiwaka et al [8] have measured the mechanical vibrations of samples indirectly through the determination of impedance characteristics. They have described the behavior of an acoustic vibration element in which the measurements were made using a laser doppler vibrometer but their analysis was based on an analogy with the vibration of a mass on a spring which is not appropriate for this situation. Analysis in terms of standing waves in a solid continuum is the correct procedure to use where the whole specimen is vibrating and the mass is distributed.

Takada [9] investigated magnetomechanical resonance in both strip and toroidal samples and was able to show that the resonance occurred at the expected frequency. Mogi et al [10] have also used a laser Doppler vibrometer to measure the ac magnetostriction at frequencies up to 4000Hz. Benda and Klima [11] calculated magnetostriction using laser speckle interferometer, by which they obtained a resolution of  $5 \times 10^{-6}$  m. Karimi *et al* [12] have looked at the magnetomechanical behavior of alloy films. Resonant behavior similar to that shown elsewhere was observed. Chicarro [13] has demonstrated that the elastic modulus can be calculated from the resonance frequency. Bayou et al [14] have investigated the field dependence of elastic modulus by measuring the  $\Delta E$  effect through changes in the resonance and anti-resonance frequencies.

Hirano *et al.* [15] described measurement of magnetostriction using a laser displacement meter and compared the results to those obtained with a laser Doppler vibrometer. The laser displacement meter was able to measure displacements as low as  $5 \times 10^{-8}$  meter and there was good agreement between the results obtained by the two methods. Moses *et al* [16] have reported a reduction of magnetostriction with frequency in non-oriented electrical steels. Here, the stress sensitivity of magnetostriction was dependant on the degree of texture.

### 3 EXPERIMENTAL DETAILS

A 40MHz arbitrary waveform generator was used for ac signal generation. A pre-amplifier was connected in parallel with the power amplifier and was used for feedback control of the power amplifier. A digital multimeter was used to monitor the average voltage induced in a secondary search coil while a power analyser

was used to display its form factor (FF). A digital oscilloscope with a high voltage isolation module (10 MS/s sampling rate) was used to display displacement output from the laser vibrometer, voltage signal in the search coil ( $V_{ind}$ ) and magnetizing signal in the primary coil. The voltage signal in the primary coil was taken as a reference signal for triggering. National Instrument Software Labview 7.0 was used for data collection and analysis purposes.

Fig. 2 shows the experimental setup. The primary coil had only 39 turns to maintain low impedance at high frequency. A 10 turn secondary coil was used for monitoring the flux density. The secondary coil was connected to the oscilloscope and the multimeter. The sample was clamped at one end with the laser beam directed on the other. The laser beam was focused on a reflective thin film, which was attached on the sample for optimum reflection back to the laser.

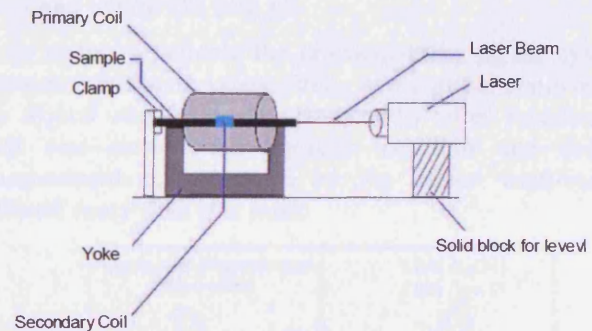


Fig. 2. Diagram of experimental setup

In the present research a single point laser vibrometer (SPLV) was used. The laser vibrometer has 12-bit digital resolution could resolve signal differences of 0.0039 volts, which corresponds to a change in length of  $\Delta l = 1.95$  nm. For samples of length 300 mm this corresponds to a strain resolution of  $6.5 \times 10^{-9}$ .

The magnetic flux density,  $B$  of the sample was measured using a flux coil wound on the sample. Under sinusoidal ac conditions this gave an average output voltage  $V$  which can be related to the amplitude of the magnetic flux density  $B_{max}$  by the equation

$$V = \frac{NA\omega B_{max}}{\sqrt{2}} \cong 4NAfB_{max} \quad (4)$$

Where  $N$  is the number of turns in the search coil,  $\omega$  is  $2\pi f$  with  $f$  being the magnetizing frequency and  $A$  is the cross sectional area of the search coil.

The magnetic field was generated using a solenoid. Excitation frequencies from dc to 3000Hz were used under voltage control to determine the magnetostrictive response of the material. The amplitude of the field strength generated by the solenoid changed with frequency even when the voltage amplitude remained

constant. The characteristics of solenoid are defined in Table 1.

Tab. 1. Characteristics of Solenoid

$l_s$	Length of solenoid	0.17	m
$d$	Diameter of Solenoid	0.1	m
R	Resistance of Solenoid	0.3	$\Omega$
L	Inductance	$\frac{\mu_0 \mu_r A_s N_s^2}{l_s} = 0.088$	mH

Where  $A_s$  is the cross sectional area of the solenoid and  $N_s$  is the number of turns in the solenoid.

From these characteristics the impedance  $Z$  was determined at various frequencies, from the standard equation,  $Z = \sqrt{R^2 + \omega^2 L^2}$  and from this the current ( $i = \frac{V}{Z}$ ) was determined at a function of voltage at different frequencies. Once the current was known the magnetic field strength was determined using the equation for a finite length solenoid [17]

$$H = \frac{Ni}{\sqrt{(\ell_s^2 + d^2)}} \quad (5)$$

The strength of the magnetic field generated by the solenoid for various applied voltages at different frequencies is shown in the following table.

Table 2. Magnetic Field Strength in Solenoid for Various Applied Voltages at Different Frequencies

Freq (Hz)	Voltage (V)	Resistance ( $\Omega$ )	Inductance (Henries)	Impedance ( $\Omega$ )	Current (Amps)	Field (A/m)	Field (Oe)
10	1	0.30	0.000088	0.30	3.333	659.0	8.28
10	5	0.30	0.000088	0.30	16.664	3295.1	41.41
10	10	0.30	0.000088	0.30	33.328	6590.1	82.82
10	20	0.30	0.000088	0.30	66.655	13180.3	165.64
10	30	0.30	0.000088	0.30	99.983	19770.4	248.47
10	40	0.30	0.000088	0.30	133.311	26360.5	331.29
10	50	0.30	0.000088	0.30	166.638	32950.7	414.11
20	30	0.30	0.000088	0.30	99.932	19760.3	248.34
50	30	0.30	0.000088	0.30	99.575	19689.7	247.45
100	30	0.30	0.000088	0.31	98.331	19443.7	244.36
500	30	0.30	0.000088	0.41	73.402	14514.3	182.41
1000	30	0.30	0.000088	0.63	47.543	9401.0	118.15
2000	30	0.30	0.000088	1.15	26.085	5158.0	64.82
4000	30	0.30	0.000088	2.24	13.389	2647.4	33.27

### 4 RESULTS AND DISCUSSION

Eddy current heating can be a significant factor when making measurements of the properties of these materials at high frequencies. This has to be taken into account preferably by making the measurements before significant rise in temperature has occurred, or by monitoring and allowing for changes in temperature when comparing results. Fig. 3 shows the increase of temperature with time

from the start of magnetizing at  $B_{max} = 1.0T$  over the frequency range of 500Hz to 4000Hz.

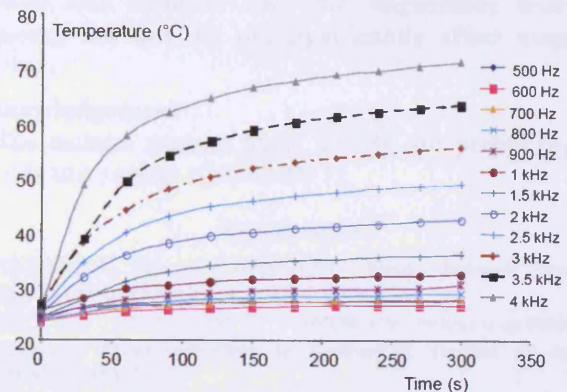


Fig. 3. Increase of temperature with time of magnetisation at different magnetising frequencies ( $B_{max} = 1.0T$ )

Magnetostriction was measured at  $B_{max} = 0.7T, 0.9T$  and  $1.0T$  and frequencies from 500Hz to 3000Hz at 250Hz increments. At these flux densities, the form factor remained within 1% of 1.11.

In order to validate the reproducibility of the system, measurements were taken: firstly at the initial condition of the digital oscilloscope and secondly after resetting it. This was carried out because the start and end of measurement points saved by the digital oscilloscope differed every time it is reset.

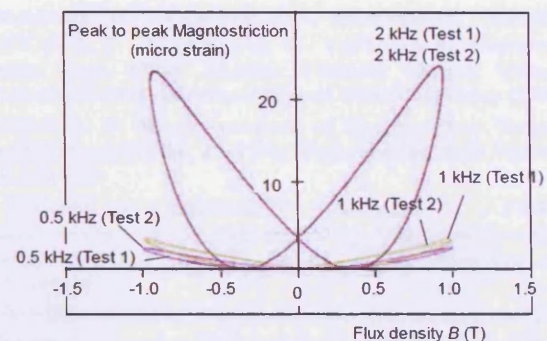


Fig. 4. Magnetostriction,  $\lambda$  vs Flux Density,  $B$  at 500Hz, 1000Hz, 2000Hz at  $B_{max} 1.0T$

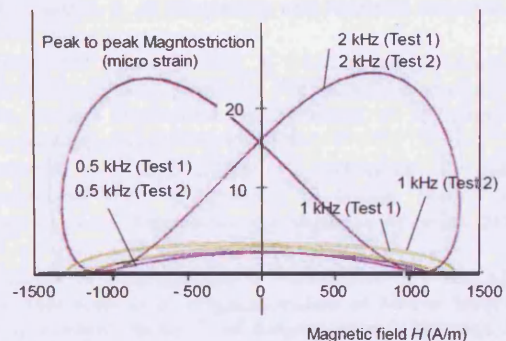


Fig. 5. Magnetostriction,  $\lambda$  vs Magnetic Field,  $H$  at 500Hz, 1000Hz, 2000Hz at  $B_{max} 1.0T$

Figs. 4-5 show the peak-to-peak magnetostriction,  $\lambda$  versus flux density  $B_{max}$  at  $1.0T$  and magnetic field  $H$  at 500Hz, 1000Hz and 2000Hz. It was observed that peak-to-

peak magnetostriction differs by less than 10% in the reproducibility tests.

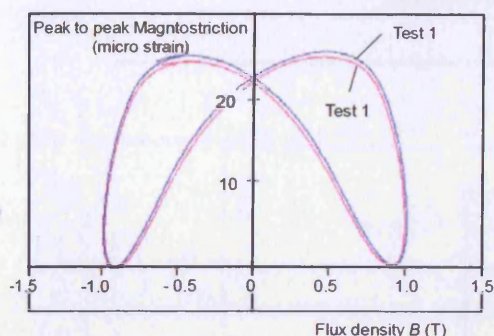


Fig. 6. Magnetostriction,  $\lambda$  vs Flux Density,  $B$  at 2250Hz at  $B_{max} = 1.0T$

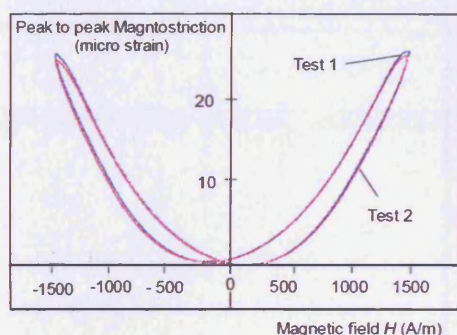


Fig. 7. Magnetostriction,  $\lambda$  vs Magnetic Field,  $H$ , at 2250Hz at  $B_{max} = 1.0T$

Figs. 6-7 shows peak-to-peak magnetostriction versus flux density,  $B$  and magnetic field,  $H$  at 2250Hz. A phase change in the plots was observed compared to figs. 4-5, confirming the characteristic of passing through a resonance point. Fig. 8 shows a plot of peak-to-peak magnetostriction  $\lambda$  versus magnetizing frequency at flux densities 0.7T, 0.9T and 1.0T. The plot shows a sharp rise of magnetostriction at 2250Hz. Another sharp rise in magnitude of peak-to-peak magnetostriction is expected at 4500Hz since the calculated resonant frequency for the sample is 4166Hz.

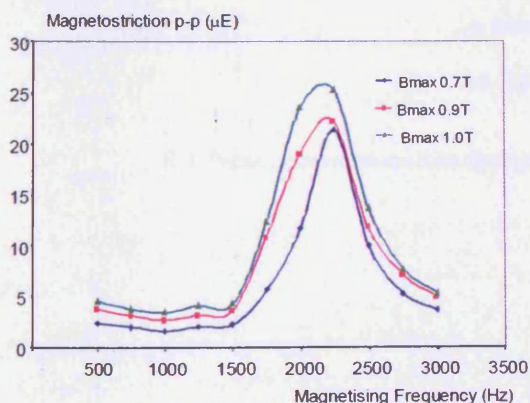


Fig. 8. Peak-peak Magnetostriction,  $\lambda$  vs Magnetising Frequency,  $\nu$  at  $B_{max} = 0.7T, 0.9T$  and  $1.0T$

## 5 CONCLUSION

It was observed that magnetostriction is not only a function of magnetic properties but also dependant on the physical condition of the sample. A resonant frequency at

2250Hz was found for the sample used under the given experimental conditions and physical dimensions. Temperature was found to rise with magnetising time and frequency but this did not significantly affect magnetostriction.

## Acknowledgement

The authors wish to thank EPSRC for partial support towards this project (GR/R10493).

## REFERENCES

- [1] ULLAKKO, RC - O'HANDLEY: Field -Induced Strain in  $Ni_2MnGa$ , Applied Physics Letters 69 (1996), 1966
- [2] JILES, DC - OSTENSON, JE - OWEN, CV: Barkhausen Effect and Discontinuous Magnetostriction in Terfenol-D, Journal of Applied Physics 64 (1988), 5417
- [3] PAULSEN, JA - RING, AP - LO, CCH - SNYDER, JE - JILES, DC: New Manganese Substituted Cobalt Ferrite Magnetostrictive Materials for Magnetic Stress Sensor Application, Applied Physics Letters - to be published (2004)
- [4] CHIKAZUMI S<sup>OSHIN</sup>: Physics of Magnetism, 1978
- [5] JAGIELINSKI, T: The Measurement of Magnetostriction Constants by the Method of Ferromagnetic Resonance by means of the Modulated Strain, Acta Physica Polonica Vol. A49 No. 6 (1976), 799-802
- [6] KAKUNO, K - GONDÓ, Y: Optical interferometric observation of magnetostrictive vibration, J. of Magnetism and Magnetic Materials, Vol. 15-18, Part 2, January-March (1980), 611-612
- [7] NAKAKTA, T - TAKAHASHI, N - NAKANO, M - MURAMATSU, K - MIYAKE, P: Magnetostriction Measurements with LASer Doppler Velocimeter, IEEE Transactions on Magnetics Vol. 30 Issue 6 (1994), 4563-4565
- [8] Wakiwaka, H - Umezawa, T - Kuwahara, K - Kamata, H - YOSHIKAWA, T - KITAZAWA, S - YAMADA, H: Measurement of Vibration Mode of an Acoustic Vibration Element Using Giant Magnetostrictive Material, Proceedings of ISEM Conference (1994)
- [9] TAKADA, S: Magnetostrictions of Electrical Iron Sheets under Controlled Magnetization, J. of Magnetism and Magnetic Materials 133 (1994), 226-228
- [10] HISASHI, M - MASAO, Y - MASATO, M - YASUO, O: Harmonic Analysis of AC Magnetostriction Measurements under Non-Sinusoidal Excitation, IEEE Transactions on Magnetics Vol. 32 No. 5 (1996), 4911-4913
- [11] BENDA - KLIMA: Magnetostriction Measurement Using Speckle Interferometry, Journal of Electrical Engineering 48 (1997), 133-136
- [12] KARIMI, A - AZCOITIA, CH - DEGAUQUE: Relationships Between Magnetomechanical Damping and Magnetic Properties of Fe-Cr(Al/Mo) Alloys, J. of Magnetism and Magnetic Materials 215-216 (2000), 601-603
- [13] CHICARRO, J M - BAYON, A - SALAZAR, F: Measurement of Field-Dependence Elastic Modulus and Magnetomechanical Coupling Factor by optical Heterodyne Interferometry, J. of Magnetism and Magnetic Materials 202 (1999), 465-472
- [14] BAYON, A - CHICARRO - SALAZAR, F: simultaneous Measurement of Field Dependence of Elastic Moduli by Laser Interferometry, J. of Magnetism and Magnetic Materials 219 (2000), 229-235
- [15] HIRANO, M - ISHIHARA, Y - HARADA, K - TOKADA, T: A Study on Measurement of Magnetostriction of Silicon Steel Sheet by Laser Displacement Meter, J. of Magnetism and Magnetic Materials 254-255 (2003), 43-46
- [16] MOSES, A J - NTATSIS, A - KOCHMANN, T - SCHNEIDER, J: Magnetostriction in Non-Oriented Electrical Steels: General Trends, J. of Magnetism and Magnetic Materials 215-216 (2000), 669-672
- [17] JILES, D: Introduction to Magnetism and Magnetic Materials, Chapman & Hall (1991)

Received 30 June 2004



---

**APPENDIX II – CORRECTION TABLE**


---

n	Correction T = t/k		
	k = 1	k = 2	k = 3
3	1.32	2.27	-
4	1.20	1.66	3.07
5	1.14	1.44	2.21
6	1.11	1.33	1.84
7	1.09	1.26	1.63
8	1.08	1.22	1.51
9	1.07	1.19	1.43
10	1.06	1.16	1.36
11	1.05	1.14	1.32
12	1.05	1.13	1.28
13	1.04	1.12	1.25
14	1.04	1.11	1.23
15	1.04	1.10	1.21
16	1.03	1.09	1.20
17	1.03	1.09	1.18
18	1.03	1.08	1.17
19	1.03	1.08	1.16
20	1.03	1.07	1.15

- Examples:**
- a) For n=10 measurements and k=1, the correction factor is 1.06  
i.e. standard uncertainty = 1.06 x estimated standard deviation
- b) For n=5 measurements of the sole source of uncertainty at a 95% confidence level, k=2, the correction factor is 1.44.  
i.e. standard uncertainty = 1.44 x estimated standard deviation  
and expanded uncertainty = 2 x standard uncertainty

II.1 Table of correction to be applied to the standard deviation for the number of measurements,  $n_u$  [6.1]